Spatiotemporal Distributions of Metabolites Involved in Barley Grain Development with Emphasis on Endosperm Formation

Dissertation

zur Erlangung des akademisches Grades

Doktor rerum naturalium (Dr. rer. nat.)

vorgelegt der

Naturwissenschaftlichen Fakultät I

Biowissenschaften

der Martin-Luther-Universität Halle-Wittenberg

von

Frau Manuela Peukert

Geboren am 02.01.1982 in Aschersleben

Gutachter/in

1. PD Dr. Hans-Peter Mock
2. Prof. Dr. Klaus Humbeck
3. Prof. Dr. Gerhard Leubner-Metzger

Halle (Saale), den 24.10.2013

Abstract

Cereal grain development is a phenomenon that involves complex regulatory pathways, the evolving and degeneration of tissues, and the bulk accumulation of storage compounds that are of outmost importance for animal and human nutrition. In this thesis, mass spectrometry based imaging (MSI) was applied as a novel approach for the study of metabolite distribution patterns in developing barley grains to identify candidate compounds that have an impact on the events of endosperm formation and grain filling.

The investigation of characteristic developmental stages of barley grains by MALDI MSI revealed highly tissue specific patterns of particular metabolites. Data mining by multivariate statistics reflected the typical developmental proceedings. In general, the specificity of molecules in the endosperm and in the nutrient transfer region increased from the prestorage stage to the storage stage, whereas the abundances of molecules in the pericarp decreased.

The endosperm constitutes specific phospholipid distributions during the storage stage of barley grain development. By means of MALDI MSI increasing gradients of particular lipids towards the periphery were obtained. These accumulations are suggested to reflect characteristics of the starch-lipid complex formation.

The integrated study on fructan distribution patterns involved targeted analyses on the metabolite, the transcript and the protein level. The grain region that realizes the transport of nutrients towards the endosperm exhibited particular accumulations of oligo fructans. The mixed levan type fructan bifurcose was found to concentrate prior to the onset of massive storage accumulation. But with the early storage stage the inulin type oligo fructans (1-kestose and nystose) highly accumulated in the tissues surrounding the endospermal cavity. By transcript analyses specific expression patterns for genes from fructan metabolism were obtained that correspond to the profiles of the individual fructans. Their differential patterns during grain development suggest particular functions concerning a transient carbon partition and a relation to stress responses, such as membrane stabilization and ROS detoxification.

The impact of phytohormones on developmental processes is well known. Their action is determined by a precisely regulated interplay with each other, and with further signaling compounds (such as sugars). The various tissue types in a barley grain suggest a specific spatial hormone composition that regulates the local occurring processes, e.g. programmed cell death in the pericarp, and cellularization and storage product accumulation in the endosperm. As phytohormones act at very low concentrations, barley grain dissections were used to quantify

abscisic acid and cytokinin in particular grain parts. Developmental stage depending distribution patterns were observed for both hormones. These were correlated to stage specific proceedings in the particular grain regions.

So far, transcriptome studies gained much information about spatiotemporal regulations of factors that affect the processes of grain development, but direct conclusions about the final end products of gene expression, the metabolites, cannot be deduced as their abundance is subjected to a network of biosynthesis, processing, transport and degradation. The presented study about metabolite distributions in barley grains provides new insights into the particular kernel constitutions at characteristic developmental stages, and emphasizes individual metabolites that are hypothesized to affect the developmental processes of nutrient import and storage product accumulation.

1. Introduction

Cereals are the worldwide most important energy sources of human and animal nutrition. To provide food to an increasing population, the enhancement of crop yield and seed quality, of tolerance against abiotic stresses, and an increased resistance against diseases are in the focus of crop plant research and of the breeding industry. Most important cereals are maize, rice, wheat, barley and sorghum, with barley on the fourth place of the cereal world production quantity (Faostat 2011, http://faostat.fao.org). Barley (*Hordeum vulgare* L.), one of the most ancient crops, belongs to Triticeae within the family Poaceae. Besides the agronomical importance for animal feed and human consumption (mostly for brewing and distilling), barley plays a central role as a model plant for genetics and breeding, plant physiology, cereal chemistry, nutrition and pathology (Ullrich, 2011). Within the crop Triticeae, barley constitutes the least complex genome (diploid) and shows high colinearity to other species, such as wheat and rye. Numerous ESTs and BAC clones are available. In addition, more than 95% (= 5.1 Gb) of the barley genome are represented in the physical map (Consortium, 2012), emphasizing its role as a model plant.

Seeds make about 70% of all food for human consumption (Bewley et al., 2013). The end usage of barley grains as food, feed or for processing is determined by the grain quality, which means the structure and composition of the mature grain. The major components (in typical order of % composition) are starch, fiber (non-starch polysaccharides), proteins, soluble sugars, lipids and ash (minerals). A comprehensive description is presented in (Byung-Kee et al., 2011). Even though barley is of great scientific and industrial interest, the complex physiological processes occurring in a grain are far from being fully understood. It is necessary to elucidate how the grain develops and acquires a specific composition that defines in the end the properties of a barley seed. The major storage organ of barley (as in all cereals) is the endosperm and the grain filling period is essential for the bulk storage in this seed organ.

The following sections give an introduction to the characteristics of grain development (1.1.), and to the processes of nutrient import and the accumulation of storage compounds (1.2.). In 1.3. approaches for the tissue specific determination of metabolite distribution patterns are introduced. The scientific aims of this thesis are outlined in 1.4.

1.1.   A General Overview on Barley Grain Development

The barley kernel comprises maternal and filial derived tissues that undergo massive changes from fertilization to the mature seed. Seed development is in general divided into three characteristic stages: prestorage, storage and desiccation. For barley, a fourth phase, the transition phase, was described. This phase represents the switch between the prestorage and the storage stage, and is characterized by dramatic changes at the transcriptional level, and for many physiological parameters (Sreenivasulu et al., 2004; Wobus et al., 2005). Below, histological and physiological characteristics of the prestorage, transition and storage stage are described in more detail as being relevant for the presented study. A histological overview of these phases is presented in Figure 1.
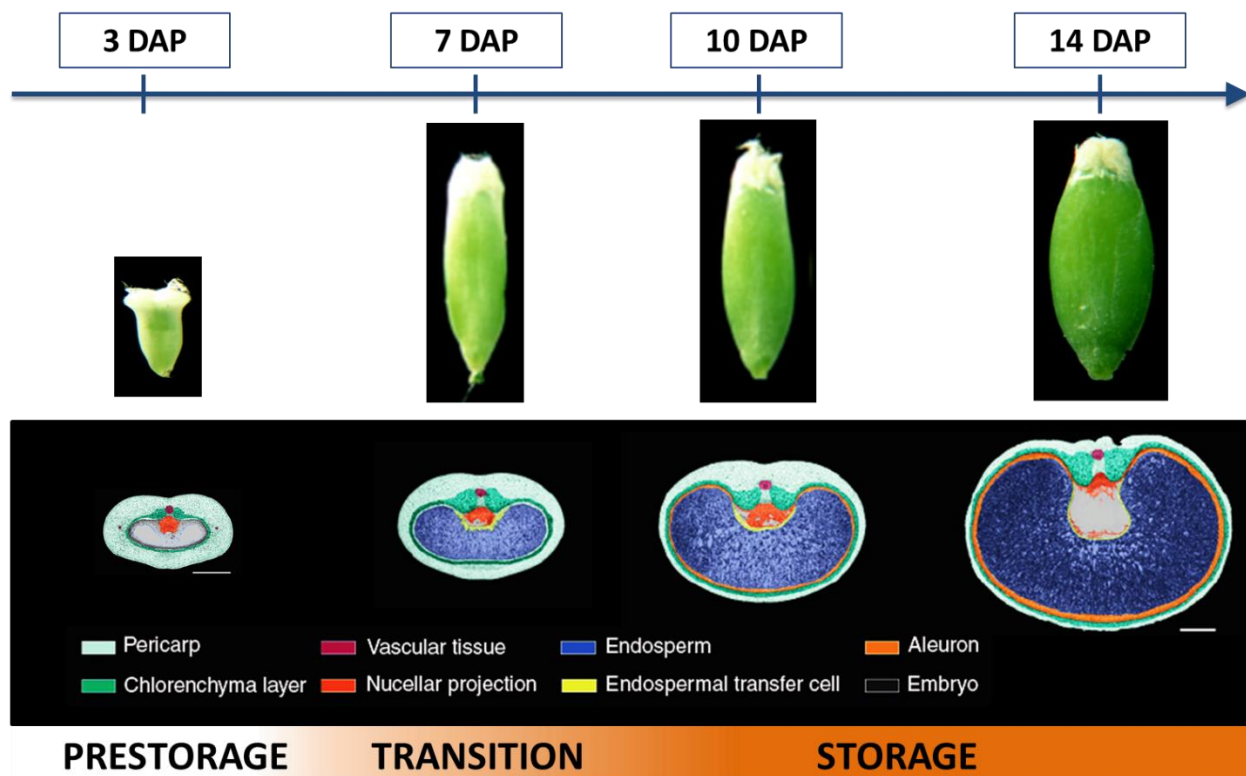
Figure 1: Histological overview of barley grain developmental stages relevant for the presented work.

A: Seed development in barley follows the general phases of cell-division (prestorage) and storage accumulation. Between both, the transition phase was described for barley that is related to massive transcriptional and physiological changes; DAP, days after pollination (according to Wobus et al., 2005).

B: Histological models of barley grain cross sections from different developmental stages indicating the morphological changes of individual tissues. Colors represent single tissues. Bars, 500µm. (Sreenivasulu et al. 2010).

The prestorage stage

After the fertilization the seed consists of the embryo sac surrounded by maternal tissues such as nucellus and pericarp. The maternal tissues comprise at this time point about 90% of the caryopsis (Sreenivasulu et al., 2010). As in other angiosperms double fertilization leads to a diploid zygote and a triploid central cell, which forms later the endosperm (Bethke et al., 2000). The period from 1 to 6 days after pollination (DAP) is designated as the prestorage stage in barley (Weschke et al., 2003) and it is characterized by cellularization processes. The formation of the embryo begins at 1 DAP (Engell, 1989). The cell divisions of the endosperm start at 3 DAP. First, mitotic events without cytokinesis and cell wall formation lead to a coenocytic tissue surrounding the fluidic filled cavity (arisen from the embryo sac cytoplasm). Then, the nuclei of the coenocyte are surrounded by cell walls forming separated alveolar cells and finally start synchronous cell divisions towards the centre (Olsen, 2001). Until 5-6 DAP the endosperm is completely cellularized (Olsen, 2001; Weschke et al., 2003; Sreenivasulu et al., 2010). The cellularization events in the filial part are accompanied by reorganizations in the maternal seed part. Grain growth during the prestorage stage occurs mainly longitudinally (as can be abstracted from Figure 1A). The scar volume scales down and the pericarp expands by cell division and elongation. The nucellus that surrounds the embryo sac undergoes programmed cell death (PCD) except the part facing the main vascular bundle, which differentiates into the nucellar projection (NP). In parallel, when the cells of the endospermal coenocyte start mitosis, the cells of that region facing the NP differentiate into the endospermal transfer cells (ETC) (Sreenivasulu et al., 2010). NP and ETC are of outmost importance for transport events (section 1.2.). According to transcript studies, the pericarp mainly serves as a feeding tissue (Wobus et al., 2005). This coincides with findings that during the early development (2-5 DAP) the pericarp displays the major sink part of the seed, which is characterized by high invertase activity and a transient accumulation of starch in this tissue (Weschke et al., 2000; Weschke et al., 2003).

The transition stage

The transition phase represents the physiological switch from cellularization to massive storage accumulation that occurs between 6 and 8 DAP (Figure 1A), and it is characterized by a dramatic reprogramming of gene expression. Processes of endoreduplication and storage product synthesis are initiated, accompanied by the expression of genes related to energy production (Sreenivasulu et al., 2004). Energy equivalents produced in the endosperm are a prerequisite for storage product

synthesis. Gene expression in the maternal pericarp switches from carbon metabolism and cell division to degradation processes as indicated by expression of glucanases and lipases. In addition, the specific expression of sucrose transporters in the ETCs is correlated to an increase of the sucrose level and to an induction of massive starch accumulation. At the same time, activity of sucrose synthase (SuSy), a major enzyme in the sucrose to starch pathway, increases dramatically between 5 and 9 DAP and is associated with the onset of storage accumulation (Weschke et al., 2000). The dominant sink for nutrient loading is no longer the maternal pericarp but shifts to the filial tissues (Zhang et al., 2007).

The storage stage

The storage stage of grain development is mainly determined by massive storage accumulation. Cells of the NP and the ETC are fully differentiated, increasing the sink strength of the endosperm. The maturing endosperm differentiates into different cell types, those surrounding the embryo, the starchy endosperm, and the peripheral cells. The latter ones comprise the aleurone layer, covering the surface of the starchy endosperm, the germ aleurone over the embryo, and the ETC facing the NP (Gubatz and Shewry, 2011). The high storage capacity of the starchy endosperm is suggested to be related to endoreduplication events that are initiated after finalization of endosperm cellularization (Sreenivasulu et al., 2010), and that are supposed to be induced by the ratio of the phytohormones auxin and cytokinin (Nguyen et al., 2007; Rijavec et al., 2009). However, the role of endoreduplication is conversely discussed. A contribution to germination was suggested as polyploid nuclei could be a source of nucleotides or nucleosides for the embryo, allowing rapid cell division during the early seedling growth as *de novo* synthesis might be time- and energy consuming (Nguyen et al., 2007). During the storage stage, cells of the endosperm (except aleurone) undergo PCD. This process is thought to facilitate nutrient hydrolysis and uptake by the embryo at germination (Nguyen et al., 2007). The degeneration starts random in its spatial pattern at the early storage stage and is present throughout the endosperm until the late storage stage (20 DAP). In contrast to PCD in the pericarp, endosperm cells do not show DNA fragmentation before 19-20 DAP (Gubatz and Shewry, 2011). In addition, the expression of PCD related genes shows fundamental differences to pericarp and NP. Here, abscisic acid (ABA) in concert with ethylene is suggested to be involved (Sreenivasulu et al., 2010).

The aleurone consists of specialized cells, and comprises three cell layers in barley. The cytoplasm of aleurone cells is dense, contains numerous small vacuoles, and is free of starch granules. The aleurone cells are rich in storage reserves, such as lipids, proteins and minerals. Lipids are stored in oil bodies stabilized by oleosins and phospholipids. Protein-carbohydrate bodies (crystalloids) and phytin-globoids are deposited in a proteinaceous matrix (Gubatz and Shewry, 2011). The aleurone is the only living endosperm part at germination and possesses a specific program for the acquisition of desiccation tolerance. Endosperm cells adjacent to the aleurone are called subaleurone cells due to their smaller shape and higher mitochondrial activity than the inner starchy endosperm cells. They contain only few or no starch granules but are rich in protein content (Gubatz and Shewry, 2011).

The storage accumulation stage is also accompanied by further embryonic cell divisions and differentiations. The first visible tissue differentiations of the embryo can be observed at 7 DAP. At first, the shoot meristem and scutellum can be distinguished, and a few days later the root meristem (Bethke et al., 2000). Embryo length continuously increases until 20 DAP (Gubatz and Shewry, 2011). The scutellum, a nursing tissue, is rich in lipid reserves and protein bodies, and also contains starch, and ferulic acid as a major phenolic compound.

The maternal pericarp is bounded by an inner and outer epidermis and encloses the green chlorenchyma layer and the non-photosynthetic layer. During the storage phase most parts of the pericarp disintegrate. Of the non-green part, only the region embedding the main vascular bundle in the ventral crease remains (Wobus et al., 2005). An expression of PCD related genes was observed between 8 and 14 DAP and is suggested to be regulated by ethylene and jasmonic acid (Sreenivasulu et al., 2010). The chlorenchyma layer consists of two cell layers and envelopes the nucellar epidermis. This tissue maintains until the end of the storage stage supplying oxygen for energy metabolism in the endosperm (Rolletschek et al., 2004).

With the beginning of the storage stage a large apoplastic gap between the NP and ETC is formed. A part of the NP undergoes PCD that contributes to the formation of the endospermal cavity. The NP constitutes three different cell types: meristematic cells undergoing active cell division are adjacent to the pericarp ground tissue, the middle zone contains differentiating/ elongating cells, and the third zone facing the ETC contains the autolysing cells and those cells showing transfer cell morphology (Thiel et al., 2008).

For the final grain composition, the storage stage is the essential developmental phase in which those regulations occur that control the onset and offset of the different storage compound

pathways. All this biosynthetic pathways have one fact in common: they depend on the assimilate import from the mother plant through the vascular bundle in the ventral crease. High import rates are necessary to keep the high turnover rates within the seed. Specialized cell systems have developed to fulfill the high, but also controlled supply of nutrients. How these cell systems work and how the influx is controlled is a crucial issue in the study of grain development. Furthermore, carbohydrate partition towards the different storage compounds has to be regulated. Factors determining the final grain composition and the way of deposition (temporally and spatially) are also in the focus of the study of grain development. The following section introduces an overview of nutrient import into the endosperm, and about the storage deposition in barley.

1.2. Assimilate Import and Accumulation of Storage Compounds in the Endosperm During the Storage Phase

The main function of the endosperm is providing nutrients to the embryo during germination. Because of its importance in human and livestock nutrition the discovery of endosperm formation and of influencing factors is inevitable. The rate of biosynthesis of storage products depends on the permanent nutrient influx. First, this is realized from the mother plant that mainly supplies the solutes in form of sucrose and minerals. Then, an effective transfer has to be ensured when the nutrients leave the phloem and move through post-sieve elements towards the filial grain part. Finally, the uptake into the endosperm has to be efficient, and to be regulated according to the requirements.

1.2.1. Transport of nutrients from the main vascular bundle into the endosperm

The filial part of the grain is covered by the seed coat between the nucellar epidermis and the inner pericarp. This coat is derived from the inner integument and comprises a cuticle, which forms a barrier against solutes. Thus, the transport of nutrients into the filial part of the grain occurs only through a region of the crease, where the seed coat is interrupted (Ugalde and Jenner, 1990b). Nutrients are imported from the mother plant through the main vascular bundle in the ventral crease (Figure 2). This bundle exceeds the whole length of the barley grain. From the phloem imported nutrients are transported through plasmodesmata along a post-sieve element pathway towards the NP (Patrick and Offler, 2001). This passive flow was supposed to be a pressure-driven bulk flow (Wang and Fisher, 1995c). Between the filial and the maternal tissues there is no direct symplastic connection. The nutrients are delivered into the extracellular space

that separates both generations (Wolswinkel, 1992). The release of nutrients occurs through specialized cells of the NP bordering the ETC, and later in development the endospermal cavity. These cells were found to exhibit transfer cell morphology that means that they contain an extensive ER network, a high number of mitochondria, and cell wall ingrowths to amplify the plasma membrane surface area (Ugalde and Jenner, 1990b; Patrick and Offler, 2001; Thiel et al., 2012). In addition, the expression of transport proteins was observed for the NP (Weschke et al., 2003; Thiel et al., 2008).
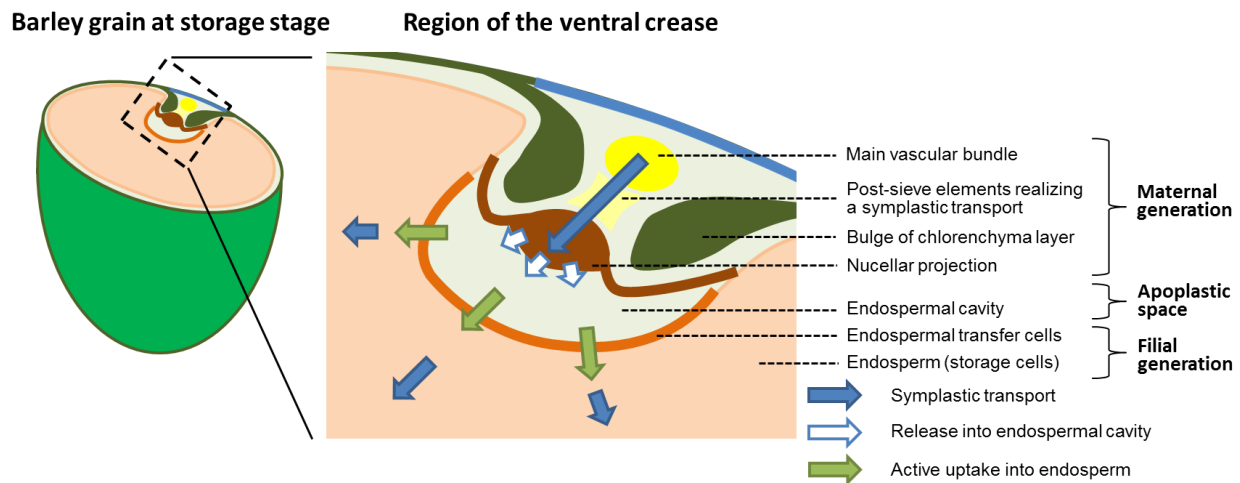
Figure 2: Generalized pathway of solute import into the developing grain.

Nutrients exit the phloem by a bulk flow and move through symplastic connected cells to specialized cells for the efflux at the nucellar projection facing the endospermal cavity. From these cells the nutrients are released into the seed apoplasm. The import into the transfer cells occurs through specialized transporters. The distribution within the storage tissue occurs again symplastically via plasmodesmata.

With the beginning of the storage stage a fluidic filled cavity between the NP and ETC is formed containing high concentrations of soluble carbohydrates (Ugalde and Jenner, 1990a). The uptake of nutrients is conducted by the ETCs that also show transfer cell morphology, and contain transporters with defined substrate specificities (Thiel et al., 2008). Sucrose and amino acid/H+ symporters function in parallel with non-selective cation channels (Zhang et al., 2007). A high density of plasmodesmata in the endosperm allows a nutrient distribution at high rates towards the places of storage product biosynthesis (Ugalde and Jenner, 1990b; Patrick and Offler, 2001).

The regulation of nutrient loading is highly dynamic and linked with developmental processes. Import reaches a plateau during storage accumulation, before declining as the seed reaches maturity (Zhang et al., 2007). The rate of grain filling defines the final seed weight and is correlated to the number of starch granules in the endosperm. In turn, the number of starch

granules depends on the number of cells. Thus, the extent of the cell division plays also a key role for the final grain yield (Jones et al., 1985; Sabelli and Larkins, 2009). Up to now, the regulation of import processes is poorly understood and has to be further addressed. This issue includes e.g. the synchronous regulation of efflux and influx, as by selective transport processes the composition of the apoplastic fluid might be affected. This in turn could influence the osmolarity of the apoplastic space. In experiments, the osmolarity of the cavity sap was found to be stable across different treatments and changing concentrations of individual sap solutes (Fisher and Gifford, 1987). Cell wall bound invertases that are expressed in cells of the NP and ETC (Weschke et al., 2003) could be involved in the regulation of cavity sap composition, but the control of enzyme activities according to short-term requirements (in case of osmotic adaption) is not yet known. A tight interplay of filial and maternal tissues for a regulation of the pH, the osmolarity, and of the nutrient supply is suggested. In this direction the communication of a sink demand by a turgor signal was proposed (Patrick and Offler, 2001).

1.2.2. Deposition of storage compounds

In cereal grains the major storage compound in the endosperm is starch. In barley, starch accounts for 50-70% of the mature grain. Other carbohydrates are cell wall polysaccharides (ß-glucans, cellulose, arabinoxylans), and a minor amount of oligosaccharides (Gubatz and Shewry, 2011). Barley starches are a mixture of amylose and amylopectin, with the latter one being the major component. Deposition of starch occurs in granules. Two size classes are abundant in barley: large A granules (≥ 10 µm) and small B granules (≤ 10 µm). The synthesis of starch is realized by the concerted action of at least five enzyme activities: sucrose synthase (SuSy), ADP-glucose pyrophosphorylase (AGPase), starch synthase (SS), starch-branching (SBE) and starch-debranching (SDBE) enzymes (Yang et al., 2004). An overview of starch synthesis is given in Figure 3. Activity of SuSy is high during the storage stage in barley and correlates with starch accumulation and expression of sucrose transporters into the endosperm (Weschke et al., 2000). A linkage of this enzyme to sink strength in the developing grain was considered (Yang et al., 2004). AGPase produces the primer of the starch chain and its activity represents the rate-limiting step in starch biosynthesis (Sabelli and Larkins, 2009). Starch synthases elongate amylose and amylopectin chains, whereas SBEs introduce branches into the chain by cleavage of α-1,4 bonds and replacement by α-1,6 bonds. The activity of SDBE is related to a structural organization of

the tightly packed amylopectin molecules and therefore to the starch granule structure (Kubo et al., 1999).
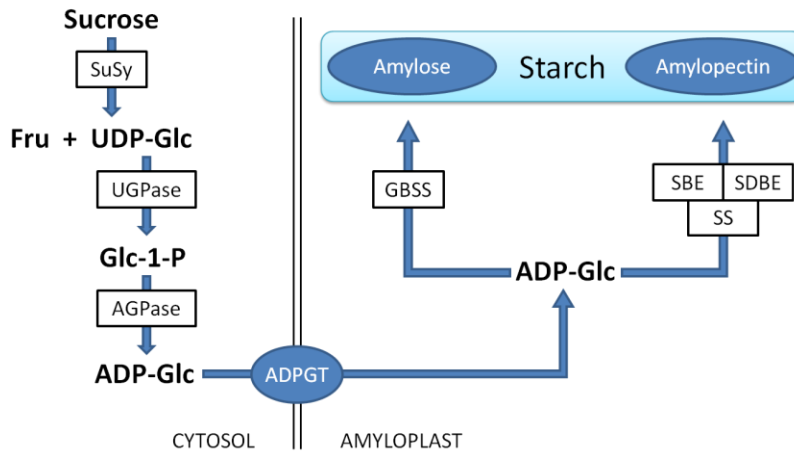
Figure 3: Generalized pathway of starch synthesis in the endosperm of cereal grains.

Abbreviations for enzymes are SuSy, sucrose synthase; UGPase, UDPglucose pyrophosphorylase; AGPase, ADPglucose pyrophosphorylase; SS, starch synthase; SBE, starch-branching enzyme; SDBE, starch-debranching enzyme. The transporter ADPGT in the amyloplast inner membrane is shown as circle, ADPglucose-transporter; Other abbreviations are Fru, fructose; UDP-Glc, UDP-glucose; Glc-1-P, glucose-1-phosphat; ADP-Glc, ADP-glucose. The figure is modified after (Thitisaksakul et al., 2012).

Cereals are the main source of protein in livestock feed worldwide. In human nutrition, storage proteins are responsible for the cohesive and viscoelastic properties of the dough that are essential quality parameters for bread making and other baked goods (Sabelli and Larkins, 2009). The major group of storage proteins in barley are the alcohol-soluble prolamins, the hordeins. These are exclusively located in the starchy endosperm (Bethke et al., 2000). The second storage protein group is globulin that is mainly stored in the aleurone cells and in the embryo (Gubatz and Shewry, 2011). Both form insoluble aggregations (protein bodies) in the lumen of the rough endoplasmic reticulum (ER). The induction of storage protein synthesis is related to the early storage stage (Bethke et al., 2000).

Storage lipids are found in different classes. In the starchy endosperm, mostly phospholipids associated to starch are found, whereas the aleurone and embryo contain oil (Finnie et al., 2010a). Oil is mostly stored in form of oil bodies that comprise a matrix of triacylglycerols (TAG) surrounded by a phospholipid monolayer, in which specific proteins, the oleosins, are embedded (Barthole et al., 2012). The amount of endospermal phospholipids was correlated with the amylose content; high amylose starches contain more phosphlipids than amylopectin starches (Cochrane, 2000). A steep gradient in the lipid level of the endosperm was detected by (Liu, 2011), with a high amount of fatty acids (FAs) in the aleurone and very low levels in the central

endosperm. Up to now, little is known about the regulation of lipid biosynthesis in the endosperm. Recent descriptions of the lipid biosynthetic pathway in legume is given by Bewley et al. (2013), and for maize by Barthole et al. (2012).

The biosynthesis of storage compounds and the regulation of it are tissue and development specific processes. Thus, the elucidation of spatial of metabolite patterns in the developing grain is of highest interest as this would help to understand the occurring processes. Up to now, the analysis of transcripts on single tissue level using micro-dissected barley grain material provides much information to grain developmental processes (Thiel et al., 2008; Thiel et al., 2009; Thiel et al., 2012). By this, the expression of specific transporters, of enzymes related to storage metabolism, of elements from phytohormone signaling, and PCD related proteins could be observed and integrated into the developmental processes of barley grains. But no information about the final products can be deduced from these data. Therefore, it is necessary to investigate also the developmental and tissue specific composition of the grains. Aspects regarding this issue are introduced within the next section.

1.3.   Resolving the Spatial Distribution Patterns of Metabolites

Metabolites are not directly deduced from the genomic information, but are parts of a complex network including processes of synthesis, processing and degradation. In biological systems an enormous variance of metabolites exists. This concerns their extremely different chemical properties (e.g. hydrophilic and hydrophobic compounds), and the immense differences in their concentrations (Kueger et al., 2012; Heinig et al., 2013). Furthermore, metabolic pathways in plants take place in different organs, tissues, cells and even in specific cellular compartments. The cellular localization of biosynthesis must not display the final localization of the metabolites, but often includes a translocation of intermediates, or of the final products. This could be shown for different secondary metabolites, e.g. for the accumulation patterns of alkaloids in opium poppy or for solanaceae species, outlined in Niemüller et al. (2012). As a consequence, the elucidation of tissue specific metabolite distribution patterns is needed to understand the characteristics and functions of particular plant tissues, and to discover the specificity of a molecular phenotype. In recent studies, the application of novel technologies has been proven to exhibit the potential to unravel such detailed insights into metabolite distributions at a high resolution. Horn et al. (2012b) showed the specific allocations of individual lipids within a cotton seed. In relation to plant defence, differences in glucosinolate distributions according to preferred

places of cotton bollworm attacks within a leaf were exhibited by using mass spectrometric imaging (Shroff et al., 2008). Different methods and techniques are applied in plant biology to elucidate the spatial distributions of metabolites (Sumner et al., 2011). In cell biology staining and hybridization techniques are routinely used for particular compounds or compound classes. The property of many metabolites to absorb light at a specific wavelength is used in confocal laser scanning microscopy. Analytical technologies include all variants of molecular spectroscopy and mass spectrometry, which capacities in terms of resolution, sensitivity and selectivity can be enhanced by a multitude of separation methods, such as gas chromatography or liquid chromatography. Current developments aim at the visualization of metabolite distribution patterns at the tissue, or even at the cellular level by nuclear magnetic resonance spectroscopy (NMR) or mass spectrometric imaging (MSI). Table 1 represents an overview of high resolution techniques for the analysis of metabolite distributions in plants and gives examples for their applications.

Table 1: Methods for studying metabolite distributions in plants at a high spatial resolution.

Three of these techniques can be used for a direct detection of compounds (FRET, MSI and NMR) whereas the other three are connected to extraction procedures in combination with subsequent analysis by means of analytical techniques such as liquid chromatography (LC) and mass spectrometry (MS). Abbreviations are: FRET, fluorescence resonance energy transfer; DESI, desorption electrospray ionization; MALDI, Matrix assisted laser desorption/ionization; NMR, nuclear magnetic resonance. According to Kueger et al. (2012).

Single Cell Level	**Organelle fractionation**	Fractionation of homogenized sample material by centrifugation (e.g. sampling of organelles through a density gradient) followed by extraction procedures.	Klie et al. (2011) Tohge et al. (2011)
	Single cell sampling	Usage of microcapillaries to collect cell sap (mainly from vacuolar cells) that is used for metabolite extractions.	Berit et al. (2010)
	FRET based nano sensors	Genetically encoded molecular nano sensors for analyses of living cells.	Chaudhuri et al. (2011) Chaudhuri et al. (2008)
Tissue Level	**DESI & MALDI MS Imaging**	Detection of a broad range of molecules from tissue or tissue sections. MALDI ionization produces intact molecules.	Shroff et al. (2008) Müller et al. (2011) Horn et al. (2012b)
	NMR	Detection of isotopes. Allows in vivo determination of distributions.	Rolletschek et al. (2004) Rolletschek et al. (2011)
	Micro-dissection	Isolation of single tissues from by a laser beam, followed by extraction procedures and different analytical methods.	Martina et al. (2005)

Matrix assisted laser desorption/ionization MS imaging (MALDI MSI) has recently been applied in plant science. The detection of intact metabolites directly from tissue sections with a high

spatial resolution is the great advantage of this technology. In the case of barley seed development MS based imaging can provide new information of metabolite accumulation patterns that exhibit the specificity of single grain tissues. As mentioned above, the processes occurring during grain filling period are of highest interest in the study of grain development, and tissue specific proceedings suggest a defined spatial pattern of metabolites regarding the underlying functionalities. Thus, MALDI MSI was applied in this work for the investigation of small molecule distribution patterns. It provides a soft ionization technique to measure biomolecules in their intact form. During the last decade the technique was widely applied in medical research and has provided a number of novel clinical markers for better diagnosis or for pharmacological studies (Chaurand et al., 2004; Schwartz et al., 2005; Cornett et al., 2006). But the investigation of plant tissues with MALDI MSI is more recent; overviews are presented in Kaspar et al. (2011) and Matros and Mock (2013). In the field of cereal grains, imaging studies were carried out by Zaima et al. (2010b), who analyzed mature rice grains showing phospholipid distribution patterns, and by Burrell et al. (2007), who analyzed premature wheat grains on the distributions of sucrose and hexose-phosphate. A comprehensive MALDI MSI study on barley grain development offers the opportunity to exhibit new information of spatiotemporal metabolite allocations. For this purpose, special attention has to be paid adapting the method for barley grain material, and for the data analysis that represents an essential challenge integrating the outcomes of complex MSI datasets into the processes of barley grain development.

1.4. Scientific Aims of the Presented Study

In this thesis the characterization of metabolite distribution patterns in developing barley grains was addressed. The major aim was to elucidate those compounds that have an impact on grain developmental processes. Events of endosperm cellularization and grain filling are of outmost biological interest as these processes display a complex network of regulation between two generations (the maternal and the filial plant). Furthermore, these processes determine the final grain composition, and thus, the quality of the grain.

- Tissue specific distribution patterns of small molecules had to be elected for the characteristic stages of grain development: the prestorage stage, the transition stage and the storage stage. Therefore, an untargeted MALDI MSI approach was applied to unravel candidate compounds that are characteristic for particular tissues and/or show developmental

specifications. Data mining using biostatistical tools should exhibit patterns of the datasets as a whole that can be correlated to grain developmental processes.

- Selected candidate compounds that are supposed to have an effect on grain developmental processes should be used for targeted analysis in order to deepen the knowledge regarding their biophysiological context. By combination of metabolite, transcript and protein approaches the source of a specific metabolite accumulation should be investigated.

- Since the knowledge about phytohormone distribution patterns is limited to transcript analyses, the aim was to elucidate phytohormone levels in barley grain dissections of the different developmental stages, as these are essential regulatory compounds of grain development. Furthermore, the interplay of sugar and phytohormone signaling plays crucial roles in the regulation of cell division and grain filling.

2.   Materials and Methods

2.1.   Plant Material

Barley (*Hordeum vulgare* L., cv. Barke) plants were grown in a greenhouse under a 16 h light, 20°C and 8 h dark, 14°C regime. Days after pollination (DAP) were defined by determining the time point of anthesis on spikelets in the centre of a spike, described by (Weschke et al., 2000). For all analyses, kernels from this spike region (about ten kernels per spike) were used. Lemma and palea were directly removed after harvest and the grains were frozen in liquid nitrogen and stored at −80°C until processing. Barley kernels from different developmental stages were taken for MALDI MSI analysis: 3 DAP (prestorage stage), 7 DAP (transition stage), 10 DAP (early storage stage) and 14 DAP (middle storage stage).

2.2.   MALDI MS *Imaging*

A detailed description of MALDI MSI for barley kernels is provided in (Peukert et al., 2012). This technique provides relative abundances of molecules at specific positions in a tissue slice. Figure 4 summarizes the general working steps.
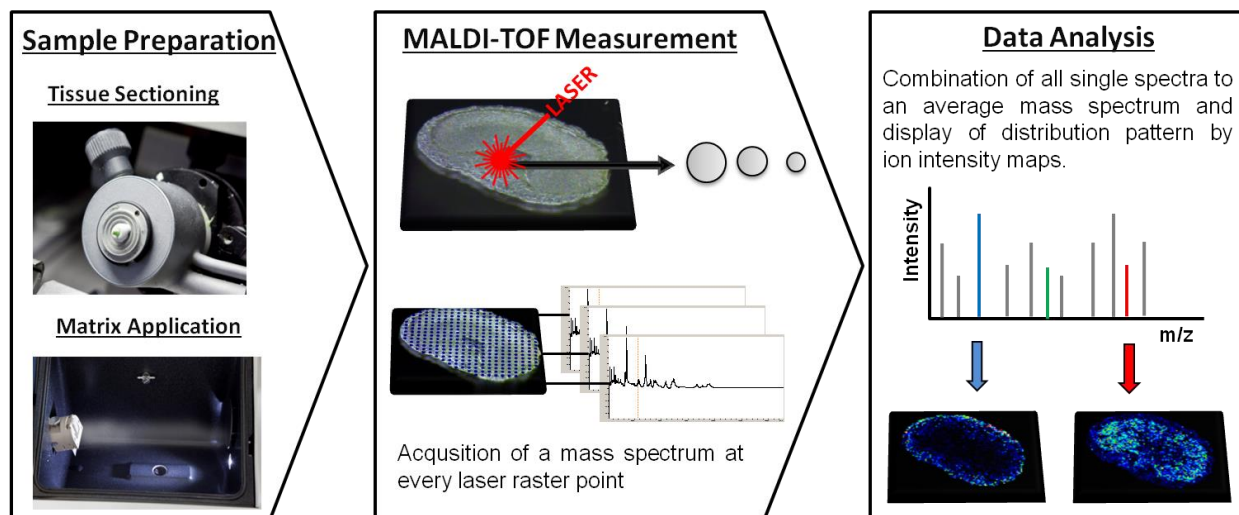
Figure 4: Principle of MALDI MS *Imaging*. Thin tissue sections are covered with a matrix that is needed for the ionization of analytes during the MALDI process. The laser of the instrument rasterizes in a defined pattern over the sample surface. At every laser raster point a single mass spectrum is acquired. At the end of the measurement all single mass spectra are combined to an average mass spectrum that is used for displaying the spatial distributions of selected *m/z* values. The color coded map shows the signal intensity of a molecular ion at every acquired laser raster point.

The sample preparation procedure is critical for the outcome of MALDI MSI and includes sectioning of the sample material and the application of a matrix. The MS instrument creates an

array of mass spectra, where each pixel/spot represents its own *m/z* profile. The gradients of ionic abundances are visualized across the tissue by two-dimensional reconstruction of ion chromatograms. Color coding is usually used to display/simplify the recognition patterns (Gross, 2011).

2.2.1. Tissue sectioning

Frozen grains were fixed at the sample holder of the cryotom (cooled to -20°C) using either optimal cutting temperature compound (O.C.T.) or water (ice) that was preferred for tissue preparations of very small sample material, such as grains from the prestorage stage, to avoid contaminations with the polymeric O.C.T. substance. Longitudinal and cross-sections of 30 µm thickness were cut and immediately thaw mounted onto indium tin oxide (ITO)-coated glass slides (Bruker Daltonics, Bremen, Germany). For complete drying samples were transferred into a desiccator for 30 minutes. Prior to matrix application images were captured with a stereomicroscope (Leica MZ6, Wetzlar, Germany) connected to a digital camera (AxioCam ICc1, Zeiss, Jena, Germany).

2.2.2. Matrix application

2,5-Dihydroxybenzoic acid (DHB) was used as matrix and diluted to 30 mg/ml in 50% (v ⁄v) methanol (MeOH) and 0.2% (w/v) trifluoroacetic acid (TFA). The matrix was applied using the ImagePrep device (Bruker Daltonics) according to the manufacturer's instructions. Spray protocols constitute of several cycles of matrix deposition, incubation and drying, controlled by the optical sensor of the instrument.

2.2.3. MALDI TOF MS measurement

The slides were fixed in a Slide Adapter II MALDI target (Bruker Daltonics) and introduced into the MALDI TOF MS instrument (ultrafleXtreme MALDI TOF/TOF, Bruker Daltonics). Measurements were performed in positive ionization mode with a mass range of *m/z* 80-1300 that covers molecular weights from very small to larch metabolites such as storage lipids or oligosaccharides. The instrument was calibrated with defined mass signals derived from a polyethylene glycol (PEG) mixture (1:1 mixture of PEG200 and 600, diluted 1:300 in 30% v/v acetonitrile and 0.1% w/v TFA), and from the DHB background prior to each imaging run. The monoisotopic masses were determined by the chemical composition of the respective calibrants.

MolE (http://rna-mdb.cas.albany.edu/RNAmods/masspec/mole.htm), an online software tool, was used for the calculations of the respective *m/z* values (Table 2).

Table 2: Calibrants for MALDI MS instrument calibration.

PEG signals were acquired from a 1:1 mixture of PEG200 and PEG600 diluted 1:300 in 30% acetonitrile and 0.1% TFA. Two DHB background signals were also included. the online software tool MolE (http://rna-mdb.cas.albany.edu/RNAmods/masspec/mole.htm) was used for calculation of expected monoisotopic peaks.

Calibrant	Calculated *m/z*	Sum formula	Corresponding ion
DHB_137	137.0233	$C_7H_4O_3$	$[M-H_2O+H]^+$
DHB_273	273.0394	$C_{14}H_8O_6$	$[2M-2H_2O+H]^+$
PEG_217	217.1052	$C_8H_{18}O_5Na$	$[M+Na]^+$
PEG_305	305.1576	$C_{12}H_{26}O_7\ Na$	$[M+Na]^+$
PEG_393	393.2101	$C_{16}H_{34}O_9\ Na$	$[M+Na]^+$
PEG_481	481.2625	$C_{20}H_{42}O_{11}\ Na$	$[M+Na]^+$
PEG_569	569.3149	$C_{24}H_{50}O_{13}\ Na$	$[M+Na]^+$
PEG_657	657.3673	$C_{28}H_{58}O_{15}\ Na$	$[M+Na]^+$
PEG_745	745.4198	$C_{32}H_{66}O_{17}\ Na$	$[M+Na]^+$
PEG_833	833.4722	$C_{36}H_{74}O_{19}\ Na$	$[M+Na]^+$
PEG_922	921.5246	$C_{40}H_{82}O_{21}\ Na$	$[M+Na]^+$
PEG_1010	1009.5770	$C_{44}H_{90}O_{23}\ Na$	$[M+Na]^+$
PEG_1054	1053.6033	$C_{46}H_{94}O_{24}\ Na$	$[M+Na]^+$
PEG_1142	1141.6557	$C_{50}H_{102}O_{26}\ Na$	$[M+Na]^+$

The software tools flexControl v3.3 and flexImaging v.2.1 (Bruker Daltonics) were used for the setup of the measurements. The laser power and lateral resolution were selected according to the needs of each experiment. The laser power had to be adjusted at every MALDI MSI run. The laser width was set to 10 μm, and 1000 shots per raster spot were acquired. The measurement of the laser raster spots was carried out in random order to eliminate influences of measurement order. In MALDI mass spectrometry imaging no separation of compounds or compound classes takes place resulting in a very dense spectrum. To ensure a sufficient mass resolution 20.000 data points per spectrum were chosen (corresponds to a sample of 0.5 Gs/s).

2.2.4. Data analysis

After the MALDI MSI measurement all acquired single spectra were combined to an overall average spectrum in flexImaging software (Bruker Daltonics), and further used for the selection of *m/z* values. The distribution patterns of selected *m/z* values were displayed in form of single or multi ion intensity maps. The interference of matrix derived signals in the spectrum is a major drawback in analysis of metabolites up to *m/z* 500 in MALDI MS. Matrix cluster, the respective adducts with sodium or potassium and fragments produce a dense background. As the matrix is applied in a vast excess compared to the analytes, a reduction of sensitivity or a suppression of

analytes in low mass range is assumed (Fuchs et al., 2010). To exclude matrix derived background signals for data analysis, the average spectrum from a blank region, measured along with the sample, was included in the spectra view. Selection of *m/z* values from the samples had to be manually carried out as current software tools for MALDI MSI data analysis are not capable to exclude default *m/z* values.

Calculation of average peak intensities from selected regions of interest (ROIs) was carried out using ClinProTools (CPT) software v2.2 (Bruker Daltonics). Therefore, grain regions were marked in flexImaging software according to the histological properties of the sections (based on pictures taken previously to the measurement). The spectra belonging to these regions were exported to CPT. As in CPT the calculations are limited in total number of imported spectra, ROIs display not a complete grain part but contained about 200 up to 600 single spectra, each. In CPT candidate peaks were selected and the average intensities for each ROI were determined. Peak intensity lists were prepared containing the data obtained by three independent experiments, and were further used for multivariate statistical analysis. Due to different ionization capacities of molecules during the MALDI process (depending on used matrix, ionization mode, suppression effects or simply applicability of MALDI process itself) and high influence of external circumstances e.g. matrix layer or adjustment of laser intensity, the MALDI MS technique is a semi-quantitative kind of measurement. Signal intensities of detected molecular ions can be compared within one single run but hardly between different sample sets. To compare the distributions of molecular ions from independent experiments total ion intensities of individual *m/z* values were normalized to relative signal intensities that display the contribution to the selected ROIs (sum of signal intensities of an *m/z* over all ROIs = 1, which represents 100%). In this way, the high dynamic range of the signals was excluded, displaying only the participation of a selected molecular ion to a specific ROI. The Neural Gas (NG) algorithm was applied for clustering analysis. This algorithm was introduced Martinetz and Schulten (1991) and is used to find common features in large datasets. It is an alternative to k-means clustering as it constitutes higher robustness. The generated prototypes represent the average of the data within one cluster. The NG clustering was applied for all datasets, respectively, and for a combined analysis of all three replicates for each developmental step. In this way, molecular ions of independent experiments were classified to groups. To proof the NG cluster analysis a k-Means clustering was applied to the datasets of 14 DAP revealing similar results. Cluster analysis was performed in corporation with Prof. Dr. Udo Seiffert (IFF Magdeburg, Germany).

The above mentioned relative signal intensities were also used for the generation of heat maps using Genesis software v1.7.6. (TU Graz, Austria).

2.2.5. Manual measurements of laser capture micro-dissected seed material

The validation of distribution patterns obtained by MALDI MSI was performed using laser capture micro-dissected seed material, described in (Thiel et al., 2008). Therefore, 30 µm thick grain sections, produced as mentioned above by using the cryotom, were thaw mounted onto MembraneSlide 1.0 PET (Zeiss) and transferred into a desiccator for 30 minutes. Laser capture micro-dissection was carried out using a PALM Laser Microbeam instrument (Carl Zeiss Micro-Imaging GmbH, Jena, Germany). The isolated tissues (at least 100.000 μm^2) were extracted using either hexane:isopropanol (1:1, v/v) or 80% (v/v) methanol. About 10 µl solvent were applied to the sample and metabolites were extracted by up and down pipetting. 2 µl of the extracts were directly spotted onto an AnchorChip 800 target plate (Bruker, Bremen, Germany). 1 µl DHB matrix (30 mg/ml in 50% v/v methanol, 0.2% w/v TFA) was added to each sample spot.

Measurements were performed using the MALDI TOF MS instrumentation. Calibration of the instrument was carried out using the PEG200 + 600 mixture (chapter 2.2.3.). Sample spots were manually measured in positive ionization mode. Mass range was set to *m/z* 80-1300. Laser intensity was adjusted according to the requirements of the measurement. The obtained data were analyzed in flexAnalysis software v3.3 (Bruker Daltonics).

2.2.6. Accurate mass measurement

During long MALDI MSI runs small mass shifts can occur. To get accurate *m/z* values manual measurements on hydrophilic and hydrophobic extracts (produced according to the extracts from micro-dissection as mentioned above) were performed, calibrating the MALDI TOF MS instrument every four spots.

2.2.7. MS/MS measurement

To integrate selected *m/z* values into a biological context, the identity of compounds has to be elected. MS/MS measurements by MALDI TOF/TOF were carried out directly on tissue sections in the particular regions. Characteristic fragment ions were used for classification of molecules to their metabolic classes. In addition online database were searched for precursor ion identities. Following databases were used:

- Lipid Mass Spec. Prediction Program v.1.5 (LIPID MAPS, http://www.lipidmaps.org/)

- Metlin, online database (Scripps Center For Metabolomics, http://metlin.scripps.edu/)

- KNApSAcK, online database (http://kanaya.naist.jp/KNApSAcK/)

2.3. Production of Recombinant Proteins and Antibodies

2.3.1. Cloning and expression of ABA-glycosyltransferase UGT71B6

For ABA-glycosyltransferase (UGT71B6) the pUni51 clone U87541 containing a full length cDNA of AT3G21780 was purchased from ABRC (Arabidopsis Biological Resource Center, Columbus, USA). Expression clones were generated using the Gateway™ system (Invitrogen, Life technologies GmbH, Darmstadt, Germany). Cloning procedure and protein expression were performed according to the instructions from the user manual "E. coli Expression System with Gateway® Technology". For amplification and control of transformants the primer combination 5'-CACCATGATCACCTCTCTTACATC-3' and 5'-CTAGCTTTCAGTTTCCGACCAAGC-3' was used. Full length PCR fragments, produced using Pfu polymerase, were eluted from an agarose gel with the PeqGOLD gel extraction kit (Qiagen GmbH, Hilden, Germany) and inserted into the vector pENTR™ TOPO® (Life Technologies). One Shot TOP10 (Life Technologies) competent *E. coli* cells were used to generate the entry clones. For the LR-clonase reaction the expression vector pDEST™17 was used. The destination vector was transformed into One Shot TOP10 competent *E. coli*. For recombinant expression of the protein, BL21-AI™ strains were transformed with plasmid preparations of positive tested clones.

Expression of recombinant proteins was induced using 0.1% L-Arabinose (w/v). Extracted proteins (in 50 mM NaH_2PO_4, 300 mM NaCl, 10% Glycerin (v/v), pH 8) were purified by Ni-NTA agarose (Qiagen) and preparative SDS gel electrophoresis. The corresponding protein band was cut from the gel and electrophoretically eluted using the BioRad Electro Eluter Modell 422 (in 25 mM Tris, 192 mM Glycine, 0.1% w/v SDS).

Identity of the eluted protein was verified by mass spectrometry. Therefore, spots were excised and tryptic digested as described by (Witzel et al., 2007). 0.5 µl of the digest solution were spotted onto a MALDI target (AnchorChip 800 MTP 384, Bruker Daltonics) and covered with 1µl matrix solution (0.7 mg/ml α-cyano-4-hydroxycinnamic acid in 90% v/v acetonitrile, 0.1% w/v TFA, 1 mM $(NH)_4H_2PO_4$). Measurement was performed with the MALDI TOF MS instrument (ultrafleXtreme, Bruker Daltonics). The peptide mass fingerprint (PMF) and corresponding MS/MS spectra were subjected to protein identification using the MASCOT

search engine (Matrix Science, London, UK) in Biotools 3.0 software (Bruker Daltonics) searching in NCBI, v*iridiplantae* index of the nonredundant database.

Antibody production in rabbit was performed by the Phytoantibodies group at the IPK Gatersleben, Germany. The antibody was purified from the obtained serum using HiTrap NHS activated HP sepharose columns (GE Healthcare, Munic, Germany). This procedure was performed according to the recommendations of the vendor.

2.3.2. Expression of fructan metabolizing enzymes

Pichia pastoris expression clones for sucrose:sucrose 1-fructosyltransferase (1-SST), fructan:fructan 1-fructosyltransferase (1-FFT), sucrose:fructan 6-fructosyltransferase (6-SFT), fructosyl 1-exohydrolase (1-FEH) and the *E. coli* strain containing the pPICZαB vector including the cDNA sequence for fructosyl 6-exohydrolase (6-FEH) were provided by Prof. Wim Van den Ende, KU Leuwen, Belgium.

Transformation of the *P. pastoris strain* X33 with the purified and linearized vector DNA, containing the full length cDNA of 6-FEH, was performed by electroporation according to the standard procedures "EasySelect™ Pichia Expression Kit" given by the vendor (Life Technologies). Also, protein expression of all constructs was carried out as recommended in the user manual. Expression was stopped after 72 hours and yeast cells were removed by centrifugation.

Purification for antibody production

For antibody production, excreted proteins were purified from the culture media by precipitation with 9 Volumes ice-cold ethanol. After centrifugation the resulting pellet was dissolved in 20mM potassium acetate buffer, pH 5. The protein extracts were conducted to preparative SDS gel electrophoresis and the corresponding bands were cut and eluted as described under 2.3.1. For the identification by tryptic digest and MS measurement (as described under 2.3.1.) a pretreatment was performed: according to Rademaker et al. (1998), the samples were chemically deglycosylated with 25% NH_4OH. 100 µg of the dried proteins were incubated with 150 µl 25% NH_4OH for eight hours at 45°C. Afterwards the solvent was evaporated and the dry pellets were diluted in 100 µl 1xPBS buffer and precipitated by chloroform/methanol: Samples were mixed in series with 400 µl MeOH, 200 µl $CHCl_3$ and 300 µl H_2O, and incubated for 5 min on ice. For the phase separation, the solutions were centrifuged at 9000*g*, 4°C for 2 min. The upper phase (water) was carefully removed and 300 µl MeOH were added for precipitation. After incubation

for 5 min on ice, samples were centrifuged at $18000g$ and 4°C for 5 min. Protein pellets were finally dried in a vacuum centrifuge and subjected to an in-solution digestion. Proteins were diluted in RapiGest^{TM} SF buffer (0.1% w/v RapiGestTM SF (Waters, Eschborn, Germany) in 20mM ammonium bicarbonate) to a final concentration of 30 µg/µl. Prior to digestion with trypsin the extracts were 10 min held at 80°C, then incubated at 60 °C for 10 min with addition of 2.5 mM final concentration DTT and finally, alkylated with 7.5 mM final concentration iodoacetamide for 30 min at room temperature in the dark. 0.6 µg Trypsin (V511, Promega) were added and the mixture was incubated over night at 37°C. After digestion, RapiGest^{TM} SF was precipitated by adjusting the pH to ~2 with 1N HCl. The resulting pellet was removed by centrifugation for 30 min at $18000g$ and 4 °C.

Identification by MALDI TOF MS was performed as described under 2.3.1.

Native extraction for enzyme assays

Native 1-FEH was taken for enzyme assays. The excreted protein was precipitated from the culture media by stepwise addition of $(NH_4)_2SO_4$ to a final concentration of 80%. The enzyme was pelleted by centrifugation ($14.000g$, 4°C, 1h) and finally dissolved in 50 mM potassium acetate buffer, pH 5. A dialyzation step was included to remove the remaining salt. This was performed by using the "Mini Dialysis Kit, 1 kDa cut-off" according to the instruction from the manufacture (GE Healthcare).

2.4. General Protein Techniques

2.4.1. Extraction of proteins from barley grains

Extraction of proteins from grounded barley grains was performed following the TCA/Acetone method from (Schlesier and Mock, 2006). The material was mixed with ten parts of extraction buffer (10% trichloroacetic acid (TCA), 0.07% (w/v) 2-mercaptoethanol in acetone) and incubated at -20°C for 45 min. The precipitated pellet (by centrifugation for 15 min, 4°C, $36,000g$) was washed using 2-mercaptoethanol in acetone (0.07% w/v) and finally dried in a vacuum centrifuge. For 2-DE the pellet was dissolved for 1 h at 37 °C under shaking conditions in rehydration buffer (8 M urea, 2% w/v 3-[(3-cholamidopropyl) dimethylammonio]-1-propanesulfonate (CHAPS), 0.005% v/v 3,3',5,5'-tetrabromphenolsulfonphthalein, 0.5% immobilized pH-gradient (IPG)-buffer, 20 mM dithiothreitol (DTT)). Solid residues were removed by purification of the solution through an Ultrafree MC Amicon filter (Durapor PVDF

0.45 µm, Millipore, Schwalbach, Germany). By dialysis against 40 times rehydration buffer using the Quant Dialysis Kit (GE Healthcare, Munic, Germany) the contaminating salts and metabolites were removed.

2.4.2.   Determination of protein concentration

Depending on the buffers in which the proteins were dissolved, the determination of protein concentration followed the method of Bradford (Bradford, 1976) or the manufactures' instructions for the 2-D Quant Kit (GE Healthcare, Munic, Germany). The latter one was used in cases the buffer contained CHAPS and DTT.

2.4.3.   2-Dimensional electrophoresis

The isoelectric focusing and subsequent SDS-PAGE followed the method described in Schlesier and Mock (2006). Amount of protein subjected to 2-D separation depended on detection method and size of the gels. For 7 cm IPG strips (pH 4-7, GE Healthcare) 50 µg protein mixture were loaded. Separation was performed using the IPGphor II unit (GE Healthcare) with the following parameters: Rehydration for 14 h, 30 min gradient to 250 V, 30 min gradient to 500 V, 30 min gradient to 3000 V and 4.40 h at 3000 V. Afterwards, IPG-strips were equilibrated for 15 min in buffer 1 (50 mM Tris/HCl pH 8.8, 6 M Urea, 30% v/v Glycerin, 2% w/v SDS, 20 mM DTT, 0.01% w/v bromphenol blue). Finally, strips were placed on top of an 10% w/v SDS polyacrylamid gel, covered with 0.5% w/v agarose and separated using a Mini Protean II Bio-Rad apparatus (Bio-Rad, Munic, Germany) with the following conditions: 30 min at 75 V and 60 min at 150 V. Gels were washed twice for 10 min in water and subjected to visualization.

2.4.4.   Colloidal coomassie brilliant blue staining

Staining of proteins followed the method by (Kang et al., 2002). Gels were incubated for 1h in cCBB staining solution (0.02 % w/v CBB-G250 in 5% w/v aluminium sulfat-(14-18)-hydrate, 10% v/v ethanol and 2% w/v phosphoric acid), followed by 30 min incubation in 10% ethanol and 2% phosphoric acid. Then, gels were washed and kept in water.

2.4.5.   Western blot analysis

Western blot analyses were performed as described in Amme et al. (2005). Proteins separated on 1-D or 2-D SDS-Page were blotted onto polyvinylidene fluoride (PVDF) membrane (Immobilon-FL, pore size 0.45 µm, Millipore, Eschborn, Germany) with a semidry apparatus (Schütt,

Göttingen, Germany). Immunodetection was performed by using respective antisera (anti-ABA-UGT, anti-1-FEH, anti-6-FEH, anti-1-SST, anti-1-FFT and anti-6SFT) and chemiluminescence visualization (infrared fluorescence detection) by using IRDye 800CW Rabbit Anti-HRP (LI-COR Bioscience GmbH, Bad Homburg, Germany).

2.5.   Metabolite Analyses

2.5.1.   Extraction of endospermal cavity sap

Cavity sap was extracted from barley grains 10, 14, 17 and 20 DAP. The frozen seeds were cut in half and the thawing sap was immediately soaked with a micro syringe and placed in 1.5 ml sample tubes on ice. Depending on the developmental stage 1-3 µl of sap per seed could be sampled. The pooled sap was heated to 90°C for 5 minutes to inactivate enzymes and finally dried in a vacuum centrifuge. Samples were stored until usage at -20°C.

2.5.2.   Dissection of seed material

Manual dissection of seed parts was performed from frozen grain material from 7, 10 and 14 DAP. With help of a pre-cooled (in liquid nitrogen) stainless steel plate, scalpel, forceps and a stereomicroscope, six grain parts could be isolated: scar region, embryo, outer pericarp, chlorenchyma layer, endosperm and the "transfer region" (displayed in Figure 43, section 3.4.). According to the needs of the following experiments, dissections from several grains were pooled.

2.5.3.   Enzyme assays

On tissue digestion

Yeast invertase (purchased from Sigma Aldrich) was diluted to 0.9 mg/ml (=37 U/ml) in 20 mM KH_2PO_4 adjusted with K_2HPO_4 to pH 5. 400 µl of this dilution were subjected into the sprayhead of the ImagePrep device (Bruker Daltonics) and applied in 50 cycles onto the tissue sections. Each cycle consists of 1.5 sec spray and 30 sec drying. As a negative control 20 mM KH_2PO_4 adjusted with K_2HPO_4 to pH 5 without enzyme were applied in the same way. Then the slide was incubated above a water bath at 55°C for 1h (to keep a moist atmosphere, but without droplet formation on the slide). Finally, the DHB matrix was applied as stated above (2.2.2.).

To directly compare signal intensities in the MALDI sum spectrum, consecutive slices were used and the treated and control section were simultaneously measured in random order.

In-vitro digestion

Cavity extracts (2.5.1.) were dissolved in 50 mM potassium acetate buffer, pH 5 (about 10 µl of original extract were dissolved in 20 µl final volume). The solution was purified by SPE using TopTip C-18 micro-spin columns (GlySci, Columbia, MD, USA). Samples were applied onto equilibrated tips and eluted with 70 µl 10% MeOH in 50 mM potassium acetate buffer, pH 5. Eluates were dried and prior to digestion assays diluted again in 50 µl 50 mM potassium acetate buffer, pH 5.

Digestions were performed in final volumes of 20µl containing 5µl purified cavity extract, and the respective enzymes: 1-FEH (6 µg/µl, expressed in *P. pastoris,* 2.3.2.), yeast invertase (2 U, purchased from Sigma Aldrich) and α-galactosidase (2 U, purchased from MegaZyme, Gernsheim, Germany). Incubations with invertase and α-galactosidase were performed at 55°C and with 1-FEH at room temperature. As negative controls, incubation mixtures with previously heated enzymes (5 min to 90°C), and without substrate were prepared. Reactions were stopped by heating to 90°C for 5 min.

Prior to MS measurements, samples were again purified with TopTip C-18 micro-spin columns (GlySci), dried in vacuum centrifuge and finally dissolved in 20 µl 70% MeOH. Measurements were carried out by MALDI TOF MS (Bruker Daltonics) and GC-MS (GCT Premier, Waters) analyses.

2.5.4.   Integrated extraction of hydrophilic and hydrophobic compounds

Seed material was extracted twice with 70% MeOH containing ^{13}C glucose standard (added to 1 nmol/2mg FW) with 400 µl/50 mg FW, and then twice with MeOH:CHCl$_3$ (2:1, v/v, 400 µl/50 mg FW). Between each step, the supernatants were collected by centrifugation at 20.000*g*, 4°C for 20 min and combined. For phase separation water was added (300 µl per 800 µl MeOH:CHCl$_3$). After a second centrifugation step (20.000*g*, 4°C for 10 min), the upper phase containing the polar compounds and the lower phase containing the apolar compounds were separated and dried in a vacuum centrifuge.

2.5.5.   Extraction of phytohormones

Extraction of ABA and CK followed a modified protocol from Kojima et al. (2009), adapted by Bernhard Bauer (Molecular Plant Nutrition group, IPK Gatersleben, Germany; personal communication). For dissected seed material 1 ml of 80% (v/v) ice-cold MeOH were applied to 50 mg FW. As internal standard 30 pmol hexadeuterated ABA (D6-ABA) were added to each

sample. All extractions were carried out in two technical replicates and a third replicate was spiked with 50 pmol of a standard phytohormone mixture (containing abscisic acid, abscisic acid glycosyl ester, *trans*-zeatin, *cis*-zeatin, iso-pentenyladenin, dihydrozeatin, *trans*-zeatinribosid, *cis*-zeatinribosid, isopentenyladenosin, dihydrozeatinribosid, salicylic acid, jasmonic acid, indole-3-acetic acid). Extraction was carried out over night at -20°C. After centrifugation (14.000*g*, 15 min, 4°C) a re-extraction for 30 min at -20°C with 400 µl ice-cold 80% (v/v) MeOH was performed. Supernatants were combined and evaporated in a vacuum centrifuge until MeOH was removed. Sample volumes were adjusted to approx. 1ml with 1% acetic acid and subjected to SPE purification. First purification was performed using Oasis HLB columns (Waters, Eschborn, Germany). From eluted extracts (in 90% v/v ACN) the organic part was removed by evaporation and samples were again adjusted to 1ml with 1% acetic acid. For the second purification step Oasis MXC columns (Waters, Eschborn, Germany) were used. The first eluate (with 90% v/v ACN) contained acidic and neutral hormones, the second eluate (5% v/v NH_3(aq) in 60% v/v ACN) contained alkaline phytohormones. Finally, all samples were dried in a vacuum centrifuge.

2.5.6.   Metabolite analysis by GC-MS

The measurement of polar and apolar seed extracts followed the protocol of (Lippmann et al., 2009). Polar seed extracts were modified in a two step process according to (Lisec et al., 2006): At first incubation with 25 µl methoxyamine hydrochloride (20 mg/ml in pyridin) for 2 h at 37 °C, and a following incubation with 25 µl N-Methyl-N-(trimethylsilyl) trifluoroacetamide (MSTFA) containing the alkane retention time standard (C7-C30, 10 µg/µl, Sigma-Aldrich, Munich, Germany) for 30 min at 37°C. For apolar extracts just the derivatization with MSTFA was performed. These steps were carried out automatically using the MultiPurposeSampler (GERSTEL, Mülheim an der Ruhr, Germany) connected to the GC-MS system. This measurement system consists of the gas chromatograph A7890 (Agilent, Böblingen Germany) coupled to a mass spectrometer GCT Premier (Waters). 1 µl of sample were injected in splitless mode at 240°C. The separation was performed using a 30 m Rxi®-5Sil MS column (Restek, Bad Homburg, Germany) with 0.25 mm inner diameter and 0.25 µm film thickness. For the polar and apolar seed extracts the following parameters for separation were used: 3 min at 80 °C, followed by a gradient of 5°C/min to 300°C for 50 min. Data acquisition was done by MassLynx 4.1 software (Waters) with 10 spectra/s in a range of 65-650 m/z in centroid mode and using the dynamic enhancement modus (DRE).

The identification of metabolites was carried out using the NIST 05 library and the Golm Metabolite Database (http://csbdb.mpimp-golm.mpg.de/csbdb/gmd/gmd.html). In addition, the retention time indices (RI), calculated in correlation to the retention times of added alkanes, were used to verify the identified metabolites. In MarkerLynx software v.4.1 (Waters) mass-retention time pairs were calculated with the following settings: time window 7-50 min, mass window 100-650, mass tolerance 0.1 Da. The datasets were taken for principle component analysis (PCA) using the statistical software tool The Unscrambler v.10.2 (CAMO, Oslo, Norway).

2.5.7. Phytohormone analysis by LC-MS

The measurement of phytohormone extracts was performed with a UPLC/MS/MS system (Xevo TQ MS, Waters), following the protocol of Bernhard Bauer (personal communication, Molecular Plant Nutrition group, IPK Gatersleben, Germany). The dried extracts were dissolved in 30% MeOH and 1% acetic acid. 10 µl of sample were injected in full loop modus and loaded onto a ACQUITY UPLC BEH C18 Column (1.7 µm, 2.1 mm x 50 mm, Waters). Separation was performed according to the following linear gradient at 0.4 ml/min: initial flow 90% solvent A (0.1% formic acid in water) and 10% solvent B (0.1% formic acid in MeOH); from 0 min to 2 min to 85% A; from 2 min to 7 min to 1% A; from 7 min to 8 min to 90% A. This was held until 9 min. Column temperature was set to 40°C. General settings for the MS were: Capillary voltage 2.0 kV; Source Temperature 150°C; Desolvation Temperature 650°C. Detection of the individual phytohormones took place in MRM mode with the following transitions for the quantification trace (Table 3).

Table 3: Detected transitions for selected phytohormones as measured by LC-MS/MS (MRM mode).

Compound	Transition
Abscisic acid	263.16 > 153.05
D6-abscisic acid	269.14 > 158.98
Abscisic acid glycosyl ester	425.25 > 263.16
Salicylic acid	136.90 > 64.98
Jasmonic acid	211.06 > 133.08
trans-Zeatin	220.09 > 136.07
cis-Zeatin	220.09 > 136.01
Iso-pentenyladenine	204.03 > 136.07
Dihydrozeatin	222.10 > 136.07
Benzyladenine	226.09 > 90.98
trans-Zeatinribosid	352.21 > 220.16
cis-Zeatinribosid	352.21 > 220.16
Isopentenyladenosin	336.15 > 136.05
Dihydrozeatinribosid	354.22 > 222.12
Benzyladenosin	358.21 > 226.10

Quantification was carried out in MassLynx software v.4.1 (Waters) according to the standard curves obtained from the phytohormone standard mixture that was measured along with the samples, covering the range from 2 nM to 5 μM.

2.5.8. Sugar quantification by LC and electrochemical detection

Quantification of sugars from cavity extracts and kernels were carried out in collaboration with Wim Van den Ende, KU Leuwen, Belgium. Separation and measurement were performed by means of LC and electrochemical detection as described in Van den Ende and Van Laere (1996).

2.6. Quantitative RT-PCR

Gene expression analysis was carried out by Dr. Johannes Thiel (Seed Development group, IPK Gatersleben, Germany) by means of qRT-PCR. Therefore, a cDNA library of micro-dissected barley grain tissues from different developmental stages was used (consisting of 21 different tissues and/or time points, non-published results of Julia Schmeichel, Seed Development group, IPK Gatersleben). Table 4 gives an overview of the selected genes and specific primer sequences.

Table 4: Primer design for qRT-PCR analyses of candidate genes from fructan metabolism based on published cDNA sequences of barley. Barley sequences were selected from public databases.

Gene name	Accession	Protein	Primer combinations
1-SST	AK366020 AK357135 AJ567377	JQ411252	F-ACTTGGTAGTCGTCGGTTAGGC R-ACCGAGCAATCAATCCACAA
1-FFT	AK354338	JQ411253	F-TTCGAACGCACTTCTGCCA R-TTCGCCACATCGGTAGCAT
6-SFT	AK253058	JQ411254	F-AAAGGCTTGTGGTGCACGAGA R-ATGCCATCGTCCTCATTGGAG
1-FEH	AK252358		F-GCAGAGGAGCAATTCGATTTTC R-CCAGGCAATGCTCATGAATG
6-FEH/CWINV2	AJ534444		F-GCCTCGTGAAGGTTTCCAAA R-ACAACGTTTACAGCAGCCGTG
INV	AK367512		F-CCCAATTGTGGCTCAGGTGTA R-TCTTCTGTGCTGTTCTGGCAA
WIRVa	AK372909	JQ411255	F-AGATGGCCTCGACGTCTTAGA R-AAAGCTACCAGTCATCGTCGG
WIRVb	AK374122	JQ411256	F-CATGCCACAAAAAGTCGCA R-GCCCCTGGAAACGTAGAAGTAC

3. Results

The presented work aims at the characterization of metabolite distribution patterns in barley grains to discover substances showing tissue as well as developmental specificity. These compounds represent candidates having an impact on the physiological processes underlying seed development. Main emphasis lies on the exploration of substances influencing the nutrient transport into the endosperm and the endosperm composition.

The following section presents the methodological adaption of the MALDI MSI approach according to the barley grain material and the scientific aims. Then, tissue specific distribution patterns of molecular ions for the four investigated developmental stages of barley grains are described. Further, particular developmentally dependent distribution patterns of ions are presented. Here, next to the results for overall tissues, the focus lies on endosperm related molecular ions. Among them there are several lipids. In the third results section reallocations of oligosaccharides during grain development and related targeted analyses are presented in detail. Finally, distribution patterns of selected phytohormones and apolar metabolites as obtained by means of LC-MS and GC-MS analysis are presented and correlated to the aforementioned results.

3.1. Method Adaption and Validation of MALDI MS *Imaging* Approach to Barley Grains

In order to elucidate the metabolite distribution patterns in barley grains, the working procedures for MALDI MSI had to be adapted to the investigated material and the intended objectives. Optimal conditions for sample preparation and measurement were elected in preceding experiments. The adapted methods were finally validated by independent analytical techniques, and the results are presented in the following subsections.

3.1.1. Sample treatment

Sectioning of barley grains

The temperature of the cryotom chamber and the cutting block was set to –20°C. At lower temperatures (> -30°C) the grain samples tended to become fragile, while turning more flexible at higher temperatures (-10°C).

Prior to sectioning the grains had to be fixed in the desired orientation at the sample holder of the cutting block. For the fixation Optimal Cutting Temperature (O.C.T.) compound was found to be convenient in case of larger samples, e.g. from 7 DAP on (Figure 5). To avoid a contamination of

very small samples (for 2/3 DAP), and of longitudinal sections with this polymeric embedding substance water (ice) was used instead. Furthermore, for the cutting of barley stems, filling the hollow shoot with beaten egg white provides more stabilization.
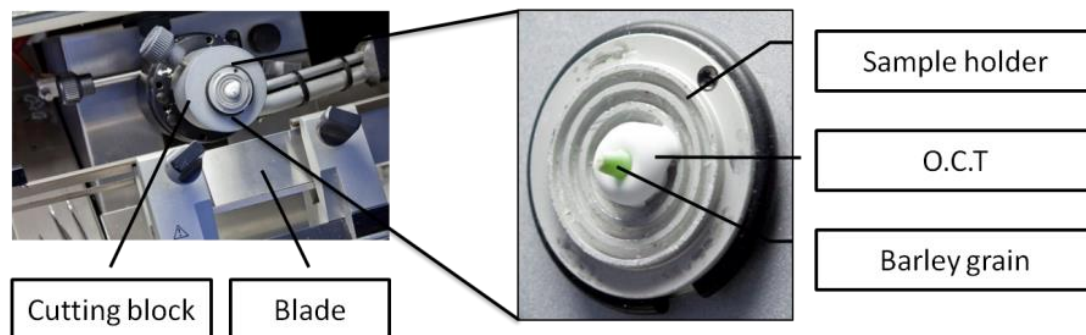
Figure 5: Cutting block of the cryotom chamber with a fixed 7 DAP barley grain.

Optimal Cutting Temperature (O.C.T.) compound is used as fixation medium to stick the kernel onto the sample holder (right). The desired part of the grain is exposed without any embedding material to the blade.

Slices of 10 to 40 µm were prepared from grains of different developmental stages. Young seeds containing higher water to dry matter proportion than grains of the storage phase, when dry matter part rises, allowed cuttings of 20 µm thickness. With the enlargement of the endosperm, the sections became more fragile and slices of 30 and 40 µm gave better cutting results. Prepared sections were thaw-mounted onto indium tin oxide (ITO) coated glass slides for approximately 20 seconds until visual dryness. To ensure complete dryness the slides were dried in a desiccator for 30 minutes. The influence of different slice thicknesses on the quality of the resulting imaging sum mass spectra was proven by simultaneous measurements of 20, 30 and 40 µm thick sections. These sections were successively prepared and placed next to each other on the slide. To avoid an influence of the measurement order, single spectra were acquired randomly from all sections within one imaging run. Exemplarily, extracts from the overlaid average spectra for the three slice thicknesses are shown in Figure 6. Differences in the signal intensity between 20 and 30 µm are marginal, but the comparison to 40 µm revealed a noticeable decrease of the signal intensity. Accordingly, a 30 µm thickness was chosen for all investigated barley developmental stages.
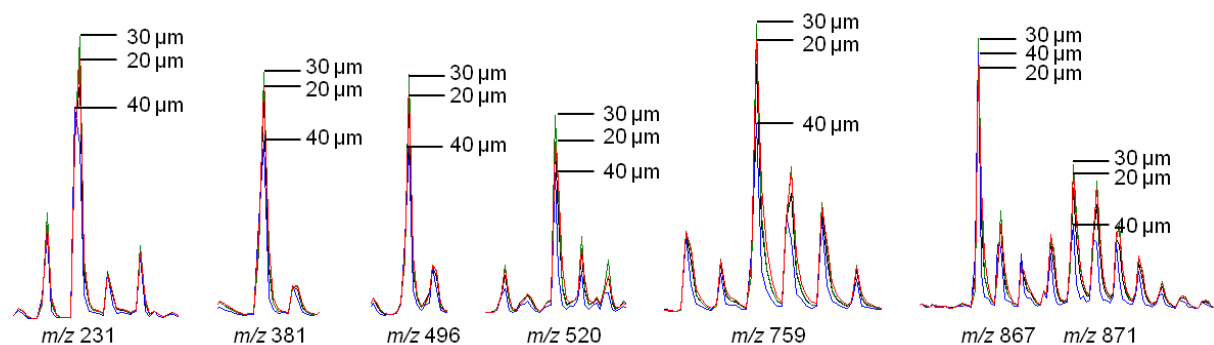
Figure 6: Influence of tissue section thickness on signal intensity in MALDI MSI.

20 µm (red), 30 µm (green) and 40 µm (blue) thick slices were prepared consecutive from a 7 DAP barley grain and measured simultaneously in one imaging run. Movement of the laser was set to random to avoid influences of measurement order.

Choice of a matrix

Generally, in the MALDI process a matrix is needed to facilitate the ionization of substances under investigation. The matrix is applied in a molar excess and co-crystallizes with the compounds. Conventionally used matrices are α-Cyano-4-hydroxycinnamic acid (HCCA), 2,5-dihydroxybenzoic acid (DHB) and sinapinic acid (SA). These are widely used in peptide and protein analyses by MALDI. For the elucidation of a suitable matrix for the metabolite measurements, those as well as some rarely used matrices were tested using polar and apolar seed extracts. Ionization capacities for the extracts and the amount of background signals derived by the matrix itself were critical properties here (every matrix produces its own background spectrum in small molecule mass range due to matrix fragmentation and cluster formation). Additionally, some standard compounds were used for further matrix tests.

For the analysis of the particular background signals the matrices were spotted on a MALDI target plate and measured in positive and negative ionization modes. The results for positive ionization are displayed in Figure 7A. Graphite particles and 1,8-bis(dimethylamino)naphthalene (DMAN) produced the least peaks, contrarily, gold nanoparticle (GNP) and SA spectra were found to be the most complex.

The metabolic seed extracts were spotted on a MALDI target and furnished with the different matrix compounds. Spectra of positive and negative mode were obtained and analyzed in FlexAnalysis software for spectra quality, signal intensity and interference with background spectra derived from the particular matrices (Figure 7B). An overview of the here tested matrices for the referred usage and their obtained suitability in small molecule mass range is provided in Table 5.The best results for ionization capacities of tested extracts were achieved by DHB and

2,5-Dihydroxyacetophenone (DAHP). Thereof, a comparison of matrix derived background signals revealed DHB as the best suited one (Figure 7B). Both matrices produce several intense background signals below *m/z* 400. For DHB a few less intense signals between *m/z* 400-600 and nearly no interfering peaks beyond *m/z* 600 were found. DHAP produces less signals between *m/z* 400 and 500 but numerous and more intense peaks in the range of *m/z* 500-700.
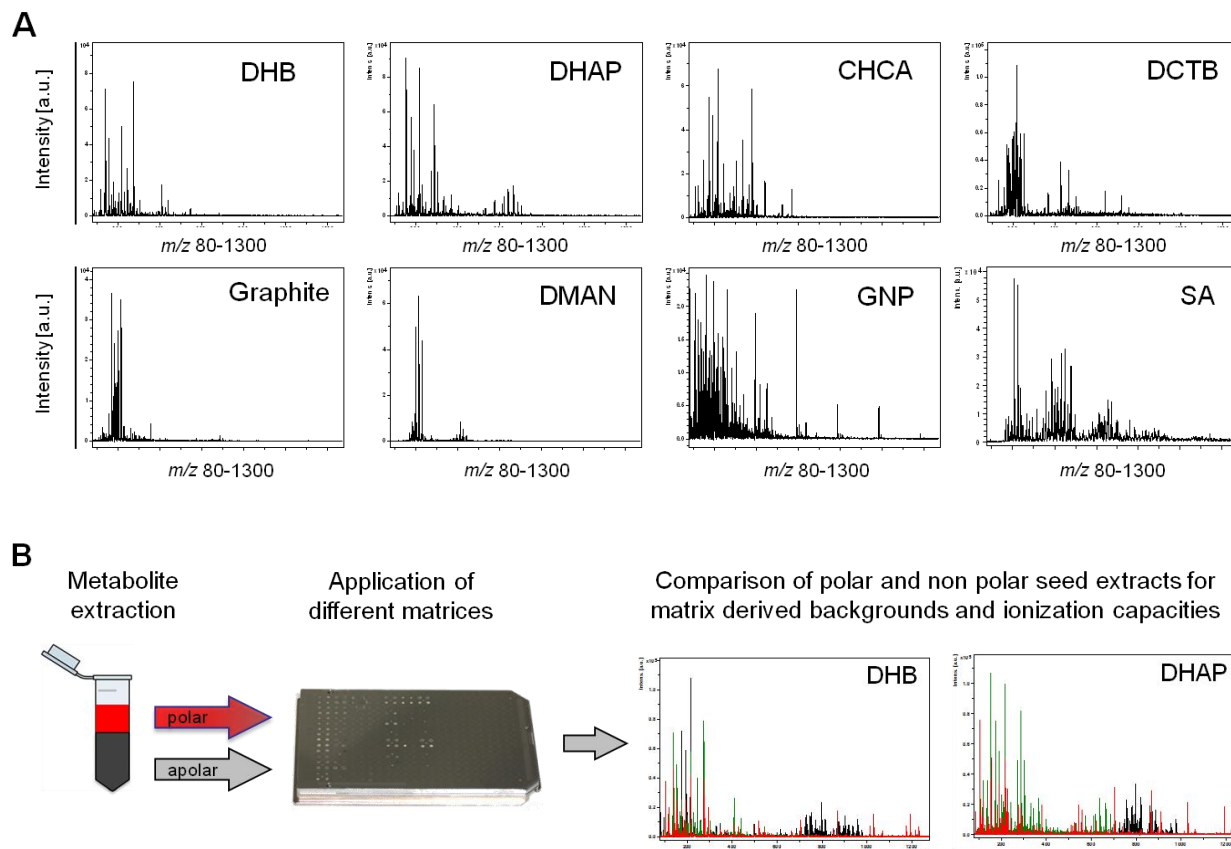
Figure 7: Choice of a suitable matrix for MALDI MSI approach by:

A: Evaluation of matrix-derived signals in low molecular mass range (here shown for the positive mode).

B: Comparison of ionization capacities of polar (red) and apolar (black) seed extracts (here shown for the positive mode). DHB and DHAP are both suited for small molecule mass range but DHAP shows more interfering background signals (displayed in green).

Abbreviations are: DHB, 2,5-dihydroxybenzoic acid; DHAP, 2,5-Dihydroxyacetophenone; CHCA, α-Cyano-4-hydroxycinnamic acid; DCTB, 2-[(2E)-3-(4-tert-butylphenyl)-2-methylprop-2-enylidene]malononitrile; DMAN, 1,8-bis-(dimethylamino)-naphthalene; GNP, gold nanoparticle; SA, sinapinic acid.

Table 5: Applicability of matrices for metabolic barley seed extracts.

Matrices were diluted to recommended concentrations. 0.5 μl of sample extracts were spotted onto a MALDI Anchor800 target plate and furnished with 1μl of the respective matrix. Measurements were carried out in positive and negative ionization mode.

Chemical compound	Acronym	Positive ionization mode	Negative ionization mode	Referred usage	References
α-Cyano-4-hydroxycinnamic acid	CHCA	Polar and apolar extracts	Polar and apolar extracts, less signals compared to positive mode	Peptides	(Zhang and Zenobi, 2004)
2,5-Dihydroxybenzoic acid	DHB	Polar and apolar extracts	Polar and apolar extracts, less signals compared to positive mode	Peptides Lipids	Cohen and Gusev (2002)
Sinapinic acid	SA	Not suited	Not suited	Proteins	Schiller et al. (2004)
1,8-Bis-(dimethylamino)-naphthalene	DMAN	Few signals	Better for polar extracts	Organic acids	Shroff and Svatoš (2009)
2-[(2E)-3-(4-tert-butylphenyl)-2-methylprop-2-enylidene]malononitrile	DCTB	Not suited	Not suited	Polymers	Ulmer et al. (2000)
2,5-Dihydroxyacetophenone	DAHP	Polar and apolar extracts	Better for apolar extracts	Peptides, glycoproteins	Wenzel et al. (2006)
Gold nanoparticle	GNP	Polar and apolar extracts	Not suited	Lipids	Spencer et al. (2008)
Graphite		Few signals	Better for apolar extracts	Lipids, organic acids	Cha and Yeung (2007)

Some standard compounds of differing metabolite classes where additionally tested for their ionization behavior in the MALDI process (Table 6). In positive ionization mode protonated ions $[M+H]^+$ as well as adducts of sodium $[M+Na]^+$ and potassium $[M+K]^+$ were observed. In some cases also water loss combined with protonation $[M-H_2O+H]^+$ was found. Organic acids showed typically better ionization in negative mode. For unsaturated fatty acids and sterols the DHAP matrix was found to be more applicable then DHB (Table 7).

Table 6: Ionization performance of standard compounds during MALDI MS measurement using DHB matrix.

All compounds were diluted in 80% methanol to mM concentrations. 0.5 µl of standards were spotted onto a MALDI Anchor800 target plate and furnished with 1µl DHB matrix (30 mg/ml in 50% methanol and 0.2% TFA). Measurements were carried out in positive and negative ionization mode.

Compound class	Compound	MW [g mol^{-1}]	Sum formula	Obtained m/z (integer)		Corresponding ion(s)
				positive	**negative**	
Favonoids	Kaempferol	286.04	$C_{15}H_{10}O_6$	287, 309	285	[M+H]$^+$, [M+Na]$^+$, [M-H]$^-$
	Rutin	610.15	$C_{27}H_{30}O_{16}$	633	609	[M+Na]$^+$, [M-H]$^-$
	Quercitrin	448.1	$C_{21}H_{20}O_{11}$	471	447	[M+Na]$^+$, [M-H]$^-$
	Kaempferol-3-Rutinosid	594.52	$C_{27}H_{30}O_{15}$	617	593	[M+Na]$^+$, [M-H]$^-$
	Sacuranetin	286.27	$C_{16}H_{14}O_5$	287, 309		[M+H]$^+$, [M+Na]$^+$
	Kaempferol-3-Glucosid	448.37	$C_{21}H_{20}O_{11}$	471	447	[M+Na]$^+$, [M-H]$^-$
Phenols	Aesculetin	178.02	$C_9H_6O_4$	179, 201	177	[M+H]$^+$, [M+Na]$^+$, [M-H]$^-$
	Scopoletin	192.04	$C_{10}H_8O_4$	193		[M+H]$^+$
	Ferulate	194.18	$C_{10}H_{10}O_4$	194,195, 217, 233		[M]*, [M+H]$^+$, [M+Na]$^+$, [M+K]$^+$
Organic acids	Malate	134.09	$C_4H_6O_5$		133	[M-H]$^-$
	Ascorbate	176.02	$C_6H_8O_6$		175	[M-H]$^-$
	Caffeic acid	180.16	$C_9H_8O_4$	181, 203	179	[M+H]$^+$, [M+Na]$^+$, [M-H]$^-$
Sugars	Raffinose	504.46	$C_{18}H_{32}O_{16}$	527, 543		[M+Na]$^+$, [M+K]$^+$
	Glucose	180.16	$C_6H_{12}O_6$	203, 219		[M+Na]$^+$, [M+K]$^+$
	Fructose	180.16	$C_6H_{12}O_6$	203, 219		[M+Na]$^+$, [M+K]$^+$
	Sucrose	342.3	$C_{12}H_{22}O_{11}$	365, 381		[M+Na]$^+$, [M+K]$^+$
	Maltose	342.3	$C_{12}H_{22}O_{11}$	365, 381		[M+Na]$^+$, [M+K]$^+$
Peptides	Glutathion ox	612.63	$C_{20}H_{32}N_6O_{12}S_2$	613, 635		[M+H]$^+$, [M+Na]$^+$
	Glutathion red	307.33	$C_{10}H_{17}N_3O_6S$	308, 330		[M+H]$^+$, [M+Na]$^+$
Lipids	α-Tocopherol	430.71	$C_{29}H_{50}O_2$	431	429	[M]*, [M+H]$^-$
	Sterylglucoside	576.85	$C_{35}H_{60}O_6$	600		[M+Na]$^+$

Table 7: Standard compounds with better ionization capacities using DHAP matrix for MALDI MS measurement.

Compounds were diluted in 80% methanol to mM concentrations. 0.5 µl of standards were spotted on a MALDI Anchor800 target plate and furnished with 1µl DAHP matrix (15 mg/ml in 75% ethanol and 0.2% TFA). Measurements were carried out in positive and negative ionization mode.

Compound class	Compound	MW [g mol-1]	Sum formula	Obtained m/z (integer)		Corresponding ion(s)
				positive	**negative**	
Sterols	Sitosterol	414.71	$C_{29}H_{50}O$	397		$[M-H_2O+H]^+$
	Cycloartenol	426.72	$C_{30}H_{50}O$	409		$[M-H_2O+H]^+$
Lipids	C18:2 Linoleic acid	280.45	$C_{18}H_{32}O_2$		279	$[M-H]^-$
	C18:1 Oleic acid	282.46	$C_{18}H_{34}O_2$		281	$[M-H]^-$

Mass spectrometric imaging of small molecules implicates a prevention of compound delocalization during the sample preparation process. Therefore, washing steps as recommended for imaging analysis of proteins are not allowed. Furthermore, the way of matrix application has to keep the localization of molecules, while allowing their effective extraction into the matrix layer (scheme shown in Figure 8). Spray application by vibrational vaporization admits small droplet sizes that are necessary for a high spatial resolution but that are large enough for a sufficient extraction into the crystallizing matrix.
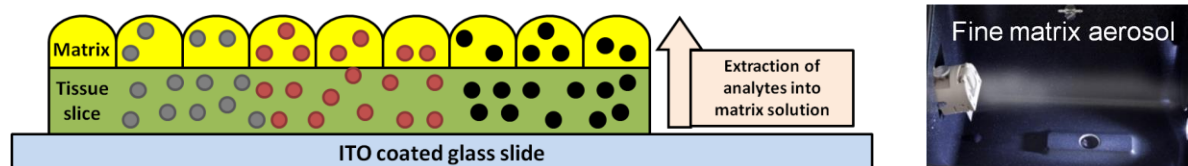
Figure 8: Principle of matrix application in MALDI MSI.

Left: Analytes from the tissue section must be extracted into small matrix droplets where they co-crystallize, which is necessary for ion formation during laser ablation.

Right: Nebulizing spray of the ImagePrep device (Bruker). Matrix is applied by vibrational vaporization through a fine metal sheet resulting in an aerosol that homogeneously lays down onto the sample slide.

3.1.2. Measurement conditions

Generating a dataset for different barley grain developmental stages implies largely varying sample sizes, from ca 1.5 mm^2 for smallest prepared sections to large slices of >1 cm length and > 5 mm width. In addition, tissue differentiation increases during grain development generating the need for high spatial resolution to keep tissue-specific information. Thus, laser spot size was set to 35 µm for larger samples and to 15-20 µm for small samples, which corresponds to ca

15.000 single mass spectra per slide, respectively. This compromise was necessary due to pollution of the source resulting in less signal intensities, when > ca 15.000 single spectra per slide were acquired. In all cases spot to spot measurement was randomized to avoid positional influences of spectra quality from source pollution.

3.1.3. Data validation

3.1.3.1. Selection of individual *m/z* values

Matrix derived signals interfere with sample signals in the mass spectrum (especially in the range *m/z* 100-500). Figure 9 exemplarily shows two signals from an MSI run of a 7 DAP longitudinal section. The peak at *m/z* 273 overlaps with the DHB background signal $[2M\text{-}2H_2O\text{+}H]^+$ and was excluded from further analysis. Contrary, at *m/z* 275 a sample signal was observed partially overlapping with the third DHB isotope, but clearly discernible due to the DHB isotopic pattern. Thus, the individual *m/z* signals from all MALDI MSI runs were selected manually by overlaying the average spectra from the blank region and from the sample.
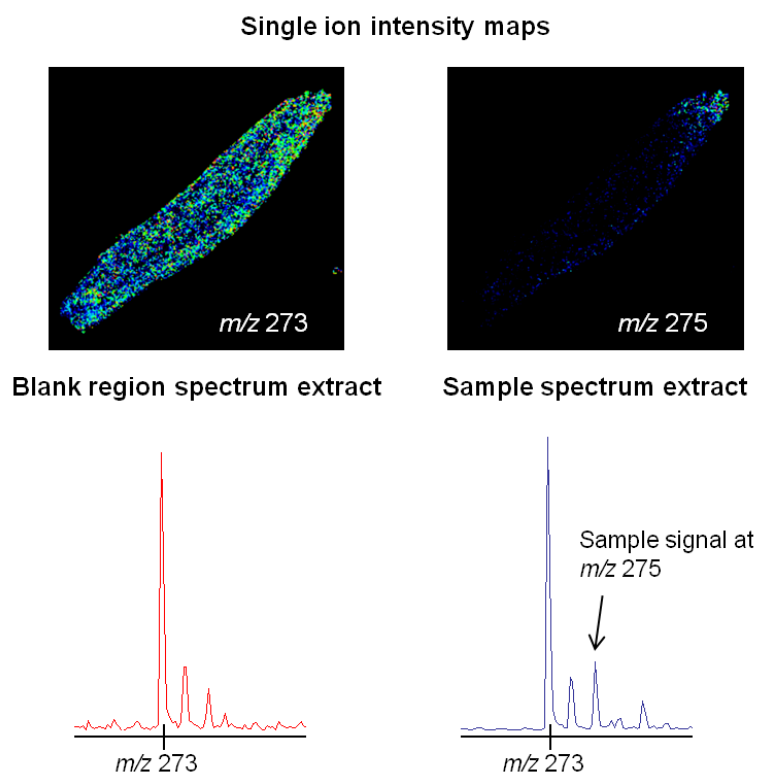
Figure 9: Illustration of DHB matrix interference with sample derived signals on a 7 DAP longitudinal section.

Matrix background signal *m/z* 273 is homogeneously distributed over the sample surface. A sample signal of *m/z* 275 overlaps with the third isotope of the matrix signal but is distributed in the scar region of the section.

3.1.3.2. Validation of distribution patterns

The influence of the different tissue types present in a barley grain on the ionization capacities has not been known. Thus a punctual validation of the obtained metabolite distribution patterns has been performed.

Validation of distribution pattern by measurements of cross sections from different grain parts

MALDI MSI analyses were also carried out on cross sections of the different grain parts for each individual developmental stage. The data were compared to specific abundances of molecular ions in the longitudinal sections. Figure 10 exemplarily shows the tissue specific distributions of molecular ions as revealed by imaging measurements of longitudinal and cross sections from 7 and 14 DAP barley grains. For both developmental stages, the tissue specificity could be confirmed.
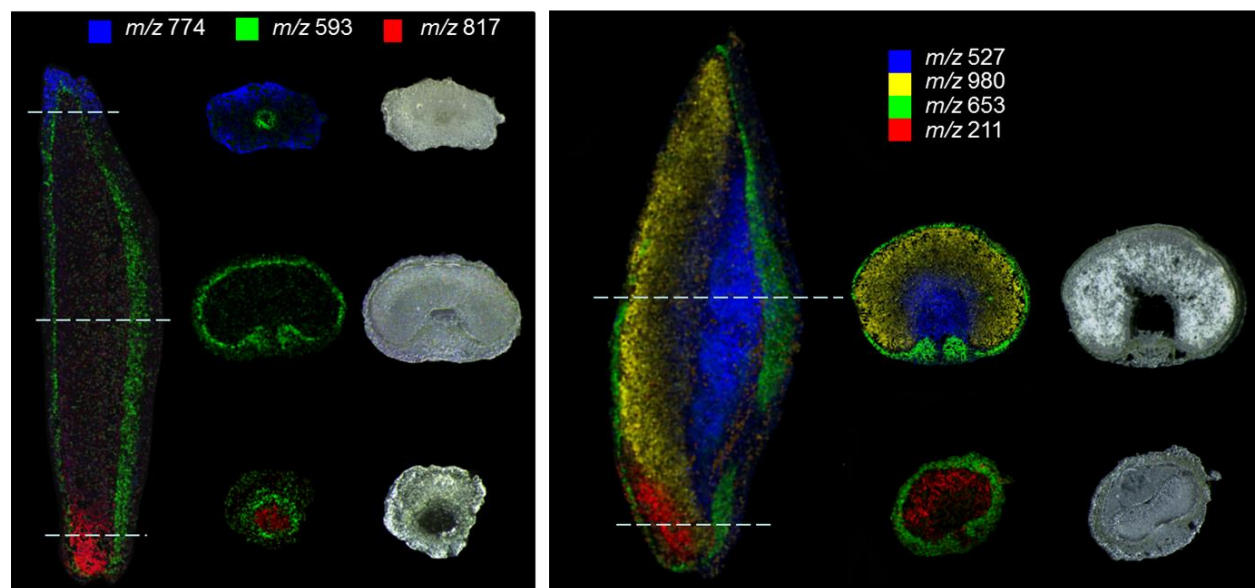
Figure 10: Validation of distribution patterns in longitudinal sections by comparison to cross sections.

Analytes were found to show the same distributions in cross sections as revealed by MALDI MSI of longitudinal sections. Measurements were carried out from 30 µm tissue sections coated with DHB matrix as described in section 2.2.

A: Grains from 7 DAP with tissue specific abundances of *m/z* 593, 774 and 817.

B: Grains from 14 DAP with tissues specific distributions of *m/z* 211, 527, 653 and 980.
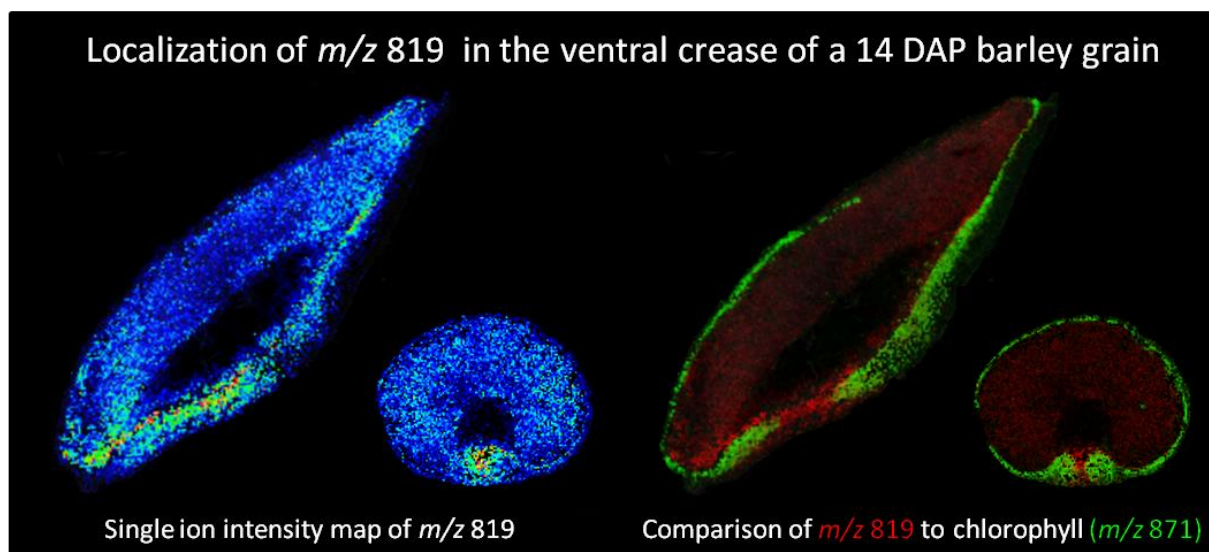
Figure 11: Assignment of particular *m/z* values to distinct tissues by comparison of MSI measurements from cross and longitudinal barley grain sections.

Specific allocation of *m/z* 819 in the ventral crease has been observed by analyses of 14 DAP cross sections. A comparison to the chlorophyll distribution revealed the highest abundance of the signal between the bulbs of the chlorenchyma layer.

Furthermore, the MSI analyses of cross sections from the grain middle part revealed more detailed information of specific molecular ion distributions as particular grain tissues are better resolved; e.g. specific distributions in the ventral crease can be easier localized and differentiated from the chlorenchyma bundles as shown in Figure 11. (The corresponding histological image of the cross section is represented in Figure 21).

Validation of molecular ion identities by MS analysis of laser micro-dissected (LMD) tissues

To confirm the MSI derived identities, and the localization of molecular ions, extracts of different laser micro-dissected tissues (pericarp, endosperm and chlorenchyma layer) from 7 DAP barley grains were analyzed for the abundance of specific signals. Therefore, 30µm thick slices were transferred onto glass slides and applied to LMD (Figure 12A). At least 100.000 µm^2 were cut for the extraction with hexane or methanol (80%), respectively (described in materials and methods 2.2.5.). Mass spectra were manually acquired from those extracts. The comparison of these MALDI spectra revealed tissue specific molecular ion patterns as presented in Figure 12C. Discriminative molecular ions have been detected with the same tissue specific patterns by MALDI MSI (shown for three examples in Figure 12B), thus, confirming the applicability of MALDI MSI technique for small molecule distribution analysis in these plant tissues.
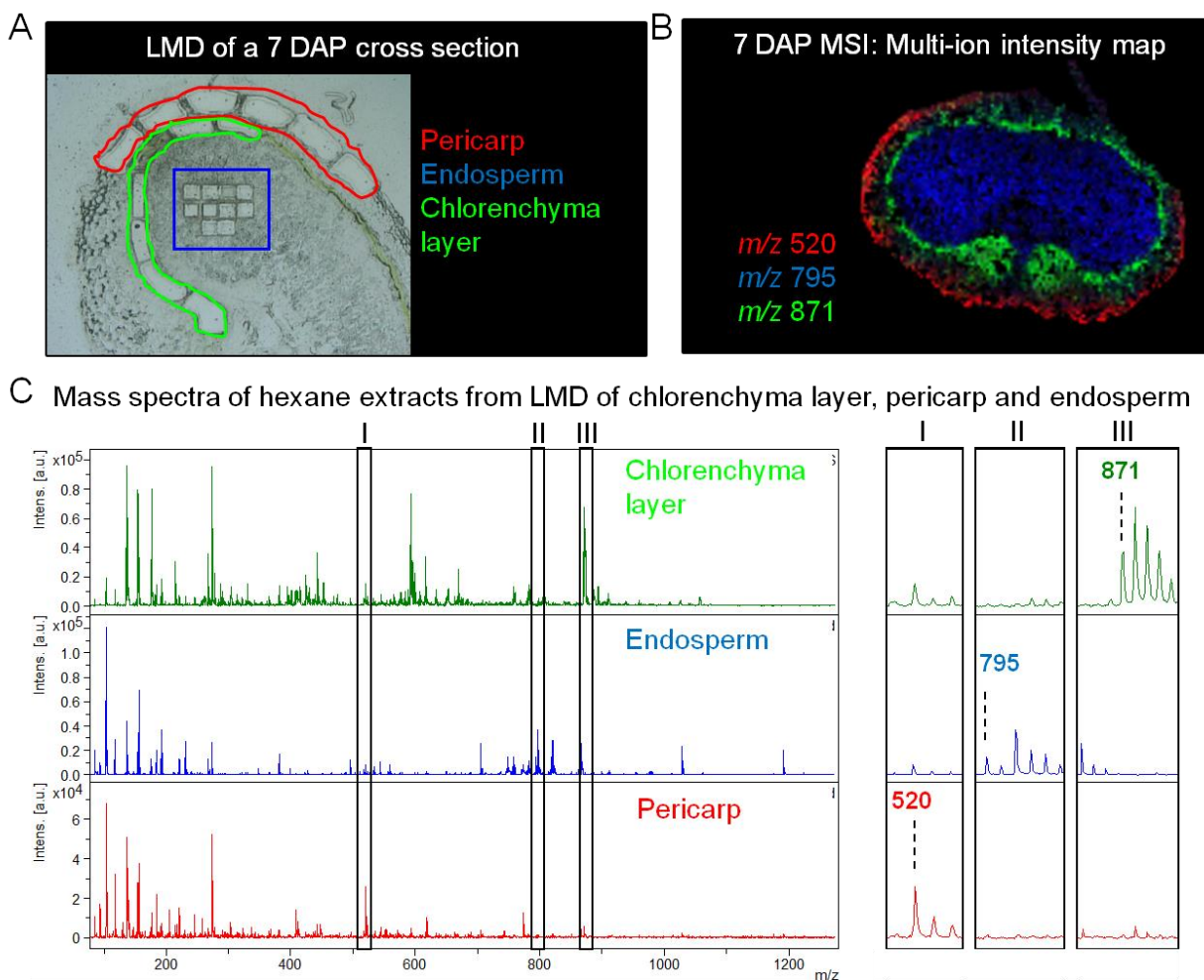
Figure 12: Validation of MALDI MSI distribution patterns by laser-capture micro dissection (LMD).

A) The picture partly shows a 7 DAP cross section with the dissected regions surrounded by colored lines (red – pericarp, green – chlorenchyma layer, blue – endosperm).

B) Multiple ion intensity map from a MALDI MSI measurement of a 7 DAP cross section illustrating the distributions of three designated molecular ions.

C) MALDI spectra of manual measurements from hexane extracts of micro dissected seed material corresponding to 12A. Enlargement shows those *m/z* values specific for the respective regions and displayed in the multi ion intensity map in 8b.

3.1.4. Summary section 3.1.

Up to now, MALDI MSI was rarely used for the investigation of plant material and in small molecule mass range. Thus, the sample preparation procedure had to be adapted to the barley grain material. Additionally, the influence of the various tissue types existing in a barley grain on the mass spectra signal patterns had to be tested. The applied method was validated and found to be suitable for a high resolution MSI analysis of metabolite distributions in barley grains from different developmental stages. Only laser capture micro dissection (LMD) is able to achieve

similar spatial resolutions but comprises a high practical and time consuming effort. Figure 13 demonstrates the working steps of the MALDI MSI approach applied for the study of grain development presented in this thesis. Experiments were carried out in triplicates for the validation of peak selection. Only those peaks detected in all three independent experiments were used for further statistical analyses.

Sample Treatment

Tissue sectioning
- Cryotom: -20°C
- Fixation: O.C.T., water, egg white
- Slice thickness: 30 µm
- Desiccator: 30 min

Matrix application
- Matrix: DHB
- Application: Oscillating spray device

Measurement

Instrument parameter
- *m/z* range: 80-1300
- 20.000 points/spectrum
- Instrument calibration: PEG 200+600
- Positive ionization mode

Imaging conditions
- 15-35 µm lateral resolution
- Randomized spot measurement

Data Analysis

Peak selection
- Comparison with matrix background
- Reproducibility

Identification
- MALDI MS/MS measurements
- Targeted LC-MS measurements of metabolic extracts
- Comparison to online databases
- Comparison to literature

Statistical analyses
- Neural gas clustering

Figure 13: Schematic representation of the experimental setup for MALDI MS *imaging* analysis of barley grain development.

Working steps and instrumental setup were applied for all investigated developmental stages and grain regions. Targeted analysis related to further identification and quantification was carried out for candidate compounds obtained by MALDI MSI approach. Multivariate statistics were applied for complete data sets comprising all detected molecular ions within three replicates.

3.2. Spatially and Developmentally Dependent Distributions of Small Molecules in Barley Grains

The major aim was to resolve the distribution patterns of small molecules during the characteristic stages of grain development, namely: prestorage stage, transition stage and storage stage. Therefore, the MALDI MSI approach as approved in preliminary experiments (section 3.1.) was applied. The total dataset comprises measurements of longitudinal and cross sections for each developmental stage. The statistical data analysis and the examination of developmental differences were carried out on measurements of longitudinal sections; measurements of cross sections were taken for the validation of obtained distribution patterns. An overview representing the sample material used, and the corresponding tissue slices from the particular regions of a 14 DAP barley grain is given in Figure 14. The MSI measurements were analyzed in a tissue specific manner for each individual time point (section 3.2.1.). Development depending changes of molecular ions were analyzed from total grain sections (section 3.2.2.), and for endosperm specific distributions (section 3.2.3.). Tentative identification of revealed *m/z* values indicated polar lipids as a major metabolite group, detected by the used protocol for MSI. The results for the identification are presented in section 3.2.4. The complete peak lists for all investigated stages contain the *m/z* values detected in all three replicates (Please refer to Appendix 1-4).
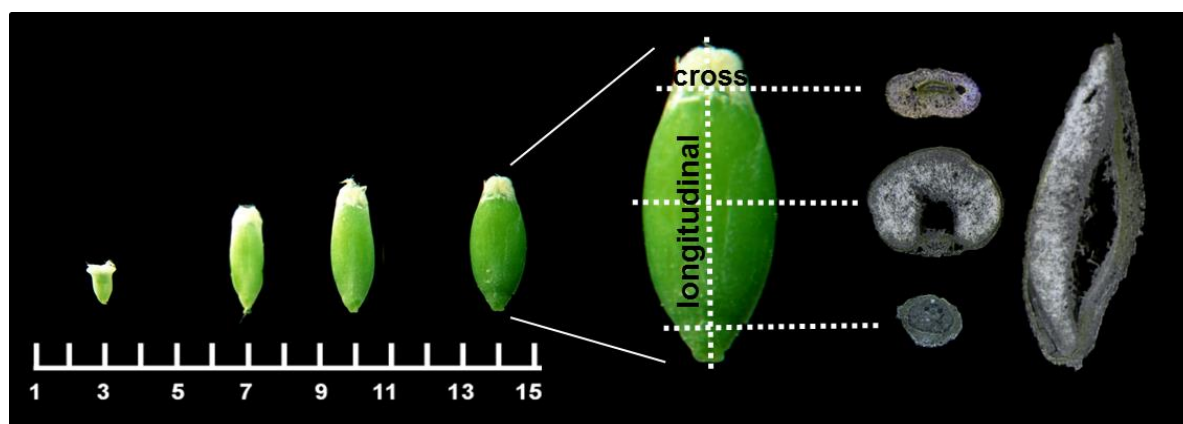
Figure 14: Sample set up for investigation of barley grain development.

For prestorage phase 2 and 3 DAP grains were used. 7 DAP represents the transition phase, when development switches from mainly cellularization to storage product accumulation in storage phase. This stage is represented by measurements from ten and 14 DAP old grains. From grains of 7, ten and 14 DAP cross sections from scar region, middle part and embryo region were prepared. For 3 DAP cross sections from scar region and near the basis were prepared. From all designated developmental steps longitudinal sections were prepared and taken for development specific analyses.

3.2.1. Tissue-specific distribution patterns of small molecules

Massive changes of the tissue constitution occur in a developing barley grain. Emergence and programmed cell death (PCD) of tissues take place in parallel at each stage. The maternal pericarp surrounding the filial part diminishes, whereas the starchy endosperm, the endospermal transfer cells (ETC), the nucellar projection (NP) develop, but later undergo PCD as well. Just the embryo and the aleurone layer persist until germination. Accordingly, specific regions of interest (ROIs) were selected for each individual stage for multivariate statistical analysis.

3.2.1.1. Distributions of molecular ions during the prestorage phase

The prestorage phase in barley describes seeds between pollination (0 DAP) and transition stage (7/8 DAP). Here, seed material of 2 to 3 DAP was used for MALDI MSI measurements. From a histological view the predominant part of the seed material is the pericarp. A thin green layer around the embryo sac is discernible. At this point of development the embryo sac is a fluidic filled cavity with beginning cellularization from the periphery (Figure 15). For data analysis five ROIs were selected, three of them represent different regions of the maternal pericarp in the longitudinal axis. One region denotes the green chlorenchyma layer and another one the embryo sac with the cellularized part.
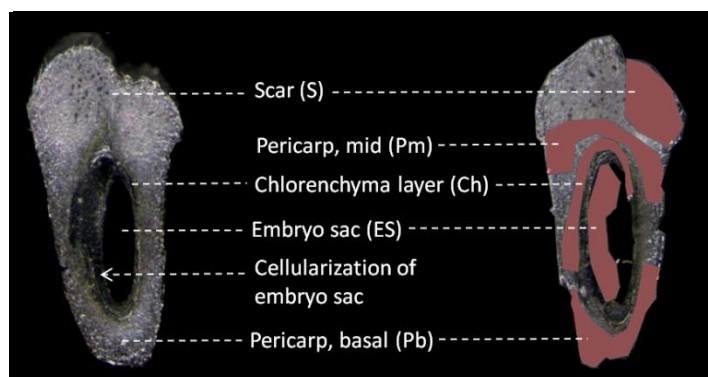
Figure 15: Longitudinal 30 μm thick cryo-sections of 3 DAP barley grain.

Right, the ROIs selected for statistical analysis are indicated. At this stage most of the grain belongs to the maternal part, surrounding the filial embryo sac.

Analyses of three replicates revealed 140 molecular ions taken into account for multivariate statistics (a complete table containing the selected molecular ions and average peak intensities is given in Appendix 1). Due to the prior observations of MALDI MSI data sets for the prestorage stage the NG cluster algorithm was initially set to three forming clusters. In Figure 16 prototypes

of the resulting clusters are given for all individual experiments (upper part), and for the combined analysis (lower part). The prototypes represent the typical profiles of the mean normalized peak intensities across the selected grain parts. The separate analysis shows that experiment two and three constitute nearly the same prototype pattern, whereas in experiment one the second cluster differs. In all three replicates the first cluster is dominated by molecular ions showing highest mean normalized peak intensities in the chlorenchyma layer. The shape of this prototype clearly reflects the high specificity of molecular ions assigned to it. The second cluster in experiment two and three accentuates the embryo sac; in experiment one a mixed pattern was observed. The third cluster slightly accentuates the maternal pericarp parts. These patterns were also observed by combined NG clustering. Distinguished grain parts and the general functionalities of those are indicated in Figure 16, lower part. The combined prototype of cluster two reflects the *m/z* values showing higher abundances in the embryo sac. Distributions in the maternal pericarp parts are less accentuated as it is reflected by the third cluster of the combined NG clustering.

Table 8 shows the numbers of molecular ions assigned to the particular clusters arisen from the individual experiments, and from the common subset. From this data 39 molecular ions were found to show different patterns within the three replicates. The classification of all *m/z* values to the respective clusters is given in Table 9.
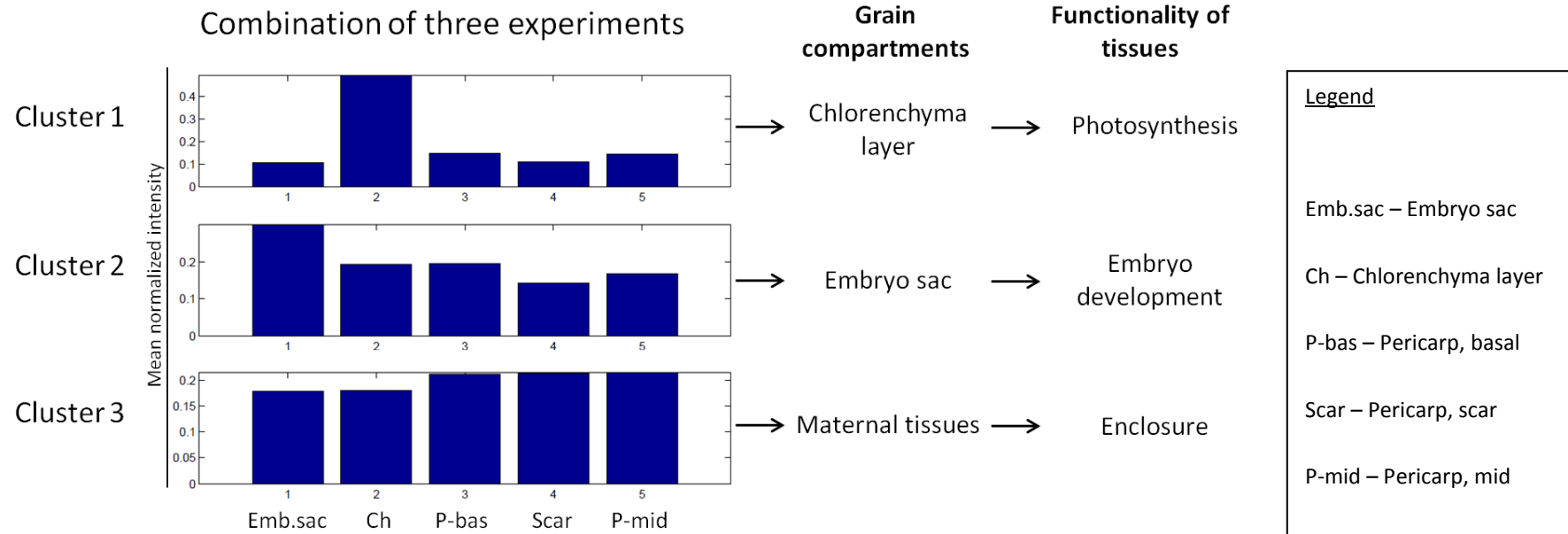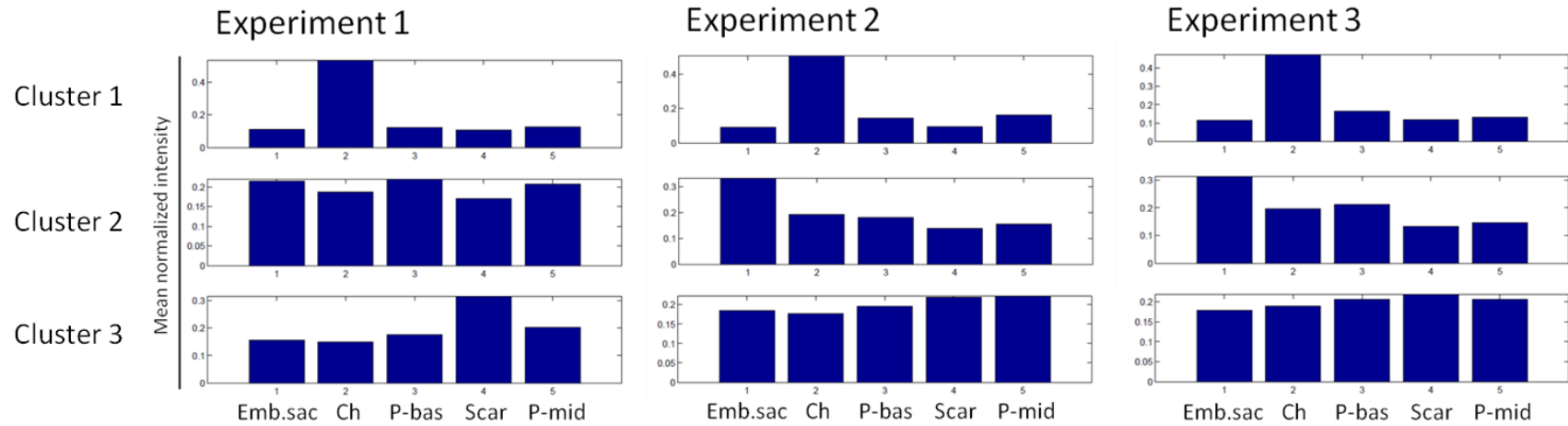
(Description next page)

Figure 16: Results of the Neural Gas (NG) cluster analysis out of MSI datasets from barley grains during the prestorage phase.

Upper part: NG clustering of three individual experiments.

Lower part: Combined NG clustering of three replicates. Grain parts that are accentuated in the respective clusters are indicated, and general functionalities of involved tissues are given.

Table 8: Numbers of assigned *m/z* values per cluster for the individual experiments and for the common subset as revealed by the combined cluster analyses of three independent MSI measurements of 3 DAP barley grains.

	Numbers of *m/z* in each cluster			Common subset
	Experiment 1	**Experiment 2**	**Experiment 3**	
Cluster 1	6	10	7	6
Cluster 2	31	51	32	24
Cluster 3	103	79	101	71
Sum	140	140	140	101

Table 9: Assignment of the individual *m/z* values from the common subset of 3 DAP barley grain MSI experiments to the particular clusters as revealed by NG cluster analysis.

Molecular ions that were not designated to the same cluster by all three experiments are indicated as different pattern. *M/z* values are displayed as integer numbers, except those, that share the same integer.

Group	Obtained *m/z* in integer numbers
Cluster 1	592, 653, 871, 885, 910, 924
Cluster 2	90, 116, 147, 148, 205, 460, 616, 651, 757, 761, 779, 781, 783, 785, 787, 795, 799, 801, 808,817, 819, 821, 823, 825
Cluster 3	94, 118, 140, 152, 156, 158, 166, 192, 193, 195, 221, 233, 254, 258, 284, 293, 294, 296, 319, 337, 350, 358, 380, 399, 412, 419, 448, 466, 479, 481, 489, 511, 520, 543, 558, 560, 576, 577, 580, 604, 615, 646, 664, 684, 689, 705, 712, 738, 744, 749, 773.4, 851, 867, 900, 918, 951, 954, 956, 969, 978, 982, 1007, 1010, 1013, 1029, 1062, 1174, 1176, 1191, 1224, 1273
Different Pattern	86, 104, 130, 136, 164, 184, 222, 230, 231, 240, 241, 246, 292, 308, 381, 423, 496, 518, 574, 597, 600, 602, 618, 747, 749, 755, 759, 773.0, 797, 805, 814, 815, 840, 976, 1009, 1081, 1111, 1213, 1243

Figure 17 shows examples for abundances of single molecular ions according to the results from the combined NG cluster analysis. The heat maps display the percentage abundance of ions in the selected ROIs. For cluster one and two the patterns of the respective prototypes are recognizable as displayed by the individual *m/z* values in the heat maps. Additionally, it is remarkable that characteristic abundances of molecular ions in the embryo sac are mainly connected to the periphery, where cellularization starts. The third cluster contains *m/z* values showing a high specificity for the scar region, and those values that are more co-localized, or show just slight increases of the signal intensity in the maternal parts.
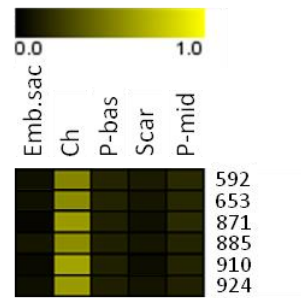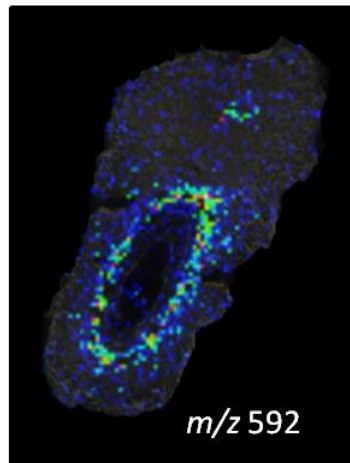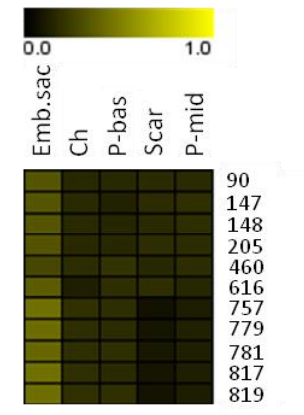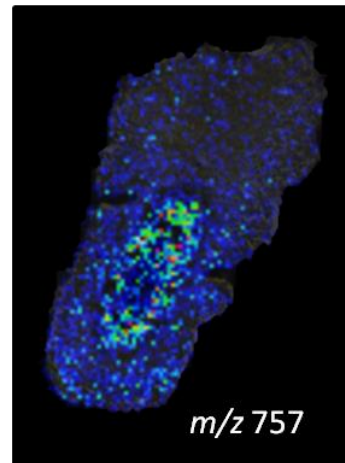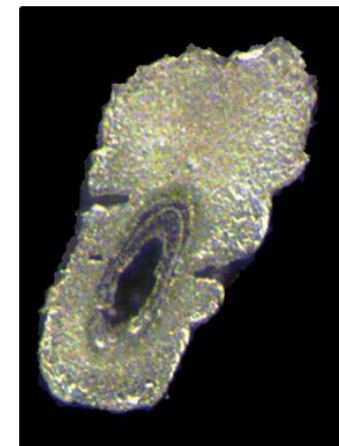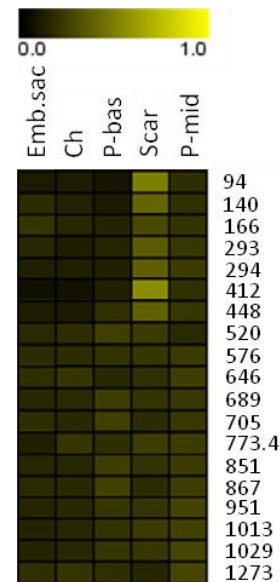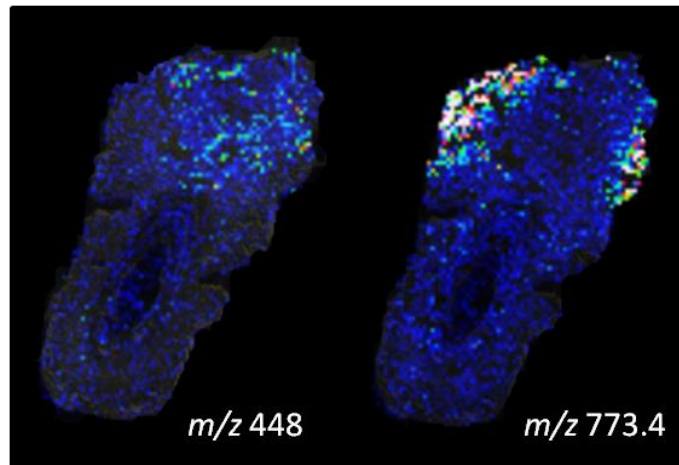
(Description next page)

Figure 17: Distributions of selected molecular ions corresponding to the groups determined by NG cluster analysis.

Distributions are illustrated by single ion intensity maps and heat maps for one replicate of a grain from the prestorage stage. Single ion intensity maps were generated in FlexImaging software. Heat maps were built using the normalized peak intensities in the Genesis software tool.

Abbreviations are: Emb.sac – embryo sac; Ch – chlorenchyma layer; P-bas – pericarp, basal; Scar – pericarp, scar; P-mid – pericarp, middle.

3.2.1.2. Distributions of molecular ions during the transition phase

At the transition phase between six and eight DAP the endosperm is fully cellularized, the endospermal transfer cells (ETC) become active and the nucellar projection (NP) has been differentiated from the nucellar epidermis in front of the ETC (Weschke et al., 2000). After mainly longitudinal growth the grain nearly exhibits its full length. As can be observed from the histological sections in Figure 18 the maternal part of the seed is still dominating.
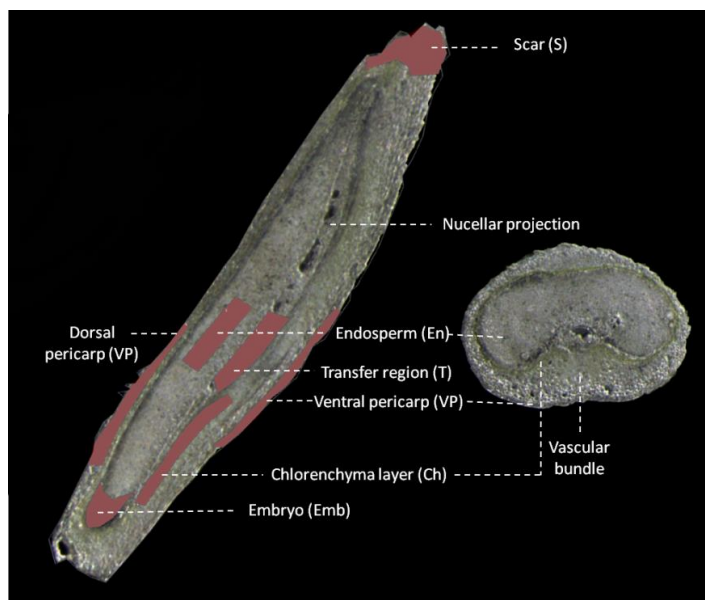
Figure 18: Histological overview of barley grain tissues at 7 DAP by longitudinal (left) and cross sections (right).

Displayed are 30 µm thick cryo-sections, prepared prior to the MSI runs. The marked regions in the longitudinal slice indicate the selected ROIs included in the multivariate statistical analysis of distribution patterns. At this developmental stage the grain is fully cellularized, the maternal part is still dominating.

Statistical analyses were carried out taking seven ROIs (displayed in Figure 18) and 114 individual *m/z* values into account. A table containing the selected molecular ions and the average peak intensities for all ROIs is given in Appendix 2. From a preliminary examination of the data

the number of the resulting NG clusters was set to four. The results of the individual and of the combined cluster analysis of the experiments are presented in Figure 19. The common functionalities of the obtained prototypes that show the typical profiles of the mean normalized peak intensities in the dedicated ROIs are indicated. Separated and combined NG clustering revealed three clusters with specific accentuations of particular tissues. The embryo (cluster one), was clearly found to differentiate from the remaining seed parts. Also the chlorenchyma layer forms one cluster (cluster four). For the pericarp tissues (ventral pericarp, dorsal pericarp and scar region) differences between the three replicates were observed. In experiment one the ventral pericarp and the scar are both dominating, whereas in experiment two the ventral pericarp, and in experiment three the scar region are highlighted. By combination of the replicates a clustering of molecular ions with a higher abundance in the scar region was observed. Cluster three reflects the prototype of molecular ions that are mainly co-localized. Those ions are supposed to be not involved in a tissue specific function at this particular developmental step.

In Table 10 the numbers of molecular ions from each replicate, and the numbers from the common subset according to the obtained clusters from the NG cluster analysis are presented. 25 individual *m/z* values showed different distribution patterns within the three experiments. The corresponding *m/z* data are given in Table 11. From that, most of the signals were found to group into the third cluster. The other clusters are formed by only a small number of assigned signals, but those show high tissue specificity (Figure 20).
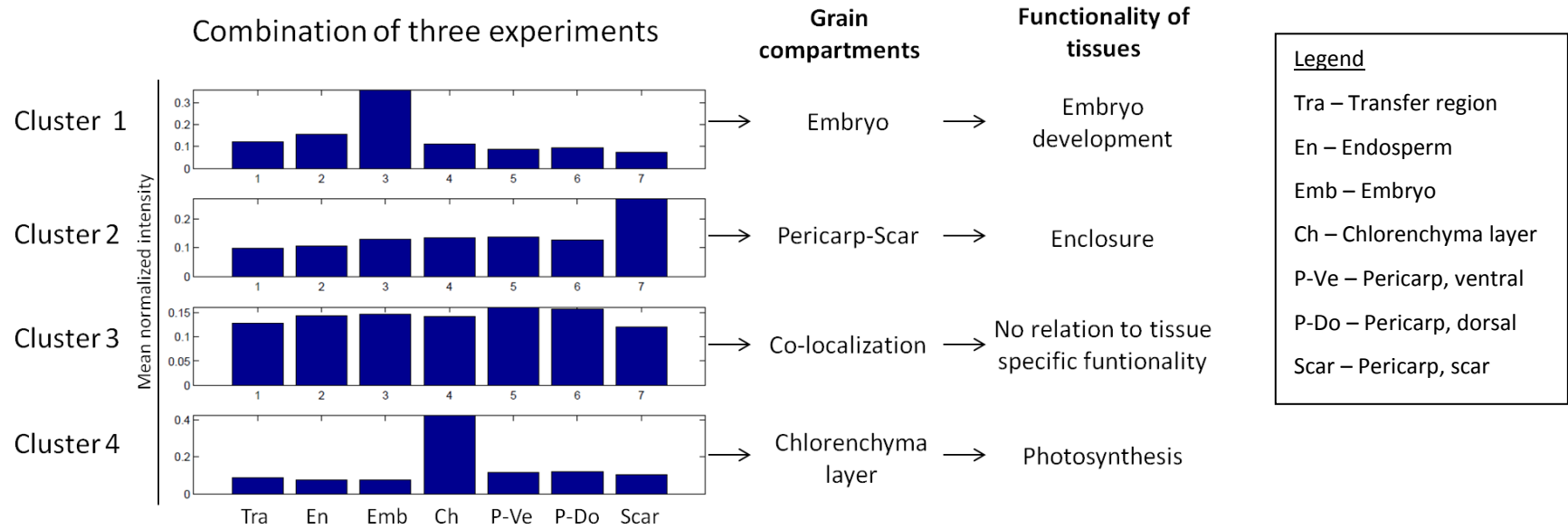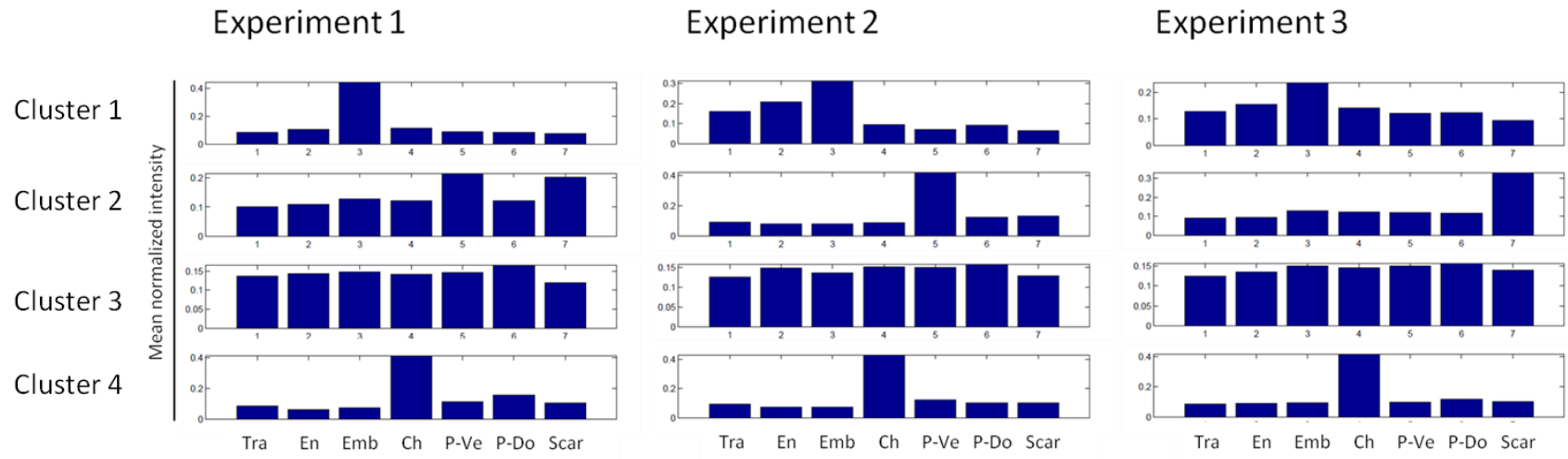
(Description next page)

Figure 19: Results of the Neural Gas (NG) cluster analysis out of MS imaging datasets from barley grains at the transition stage.

Upper part: NG clustering of the individual experiments.

Lower part: NG clustering of the combination of three replicates. The grain parts that are accentuated in the respective clusters are indicated, and the general functionalities of the involved tissues are given.

Table 10: Numbers of assigned *m/z* values per cluster for each experiment and for the common subset as revealed by the combined cluster analysis of three independent MSI measurements of 7 DAP barley grains.

	Numbers of *m/z* values in each cluster			Common subset
	Experiment 1	**Experiment 2**	**Experiment 3**	
Cluster 1	13	11	8	8
Cluster 2	12	9	15	6
Cluster 3	85	86	86	71
Cluster 4	4	8	5	4
Sum	114	114	114	89

Table 11: Assignment of the particular *m/z* values from the common subset of 7 DAP barley grain MSI experiments to the clusters revealed by NG clustering.

Molecular ions that were not designated to the same cluster by all three experiments are indicated as different pattern. *M/z* values are displayed as integer numbers, except those, that share the same integer.

Group	Obtained *m/z* in integer numbers
Class 1	616, 747, 757, 779, 781, 795, 817, 818
Class 2	94, 140, 241, 294, 448, 773
Class 3	90, 104, 130, 136, 148, 158, 164, 184, 192, 193, 195, 222, 230, 231, 233, 254, 268, 284, 308, 381, 399, 407, 423, 428, 466, 489, 508, 518, 522, 527, 543, 558, 560, 575.5, 576.5, 580, 618, 664, 688, 689, 705, 738, 751, 753, 755, 759, 761, 783, 785, 787, 799, 801, 823, 825, 867, 900, 906, 927, 945, 951, 969, 976, 1013, 1029, 1062, 1068, 1176, 1191, 1215, 1224, 1231
Class 4	592, 653, 871, 910
Different Pattern	86, 116, 118, 147, 175, 182, 221, 240, 258, 348, 460, 520, 574, 600, 615, 744, 749, 771, 773, 797, 814, 821, 851, 885, 924

Distribution patterns according to the NG cluster analysis are illustrated in Figure 20. The single ion intensity maps of selected molecular ions exemplarily show the patterns of the particular prototypes within a tissue slice. The heat maps illustrate the mean normalized signal intensities across the ROIs from one of the replicates. The distributions in the embryo (cluster one) and the chlorenchyma layer (cluster four) are highly specific. Those ions that are higher abundant in the scar region are grouped into cluster two, which belongs to the maternal enclose of the filial part. Cluster three contains signals with homogenous distributions and with slight increases in the pericarp (dorsal as well as ventral) as can be observed from the heat maps in Figure 20.

Cluster 1 — m/z 817

Cluster 2 — m/z 140

Cluster 3 — m/z 1231, m/z 575.5
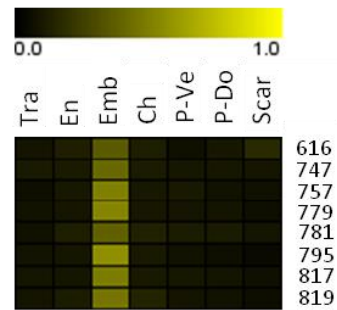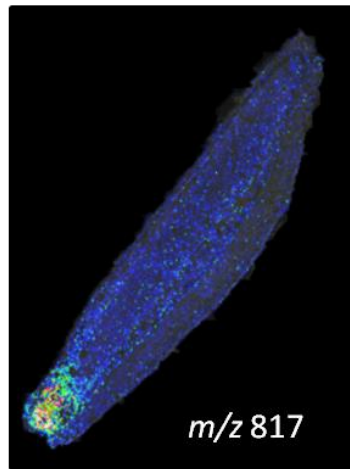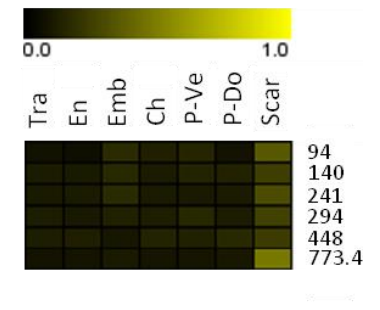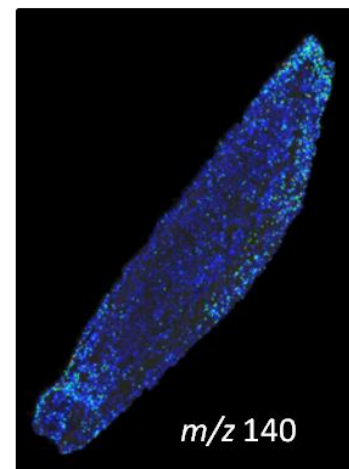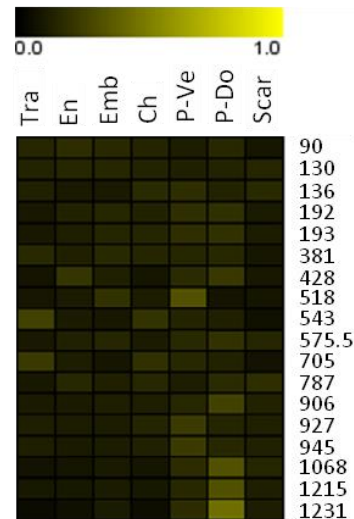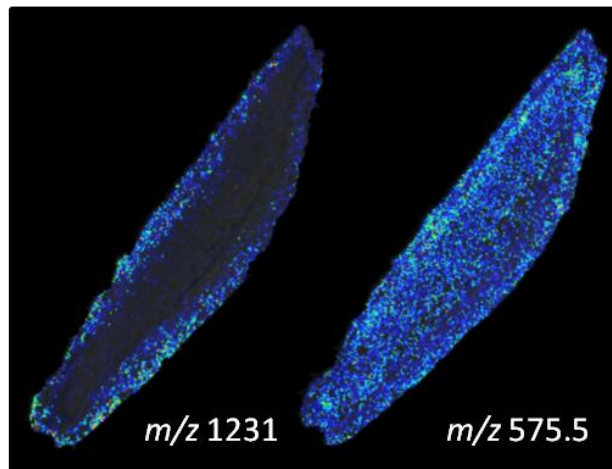
(Continued on next page)
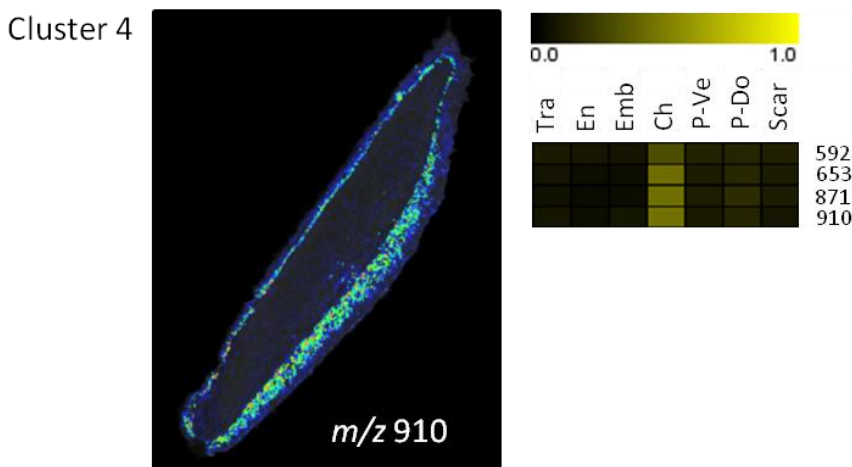
Figure 20 (continued): Distribution patterns of selected molecular ions corresponding to the groups determined by NG cluster analysis.

The distribution patterns are shown for one replicate of the 7 DAP barley grain MSI measurements by single ion intensity maps, and by heat maps. Single ion intensity maps were generated in FlexImaging software. The heat maps were built using the normalized peak intensities in the Genesis software tool.

Abbreviations are: Tra – Transfer region; En – Endosperm; Emb – Embryo; Ch – Chlorenchyma layer; P-Ve – Pericarp, ventral; P-Do – Pericarp, dorsal; Scar – Pericarp, scar

3.2.1.3. Distributions of molecular ions during the storage phase

During the storage phase the grains accumulate large amounts of starch in the rising endosperm, but also storage proteins and lipids are synthesized. Henceforth, the high storage production rates determine the further seed growth. Here, grains of 10 and 14 DAP were investigated. Clear differences between both storage phase stages were revealed from the histological observations. Remarkable are the rising endosperm, the formation of the cavity and the reduction of the pericarp surrounding the seed (Figure 21).
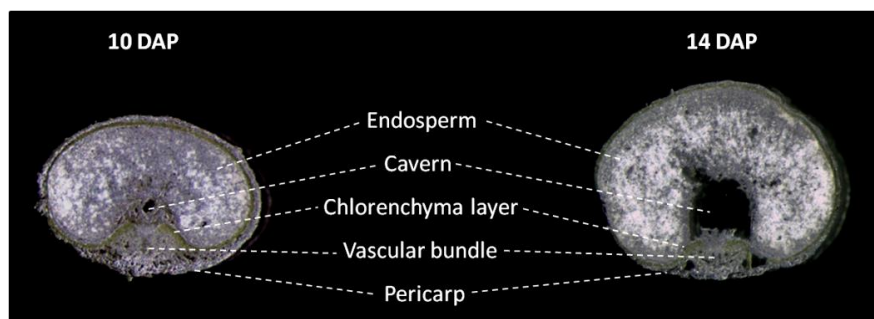
Figure 21: Histological representation of 10 and 14 DAP barley grain cross sections.

The cryo-sections were prepared from the grain middle part. Most obvious differences between both storage phase stages are the emerging cavity, the further diminishing of the pericarp and the increase of the endosperm.

10 DAP, representing the early storage phase

The early storage phase of barley grains is characterized by seeds of 10 DAP. The ETC actively transport the nutrients into the rising endosperm. A part of the NP starts to undergo PCD, visible by the emerging cavity. The endosperm now represents the major part of the grain, compared to 7 DAP, when this organ is completely cellularized but still soft and thin (Figure 18).

For the statistical analysis of distribution patterns 114 signals detected in three independent experiments were taken into account in relation to the normalized mean peak intensities from nine regions of interest (ROIs). The ROIs represent the main tissue types as chosen by means of the histological images (Figure 22).
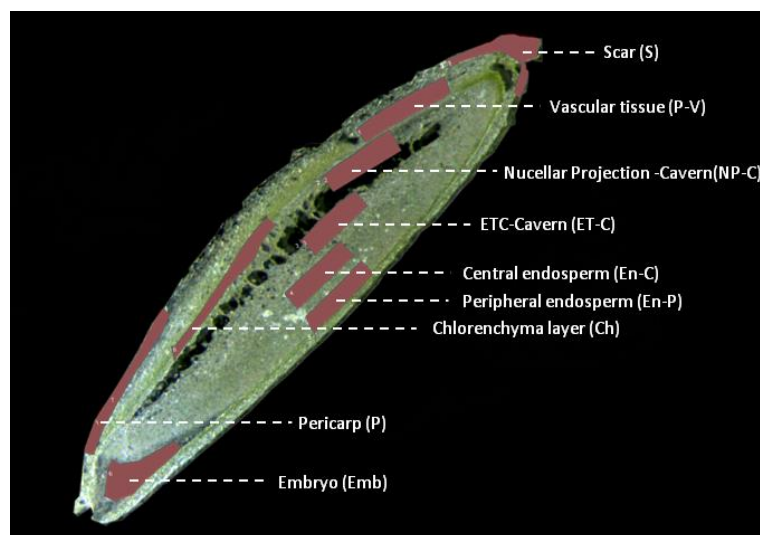
Figure 22: Longitudinal section of a 10 DAP barley grain.

Displayed is a 30 μm thick cryo-section. The indicated selected ROIs cover the different histological parts as been distinguishable from the cryo-section. Here, the filial part dominates the grain volume. Nucellar projection starts to undergo PCD, visible by the arising cavity.

The number of groups generated by the NG cluster analysis was set to five. This number resulted from preliminary observations of the imaging datasets. The prototypes displaying the center of each cluster are illustrated in Figure 23, for each replicate (upper part), and for the combination of all three replicates (lower part). Corresponding functional groups are indicated in the combined cluster analysis. In all experiments the embryo and the chlorenchyma layer dominate clusters one and two. For the third cluster mixed patterns were observed, accentuating the scar in the first experiment, the NP and the ETC in the second experiment, and showing more co-localized abundances of molecular ions in the third experiment. The Combination of all three data

sets revealed a prototype comprising a more homogenous distribution pattern of molecular ions, but with a slight increase of signal intensities for the tissues that are responsible for the transport of nutrients into the endosperm (including the vascular tissue, NP and ETC). Cluster four highlights by individual and by combined NG clustering the molecular ions that are more abundant in the rising endosperm. Here, a relation to storage product accumulation is supposed. The signals that show higher abundances in the pericarp are grouped into cluster five by the cluster analysis of each experiment and by the combined clustering.

The numbers of *m/z* values classified to the particular clusters from the combined analysis are given in Table 12 for each experiment and for the common subset. Cluster two is represented by only three molecular ions. 45 signals were found with differing distributions between the three experiments. Most ions showed a similarity to the prototype shapes of clusters three and four. The classified *m/z* values are listed in Table 13. A complete list containing all selected *m/z* values and the average signal intensities in the particular ROIs is presented in Appendix 3.
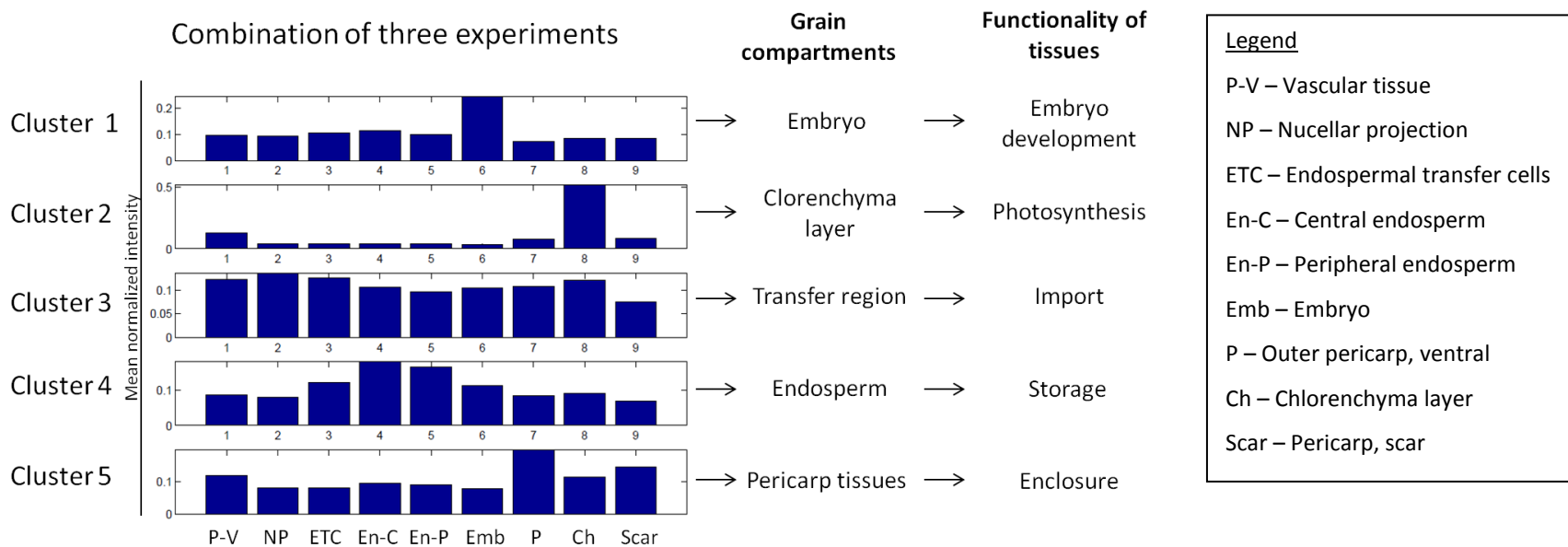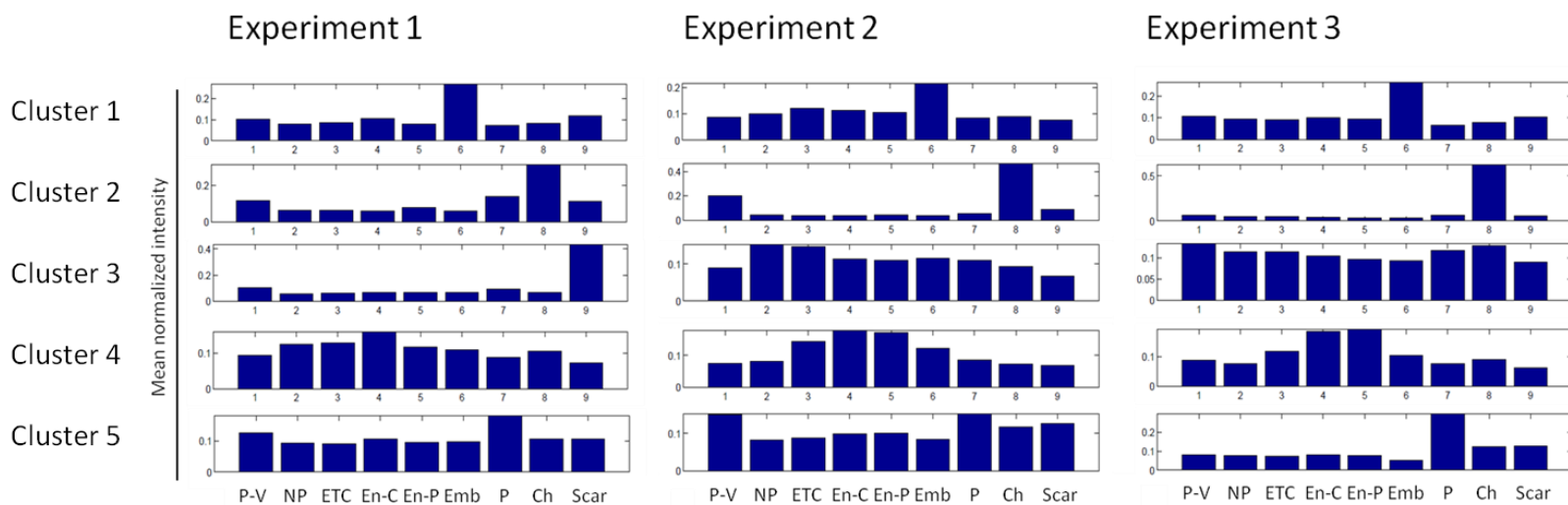
Figure 23: Results from the Neural Gas (NG) cluster analysis out of MSI datasets from barley grains at 10 DAP.

Upper part: NG clustering for the individual experiments.

Lower part: NG clustering for the combined analysis of three replicates. The grain parts that are accentuated in the respective clusters are indicated and the general functionalities of the involved tissues are given.

Table 12: Numbers of assigned *m/z* values per cluster for each experiment and for the common subset as revealed by the combined cluster analysis of three independent MSI measurements of 10 DAP barley grains.

	Number of *m/z* values in each cluster			Common subset
	Experiment 1	**Experiment 2**	**Experiment 3**	
Cluster 1	15	19	19	11
Cluster 2	3	4	4	3
Cluster 3	41	43	33	23
Cluster 4	27	31	37	23
Cluster 5	28	17	21	9
Sum	114	114	114	69

Table 13: Assignment of the particular *m/z* values from the common subset of 10 DAP barley grain MSI experiments to the clusters revealed by NG cluster analysis.

Molecular ions that were not designated to the same cluster by all three experiments are indicated as different pattern. *M/z* are displayed as integer numbers, except those, that share the same integer.

Group	Obtained *m/z* in integer numbers
Cluster 1	118, 140, 158, 221, 241, 254, 616, 757, 779, 795, 819
Cluster 2	653, 871, 910
Cluster 3	104, 192, 193, 195, 222, 230, 231, 233, 321, 381, 423, 527, 543, 562, 576.5, 618, 705, 738, 814, 867, 924, 954, 976
Cluster 4	86, 148, 428, 496, 508, 534, 575.5, 628, 749, 751, 755, 759, 761, 773.0, 775, 785, 787, 797, 799, 821, 823, 825, 980
Cluster 5	205, 448, 518, 520, 558, 560, 743, 773.4, 927
Different Pattern	90, 94, 116, 130, 136, 146, 147, 184, 240, 294, 299, 337, 348, 399, 574, 592, 600, 651, 688, 689, 747, 771, 781, 783, 817, 840, 851, 900, 918, 920, 935, 956, 978, 1013, 1026, 1029, 1062, 1068, 1102, 1174, 1176, 1191, 1215, 1224, 1231

Illustrations of distribution patterns according to the clusters are represented by selected single ion intensity maps and by heat maps in Figure 24. Cluster one emphasizes the embryo compared to the other designated grain parts. Three molecular ions were found to be highly specific for the chlorenchyma layer as they were nearly absent in the other tissues. The signals that were more homogenously distributed and those that showed increased signal intensities in the transfer region are grouped in cluster three. The illustrations for cluster four reflect the higher signal intensities in the endosperm. Cluster five contains the molecular ions that were more abundant in maternal

pericarp parts. Three of them were found to be mainly distributed in the scar region (*m/z* 205, 743 and 773).
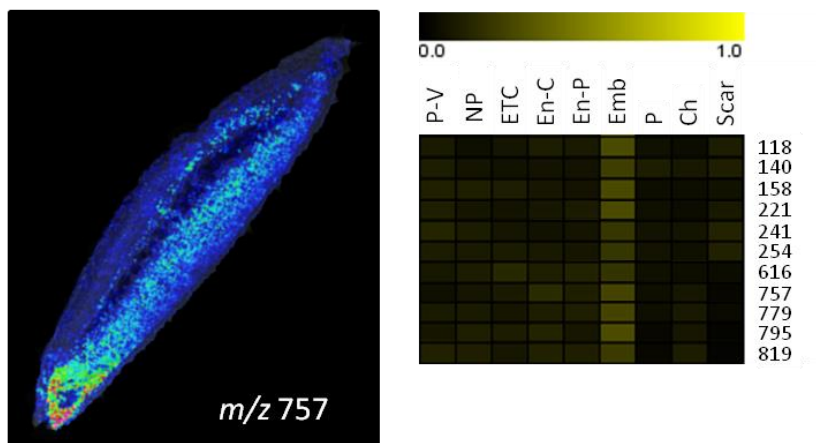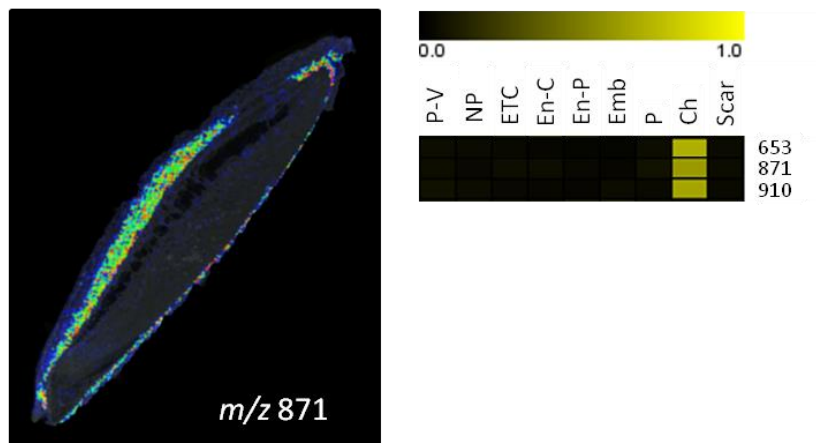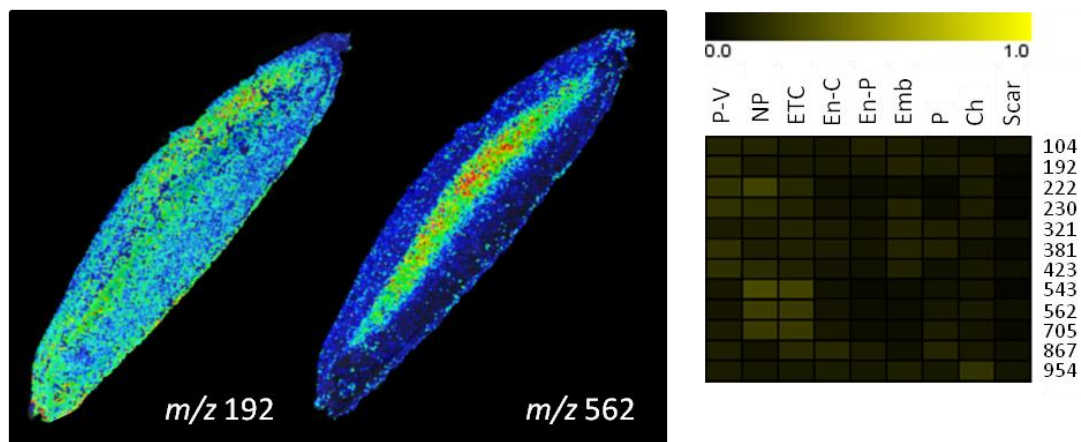
(Continued on next page)
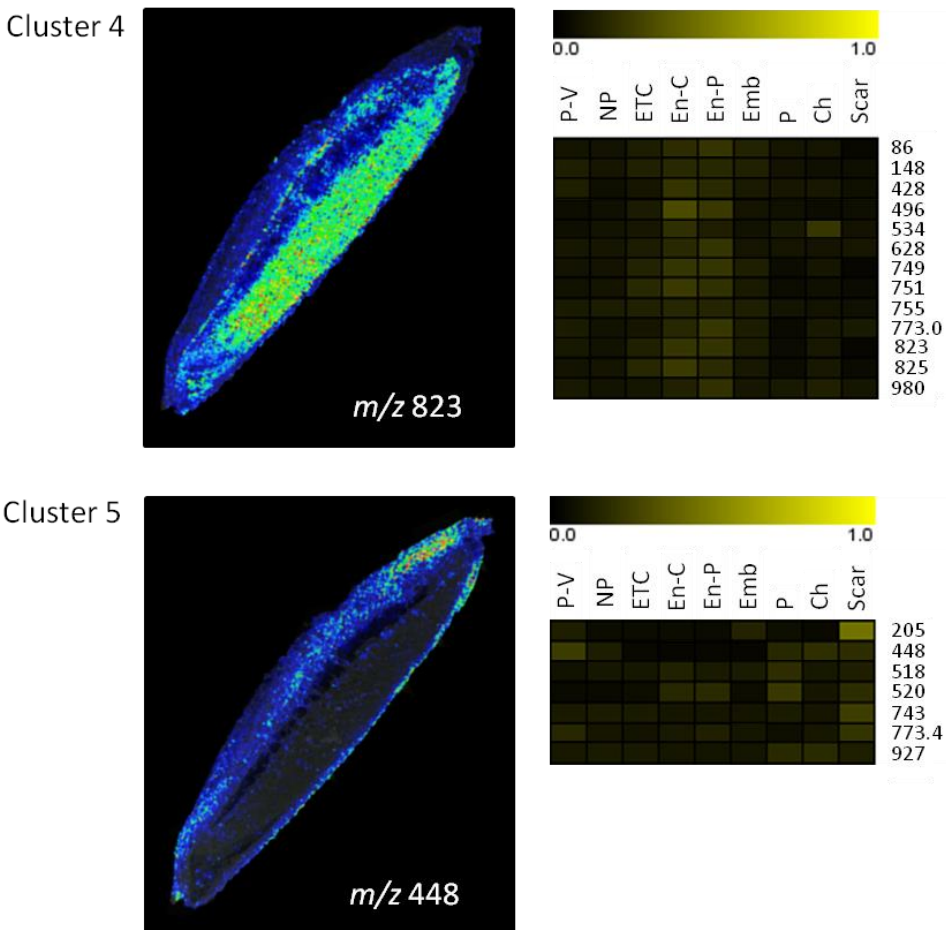
Figure 24 (continued): Distribution patterns of molecular ions according to the NG clustering results from 10 DAP barley grain MSI experiments.

The distribution patterns are illustrated for one replicate of the 10 DAP MSI runs by single ion intensity maps and by heat maps. Single ion intensity maps were generated in FlexImaging software. The heat maps display normalized peak intensities in the selected ROIs and were built using the Genesis software tool.

Abbreviations are: P-V – Vascular tissue; NP – Nucellar projection; ETC – Endospermal transfer cells; En-C – Central Endosperm; En-P – Peripher endosperm; Emb – Embryo; P – Outer pericarp, ventral; Ch – Chlorenchyma layer; Scar – Pericarp, scar

14 DAP, representing the middle storage phase

At 14 DAP most of the pericarp is degraded. This is mainly observable at the dorsal site where just a thin tissue layer above the chlorenchyma layer is visible (Figure 21). Only at the ventral site, where the main vascular bundle is localized, the pericarp is almost intact. The endosperm is the most voluminous grain part, accumulating high amounts of starch (Figure 25). All nutrients entering the endosperm have to pass the fluidic filled cavity that emerges in front of the endospermal transfer cells (ETC). Parts of the nucellar projection (NP) are degraded.
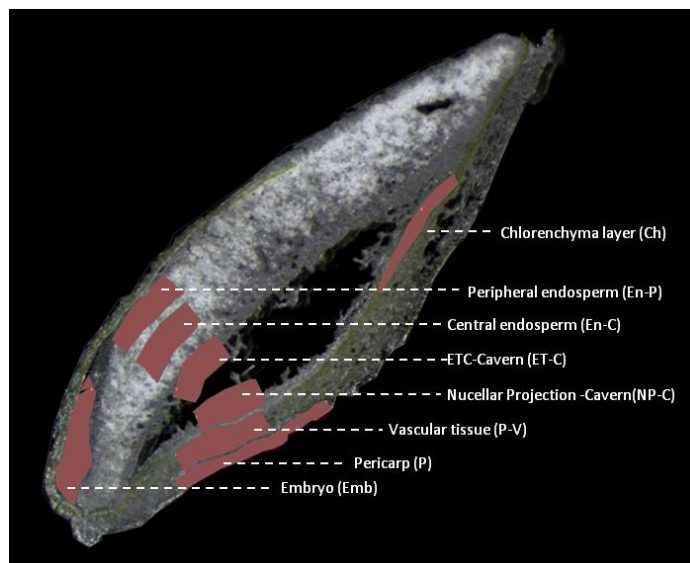
Figure 25: Longitudinal section of a 14 DAP barley grain.

The 30 μm thick cryo-section displays the ROIs selected for statistical analysis. The ROIs cover the different histological parts as been distinguishable from the cryo-section. The scar has been excluded due to tissue disintegration and to disruption during the cutting. At this stage a large cavity has been formed and the endosperm displays the main grain part.

Multivariate statistical analyses were carried out including 133 individual *m/z* values and eight ROIs (marked in Figure 25); the scar region was excluded due to the nearly complete degradation, and partial disruption during the cutting process. The NG cluster algorithm was initially set to five. This number was emerged from prior observations of the datasets and has been proven by an automatic cluster generation by the applied algorithm. The results of NG cluster analysis for the separate experiments and for the combined analyses are displayed in Figure 26. The prototypes represent the mean normalized peak intensities across the selected ROIs for the individual clusters. A grouping of molecular ions according to a general functionality of the involved grain parts was observed. The patterns of clusters four and five are mostly obvious. The *m/z* values in cluster four show high specificity for the chlorenchyma layer (Ch), indicating a relation to the photosynthetic apparatus. Embryo specific molecular ions were grouped to cluster five. Signals with higher intensities in the endosperm were grouped to cluster one, indicating a relation to storage product accumulation. Cluster two is characterized by *m/z* signals that are higher abundant in those grain regions that have an impact on the transfer of nutrients into the endosperm, namely: NP, cavity and ETC. The prototype patterns for cluster one, two, four and five were obtained by the separated cluster analysis of the individual

experiments and also by the combined clustering. Cluster three shows different patterns for the three replicates, but it generally contains the signals that are higher abundant in maternal tissues like the outer layer of the pericarp (P), the vascular part (P-V), and also the chlorenchyma layer. The separate analysis of the experiments revealed similar cluster patterns, but the numbers of assigned peaks differs from experiment to experiment, indicating unclear distribution patterns of several molecular ions (Table 14). Here, 55 signals were indicated as unclear pattern. Clusters four and five are represented by only a small number of signals, but showed the most tissue specificity. The classification of all 133 individual *m/z* values is given in Table 15. Those that were not put into a distinct class by all three replicates are designated as different pattern. A complete table containing the average peak intensities and the results from the cluster analyses of the individual experiments is given in attachments (Appendix 4).

Typical distribution patterns as observed by the NG cluster analysis are illustrated in Figure 27 in form of single ion intensity maps and heat maps from one of the replicates. Distributions in the chlorenchyma layer (cluster four) are highly specific, and the signals are nearly absent in the other grain parts. For clusters one, two, three and five increases of signal intensities in the respective grain parts are observable, but the molecular ions are not unique for one of the tissues. Abundances in the transfer region are in most cases connected to the cavity as observed by the examination of distribution patterns in single ion intensity maps. Molecular ions belonging to cluster five show specific increases in the embryo part of the grain.
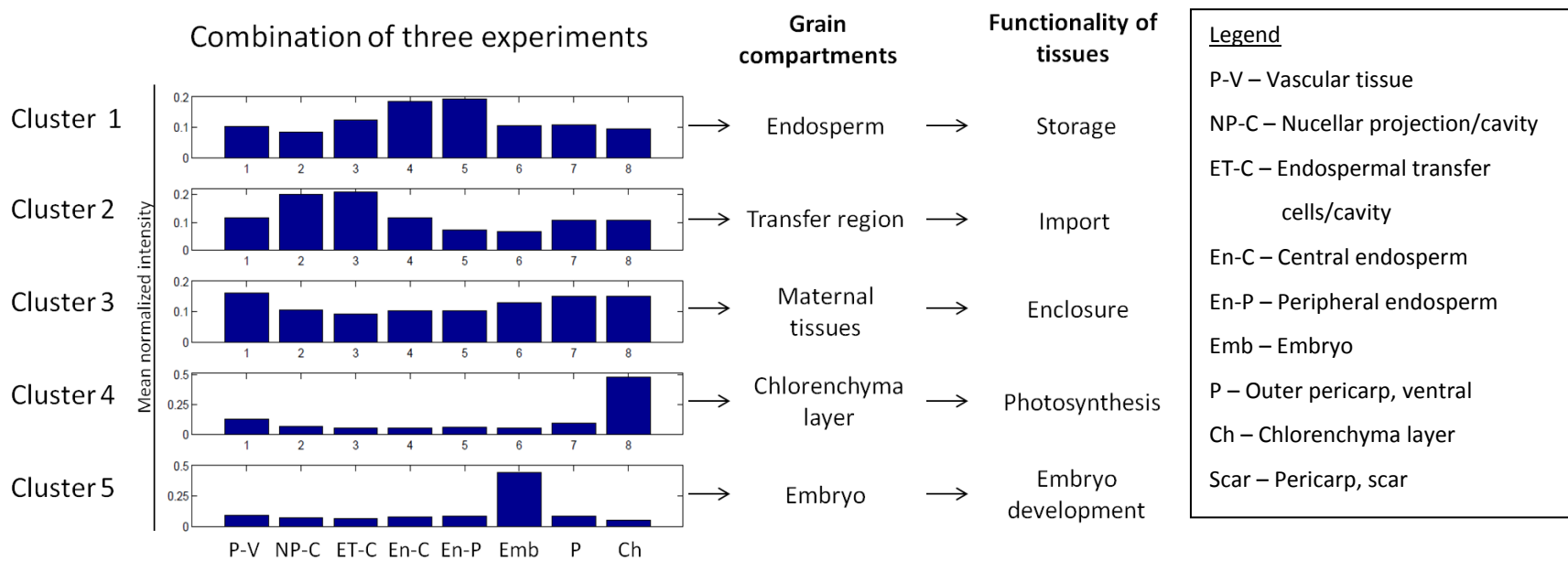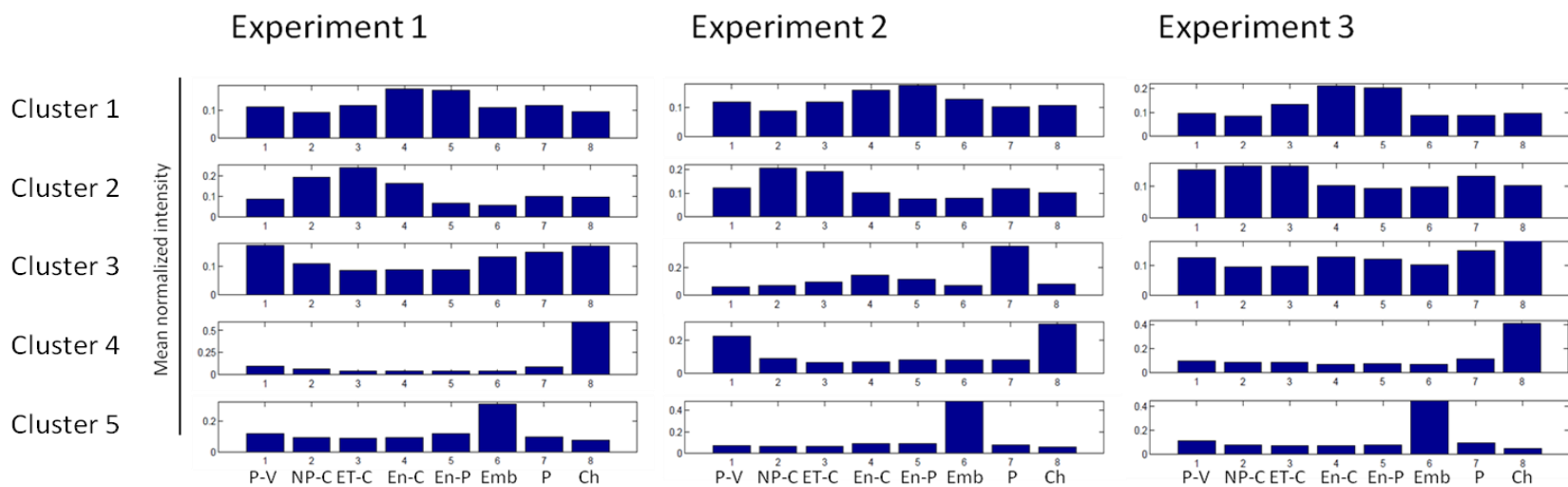
(**Description next page**)

Figure 26: Results from the Neural Gas (NG) cluster analyses out of MS imaging datasets from barley grains at 14 DAP.

Upper part: NG prototype patterns of five clusters obtained for three individual experiments.

Lower part: NG clustering for the combined analysis of three replicates. The grain parts that are accentuated in the respective clusters are indicated and the general functionalities of involved tissues are given.

Table 14: Numbers of assigned *m/z* values per cluster for each experiment and for the common subset as revealed by the combined cluster analysis of three independent MSI experiments of 14 DAP barley grains.

	Number of *m/z* belonging to each class			Common subset
	Experiment 1	**Experiment 2**	**Experiment 3**	
Cluster 1	51	47	44	32
Cluster 2	16	26	19	10
Cluster 3	53	46	49	27
Cluster 4	6	5	10	4
Cluster 5	7	9	11	5
Sum	133	133	133	78

Table 15: Assignment of particular *m/z* values to clusters determined by the combined NG clustering of three MALDI MSI experiments from 14 DAP barley grains.

Molecular ions that were not designated to the same cluster by all three experiments are indicated as different pattern. *M/z* are displayed as integer numbers, except those, that share the same integer.

Group	Obtained *m/z* in integer numbers
Class 1	86, 124, 148, 184, 240, 337, 428, 487, 496, 520, 534, 558, 575.5, 749, 751, 755, 759, 761, 773.0, 785, 787, 797, 799, 801, 818, 821, 823, 825, 935, 956, 980, 1007
Class 2	147, 222, 402, 415, 527, 543, 562, 576.5, 673, 689
Class 3	104, 130, 136, 348, 448, 460, 489, 616, 618, 747, 757, 771, 779, 781, 795, 803, 805, 817, 819, 885, 924, 954, 1068, 1102, 1174, 1215, 1231
Class 4	592, 653, 871, 910
Class 5	116, 118, 158, 221, 254
Different Pattern	94, 140, 146, 191, 192, 193, 195, 211, 214, 230, 231, 233, 241, 293, 299, 321, 381, 399, 479, 518, 533, 560, 574, 597, 600, 602, 628, 651, 675, 679, 689, 705, 738, 743, 744, 773.4, 783, 814, 840, 851, 867, 894, 900, 918, 920, 958, 976, 982, 1013, 1026, 1029, 1062, 1176, 1191, 1224

Cluster 1 — *m/z* 428

Cluster 2 — *m/z* 527

Cluster 3 — *m/z* 1231

Cluster 4 — *m/z* 871
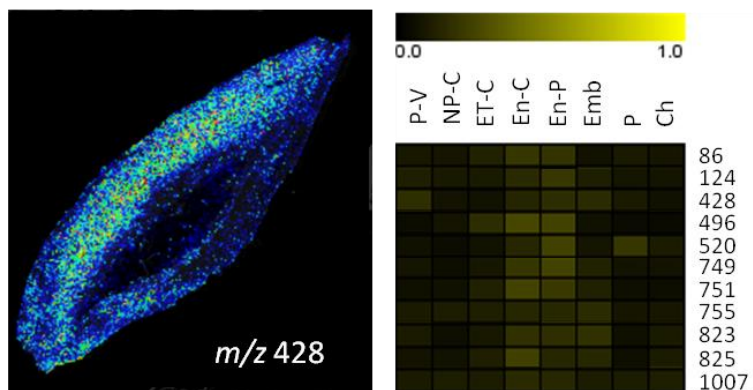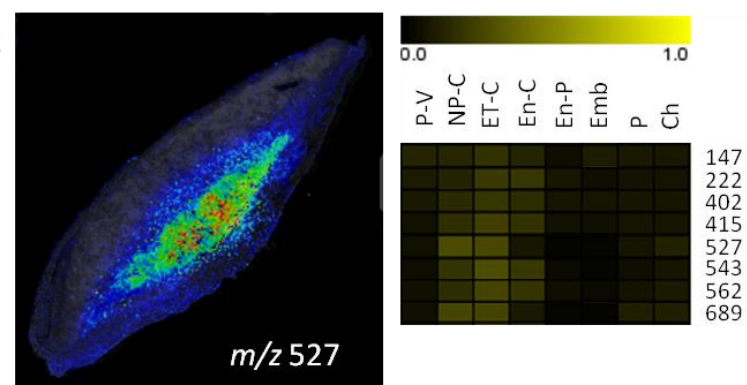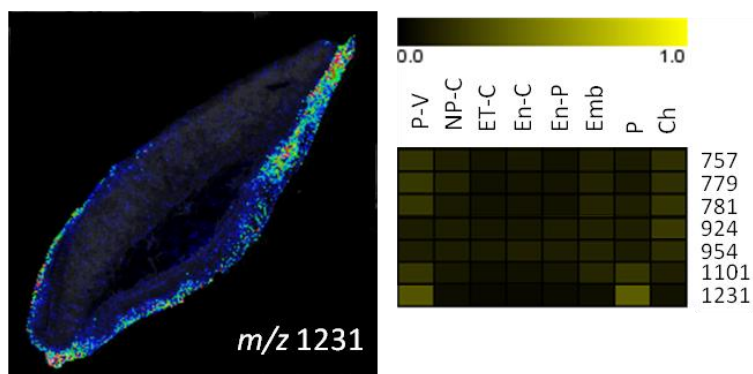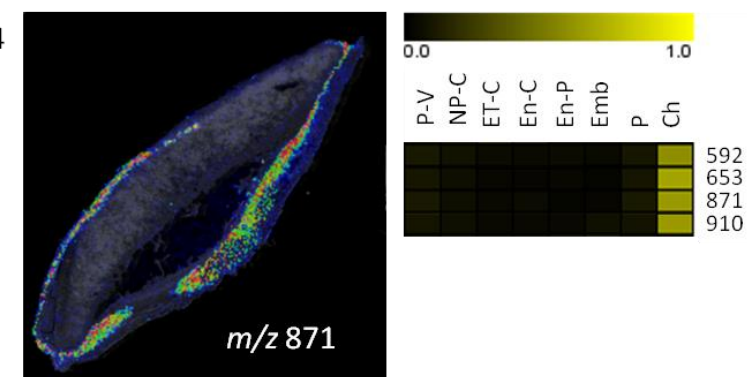
(Continued on next page)
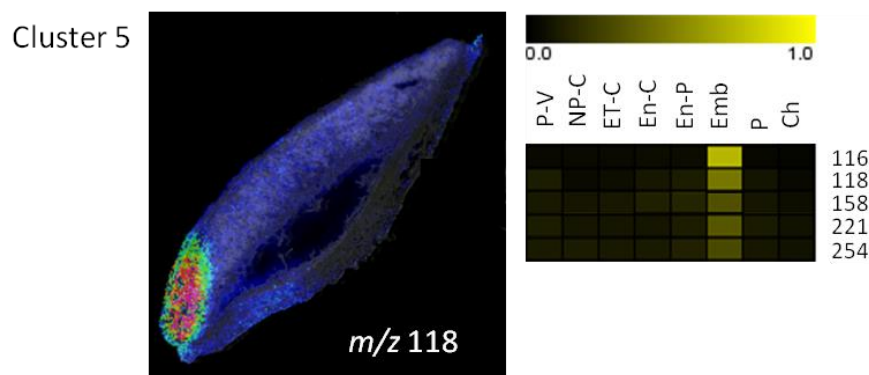
Figure 27 (continued from page xxx): Distribution patterns of molecular ions in one replicate of a 14DAP barley grain according to NG clustering results.

Single ion intensity maps display the distributions of selected molecular ions over the complete sample surface. These were generated in FlexImaging software. The heat maps were built in the Genesis software tool using normalized peak intensities, and display the abundance of molecular ions in the selected ROIs.

Abbreviations are: P-V – Vascular tissue; NP – Nucellar projection/cavity; ET-C – Endospermal transfer cells/cavity; En-C – Central endosperm; En-P – Peripher endosperm; Emb – Embryo; P – Outer pericarp, ventral; Ch – Chlorenchyma layer.

3.2.2. Developmentally specific distributions of molecular ions

The aim was to elucidate differences of molecular ion abundances between the investigated developmental stages to unravel molecules that display candidate compounds having an impact on developmental processes, and especially on the grain filling. Therefore, the detected signals from all stages were compared for the presence of unique *m/z* values, and the changes of relative signal intensities were examined.

Molecular ions that were specifically detected at particular developmental stages are listed in Table 16. The assignment to seed regions, where these molecular ions are most abundant, allowed tentative functional correlations. Specific molecular ions during the prestorage phase are mostly abundant in the pericarp and in the scar; tissues that firstly undergo PCD. At the transition stage least specific signals were observed, as this point of time represents a physiological switch to the beginning of massive storage accumulation in the filial part, whereas the maternal pericarp starts to degrade. During the storage phase the endosperm as well as the tissues involved in the import of nutrients (designated as transfer tissues) are fully developed, and several molecular ions were found to be related to these regions.

Table 16: Development-specific abundances of individual *m/z* signals.

Presented are signals that were detected in all three replicates at only one of the developmental stages. Assignment to the grain parts is according to the average peak intensities of the particular regions of interest (ROIs).

The maternal tissues comprise the outer pericarp and the vascular tissue. The transfer region comprises the nucellar projection, the endospermal transfer cells and the cavity. Unspecific pattern means that the highest signal intensities were obtained in different ROIs of the particular replicates.

	Maternal tissues	Scar	Endosperm	Transfer region	Clorenchyma layer	Embryo	Embryosac	Unspecific pattern
Prestorage Phase	319	156			815		808	152
	350	166						292
	358	246						419
	380	296						598
	481	412						1081
	511							1111
	604							1213
	646							1243
	684							
	712							
	1273							
Transition Phase	906							268
	945							407
Storage Phase	1102		124	214	533	146		321
			487	299	803			597
			534	402	894			601
			628	415	1026			675
			817	562				
			920	673				
			935	679				
			980					

Those signals that were detected at the different developmental stages were compared for their differences in distribution pattern, and for the relative changes of their signal intensities. The DHB background measured along with all sample sets was used as an internal standard. The percentage peak intensities of the individual molecular ions to the mean DHB background were determined for the different developmental stages. Signals showing increasing or decreasing signal intensities during development are listed in Table 17. All other molecular ions were found to be unchanged.

The diagrams in Figure 28 exemplarily show changes of molecular ion/DHB background ratios through the investigated developmental stages (as listed in Table 17). For *m/z* 86.1 a high

increase at the storage phase was detected. For *m/z* 689.3 the ratio also increases at 14 DAP. The examples in the lower part of Figure 28 display decreasing signal intensities of molecular ions. *M/z* 254.2 steeply decreases from 3 to 7 DAP and remains then unchanged. For *m/z* 422.9 a steady decline from a high abundance during the prestorage phase (3 DAP) to the early storage stage was obtined. At 14 DAP the compound was not longer detected.

Table 17: Molecular ions showing a development-specific accumulation as revealed by correlation of peak intensities to matrix background.

The numbers display the percentages of the particular ions related to the mean DHB background (=100%). The mean DHB background corresponds to the mean intensity of five DHB background signals (*m/z* 137, 154, 177, 273, and 409) from the blank region measured simultaneously in all imaging runs. Changing tendencies during development are indicated as increasing trend (i) and decreasing trend (d); n.d. – not detected.

m/z	3 DAP			7 DAP			10 DAP			14 DAP			Trend
	Exp.1	Exp.2	Exp.3	Exp.1	Exp.2	Exp.3	Exp.1	Exp.2	Exp.3	Exp.1	Exp.2	Exp.3	
86.1	1.6	3.4	2.5	2.1	2.5	2.3	2.4	6.0	34.4	45.0	21.0	5.6	i
94.1	8.4	10.9	3.5	6.2	7.2	5.9	6.5	9.4	26.1	25.7	12.7	7.8	i
164.1	1.9	6.4	6.5	1.1	4.1	5.4		n.d.			n.d.		d
184.1	4.8	16.9	11.3	6.6	10.8	5.1	9.3	25.6	75.0	81.5	59.7	20.6	i
254.2	2.3	3.0	3.1	1.2	1.7	2.6	1.3	1.4	2.0	1.6	1.9	1.9	d
321.2		n.d.			n.d.		3.4	1.5	3.7	4.8	8.2	6.1	i
422.9	4.7	12.4	14.1	2.4	6.6	7.8	4.1	3.8	3.9		n.d.		d
496.4	1.4	1.9	3.6		n.d.		3.2	4.2	4.3	5.7	7.7	4.4	i
527.2		n.d.		3.4	3.4	4.2	3.3	4.0	7.5	18.4	13.6	11.5	i
534.3	.	n.d			n.d.		2.7	2.7	3.2	4.8	5.3	3.3	i
543.1	9.9	23.1	22.0	10.7	13.3	14.8	17.0	18.4	35.8	41.2	54.0	41.3	i
580.1	2.5	4.5	4.9	1.5	3.1	3.9		n.d.			n.d.		d
615.0	2.2	5.0	6.5	1.3	2.5	3.9		n.d.			n.d.		d
664.2	2.0	3.3	5.3	1.5	2.2	3.7		n.d.			n.d.		d
688.4		n.d.		2.0	2.0	3.5	2.2	3.8	3.2	4.7	5.3	2.5	i
689.3	3.8	6.0	7.8	6.1	4.1	6.0	4.3	7.1	11.4	20.6	12.0	12.1	i
705.2	20.2	36.6	45.1	21.8	27.4	30.6	25.4	35.5	63.1	48.3	48.1	45.3	i
751.0		n.d.		1.8	2.1	4.1	2.5	3.9	5.4	3.8	5.9	6.8	i
771.0		n.d.		1.7	3.0	4.2	2.0	3.1	4.4	2.8	4.9	4.6	i
950.7	2.5	4.2	5.2	1.5	2.0	3.4		n.d.			n.d.		d
968.6	2.5	3.8	4.7	1.5	2.1	3.4		n.d.			n.d.		d
979.6		n.d.			n.d.		2.0	2.8	2.9	2.6	4.5	4.6	i
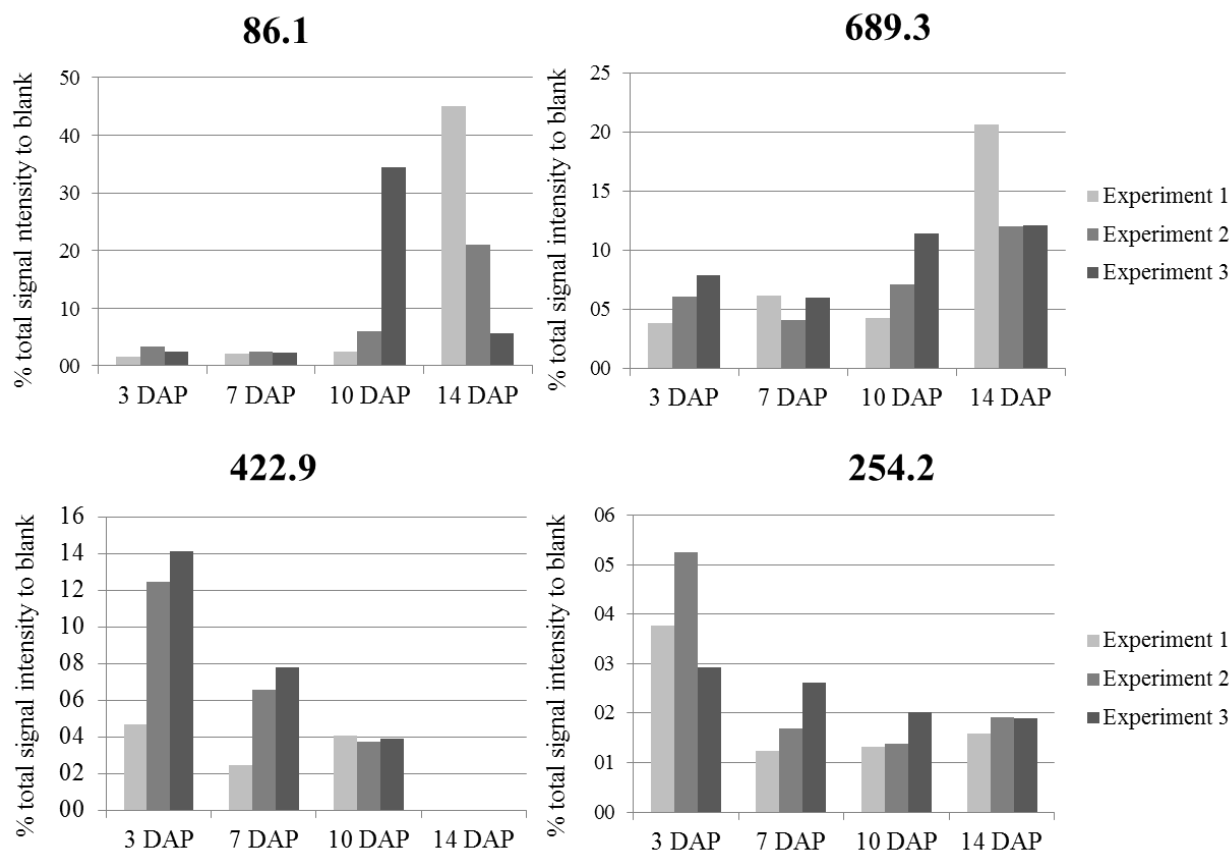
Figure 28: Examples of molecular ions with changes in the ion to background ratios during grain development.

Upper part: Two selected mass signals with increasing signal intensities during development are displayed.

Lower part: Two examples for decreasing signal intensities during development are shown. For *m/z* 422.9 no signal was detected at 14 DAP.

Bar heights correspond to the percentage signal intensity of the selected ion related to the DHB background (=100%). The DHB background corresponds to the mean intensity of five DHB background signals (*m/z* 137, 154, 177, 273, and 409) from the blank region measured simultaneously in all imaging runs.

The differences in development specific abundances of molecular ions were often observed to be related to reallocations. Especially for oligosaccharides and phospholipids a high specificity was obtained by the MALDI MSI approach. Analyses regarding particular sugar distributions are elaborated in section 3.3. The results for endosperm specific developmental changes are represented in section 3.2.3. Among them, some molecular ions were identified as lipids.

3.2.3.   Changes in endospermal distribution patterns during grain development

The main emphasis of this work lies in the elaboration of candidate compounds showing specific distributions related to the endosperm development. Starch is the major storage compound but

also storage lipids and proteins are synthesized during the storage phase. At the transition phase the endosperm is fully cellularized and the cells start to accumulate storage products. The final composition of this storage tissue has major impacts on seed quality parameters.

Here, mass signals showing differences in their relative peak intensities in the developing endosperm were elucidated. Mean peak intensities of the ROIs that represent the endosperm were related to the mean DHB background. The prestorage phase was excluded from this analysis as the endosperm was not cellularized at 2/3 DAP. Several signals with increasing intensities over time were found (Table 18), but no signals with decreasing tendencies for the endosperm could be observed. This reflects that the endosperm represents an evolving tissue and cellular activities until 14 DAP are mainly related to synthesis processes. All the other detected molecular ions exhibited no changes as been observed by the applied approach.

The diagrams in Figure 29 illustrate particular *m/z* values with considerable changes of signal intensities. Five to seven fold increases in the endosperm from 7 to 14 DAP were observed for *m/z* 520.3, 575.5, 749.0 and 796.6. Two of them (m/z 520.3 and 796.6) belong to the phospholipid class and were found to be endosperm specific during the storage stage. The three signals *m/z* 919.7, 955.6 and 979.6 were found to be endosperm as well as storage stage specific as they were not detected at 7 DAP. In addition, the *m/z* 920 and 980 exhibited gradients within the endosperm with a higher abundance at the periphery (shown for *m/z* 980 in Figure 30). The identity of these molecular ion species is not clarified so far.

As indicated above, different spatial patterns were observed for several endosperm specific molecular ions. Here, the analyses of cross sections provided better visualization. Some molecular ion species were found to accumulate in a homogeneous pattern in the endosperm (Figure 30A), whereas others constitute higher signal intensities in the peripheral part of the endosperm (Figure 30B). These accumulation gradients became apparent with proceeding of the storage stage, and were best revealed at 14 DAP. Table 19 lists endosperm specific molecular ion species according to their patterns. The detection was carried out using a new software tool, SCiLS Lab (Version 1.0, non-commercial license). The provided tool "Find Co-Localized m/z Values" helps to detect signals with a predefined pattern.

In addition, for *m/z* 520 a reallocation was observed. During the early developmental stages (prestorage and transition stage) this molecular ion was more abundant in the pericarp. With the massive enlargement of the endosperm and the diminishing of the pericarp higher signal intensities were found in the filial endosperm tissue (Figure 30C).

Table 18: Molecular ions showing increasing peak intensities in the developing endosperm.

The numbers display the percentage of the particular ions to the DHB background (=100%). The DHB background corresponds to the mean intensity of five DHB background signals (*m/z* 137, 154, 177, 273, and 409) from the blank region measured simultaneously in all imaging runs. n.d – not detected.

m/z	7 DAP			10 DAP			14 DAP		
	Exp. 1	Exp. 2	Exp. 3	Exp. 1	Exp. 2	Exp. 3	Exp. 1	Exp. 2	Exp. 3
86.1	2.2	3.3	2.4	3.3	9.8	59.0	75.5	31.4	10.1
184.1	5.5	13.2	4.5	10.5	36.8	124.8	111.0	79.6	34.8
321.2		n.d.		3.3	1.2	3.1	4.9	4.8	4.4
496.4		n.d.		8.3	9.5	9.9	12.3	18.3	10.0
520.3	2.6	1.5	3.0	6.2	8.8	7.4	8.6	15.0	8.5
534.3		n.d.		5.9	4.3	4.4	8.5	11.0	6.7
558.3	1.9	1.5	2.9	4.9	4.8	4.3	6.9	10.3	6.8
560.4	1.8	1.6	3.0	2.1	2.3	2.8	4.5	3.9	3.0
575.5	2.1	2.1	3.9	4.7	7.5	11.0	7.4	11.4	9.8
576.5	3.5	4.7	5.5	4.0	6.9	12.7	12.8	11.0	6.8
599.5	1.8	2.3	3.5	3.4	5.0	7.2	4.4	7.8	6.2
688.4	1.3	1.4	3.2	1.8	3.9	3.5	6.4	5.7	2.2
749.0	3.5	4.4	6.8	8.7	14.8	21.9	15.0	27.5	27.8
751.0	2.4	3.1	5.3	4.3	6.3	10.3	7.4	11.2	12.8
773.0	2.3	4.6	5.6	4.3	9.8	14.1	6.6	15.5	15.7
784.6	5.0	6.8	9.1	6.5	17.1	20.0	7.5	16.7	20.6
786.7	2.8	3.1	5.1	5.9	8.2	9.5	5.5	10.7	11.7
796.6	10.5	14.6	19.4	24.1	41.1	54.7	36.7	68.4	73.0
824.6	2.6	4.1	6.0	6.6	7.2	9.3	6.5	11.4	13.2
917.7		n.d.		1.8	1.5	2.1	1.8	3.9	3.1
919.7		n.d.		1.9	1.5	2.2	2.0	3.9	3.0
955.6		n.d.		2.6	2.8	3.4	3.2	6.6	6.0
979.6		n.d.		2.8	3.6	4.3	4.1	9.3	9.7
1029.3	16.5	12.0	21.2	13.5	29.4	40.3	30.3	25.2	24.0
1191.4	14.2	6.9	12.8	13.0	26.7	33.1	26.2	24.1	21.9
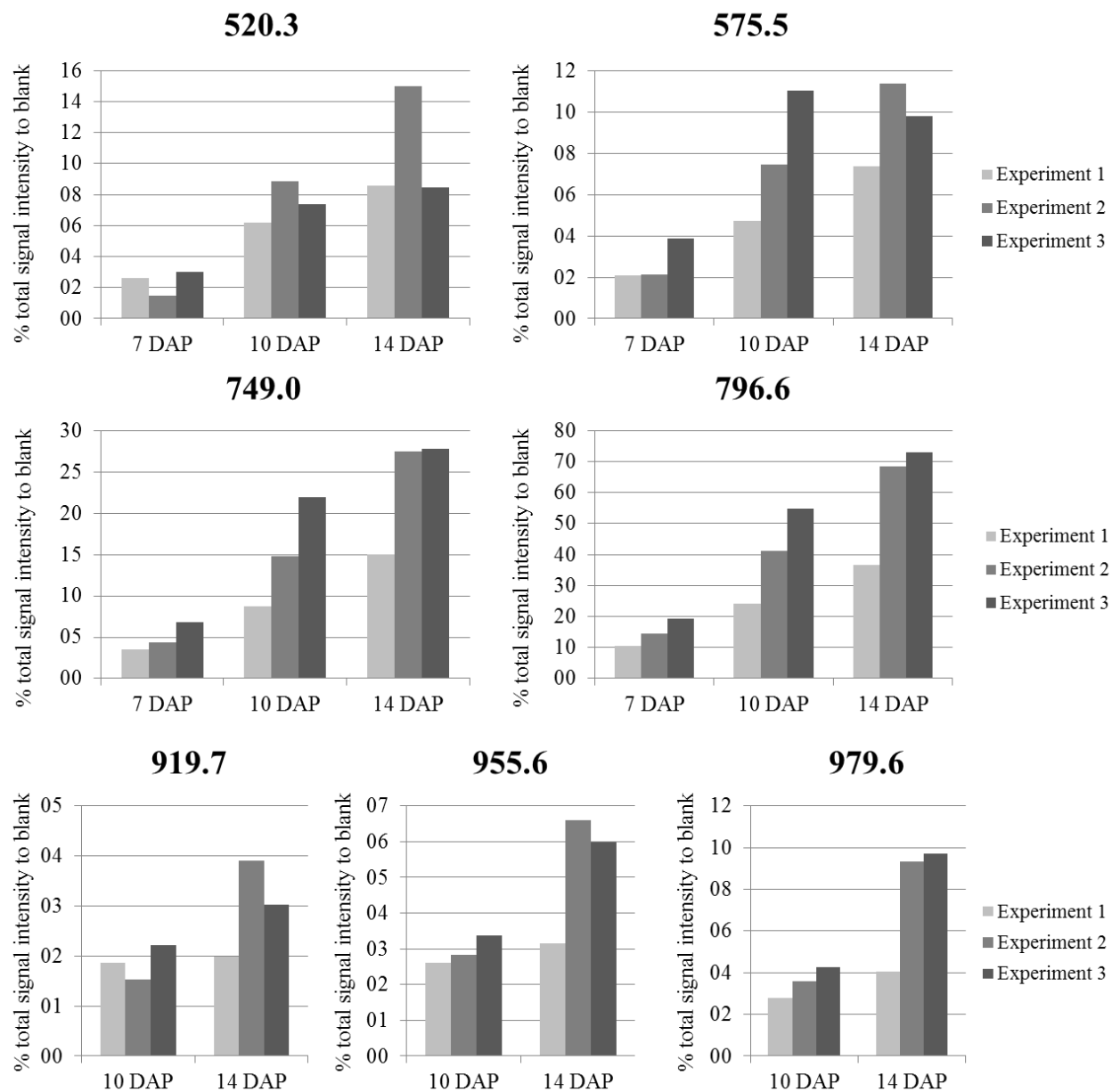
Figure 29: Endosperm specific changes of molecular ion intensities during the storage phase.

Upper part: The four selected *m/z* signals show substantial increasing signal intensities from 7 DAP to 14 DAP.

Lower part: The presented signals were not detected at 7 DAP. From 10 to 14 DAP an increase in the relative signal intensity was observed.

Bar heights correspond to the percentage signal intensity of the selected ions in the endosperm related to the DHB background (=100%). The DHB background corresponds to the mean intensity of five DHB background signals (*m/z* 137, 154, 177, 273, and 409) from the blank region measured simultaneously in all imaging runs.

Table 19: Distribution patterns in the endosperm as observed by the analyses of barley grain cross sections from 14 DAP. Detection of *m/z* values was carried out in SCiLS Lab software (Version 1.0).

***M/z* values with an increasing gradient from the central endosperm to the periphery**	520, 558, 575, 600, 602, 773, 783, 819, 821, 894, 896, 918, 920, 934, 956, 978, 980
Homogeneously distributed *m/z* values in the endosperm	337, 487, 496, 511, 534, 749, 751, 759, 793, 797, 799, 811, 823, 835, 1006, 1055, 1062
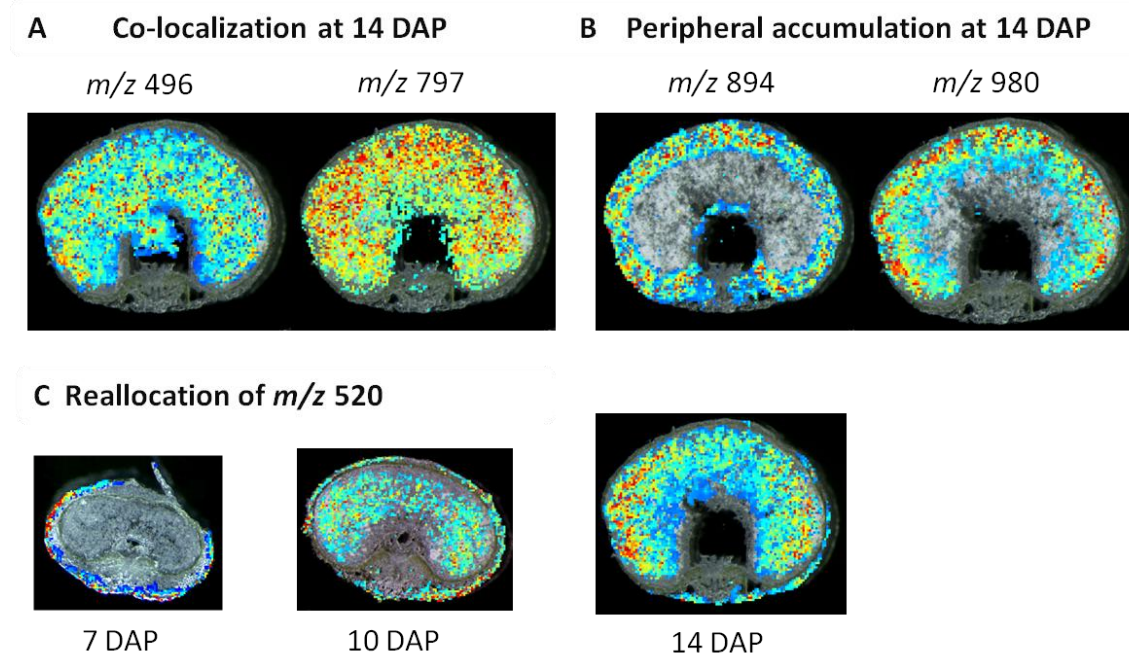
Figure 30: Endosperm specific spatial distributions of molecular ions during the storage phase.

A) Displayed are examples of homogeneously distributed molecules, belonging to phospholipid classes, *m/z* 496 (lysophosphatidylcholine 16:0) and *m/z* 797 (phosphatidylcholine 16:0/18:2).

B) Shown are molecular ions with higher abundance in the peripheral endosperm during the storage phase.

C) During early development *m/z* 520 (lysophosphatidylcholine 18:2) was located in the maternal pericarp, while not being detected in the endosperm. During the storage phase the signal intensity for this molecule increases in the endosperm and vanishes with the diminishing pericarp from the seed enclosure.

Overlays of single ion intensity maps and histological images were generated in SCiLS software (Version 1.0, Non-commercial license). Tentative identifications are given in section 3.2.4.

3.2.4. Tentative identification of compounds

Many signals that show tissue and developmentally specificity were observed by the applied MALDI MSI approach. To integrate these molecular ions into a physiological context of grain development, the identification of them displays a main objective of this study.

A combination of data base searches, comparison to literature data and MS/MS measurements were used for a tentative classification of several substances. In the case of oligosaccharides different enzyme assays were performed for the identification (for detailed results please refer to

section 3.3.). Phospholipids, namely phosphatidylcholines (PCs) and lysophopatidylcholines (LPCs), were classified by their typical fragment ions of *m/z* 104 and 184 and by the neutral loss of *m/z* 59. Some sphingolipids contain also a phosphocholine headgroup (*m/z* 184) but can be differentiated from PCs by the nitrogen rule. A neutral loss of *m/z* 162 is related to a hexose loss, and has been found to be typical for oligosaccharide fragmentation but also for the fragmentation of glycosphingolipids.

MALDI MS/MS measurements were directly performed onto tissue sections, at those positions where the highest signal intensity of a distinct molecular ion was observed (exemplarily displayed in Figure 31). The fragmentation was induced by the supply of high laser energy resulting in the decay of the precursor ions. As the fragments exhibit the same kinetic energy like their corresponding precursor, time windows were set in which the precursor could enter the analyzer with its specific fragment ions. Small time windows were set if several precursor ions had similar *m/z* values, but this resulted in a loss of signal intensity. Overlapping signals could not been isolated (e.g. if the second or third isotope of one molecule overlaps with the first isotope of another).

All tentatively identified molecular ions are listed in Table 20. Several compounds could be validated by literature data. For numerous of the detected *m/z* values no clear fragment pattern could be observed by MALDI MS/MS due to low signal intensities of precursor ions or too much interference with neighboring signals. For some of those signals tentative identifications out of literature data are given. These literature data are also related to a detection of molecules by MALDI TOF MS. Further identifications need targeted analysis as it is represented for oligosaccharides in section 3.3.

Figure 31: Exemplary representation for the identification of a phospholipid.

The precursor ion *m/z* **520** is located in the outer pericarp of a **7 DAP barely grain cross section. The MS/MS measurement was directly carried out on the tissue section in the particular region. The fragment spectrum revealed a phosphocholine fragment ion, typical for the lipid class phosphatidylcholines. The lipid mass prediction tool (Lipid MS Predictor, Version1.5, 2009 by Lipid Maps library) calculates on the precursor *m/z* value, headgroup and kind of adduct ion the related carbon chain. As only one carbon chain is connected to the molecule, it is identified as lysophosphatidylcholine 18:2.**

Table 20: Tentative identifications of detected molecular ions.

The data were obtained by MS/MS measurements, data base search using Lipid MS Predictor (Version1.5, 2009 by Lipid Maps library) and references from literature. In some cases multiple identifications are given as from the obtained *m/z* values the adduct ion could not clearly been distinguished. The green marked molecular ions were found to be endosperm specific during the storage phase (section 3.2.3.). The values for the oligosaccharides are not included here as they are given in the following section (3.3.), where detailed results for sugar analyses are presented.

Abbreviations are: LPC – lysophosphatidylcholine, PC – phosphatidylcholine, n.o. – not obtained, DGDG – digalactosyl-diacylglycerol, HexCer – hexosylceramide.

Precursor	Fragments	Ion	Tentative identification	Literature
184.1	60, 86, 125, 146, 162, 166	[M+H]$^+$	Phosphocholine	
496.4	86, 104, 184	[M+H]$^+$	LPC (16:0)	Zaima et al. (2010b), Fuchs et al. (2007), Enomoto et al. (2011)
518.3	86, 104, 163, 184, 459	[M+H]$^+$	LPC (18:3)	
520.3	86, 104, 184, 258, 321, 502	[M+H]$^+$	LPC (18:2)	Zaima et al. (2010b), Fuchs et al. (2007), Enomoto et al. (2011)
522.3	n.o.	[M+H]$^+$	LPC (18:1)	Zaima et al. (2010b)
533.3		[M+H]$^+$	Pyropheide *a*	Suzuki et al. (2009)
534.3	39, 86, 104, 163, 184, 475	[M+K]$^+$	LPC (16:0)	
538.3	184	[M+H]$^+$	LPC (19:0)	
538.3	184	[M+Na]$^+$	LPC (18:4)	
556.3	86, 104, 163, 176, 184, 205, 345, 459, 497, 533	[M+K]$^+$	LPC (18:3)	Enomoto et al. (2011)
558.3	39, 86, 104, 163, 184, 405, 499	[M+K]$^+$	LPC (18:2)	Zaima et al. (2010b)
566.3	184	[M+Na]$^+$	LPC (20:4)	
592.3		[M*]$^+$	Pheide *a*	Suzuki et al. (2009)
650.5	184, 507	[M+H]$^+$	PC 26:0	
674.5	163, 184, 481, 613	[M+K]$^+$	PC 25:0	
676.5	184	[M+H]$^+$	PC 28:1	
678.5	184	[M+H]$^+$	PC 28:0	
688.4	39, 86, 163, 184, 347, 509, 527, 564, 629	[M+K]$^+$	PC 26:0	
738.1	39, 163, 184, 576, 581, 583, 596, 598		Sphingolipid	
756.6	184, 599	[M+H]$^+$	PC (34:3)	Devaiah et al. (2006)
756.6	184, 599	[M+Na]$^+$	PC (32:0)	
758.6	184	[M+H]$^+$	PC (34:2)	Horn et al. (2012b), Devaiah et al. (2006), Fuchs et al. (2007), Veloso et al. (2011), Enomoto et al. (2011)
760.6	n.o.	[M+H]$^+$	PC (34:1)	Horn et al. (2012), Fuchs et al. (2007), Veloso et al. (2011), Enomoto et al. (2011)

		[M+H]$^+$	PC 36:6	
778.5	147, 184, 598, 720	[M+Na]$^+$	PC 34:3	
		[M+K]$^+$	PC 33:4	
780.6	147, 184, 598, 722	[M+H]$^+$	(PC 36:5)	Veloso et al. (2011)
		[M+Na]$^+$	(PC 34:2)	
782.6	184	[M+H]$^+$	PC (16:0/20:4)	Zaima et al. (2010b); Horn et al. (2012b), Enomoto et al. (2011)
		[M+Na]$^+$	PC (34:1)	Fuchs et al. (2007)
		[M+K]$^+$	PC 33:2	
		[M+Na]$^+$	PC 34:0	Veloso et al. (2011)
784.6	n.o.	[M+H]$^+$	PC 36:3	Horn et al. (2012b), Devaiah et al. (2006), Veloso et al. (2011), Enomoto et al. (2011)
786.7	163, 184, 348, 440	[M+H]$^+$	PC (18:0/18:2)	Devaiah et al. (2006), Fuchs et al. (2007), Veloso et al. (2011), Enomoto et al. (2011)
794.6	86, 163, 184, 736	[M+K]$^+$	PC 34:3	
		[M+K]$^+$	PC 35:3	
796.6	86, 163, 184, 575, 738	[M+K]$^+$	PC (16:0/18:2)	Murphy et al. (2011)
798.6	39, 86, 163, 184, 738	[M+K]$^+$	PC (34:1)	Zaima et al. (2010a)
800.6	n.o.	[M+H]$^+$	PC (38:9)	Vieler et al. (2007)
804.6	39, 86, 147, 163, 184, 198, 600, 622, 635, 739, 746	[M+Na]$^+$	PC (36:4)	Veloso et al. (2011)
820.6	86, 163, 184, 762	[M+K]$^+$	PC (16:0/20:4)	Zaima et al. (2010b)
822.6	86, 163, 184, 762	[M+K]$^+$	PC (36:3)	Zaima et al. (2010a)
824.6	86, 163, 184, 764	[M+K]$^+$	PC (36:2)	Zaima et al. (2010a)
870.6	593, 533	[M-Mg2$^+$+3H]$^+$	Chorophyll *a*	Vieler et al. (2007)
884.7	n.o.	[M+Na]$^+$	HexCer (34:0)	Tanaka et al. (2011)
909.6	n.o.	[M+Na]$^+$	PI (38:4)	Fuchs et al. (2007)
957.6	n.o.	[M+Na]$^+$	DGDG (36:7)	Vieler et al. (2007)
968.7	n.o.	[M+Na]$^+$	HexCer (40:1)	Tanaka et al. (2011)
975.6	n.o.	[M+K]$^+$	DGDG (36:6)	Vieler et al. (2007)

3.2.5.   Summary section 3.2.

Grain development coincides with massive histological changes, demonstrated not only by an increase of seed size, but also by degradation, emergence and specialization of tissues. In particular, the endosperm becomes the main grain part at the storage phase evolving from the fluidic filled embryo sac. High import rates are necessary to facilitate seed development, and

specialized tissues are needed to support the transfer of nutrients from the main vascular bundle to the filial part, e.g. nucellar projection and endospermal transfer cells.

The results of the MSI analysis clearly display the increase of grain complexity and tissue specificity from the prestorage phase to the storage phase. The grouping of detected *m/z* values to functional units by means of Neural Gas clustering is supposed to be related to the adaption of the metabolic status of the tissues according to their functionality. The increment of complexity is additionally indicated by a principal component analysis of signals from depicted ROIs of selected developmental stages (Figure 32).
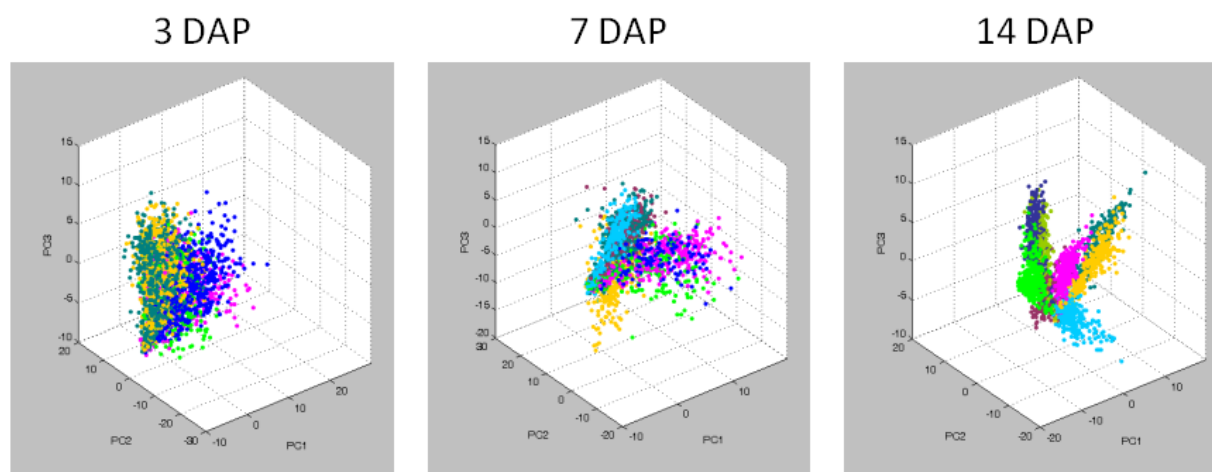
Figure 32: Increment of grain complexity depicted by principal component analysis (PCA) of peak distributions from grains of 3, 7 and 14 DAP. Colors display selected ROIs for each developmental phase. During the prestorage stage just minor grouping was obtained. At 7 DAP a progressing formation of signals according to a tissue affiliation is recognizable, climaxing at 14 DAP, when the signals of particular ROIs form distinct groups.

At all investigated time points a cluster highlighting the chlorenchyma layer was observed, indicating the presence of highly specific molecular ions belonging to this tissue. The outer pericarp forms also a separate cluster, although the composition of corresponding molecular ions changes during development. The same was observed for the embryo, that forms a separate cluster (from 7 DAP on, when the embryo was recognizable), but completely altered in its arrangement. These findings imply that physiological processes occurring in these defined grain parts are highly restricted to them. With the transition to storage accumulation, which starts at 7 DAP, considerable changes occur for the regions of nutrient import and storage deposition. On a small molecule level these changes were not yet obtained for 7 DAP by means of MALDI MSI. But from the early storage stage on (10 DAP), separate clusters for the transfer region and the

endosperm could be distinguished highlighting the peculiarities of both seed parts for the storage accumulation stage.

From all tissues, the most interesting molecular ion patterns were observed for the endosperm and the transfer region. Several molecular ions were detected showing increasing signal intensities in the rising endosperm. Some of them were identified to belong to the phospholipid classes of phosphatidylcholines and lysophosphatidylcholines. The distribution patterns of oligosaccharides exhibited massive changes during grain development. Thus, they were suggested to be involved in physiological processes that are important for the transport and/or the storage accumulation. These molecular species were taken as candidate compounds for further targeted analyses, which are presented in section 3.3.

3.3.   Reallocations of Oligosaccharides with the Beginning of the Storage Phase

Development and tissue-specific distributions of molecular ions during barley grain development were revealed by the MALDI MSI approach as described in section 3.2. Tentative identifications revealed candidate compounds, chosen for further targeted analysis. Among them, oligosaccharides were found to show highly specific distributions during the storage phase and are assumed to have an impact on grain filling processes.

Sucrose plays the central role in plant primary metabolism. It is the main end product of photosynthesis and the major transport form of sugars. The transport from the mother plant into the developing grain occurs mostly through the vascular bundle, located in the ventral crease. Especially, for the synthesis of starch, the main storage compound of cereal grains, a massive import of sucrose during the storage phase is required. The utilized MALDI MSI approach allowed the detection of small oligosaccharides up to a degree of polymerization (DP) of 7. During the ionization process in the MALDI source the sugars tend to form adduct ions with sodium or potassium. Direct investigations of tissue sections revealed a higher rate of potassium adducts so that images shown here regard to the $[M+K]^+$ ions.

In this section, the identification of oligosaccharides by MS/MS is presented (3.3.1.). The specific distribution patterns during development are shown in 3.3.2. Targeted analyses went for digestion assays (3.3.3.) and a quantification of the respective sugars (3.3.4.). It is hypothesized that these kind of sugars are not transported into the developing grain, but are synthesized in the tissues

connected to the cavity. Initial results regarding this proof of *de novo* synthesis by transcriptomic and proteomic approaches are described in 3.3.5.

3.3.1. Identification of oligosaccharides by MALDI MS/MS measurements

Oligosaccharides are composed of hexose subunits that form glycosidic bonds by the elimination of a water molecule. That reveals a nominal mass difference between the single DP's of *m/z* 162. During MS/MS analysis the glycosidic bonds can be broken by an increase of the laser energy, resulting in a pattern of different DP's in the MS/MS spectrum. Here, oligosaccharides were identified directly by MS/MS fragmentation of precursor ions from the tissue sections (exemplarily displayed in Figure 33).
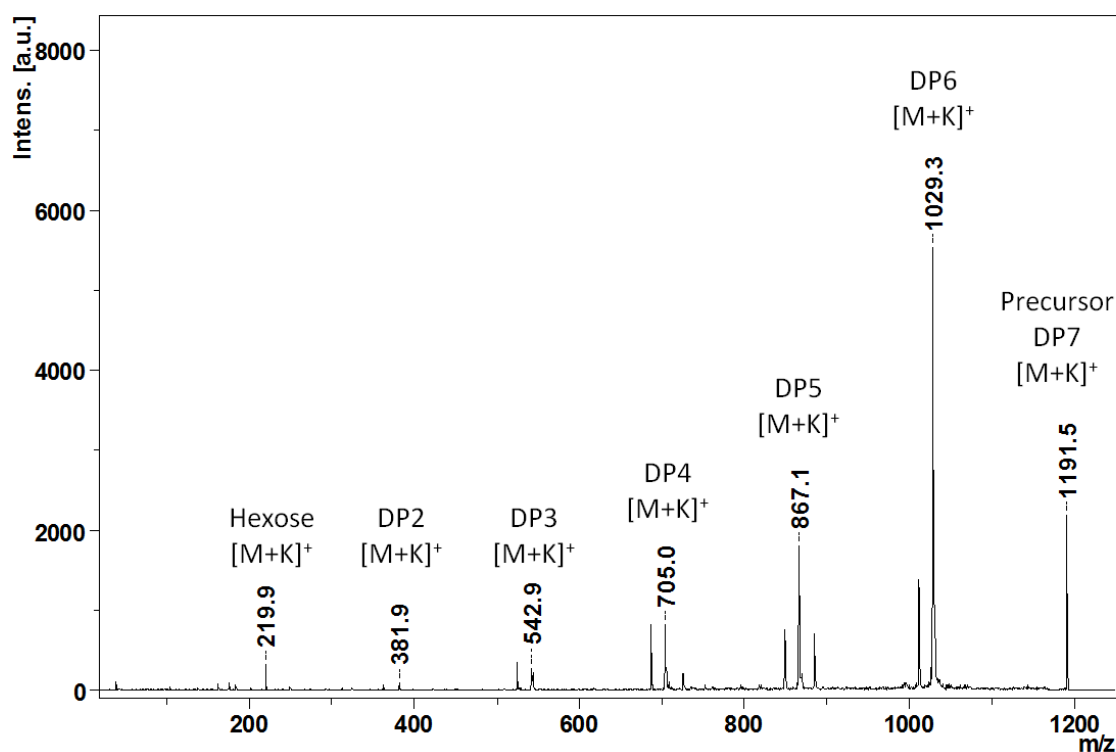
Figure 33: Identification of Oligosaccharides by MALDI MS/MS measurements from tissue sections.

The fragmentation pattern of the precursor ion *m/z* 1191 revealed the typical mass differences of *m/z* 162 between fragment ions down to hexose monomers. Thus, the precursor was identified as an oligosaccharide of DP 7.

Additionally to the breakdown of hexose subunits, the MS/MS measurements revealed a neutral loss of a water molecule (M-H_2O+K]$^+$ for each particular fragment ion. As it was observed for the precursor ions, also the sugar fragments formed adduct ions with potassium (Table 21). While MALDI MS/MS analysis allowed an assignment of oligosaccharides by their specific fragment

patterns, a clear identification of the hexose subunits was not possible, as hexoses such as fructose, glucose and galactose share all the same molecular mass. Therefore, targeted analyses were carried out (please refer to section 3.3.3.).

Table 21: Determination of MALDI MS/MS fragment patterns from oligosaccharides.
Given are the potassionated precursor ions used for MS/MS fragmentation and the corresponding fragment ions.

Sugar molecule	Precursor ion $[M+K]^+$	Chemical formula	Observed fragment ions [m/z]	Corresponding ions
Disaccharide	381	$C_{12}H_{22}O_{11}$	201.3	$[Hexose-H_2O+K]^+$
			219.3	$[Hexose +K]^+$
Trisaccharide	543	$C_{18}H_{32}O_{16}$	363.1	$[Disacch.-H_2O+K]^+$
			381.1	$[Disacch. +K]^+$
Tetrasaccharide	705	$C_{24}H_{42}O_{21}$	363.0	$[Disacch.-H_2O+K]^+$
			381.1	$[Disacch. +K]^+$
			525.0	$[Trisacch.-H_2O+K]^+$
			543.0	$[Trisacch.+K]^+,$
Pentasaccharide	867	$C_{30}H_{52}O_{26}$	363.0	$[Disacch.-H_2O+K]^+$
			381.0	$[Disacch. +K]^+$
			525.0	$[Trisacch.-H_2O+K]^+$
			543.1	$[Trisacch.+K]^+$
			687.2	$[Tetrasacch.-H_2O+K]^+$
			705.2	$[Tetrasacch.+K]^+$
Hexasaccharide	1029	$C_{36}H_{62}O_{31}$	525.0	$[Trisacch.-H_2O+K]^+$
			543.1	$[Trisacch.+K]^+$
			687.1	$[Tetrasacch.-H_2O+K]^+$
			705.1	$[Tetrasacch.+K]^+$
			849.1	$[Pentasacch.-H_2O+K]^+$
			867.2	$[Pentasacch.+K]^+,$
Heptasaccharide	1191	$C_{42}H_{72}O_{36}$	219.9	$[Hexose +K]^+$
			362.7	$[Disacch.-H_2O+K]^+$
			381.9	$[Disacch. +K]^+$
			524.9	$[Trisacch.-H_2O+K]^+$
			542.9	$[Trisacch.+K]^+$
			687.0	$[Tetrasacch.-H_2O+K]^+$
			705.0	$[Tetrasacch.+K]^+$
			849.1	$[Pentasacch.-H_2O+K]^+$
			867.1	$[Pentasacch.+K]^+$
			1011.3	$[Hexasacch.-H_2O+K]^+$
			1029.3	$[Hexasacch.+K]^+$

3.3.2. Specific accumulations of oligosaccharides during the storage phase

Analyses of developmentally depending distribution patterns revealed specific changes of the identified oligosaccharides between the prestorage stage (3 DAP) and the storage phase (14 DAP). To this reason, imaging experiments were extended to the analysis of cross sections from 17 and 20 DAP old barley grains, representing the late storage phases.

The results of MALDI MSI measurements are illustrated in Figure 34, displaying the disaccharide, trisaccharide and hexasaccharide distributions in cross sections of different developmental stages. During the early development (3 and 7 DAP) the disaccharide was found to be co-localized, but at 10 DAP an increased abundance in the endosperm was observed that was clearly visible at 14 DAP. Furthermore, at 14 DAP the disaccharide exhibited higher signal intensities around the endospermal cavity as well. During the late storage phase (17 and 20 DAP) the disaccharide is more accumulated in the cavity surrounding tissues, namely, in the endospermal transfer cells (ETC), and in the nucellar projection (NP). All detected oligosaccharides of DP 3 to DP 7 showed a higher distribution in the maternal pericarp during the prestorage phase (3 DAP). At 7 DAP co-localizations for all oligosaccharides were observed. With the early storage phase (10 DAP) an enrichment of the small oligosaccharides of DP 3 and 4 in the area of the emerging cavity was revealed, whereas the higher oligosaccharides of DP 5, 6 and 7 showed more intense signals in the endosperm. These patterns were increasingly exhibited at 14 DAP and persisted at the late storage phases (17 and 20 DAP): Tri- and Tetra-saccharides particularly accumulated in the area around the cavity. Larger oligosaccharides (DP 5 to 7) were enriched in the central endosperm.
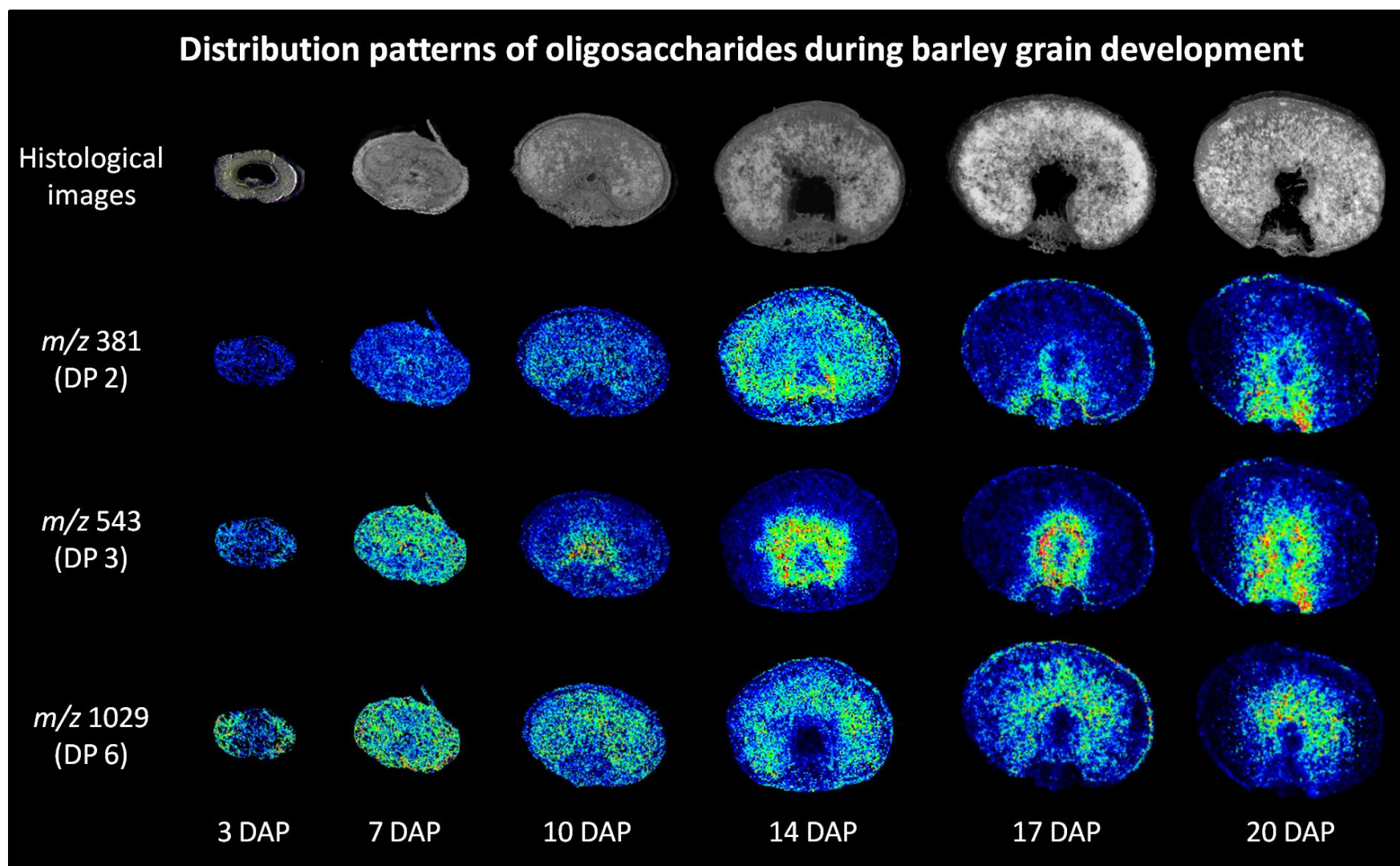
Figure 34: Distribution patterns of oligosaccharides during barley grain development.

Shown are MALDI MSI single ion intensity maps displaying the distributions of oligosaccharides of DP 2 (*m/z* 381), DP 3 (*m/z* 543) and DP 6 (*m/z* 1029) in cross sections of investigated developmental steps along with the corresponding histological images.

3.3.3. Enzymatic identification of sucrose and oligo fructans in the emerging cavity

The aim was to identify the hexose subunits of the detected oligosaccharides. Different sugar classes are known to be present in barley grains; those of the raffinose family (sucrose + galactose subunits), and those of the fructan class (sucrose + fructose subunits). The most abundant disaccharide is sucrose, but maltose is present in barley grains as well. As mentioned above, MALDI MS/MS analysis was not suited for a clear identification of the oligosaccharide composition, as the hexose monomers share the same molecular mass. Therefore, digestion reactions using specific sugar hydrolyzing enzymes were carried out. Invertase (INV) and α-galactosidase (GAL) were commercially obtained. For the fructosyl 1-exohydrolase (1-FEH) a *Pichia pastoris* expression clone was kindly provided by Prof Wim Van den Ende (KU Leuwen, Belgium).

To confirm the substrate specificity of the used enzymes, tests with different standard sugar compounds were performed. The treatments revealed a high specificity of 1-FEH for fructosyl oligomers. These were degraded to fructose monomers and to sucrose that cannot be degraded by 1-FEH. The invertase (INV) degrades sucrose to fructose and glucose. In addition, this enzyme was found to be capable to digest fructosyl oligosaccharides such as 1-kestose and nystose and hydrolyzed them into the monomers. This is also described by Nilsson et al. (1987). Sugars from the raffinose family were not degraded by INV. These types of sugars (raffinose and stachyose) were specifically hydrolyzed by GAL. The outcomes of these enzymatic pretests are summarized in Table 22.

Table 22: Standard oligosaccharide compounds used for the confirmation of the substrate preferences of the selected enzymes.

Digestion assays were performed according to the specifications of the respective enzymes using a 1mM concentration of the particular sugars. Measurements were carried out by MALDI TOF MS. + denotes degradation; – denotes no degradation.

Compound	Digestion with INV	Digestion with 1-FEH	Digestion with α-GAL
Sucrose	+	–	–
Trehalose	–	–	–
Maltose	–	–	–
Raffinose	–	–	+
1-Kestose	+	+	–
Maltotriose	–	–	–
Nystose	+	+	–
Stachyose	–	–	+

The digestion with INV was directly performed onto tissue sections of 14 DAP barley grains and subsequently analyzed by MALDI MSI. To keep the distribution patterns of the molecules, the enzyme was sprayed onto the sections and incubated prior to matrix application (a detailed description is given in section 2.5.3.). The simultaneous MSI measurement of treated sample and control secured the direct comparison of signal intensities between both samples. Figure 35 shows a typical result from an on-tissue digestion experiment. Here, an intense signal at *m/z* 219 after digestion was observed due to the degradation of sucrose and to the release of fructose from fructosyl oligosaccharides. This result is also presented by single ion intensity maps (lower part of Figure 35). The abundance of the product ion *m/z* 219 is displayed by an intense blue coloration as revealed for the digested tissue section and not for the control section. Invertase treatment leads to a nearly complete remove of the DP 2 substrate ion and of the DP 3 oligomer, shown by the less green colored intensity in the digested tissue slice. As been exhibited from the cavity average spectrum of the digested tissue slice, also oligosaccharides of DP 5, 6 and 7, which are present in cavity as well, were partly degraded (Figure 35, upper part). Hence, the MSI experiments of on tissue digested samples revealed a high accumulation of sucrose, and in addition, indicated an accumulation of fructosyl oligosaccharides in the cavity.

Average spectrum of the control cavity

Average spectrum of the digested cavity

Samples

Product ion 219 [M+K]$^+$

Substrate ion [381 M+K]$^+$

Substrate ion [543 M+K]$^+$
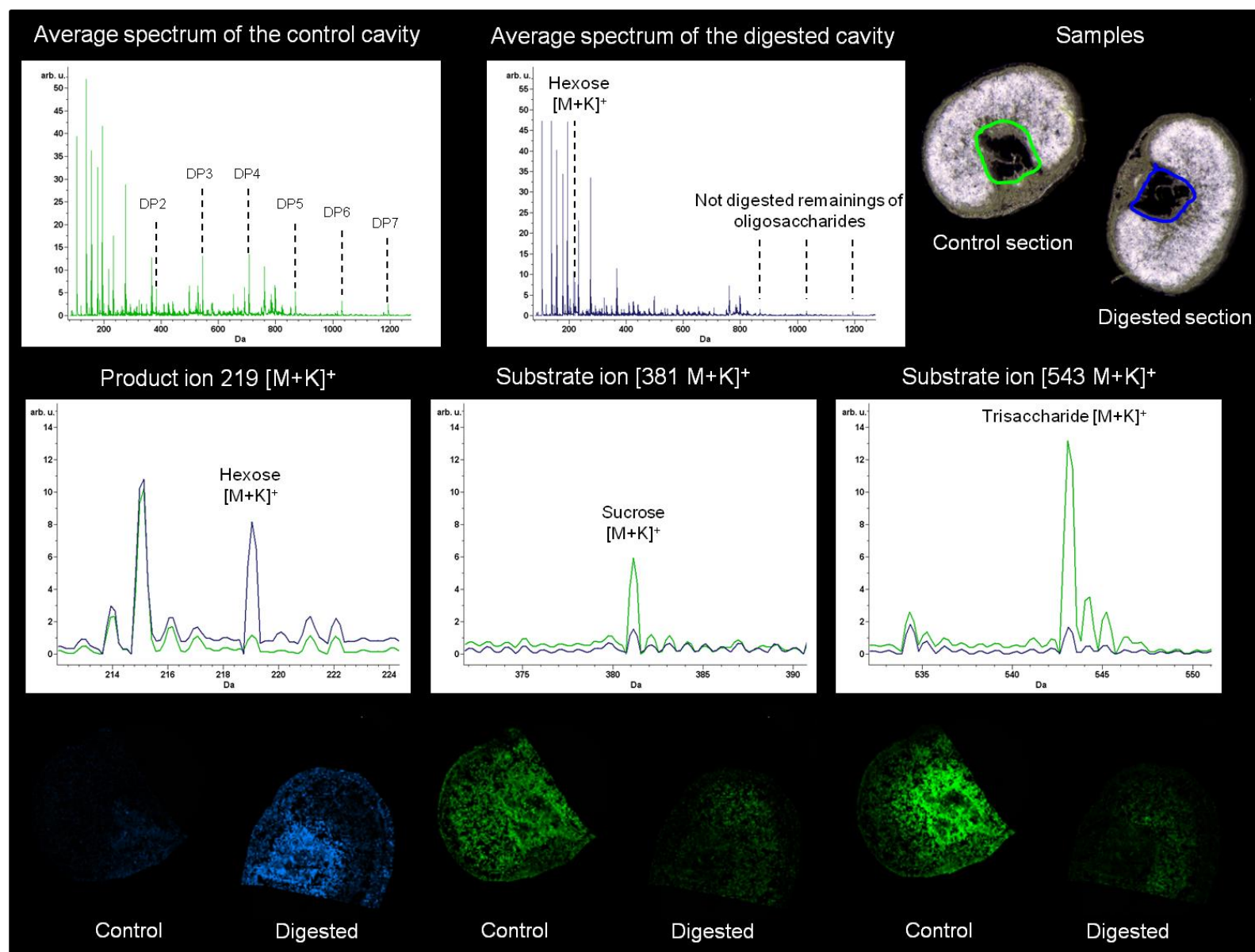
(Description next page)

Figure 35: MALDI MSI of on-tissue digested and control sections from a 14 DAP barley grain.

Upper part: Shown are the average spectra of the cavity for the control section (green) and for the digested one (blue). The typical pattern for oligosaccharides was obtained in the control, whereas after digestion a nearly complete degradation of the sugar signals was observed. Close ups into the overlay of both average spectra illustrate the differences in the signal intensities. The product ion at *m/z* 219 was absent in the control (green). The substrate ions sucrose (*m/z* 381) and the trisaccharide (*m/z* 543) were present in the control, but vanished after digestion. The average spectra were generated in ClinProTools software (Bruker).

Lower part: The single ion intensity maps display the distributions of the molecular ions according to the spectra extracts above. The light blue demonstrates a high signal intensity of the product ion in the digested tissue slice, whereas light green denotes high signal intensities for the substrate ions in the control section that are much reduced in the digested sample.

The identification of the oligosaccharide composition by *in situ* digestion was complemented by *in vitro* assays. The sap of the emerging cavity was collected, purified by SPE and taken for enzyme treatments (details are given in section 2.5.3.). The analyses were carried out by MALDI TOF MS and validated by GC-MS. *In vitro* digestion of the cavity sap with invertase (summarized in Table 23) revealed a complete digestion of sucrose as the molecular ion *m/z* 381 was not detectable, and an intense signal appeared for the resulting hexoses at *m/z* 219 (Figure 36). Additionally, invertase is able to break down fructosyl-oligomers as it was shown by digestion of the standards 1-kestose and nystose (Table 22). Equally to the results from the on tissue digestion with invertase, a partial degradation of the oligosaccharides was confirmed. Using the enzyme 1-FEH a complete degradation of sugars of DP 3 to DP 7 was revealed for the cavity sap. Here, product ions are sucrose (*m/z* 381) that cannot be degraded by 1-FEH, and the hexose subunits (*m/z* 219) (Figure 36, Table 23). On the contrary, the digestion with GAL resulted in no difference of the sugar pattern compared to the negative control, and a monomer was rarely detectable (Figure 36). These experiments additionally demonstrated that a high accumulation of oligosaccharides in the cavity is related to fructosyl oligomers.
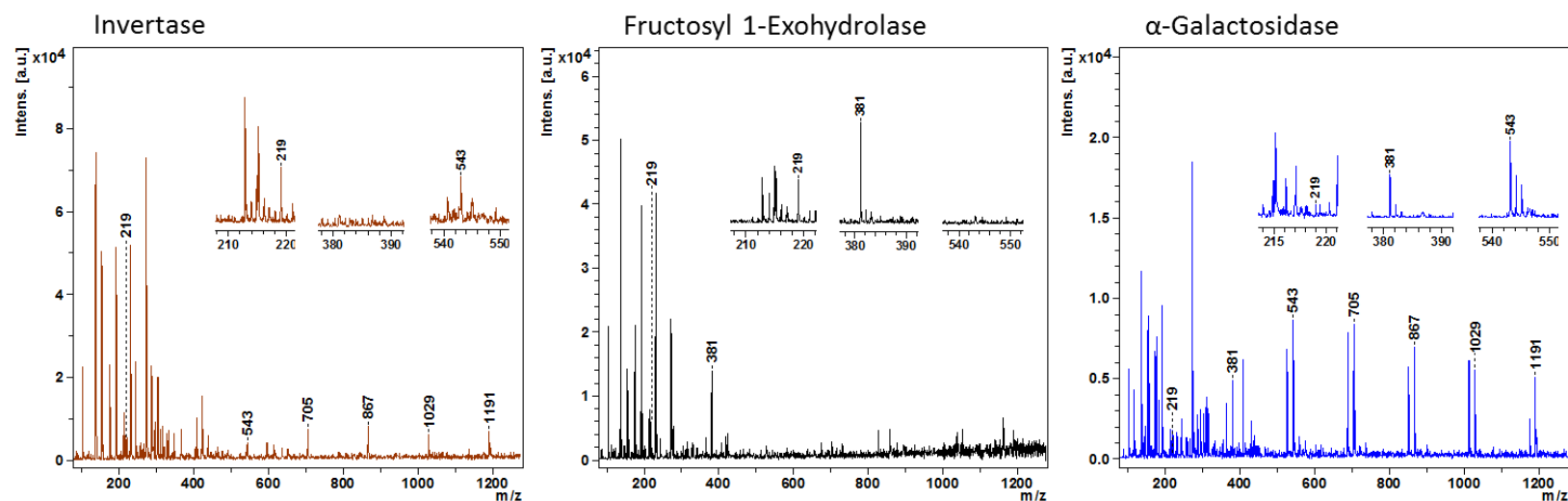
Figure 36: Representative MALDI mass spectra of digested cavity extracts.

The profiles show the sugar patterns after treatment with the particular enzymes. The enlargements illustrate the substrate ions (*m/z* 381 and 543), and the formation of the product ion (*m/z* 219). Invertase digestion revealed a complete degradation of sucrose and partly a degradation of the oligosaccharides. Fructosyl 1-exohydrolase completely cleaved all oligosaccharides, resulting in the formation of the product ions sucrose (*m/z* 381) and the hexoses (*m/z* 219). The sugar pattern after treatment with α-galactosidase didn't changed compared to non-treated samples, with the tri- and tetrasaccharide as the most intense signals.

Table 23: Summary of the results for *in vitro* digestion of cavity sap from 14 DAP barley grains.

Cavity sap was digested using three different enzymes specific for the breakdown of particular oligosaccharides: Invertase, fructosyl 1-exohydrolase and α-galactosidase. The negative control was treated with buffer, but without enzymes. Enzyme assays were analyzed by MALDI TOF MS measurements. + denotes detection; - denotes no detection.

Compound	Invertase	Fructosyl 1-exohydrolase	α-Galactosidase	Negative control
Hexose	Intense signal	Intense signal	Low signal	Low signal
Disaccharide	–	Highest intensity	+	+
Trisaccharide	Low signal	–	Intense signal	Intense signal
Tetrasaccharide	+	–	Intense signal	Intense signal
Pentasaccharide	+	–	+	+
Hexasaccharide	+	–	+	+
Heptasaccharide	+	–	+	+

GC-MS analysis of digestion assays confirmed the results from MALDI TOF MS measurements (Table 24). The treatment of cavity sap with 1-FEH that cleaves fructosyl oligomers into fructose subunits and sucrose revealed for both developmental stages an obvious increase of the sucrose signal and of the fructose signal. In contrast, the glucose level didn't change as the enzyme is not able to cleave sucrose. For 1-kestose a mixed pattern was observed due to the successive breakdown of larger oligo fructans (such as nystose and fructans of DP 5, 6 and 7) forming 1-kestose as an intermediate product. Even after 30 minutes the hydrolyzation was not completed. The digestion with invertase revealed almost complete sucrose degradation after ten minutes, and in addition of 1-kestose. For α-galactosidase no differences were obtained between the negative control (cavity sap treated with the inactivated enzyme), and the cavity sap treated with the active enzyme. Thus, the presence of high amounts of 1-kestose in the cavity sap was verified.

Table 24: Determination of sugars by GC-MS after enzymatic digestion of cavity sap.

Purified cavity sap from 14 and 20 DAP old barley grains was treated with respective enzymes for two time intervals. As a control enzymes were heated to 95°C prior to addition to samples. Subsequently after digestion samples were again purified by SPE to remove proteins. Displayed are peak areas of extracted ions according to the respective sugar compounds.

Enzyme	Kernel age	Incubation	Peak area				Result
			Fructose	Glucose	Sucrose	1-Kestose	
1-FEH	14 DAP	Control	1.7	4.0	21.3	2.4	- Sucrose and fructose are formed as products in a time dependent manner - 1-kestose as intermediate degradation product of the hydrolyzation of larger oligo fructans
		10 min	19.9	5.7	109.4	11.9	
		30 min	51.5	8.7	179.5	4.1	
	20 DAP	Control	0.7	2.9	70.2	3.1	
		10 min	15.8	5.0	177.5	18.4	
		30 min	32.6	4.1	205.6	8.8	
INV	14 DAP	Control	1.8	4.8	21.1	0.8	- Complete degradation of sucrose and 1-kestose after 30 minutes - Glucose and fructose are formed as products in a time dependent manner
		10 min	45.1	38.5	0.6	0.1	
		30 min	122.2	85.0	0.1	n.d.	
	20 DAP	Control	0.6	3.0	64.4	3.5	
		10 min	325.3	268.7	0.9	0.1	
		30 min	382.8	294.2	0.0	0.0	
GAL	14 DAP	Control	3.4	7.1	48.7	34.6	- No degradation of sucrose and 1-kestose - Levels of hexoses didn't change
		10 min	4.4	8.9	51.7	36.4	
		30 min	3.5	7.2	38.2	30.7	
	20 DAP	Control	0.9	3.6	123.9	40.7	
		10 min	2.3	5.1	152.2	42.2	
		30 min	1.9	5.3	140.9	41.6	

3.3.4. High quantity of 1-kestose and nystose in the cavity during the storage phase

The aim was to quantify the sugars in the cavity in dependence of the developmental stage of the grains. In addition, the proportion of the sugar concentration in the sap to the sugar concentration in the remaining kernel, and to earlier stages of grain development was elucidated. As described before, fructosyl oligosaccharides were found accumulate with the beginning of the storage stage in the region of the emerging cavity. From MALDI MS measurements no conclusions about the absolute quantities can be made. Thus, targeted analyses by LC separation and amperometric detection were performed in collaboration with Prof Wim Van den Ende (KU Leuwen, Belgium). The results for the quantification of hexoses, sucrose and of oligo fructans are presented in Table 25. For each developmental step seeds from two independent harvests were prepared.

Table 25: Determination of sugar concentrations in developing barley grains.

Given are the concentrations of hexoses and oligosaccharides related to fructan metabolism in extracts of cavity sap, transfer tissues, remaining kernels and total kernels. The concentrations correspond to fresh weight (FW) in µmol/g. Quantification was done by LC separation and electrochemical detection.

Developmental Stage	Sample	Sugar concentration [µmol/g FW]					
		Glucose	**Fructose**	**Sucrose**	**1-Kestose**	**Nystose**	**Bifurcose**
3 DAP	Total kernels	6.90	8.22	9.38	3.63	0.59	4.92
3 DAP	Total kernels	4.08	4.66	7.49	3.69	0.65	3.91
7 DAP	Transfer tissues	4.72	3.99	15.66	3.02	0.34	6.34
	Remaining kernels	4.34	3.57	9.76	2.67	0.26	3.55
	Total kernels	5.73	4.10	11.35	3.61	0.35	5.20
7 DAP	Transfer tissues	2.54	2.26	12.83	2.30	0.38	4.93
	Remaining kernels	2.10	1.27	4.78	1.09	0.17	1.77
	Total kernels	4.70	2.39	8.64	2.98	0.39	4.07
10 DAP	Cavity extract	5.68	7.92	19.24	13.10	5.22	3.83
	Remaining kernels	0.12	0.12	0.69	0.12	0.04	0.12
	Total kernels	1.44	1.31	5.38	1.29	0.36	1.52
10 DAP	Cavity extract	2.88	3.25	19.86	14.52	5.86	5.01
	Remaining kernels	0.80	0.70	3.03	0.63	0.14	0.93
	Total kernels	3.38	2.68	10.51	2.85	0.69	4.27
14 DAP	Cavity extract	2.66	5.29	21.13	26.56	8.34	1.43
	Remaining kernels	0.08	0.14	0.82	0.15	0.04	0.09
	Total kernels	0.37	0.57	2.97	0.81	0.25	0.47
14 DAP	Cavity extract	4.04	7.38	18.28	24.69	6.95	0.88
	Remaining kernels	0.14	0.22	0.94	0.27	0.06	0.07
	Total kernels	0.37	0.47	1.88	1.01	0.25	0.14

Most remarkable are the steeply ascending concentrations of 1-kestose in cavity extracts from 10 DAP on (Figure 37b, Table 25). The concentration of this sugar in dissected transfer tissues at 7 DAP was found to be similar compared to the total grain concentration, and was even the same at 3 DAP. A similar kinetic pattern was obtained for nystose. The concentration of this molecule rises in the cavity during the storage stage as well, but not to the same extent as it was observed for 1-kestose (Figure 37c, Table 25). Sucrose also accumulates in cavity extracts compared to the total kernel concentration. Actually for this molecule, higher concentrations in the transfer tissues at 7 DAP were revealed. But just a slight increase was found from 7 to 14 DAP for the transfer tissues/cavity concentrations (Figure 37a, Table 25). For total kernels the concentrations of 1-kestose and sucrose decreased, pointing out that a reallocation for both molecules occurs during barley grain development. A converse result was found for bifurcose. The highest concentrations were obtained in the transfer tissues at 7 DAP. To 10 DAP a slight decrease, followed by a steep decline to 14 DAP was measured, indicating a diverse, developmentally depending distribution of this structural isomer to nystose (Figure 37d, Table 25). For the hexoses, accumulations in the cavity sap were observed as well, but decreasing total kernel concentrations of fructose and glucose were obtained through the investigated developmental stages.
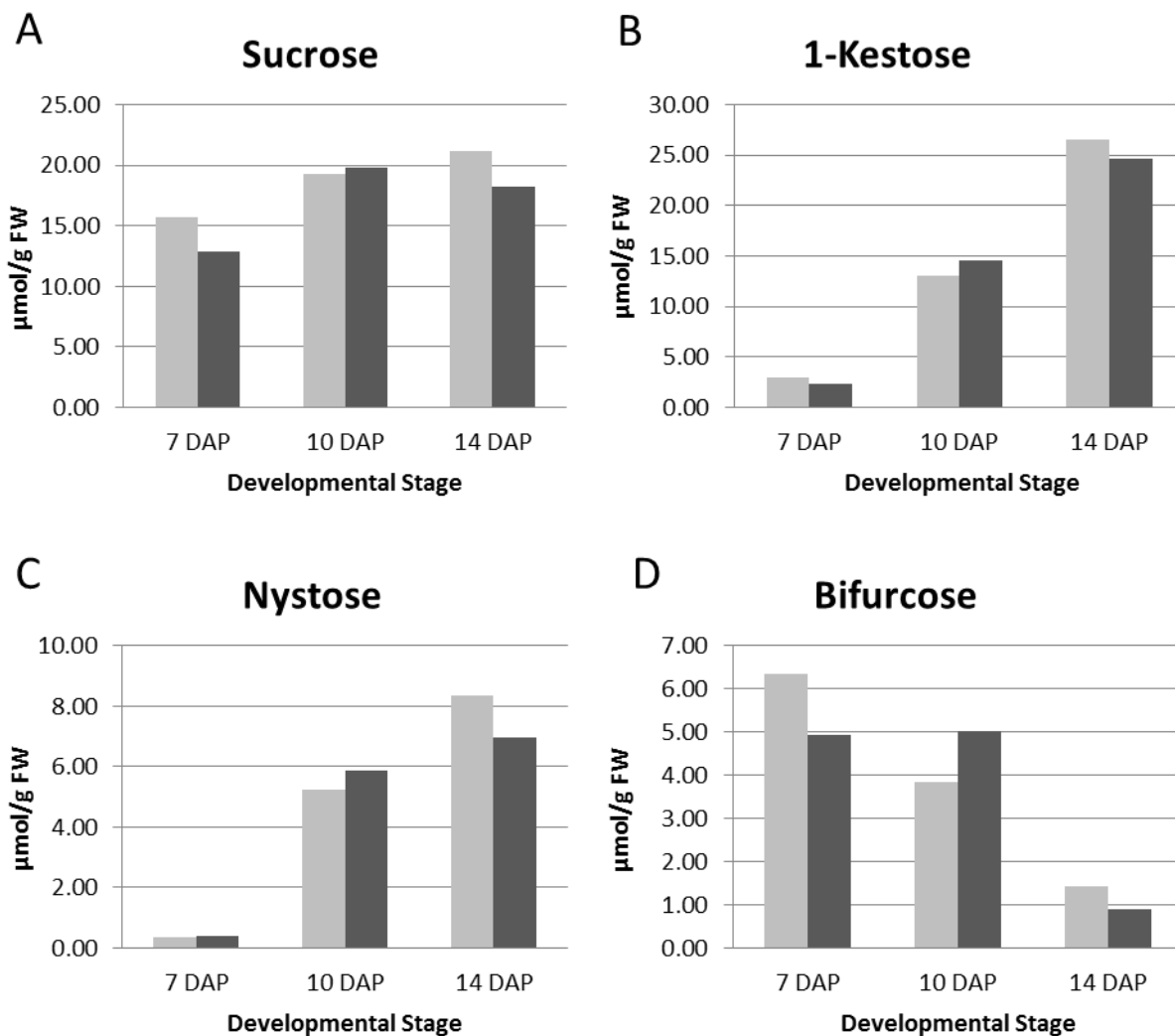
Figure 37: Developmentally depending sugar concentrations in separated transfer region (7 DAP) and cavity extracts (10 and 14 DAP) of barley grains.

The diagrams illustrate the outcomes (as shown in Table 26) from the quantification by means of LC and electrochemical detection.

a) For sucrose a slight increase from 7 to 14 DAP for the transfer tissues/cavity extracts was observed.

b) 1-Kestose revealed the highest developmental differences in its concentration, steeply increasing from 7 to 14 DAP.

c) Nystose also exhibited a high increase of the cavity sap concentration.

d) For the bifurcose concentration a contrary pattern was obtained. This compound diminishes from 7 to 14 DAP.

3.3.5. Investigation of a oligo fructan biosynthesis in barley grains

Sucrose is known to be the major transport form of carbohydrates from source to sink organs. Also hexoses like glucose or fructose in principle can be transported through the phloem, but the presence of oligo fructans in the phloem sap was not determined (Amiard et al., 2003). It is assumed that a high accumulation of 1-kestose and nystose associated to the emergence of the cavity resulted from *de novo* synthesis in this region. MALDI MSI measurements of stem tissues that were cut directly below the spikes revealed that oligo fructans are not accumulated in such high dimensions as it was observed for grains during the storage phase (Figure 38). In addition, determination of the individual oligo fructans in stem tissues beneath the spikes from the different developmental stages revealed just minor amounts (Appendix 5). In order to provide evidences for a *de novo* biosynthesis of oligo fructans in grains, transcriptomic and proteomic approaches were chosen.
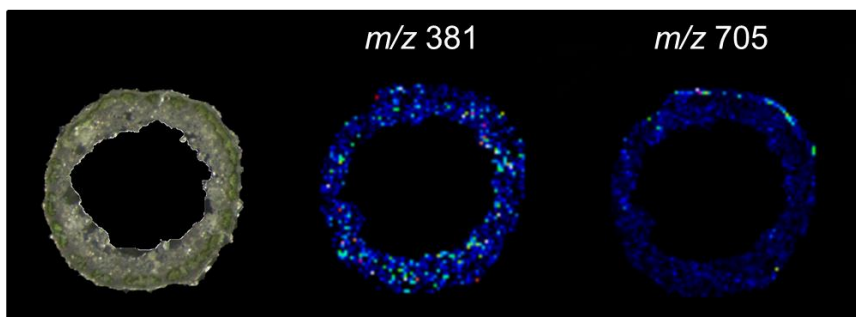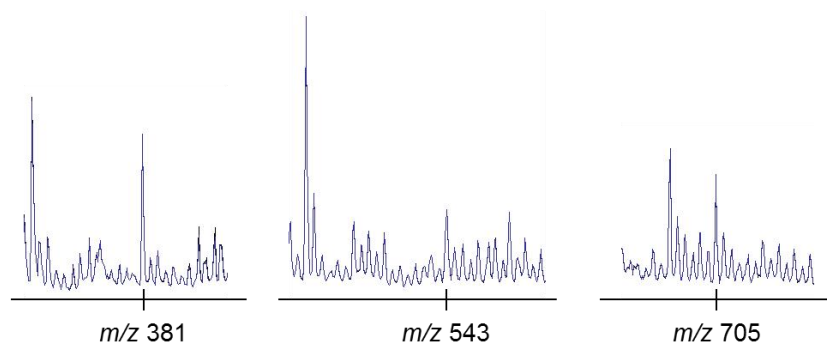
Figure 38: MALDI MSI of a 14 DAP barley stem.

The stem was directly cut beneath the spike. Measurement was carried out in same way as described for grain tissues.

A) The morphological image (left) shows a hollow stem. The single ion intensity maps for sucrose (*m/z* 381) and the tetrasaccharide (*m/z* 705) display an unspecific distribution of molecular ions over the sample surface.

B) Extracts from the sum mass spectrum indicate only low signal intensities for the sugars of DP 2, 3 and 4. Among them, the highest signal intensity was observed for sucrose (*m/z* 381). Tri- and tetrasaccharides are just slightly above the noise.

3.3.5.1. Tissue and developmentally specific gene expression for fructan metabolism

The expression of genes involved in fructan metabolism was proven by qRT-PCR analysis. The experiments were carried out in collaboration with Dr. Johannes Thiel (IPK Gatersleben, Seed Development Group) using cDNA libraries from micro-dissected seed material of different developmental stages of barley. As the highest accumulations of 1-kestose and nystose were found in those grain parts, where the transfer of nutrients is mediated, the analyses were performed for the nucellar projection (NP), the endospermal transfer cells (ETC) and the endosperm. Specific Primers for the candidate genes (Figure 39) were generated based on published gene sequences for 1-SST, 1-FFT, 6-SFT, 1-FEH, and 6-FEH from barley. As these enzymes are related to invertases (sequence homologies and sucrose cleaving capacities of 1-SST, 1-FFT and 6-SFT), sequences of a barley extracellular invertase, and of two isoforms of vacuolar invertases were additionally included in the qRT-PCR analyses (for details please refer to section 2.6.).
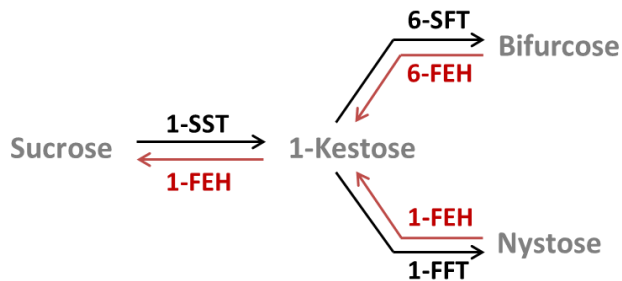
Figure 39: Schematic view of enzyme activities from fructan metabolism.

The biosynthetic genes from fructan metabolism (1-SST, 1-FFT and 6-SFT) were found to be specifically expressed in a tissue and developmentally depending manner (Figure 40). 1-SST, responsible for synthesis of 1-kestose out of two molecules sucrose (Figure 39), is expressed in both cell types of the NP at the transition stage (7 DAP), and in the dividing cells of the NP at the early storage phase (10 DAP), when NP2 starts to degenerate. Additionally, 1-SST expression was found in the endosperm at 5 DAP with decreasing levels to 7 and 10 DAP. Expression of 1-FFT relates to 1-SST. This enzyme catalyzes the elongation of 1-kestose to nystose and was also revealed to be specific for the NP, especially for the dividing part of the NP at 7 and 10 DAP. In contrast, the expression of 6-SFT is specific for the endosperm at the prestorage stage (5 DAP) and at the transition phase (7 DAP). This enzyme is involved in the synthesis of bifurcose and further of levan type fructans.
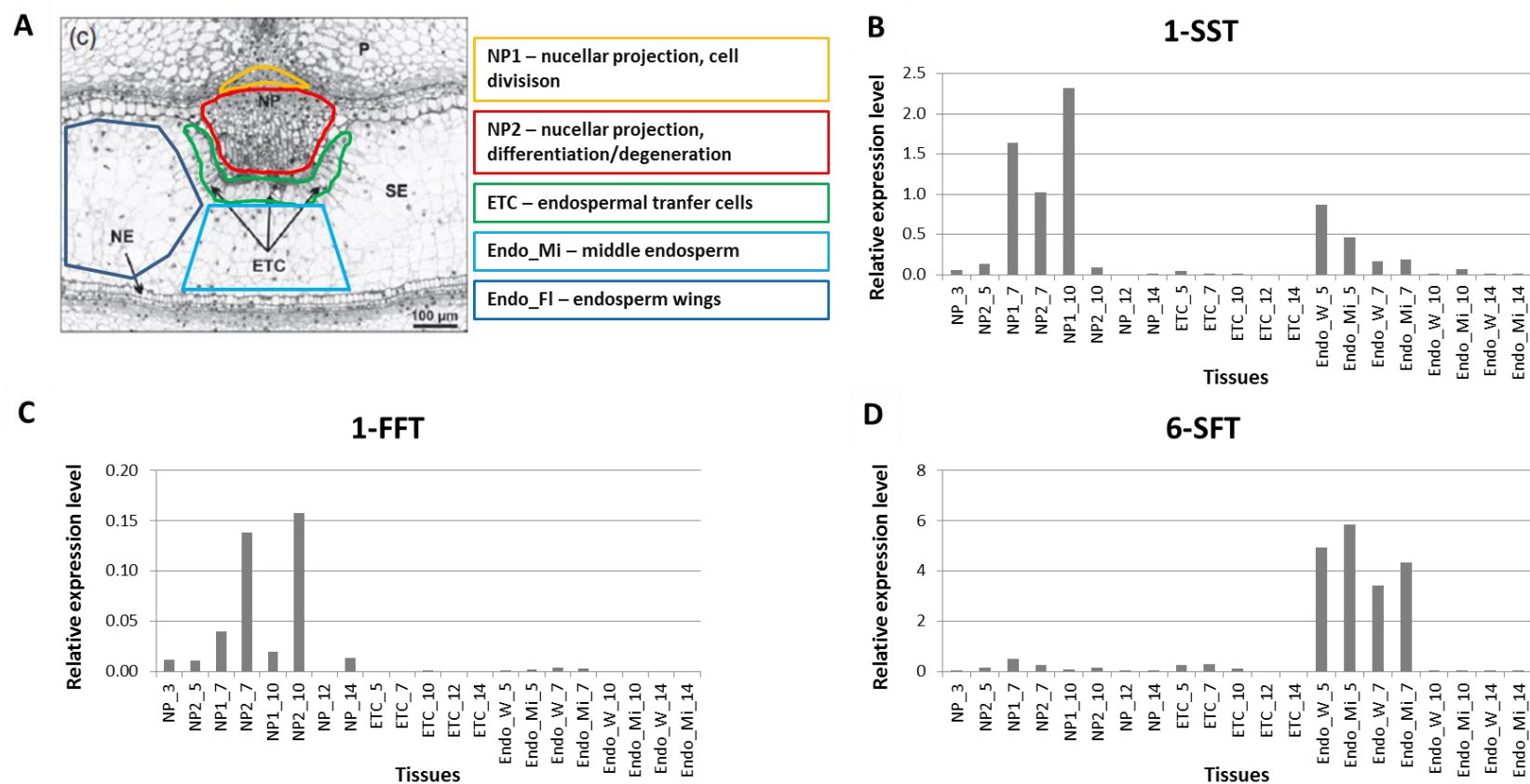
Figure 40: Tissue- and development-specific expression of genes from biosynthetic pathway of fructans.

A) Median cross section of a 5 DAP barley grain indicating the regions of micro-dissected seed material, used for qRT-PCR analyses. The morphological image is published in Thiel et al. (2012).

B) Expression of 1-SST was found to be highest in the nucellar projection (NP) at 7 and 10 DAP, additionally an early expression in the endosperm was found.

C) Also the 1-FFT expression levels are specific for NP and highest at 7 and 10 DAP.

D) 6SFT, involved in the biosynthesis of bifurcose was found to be highly expressed in the endosperm at 5 and 7 DAP.

The tissue abbreviations correspond to Figure A. The last numbers represent the developmental stage in DPA (days after pollination). The total NP tissue was isolated at 3 DAP and from 10 DAP on (according to the tissue properties at the particular stages).
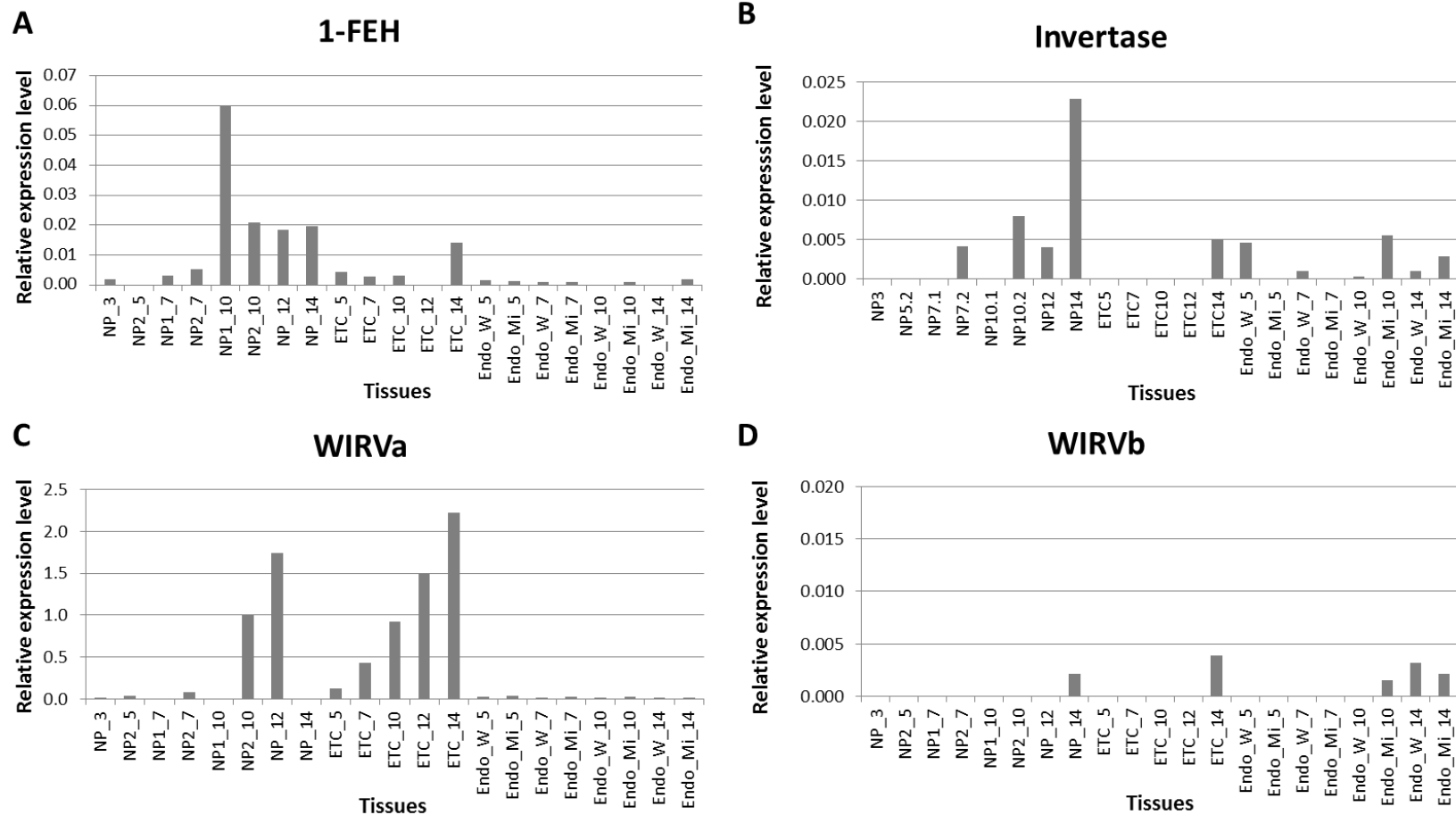
Figure 41: Tissue- and development-specific expression of hydrolyzing enzymes as revealed by qRT-PCR.

a) Expression of 1-FEH was found to be specific for the storage phase in cells of the NP and at 14 DAP in the ETC, but at a generally low level.

b) Even lower is the expression of the extracellular invertase.

c) For WIRVa the highest expression levels of the degrading enzymes were found, specifically expressed in the NP and the ETC at the storage phase.

d) For WIRVb only a trace level of expression was determined.

The tissue abbreviations correspond to Figure 40A. The last numbers represent the developmental stage in DPA (days after pollination). The total NP tissue was isolated at 3 DAP and from 10 DAP on (according to the tissue properties at the particular stages).

The gene expression analysis of fructan exohydrolases and invertases revealed a high specificity of the vacuolar invertase WIRVa for the storage phase, and for the NP and ETC (Figure 41). A low expression level was determined for 1-FEH, but also specific for the NP and ETC during the storage phase. The gene expression of the extracellular invertase is low as well. The highest expression for this gene was observed at 14 DAP in the NP. For the vacuolar invertase WIRVb just a marginal expression was observed and for 6-FEH no expression was obtained by qRT-PCR (not shown).

From the qRT-PCR analyses it can be concluded that the expression of genes related to the biosynthesis of 1-kestose and nystose is specific for those grain parts, where highest concentrations of these metabolites where observed. The highest expression levels were found between the transition and the beginning storage phase (between 7 and 10 DAP), at this period, when the metabolite accumulation starts. Expression of genes from fructan hydrolyzing pathway was found to be highest between 10 and 14 DAP. For 1-FEH that possesses substrate preference for ß(2,1) linked fructosyl residues (like for 1-kestose or nystose) a low expression level was observed. For the vacuolar invertase WIRVa, which is highly expressed during the storage phase, the ability to degrade oligo fructans is not known and further experiments are needed for a characterization of this enzyme.

3.3.5.2. Detection of proteins involved in fructan metabolism

The aim was to identify the enzymes that are involved in the fructan biosynthetic pathway in protein extracts of barley kernels. As a gene expression of all involved proteins was observed for 7 DAP (Figure 40), the extraction was performed using total barley grains from this developmental stage. The proteins were separated by 2-D gel electrophoresis. From the Coomassie stained gels the protein spots were cut according to expected protein sizes, and used for tryptic digest and subsequent MALDI TOF MS measurement.

This experiment revealed the identification of 6-SFT (Figure 42). Thus, the protein expression of this enzyme coincides with the results from the qRT-PCR analysis, where the highest expression level of this enzyme, among all of the fructan biosynthetic genes, was revealed at this particular developmental stage (7 DAP). In addition, the protein expression also conforms with the high concentration of bifurcose at 7 DAP. The detection of 1-SST and 1-FFT was not successful using the total grain extracts of 7 DAP.

2D-SDS Gel separation of seven DAP water soluble protein extract

Spot 23: Mascot Search Result
Match to: gi|1552333
Score: 174
sucrose:fructan 6-fructosyltransferase [Hordeum vulgare subsp. vulgare]
Nominal mass (M_r): 69366
Calculated pI value: 5.20
Sequence Coverage: 6%

```
  1 MGSHGKPPLP YAYKPLPSDA ADGKRTGCMR WSACATVLTA SAMAVVVVGA
 51 TLLAGLRMEQ AVDEEAAAGG FPWSNEMLQW QRSGYHFQTA KNYMSDPNGL
101 MYYRGWYHMF YQYNPVGTDW DDGMEWGHAV SRNLVQWRTL PIAMVADQWY
151 DILGVLSGSM TVLPNGTVIM IYTGATNASA VEVQCIATPA DPNDPLLRRW
201 TKHPANPVIW SPPGVGTKDF RDPMTAWYDE SDETWRTLLG SKDDHDGHHD
251 GIAMMYKTKD FLNYELIPGI LHRVVRTGEW ECIDFYPVGR RSSDNSSEML
301 HVLKASMDDE RHDYYSLGTY DSAANTWTPI DPELDLGIGL RYDWGKFYAS
351 TSFYDPAKNR RVLMGYVGEV DSKRADVVKG WASIQSVPRT VALDEKTRTN
401 LLLWPVEEIE TLRLNATELT DVTINTGSVI HIPLRQGTQL DIEASFHLDA
451 SAVAALNEAD VGYNCSSSGG AVNRGALGPF GLLVLAAGDR RGEQTAVYFY
501 VSRGLDGGLH TSFCQDELRS SRAKDVTKRV IGSTVPVLDG EALSMRVLVD
551 HSIVQGFDMG GRTTMTSRVY PMESYQEARV YLFNNATGAS VTAERLVVHE
601 MDSAHNQLSN EDDGMYLHQV LESRH
```

Figure 42: Identification of barley 6SFT in soluble protein extract of 7 DAP barley grains.

Proteins were separated by 2-D SDS gelelectrophoresis (pH 4-7). Spots were picked according to protein size and subsequently supplied to tryptic digest. Data base search following MALDI TOF MS and MS/MS measurements were carried out using NCBI *Viridiplantae* 2010.

A second approach to detect the enzymes from fructan metabolism in barley grains was a Western blot analysis. The involved enzymes were recombinantly expressed in *Pichia pastoris* and used for an antibody production in rabbit (details are given in 2.3.2.). Pretests revealed a high rate of reactions of the particular antisera with the other recombinantly expressed proteins (data not shown). The highest specificity was observed for anti-1-FEH that only additionally detected 6-FEH. By Western blot experiments with 2-D separated proteins from barley grains mixed patterns of spots were observed using anti-1-FEH and anti-1-FFT, indicating unspecific reactions as well (data not shown). These cross reactions are explained by the high homology of the proteins with each other on the amino acid level. Furthermore, the enzymes from fructan metabolism are also homolog to invertases. Thus, the targeted proteins have not specifically been detected by Western blot analysis.

3.3.6. Summary section 3.3.

MALDI MSI experiments revealed highly specific distribution patterns of oligosaccharides during barley grain development. By targeted analyses an accumulation of 1-kestose and nystose related to the emergence of the endospermal cavity were revealed, contrary the concentration of bifurcose was decreasing in the same grain region, and also in the remaining kernels. The high amounts of oligo fructans are suggested to be synthesized *de novo* within the grain. Transcript analyses by qRT-PCR revealed a high gene expression of 1-SST in cells of the nucellar projection from the transition phase (7 DAP) to the early storage phase (10 DAP). Additionally, the expression of 1-FFT showed the same spatiotemporal distribution. Enzymes related to these transcripts are specific for the biosynthesis of 1-kestose and nystose. For 6-SFT a high gene expression in the endosperm at 5 and 7 DAP was obtained. This enzyme participates in the synthesis of bifurcose, that was found to be highest concentrated at 7 DAP. Furthermore, by a 2-D protein approach and MS detection the 6-SFT has been identified. So far, 1-SST and 1-FFT could not be detected by the used protein approach. Future experiments should confine the sample material to the specific localization and time point of gene expression for a better access to the targeted proteins. In addition, highly specific peptide antibodies should reduce cross reactions to homolog proteins in order to specify the Western blot analyses.

3.4. Distribution Patterns of Metabolites by the Analysis of Dissected Seed Material

In the previous sections the results from the MALDI MSI approach for the analysis of metabolite distribution patterns were presented. The big advantages of this approach are the preservation of the spatial metabolite constitution in a tissue section, and the high resolution of molecular ion distributions that can be obtained. In this study, MALDI MSI applicability mainly relates to the analyses of lipids and sugars. As from preliminary experiments examined, also phenols and organic acids can be ionized in the MALDI process. But the extent of the plant metabolic composition cannot be visualized by one MSI approach. The interplay of ionizability by laser excitation, the intermolecular interference, the dynamic range and the sensitivity of the instrument are major factors of what can be extracted from a MALDI mass spectrum. In this section results from alternative methods using dissected seed material are presented. Therefore, seeds of the aforementioned developmental steps were dissected into the main grain parts. These

are the scar region, the embryo region, the endosperm, the outer pericarp, the chlorenchyma layer and the so called transfer region that contains the vascular bundle, the nucellar projection, but also remains of the pericarp and the chlorenchyma layer. Figure 43 illustrates the dissected seed material from a 10 DAP barley grain. This material was used for the analysis of selected phytohormone distributions as reported in 3.4.1. Further, polar and apolar extracts were conducted to GC-MS analysis; initial results are outlined in 3.4.2.
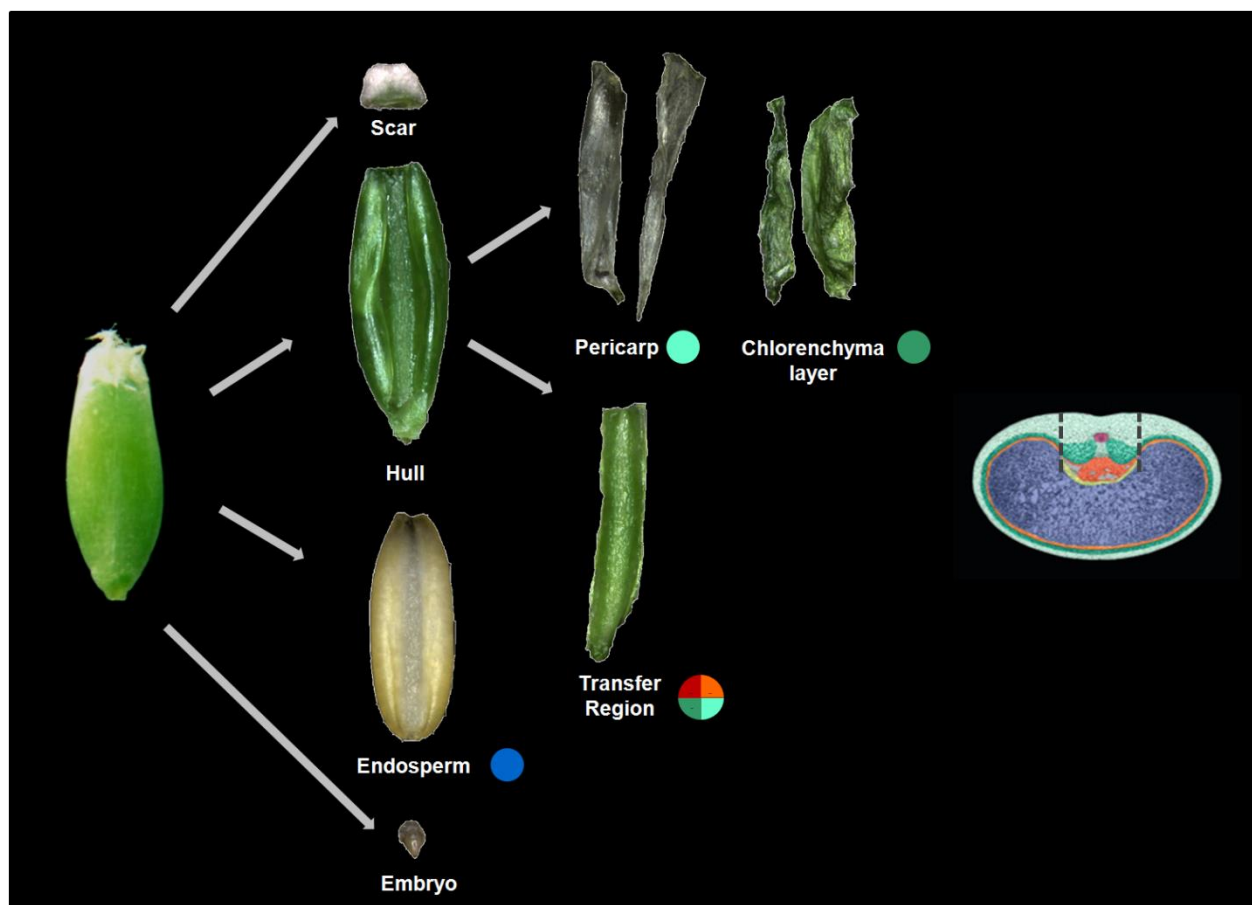
Figure 43: Illustration of dissected seed material from a 10 DAP (days after pollination) barley grain.

Dissections from frozen grains were carried out on a cooled metal plate. The separated tissues were immediately frozen in liquid nitrogen. Depending on the requirements of the following analyses, tissue material from several seeds was pooled.

Colored circles correspond to the tissues displayed in the model cross section on the right sight of the figure. The dashed lines in the model image indicate the cutting positions for the transfer region.

3.4.1. Phytohormone distribution patterns during grain development

Phytohormones are known to play essential roles in the regulation of physiological processes. Functions of particular phytohormones during the grain development were indicated by transcriptome studies (Sreenivasulu et al., 2006; Thiel et al., 2008; Becraft and Yi, 2010). The impact of abscisic acid (ABA) on seed dormancy and desiccation tolerance is well known. During grain development ABA is also meant to mediate the storage product accumulation. Cytokinins (CKs) are known for their major impact on cellularization processes, but also for their influence on primary metabolism, on meristematic activity, or for their role in biotic and abiotic stress responses. There exist different biologically active forms of cytokinins; the highest activities were exhibited for *trans*-zeatin (tZ) and isopentenyladenine (iP). The interconversion to CK ribosides (R) is considered to be an important mechanism in regulating the concentration of active compounds, and in addition, they might function as a translocation form (Schmülling, 2004; Sakakibara, 2006).

The distribution patterns of both hormones in the particular grain regions during development were not reported so far, and were addressed in this analysis. Both, ABA and CK can be transiently inactivated through glycosylation reactions. The detection of the ABA-glucoside encouraged proving the abundance of the ABA glycosyltransferase (ABA-GT) in barley seeds as this enzyme has not yet been described for barley. To better compare the proportions of the hormones in the different seed dissections, the quantification data were normalized to percentage of the total amount.

For ABA a nearly homogeneous distribution was observed through the investigated developmental stages (Figure 44). The total concentration was found to decline from 7 to 10 DAP and to increase again from 10 to 14 DAP (Table 26). This means that in all tissues the ABA content changes to similar extends. The glycosylated form was found to be more concentrated in the endosperm at 7 and 10 DAP, but its proportion in the scar region rises to 14 DAP (Figure 44). The total amount of this ABA conjugate was lower compared to the biological active one (Table 26), and the total concentration slightly decreased from 7 to 14 DAP.

The quantification of CKs in grain dissections revealed a high concentration of *trans*-zeatin (tZ) and of *trans*-zeatin riboside (tZR). Specific distributions in the different grain parts were revealed for both CK types (Figure 44). At 7 DAP the tZ concentration is dominating in the filial parts, especially for the embryo region the highest proportion was observed with more than 50%. This

proportion decreases during the storage phase (as obtained for 10 and 14 DAP) and finally changes to a higher concentration in maternal seed parts, like the outer pericarp and the scar region. The distribution of tZR was found to be similar at 7 DAP as obtained for tZ, but the decrease in the filial proportion showed a less extend. At 14 DAP the embryo still contains the highest amount of tZR. The total concentrations of tZ and tZR are similar and generally decrease from 7 to 14 DAP (Table 26), to a comparable extend.
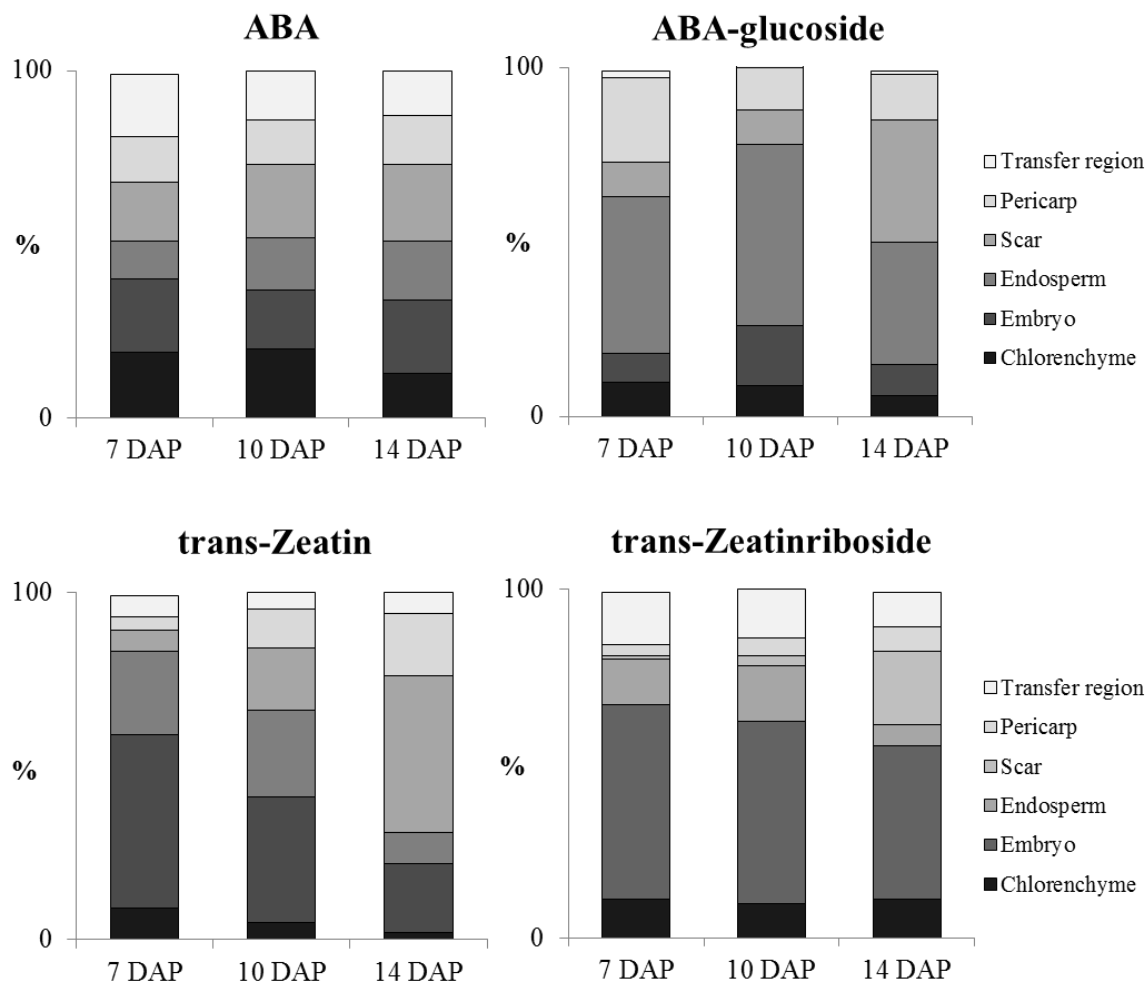
Figure 44: Tissue proportions of abscisic acid (ABA), ABA-glucoside, *trans*-zeatin (tZ) and *trans*-zeatin riboside (tZR) during barley grain development.

The concentrations of the hormones in the particular seed parts were calculated to the percentage of the total amount. Three biologically independent samples were taken for the quantification of samples from 7 and 10 DAP; two independent biological replicates underlie the quantifications for 14 DAP. Analyses were carried out by means of LC coupled to MRM.

Table 26: Determination of abscisic acid (ABA), ABA-glucoside, *trans*-zeatin (tZ) and *trans*-zeatin riboside (tZR) concentrations in barley seeds.

Total concentrations were revealed by summarizing the concentrations from the single grain parts. For 7 and 10 DAP three biologically independent samples were taken for the quantification. For 14 DAP two independent biological replicates were used. Analyses were carried out by means of LC coupled to MRM.

	Total ABA [ng/g FW]			Total ABA-glucoside [ng/g FW]		
	7 DAP	**10 DAP**	**14 DAP**	**7 DAP**	**10 DAP**	**14 DAP**
Mean	200.04	136.53	185.48	9.94	8.16	5.67
σ	53.30	26.17	13.69	2.96	3.75	2.07
	Total tZ [ng/g FW]			Total tZ riboside [ng/g FW]		
	7 DAP	**10 DAP**	**14 DAP**	**7 DAP**	**10 DAP**	**14 DAP**
Mean	168.97	154.54	78.76	182.36	133.46	65.52
σ	30.41	24.92	3.01	36.89	24.12	7.09

ABA can be inactivated through glycosylation or oxidation. The ABA-glucoside is discussed to be a storage and/or a transport form. The activity of ABA can be restored by the action of a glycosidase (Sauter et al., 2002) that is specifically expressed in the barley endosperm and the embryo (Seiler et al., 2011). The glucose ester of ABA was detected in higher amounts in the endosperm compared to the other seed dissections (Figure 44), but an expression of the ABA-glycosyltransferase (ABA-GT) in grains is not yet known. To detect this enzyme, the ABA-GT UGT71B6 from *Arabidopsis thaliana* was recombinantly expressed in *E. coli* and used for antibody production.

1-D and 2-D separated proteins from the different developmental stages were probed with the purified antiserum against ABA-GT (data not shown). Developmental differences were observed in both approaches at the corresponding protein size for UGT76B1 (53.8 kDa). But detection of several bands (1-D) and spots (2-D) suggested unspecific reactions with proteins sharing similar protein motifs, as it is known for proteins from the UDP-glycosyltransferase family. Thus, the specificity of the antibody was not given for a precise detection of the ABA-GT in barley.

3.4.2. Metabolite profiles of dissected seed material through grain development by means of GC-MS analysis

It's a matter of principle that in the MALDI MS application the mass range between *m/z* 100-500 is highly interfered by matrix background signals. To perform an untargeted analysis of metabolite distributions in that mass range the GC-MS technique is a convenient system to measure small polar and apolar substances.

Seed dissections of three developmental stages were applied to an integrated extraction of polar and apolar compounds (details are given in section 2.5.4.). Evaluated mass-retention time pairs were used for a principle component analysis (PCA) to initially visualize a grouping of the samples. For the polar seed extracts no specific groups, except for scar region were observed (data not shown). In addition, the comparison of peak heights from identified amino acids revealed no explicit pattern according to the developmental stage or tissue group.

By PCA of the apolar seed extracts a separation of the embryo region from 10 and 14 DAP was found (Figure 45). Also the scar and the pericarp from 7 and 10 DAP formed a separated group. All other tissues are grouped in close proximity as it is indicated by the green circle. The maximum normalized peak heights of identified compounds were compared, and according to the considered patterns from the PCA, pregnant distributions of several compounds were found.
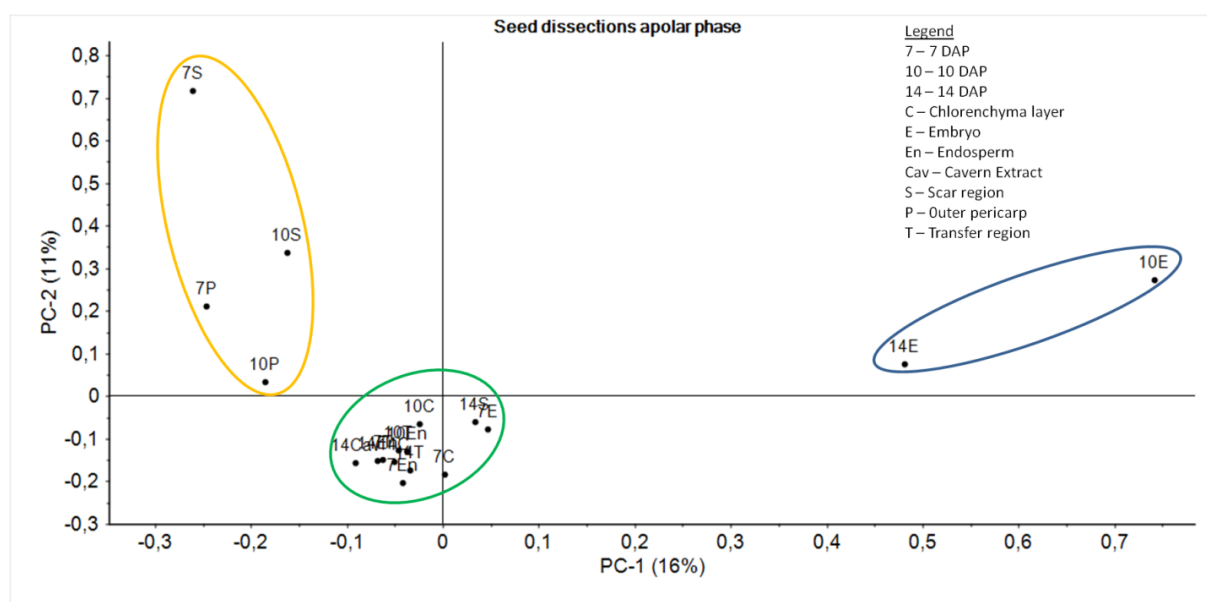
Figure 45: Principal component analysis of GC-MS data from apolar seed extracts of barley grain dissections. Mean normalized mass-retention time pairs as obtained by MarkerLynx software (Waters, Germany) from all samples were conducted to PCA.

In Figures 46 and 47 metabolites showing tissue and developmentally specific patterns are presented. Figure 46 illustrates six compounds showing high tissue specificity. It is obvious that the identified compounds in the filial fraction showed increasing signal intensities during development, whereas those from the maternal seed parts decreased. This corresponds to the patterns obtained by PCA (Figure 45), where the embryo and the pericarp specifically grouped. The same trends were also obtained by the MALDI MSI analyses as molecular ions specific for

the maternal enclosing tissues showed decreasing signal intensities, whereas those from the filial parts rose. Figure 47 exemplarily outlines mixed distribution patterns observed for six compounds.
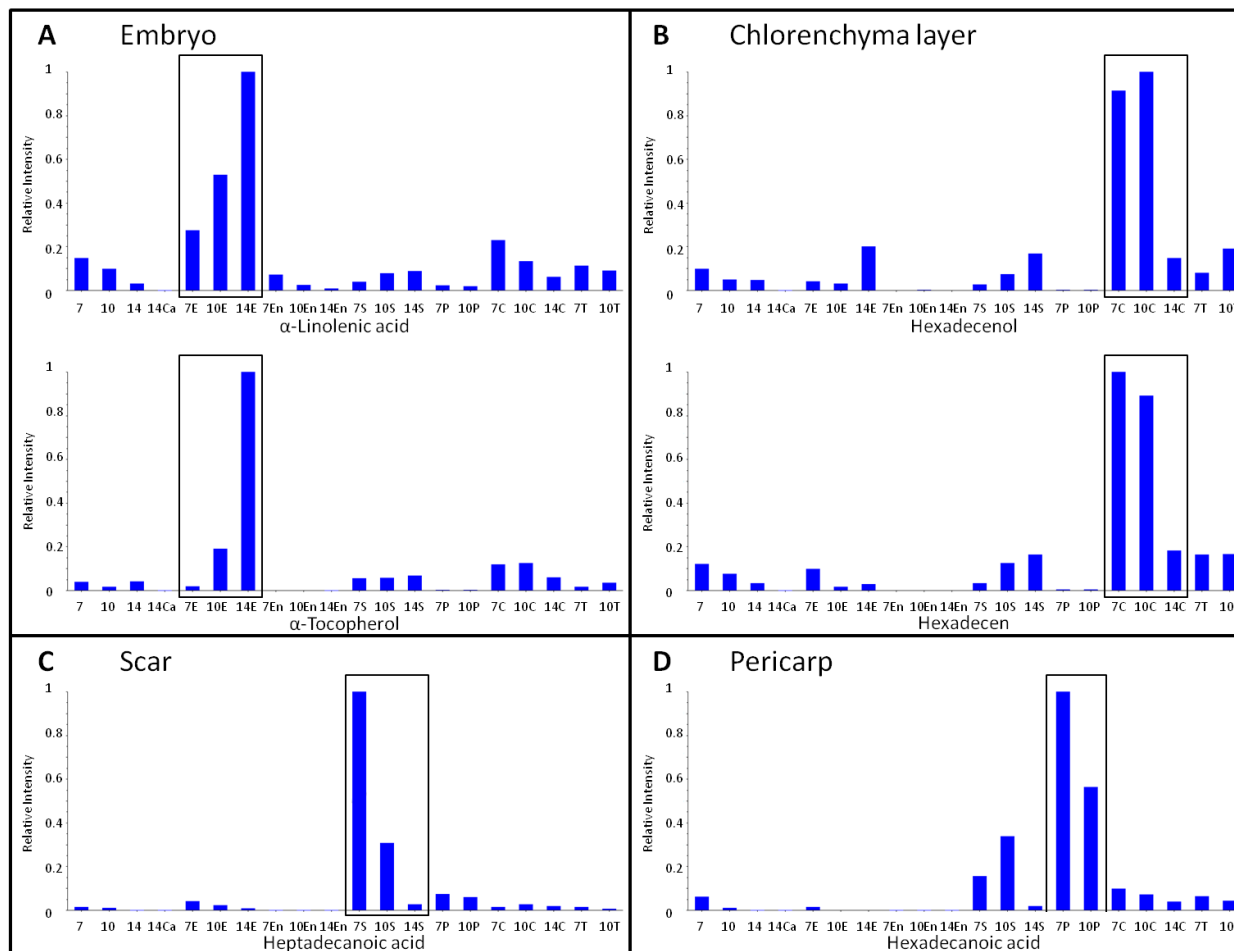
Figure 46: Tissue specific distributions of compounds as revealed by GC-MS analysis of dissected barley grains. Bar plots represent the maximum normalized peak intensities.

A – Increasing signal intensities were observed for α-linolenic acid and α-tocopherol in the embryo from 7 to 14 DAP.

B – In extracts of the chlorenchyma layer a steep decline of hexadecenol and hexadecen from 10 to 14 DAP was observed

C and D – Decreasing signal intensities of fatty acids in extracts of the scar and the outer pericarp are displayed.

Abbreviations are as follows: 7, 7 DAP; 10, 10 DAP; 14, 14 DAP; Ca, cavity extract; C, chlorenchyma layer; E, embryo; En, endosperm; S, scar region; P, outer pericarp; T, transfer region.
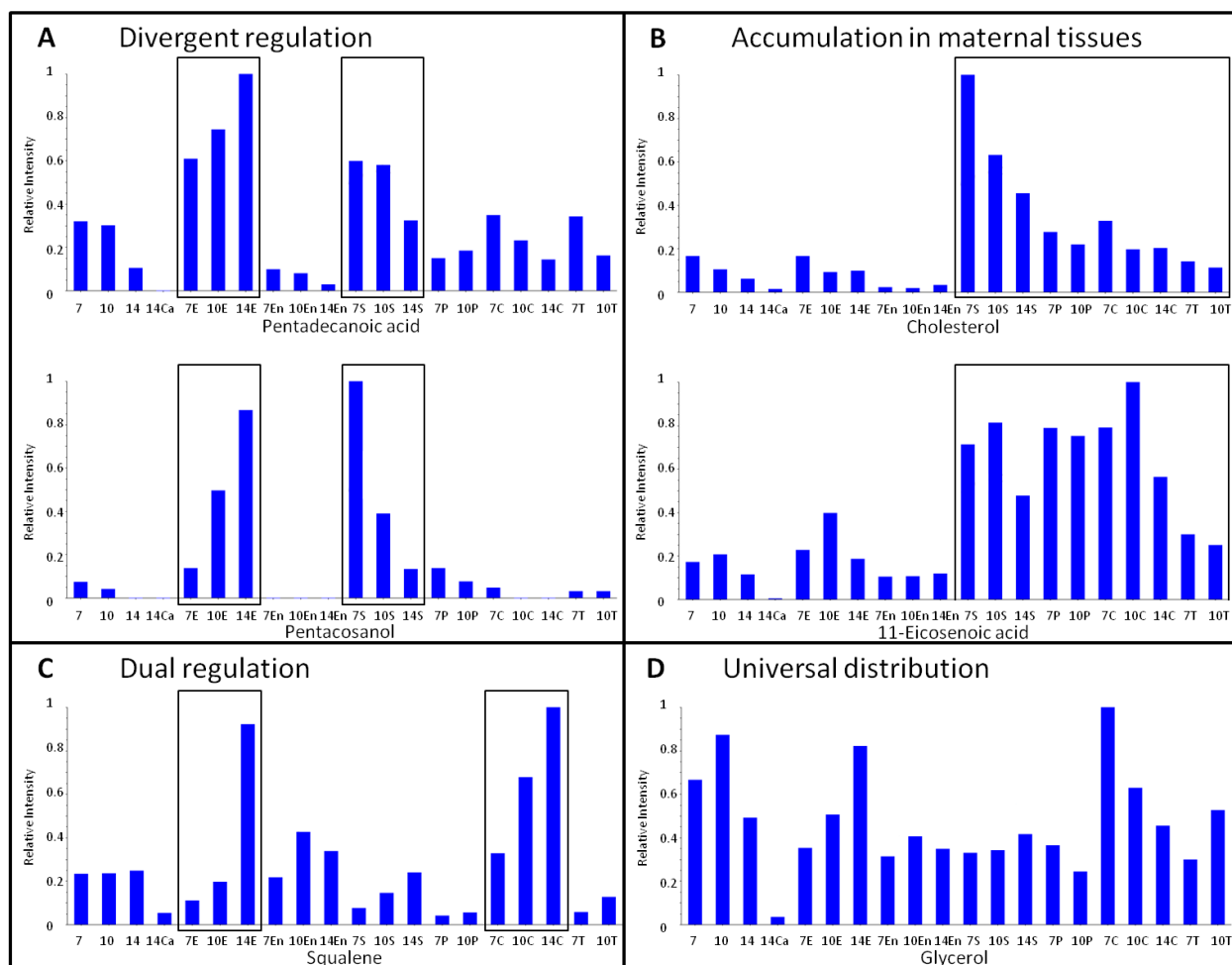
Figure 47: Mixed distribution patterns of compounds in apolar seed extracts of barley grains. Bar plots represent the maximum normalized peak intensities, obtained by GC-MS analysis.

A – For pentadecanoic acid and pentacosanol increasing signal intensities were observed for the embryo region, concurrently these compounds decreased in the scar region.

B – A generally higher amount in maternal tissues was found for cholesterol and eicosenoic acid. The cholesterol signal intensity declines from 7 to 14 DAP.

C – Squalene was found to increase in the embryo and chlorenchyma layer.

D – Glycerol is abundant in all tissues, with exception of the extracted cavity sap. For the embryo a slight increase was found. This compound diminishes in the chlorenchyma layer.

Abbreviations are as follows: 7, 7 DAP; 10, 10 DAP; 14, 14 DAP; Ca, cavity extract; C, chlorenchyma layer; E, embryo; En, endosperm; S, scar region; P, outer pericarp; T, transfer region.

3.4.3. Summary section 3.4.

By the analysis of dissected seed material specific distribution patterns of small molecules were revealed. These approaches are convenient to extend the results from the MALDI MSI analysis.

In this study, quantitative profiles for ABA and CK for three developmental stages were obtained, showing distinct differences in the particular seed dissections. These patterns extend the

information on phytohormone distributions that are so far related to the expression patterns of biosynthetic genes and signaling components. In the future, this approach has to be extended to the analysis of other hormones as the action of hormones is determined by their specific interplay.

GC-MS measurements of barley grain dissections revealed specific developmental differences of lipid distributions. Those that were detected in the maternal tissues mostly exhibited decreasing concentrations from 7 to 14 DAP, whereas the levels of embryo specific lipids increased. These patterns were also obtained by the MALDI MSI experiments, and additionally demonstrate the degradation processes occurring in the pericarp, and the accumulation processes in the filial part of the grain.

4.   Discussion

Highly specific tissue and developmentally depending differences of metabolite distribution patterns in barley grains were observed by means of MALDI MSI. This thesis focuses on those metabolites that have an impact on the final grain composition. In this regard, the region for the transfer of nutrients into the filial part of the grain, and the main storage tissue, the endosperm, were of outmost interest. Several aspects that are supposed to affect endosperm filling indicated a complex regulatory network. This chapter aims at the functional correlation of characteristic metabolite distributions to the context of grain development. The discussed key results are as follows:

- MALDI MSI has been proven to be applicable for the spatial analysis of grain development. Data mining revealed the formation of clusters that display the functional units of a grain and that emphasize the rising complexity during grain development (4.1.)

- Fructans highly accumulate in and around the emerging cavity during the storage stage. Targeted approaches revealed their physiochemical background and their distribution patterns could be related to gene expression and protein data, implying a spatiotemporal regulation of biosynthesis (4.2.).

- Most of the identified metabolites are phospholipids. Several of them showed specific accumulations in the developing endosperm. These can be correlated with seed quality parameters, and their spatial abundance displays a linkage to storage product accumulation patterns (4.3.).

- The concentrations of the phytohormones ABA and CK showed tissue and developmentally depending differences as observed by a targeted LC-MS approach. The role of these key regulators in seed development is discussed in section 4.4.

The information about spatiotemporal distributions of metabolites gains the knowledge from mainly transcriptome related studies of seed development in barley and the results of this work can be used for future investigations as outlined in chapter 5.

4.1. MALDI MSI Approach Revealed Tissue and DevelopmentallySpecific Differences of Distribution Patterns of Molecular Ions

The high spatial resolution that can be obtained by MALDI MSI and the simultaneous detection of many individual signals in one imaging run were the key advantages decisive for choosing this technique for the investigation of barley grain development. Metabolite distributions were analyzed for characteristic stages of grain development: prestorage stage, transition stage and storage stage.

Data mining by multivariate statistics was appropriate to validate the obtained metabolite distribution patterns and to compare the developmental stages. With the Neural Gas (NG) clustering algorithm specific functional groups were highlighted (4.1.1.). The principle findings are summarized in Figure 48 and the subsections where the individual results are discussed are given as well.
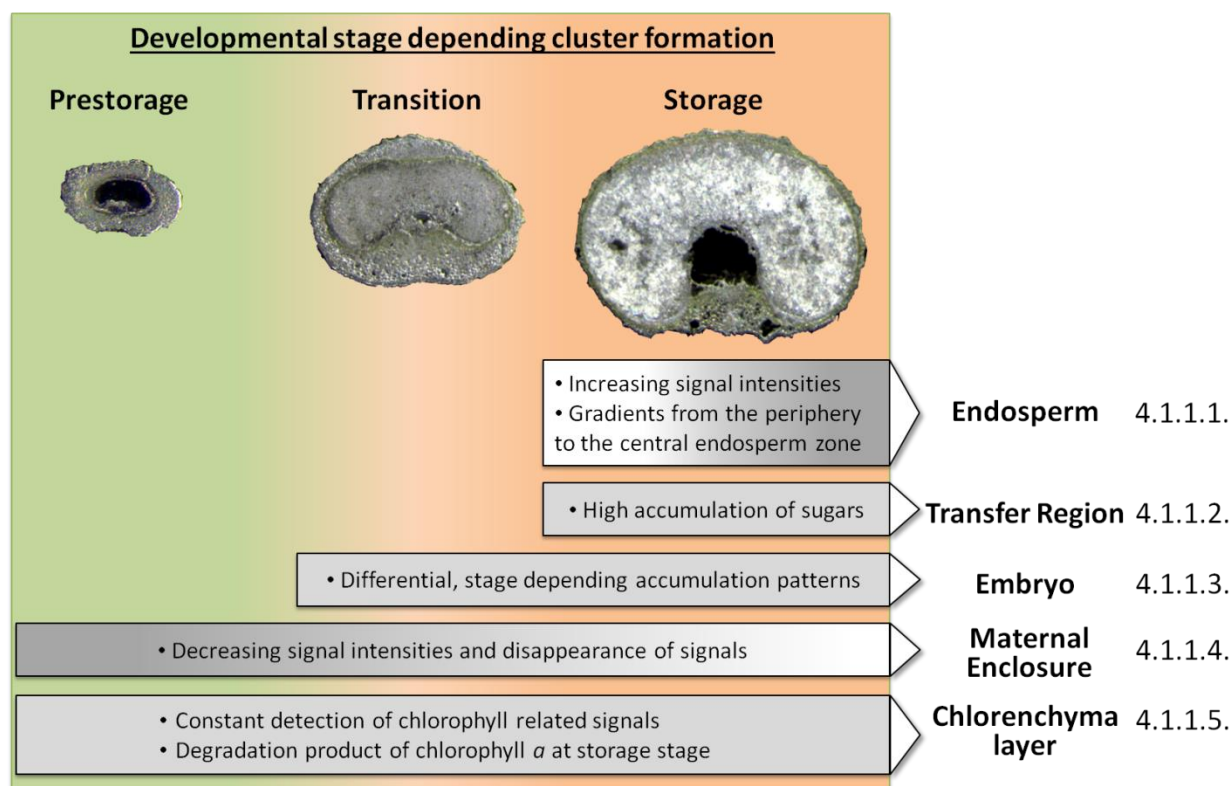
Figure 48: Summary of the results from the MALDI MSI approach of barley grain development.

Illustrated are the occurrences of specific clusters that relate to functional units of the developing grain. Tissue specificity rises during development and is highest at the storage phase. Considerable features of molecular ion assignments to the respective clusters are indicated in the grey boxes. The section numbers where the results are discussed are given on the right side.

Many signals were found to be developmental stage dependent. Their abundances were either specific for an individual stage or showed relative changes of signal intensities during development (4.1.2.). The identification of molecular ions revealed a high proportion of phosphatidylcholines and intense signals for oligosaccharides. The choice of the matrix but also the chemical structures of the analytes have crucial impacts on signals that can be extracted from a MALDI mass spectrum (outlined in 4.1.3.).

4.1.1. Correlation of MALDI MSI clustering data to functional units of the barley grain

The NG cluster analyses were based on mean signal intensities of molecular ions for defined regions of interest (ROIs). The shapes of the obtained cluster prototypes indicated a grouping of detected signals according to the functional units of the grain (Figures 16, 19, 23, 26). With the progression of development, the rising complexity of tissues was indicated by more specific distribution patterns of molecular ions (Figure 32), and it is also represented by the numbers of assigned ROIs and the numbers of clusters for each developmental step (Table 27).

Table 27: Numbers of selected regions of interest (ROIs) and of resulting clusters for the investigated developmental stages. ROIs were chosen according to obvious histological properties of longitudinal grain sections that were applied to MALDI MSI.

Developmental phase	Kernel age	Numbers of ROIs	Numbers of clusters
Prestorage stage	2/3 DAP	5	3
Transition stage	7/8 DAP	7	4
Early storage stage	10 DAP	9	5
Mid-storage stage	14 DAP	8	5

4.1.1.1. Specific phospholipid constitution of the endosperm during the storage stage

The generation of a specific NG prototype that emphasizes the endosperm was related to the storage stage. A large part of the molecular ions that are grouped to the endosperm cluster belong to the phosphatidylcholines. The specific phospholipid constitution of the endosperm can either be related to a particular plasma membrane configuration as the distribution of nutrients in the endosperm mainly occurs by diffusion through plasmodesmata (Wang et al., 1995a; Gubatz and Shewry, 2011). For several of the endosperm specific molecular ions the relative ion intensities were found to increase from 10 to 14 DAP (Table 18). In that case, the phospholipids are suggested to be part of association complexes that are formed of starch, protein and lipid molecules (Finnie et al., 2009; Finnie et al., 2010b). More detailed information to this is given in section 4.3.

4.1.1.2. The formation of a transfer region cluster relates to the storage stage

The transfer region represents the functional unit that is involved in the transport of nutrients into the endosperm and constitutes the following tissue types: parts of the ventral crease, the nucellar projection (NP), the endospermal cavity and the endospermal transfer cells (ETC). The very high signal intensities of oligosaccharides associated to the cavity were mostly obvious during the storage stage and contributed to the formation of this cluster. Lim and Gifford (1984) already detected a high concentration of sugars in the cavity, but here, the highest abundance was related to the surrounding tissues, namely NP and ETC (Figure 34). These specific accumulations motivated for targeted investigations and are discussed in detail in section 4.2. The molecular ions grouped to the transfer region cluster are supposed to reflect a special cell constitution that might be involved in maintaining the large capacity of transport events. This can relate to specific membrane configurations due to the plenty of plasmodesmata that realize the transfer of nutrients from the main vascular bundle towards the NP (Wang and Fisher, 1995c; Patrick and Offler, 2001). Several of the molecular ions from this cluster are assumed to belong to lipid classes (e.g. *m/z* 562.3, 576.5 or 923.6) and display candidates for integral membrane compounds. Moreover, the cells of the ventral crease and NP contain large vacuoles and are known for the accumulation of secondary metabolites such as tannins or proanthocyanidins (Gubatz and Shewry, 2011). Particular detected *m/z* values could also be related to secondary metabolism. The specific role of these metabolites for transport events is not fully understood, but the barley *seg1* mutant, which lacks the central vacuoles are affected in grain filling due to the early degeneration of cells from the ventral crease (Frederick et al., 1984).

4.1.1.3. Developmentally depending accumulation patterns in the embryo

Embryo emphasizing clusters resulted for the developmental stages of 7, 10 and 14 DAP by the NG cluster analyses. The comparison of assigned *m/z* values to the particular clusters revealed high differences. At 7 DAP several phospholipids were accumulated in the embryo but at 14 DAP high accumulations of low molecular mass compounds were detected. All compounds that were embryo specific at 7 DAP were later in development (14 DAP) assigned to the maternal enclosure cluster. The heat map in Figure 27 (cluster 3) shows that this molecules are higher abundant in ventral part of the pericarp, where the main vascular bundle is located. Here, a specific cell constitution related to the needs of the nutrient import is suggested; e.g. the identified phospholipids could be an integral part of plasma membranes. 10 DAP displays an

intermediate state containing both, the compounds of high molecular mass from 7 DAP and those of low molecular mass from 14 DAP (Figure 49). During the prestorage stage the embryo constitutes a very minor part of the grain (Engell, 1989) and couldn't been distinguished in barley grain cryo-sections for data mining.
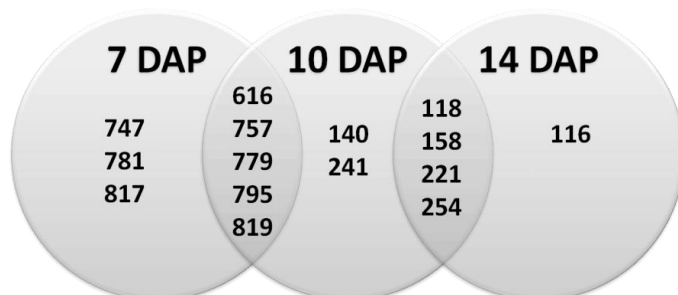
Figure 49: Assignment of individual *m/z* values to embryo clusters as observed by Neural Gas cluster analysis for different developmental stages. The overlaps between 7 and 10 DAP as well as 10 and 14 DAP display shared *m/z* values.

Up to now, little is known about the metabolic composition of the embryo during early stages of development. The obtained results indicate a switch of metabolic pathways according to the developmental proceedings. The period between 7 and 10 DAP is characterized by cellularization processes and the differentiation of the root and shoot meristem, and of the scutellum (Bethke et al., 2000). Generally, the embryo becomes functional and capable of germination during this period (Black et al., 2006). During the storage stage, the length of the embryo increases and it acquires desiccation tolerance (Gubatz and Shewry, 2011). The accumulation of low molecular mass metabolites during this stage might be related to the activation of metabolic processes that are involved in the acquisition of desiccation tolerance. Different proposed mechanisms involve a phytohormonal regulation (Leung and Giraudat, 1998; Finkelstein et al., 2002; Frey et al., 2004), an involvement of carbohydrate, protein and lipid metabolism (Nedeva and Nikolova, 1997), and a relation to membrane stabilization (Blackig et al., 1996; Ingram and Bartels, 1996; Golovina and Hoekstra, 2003; Minorsky, 2003).

4.1.1.4. Clusters for the maternal enclosure differ in their particular assignment of mass signals

Between the clusters that represent the maternal enclosure at the different developmental stages no congruities in the assignment of particular *m/z* values were observed. This functional unit

contains mainly the non-green part of the pericarp and the scar region. At 3 DAP the seed volume is dominated by these tissues. Many compounds of low and high molecular mass were assigned to this cluster. Obvious is the higher abundance of oligosaccharides with a degree of polymerization (DP) of 3-7. This coincides with the findings from Schnyder et al. (1993a) who observed a partitioning of large amounts of water soluble carbohydrates into the pericarp until 5 DAP in wheat. Phospholipids were detected in this region as well. But most molecular ion identities are not known and need further targeted investigations. Until the storage stage the assigned *m/z* values completely changed. These differential cluster constitutions are traced back to specific developmental processes occurring in the pericarp. This tissue possesses feeding functionality for the filial part, indicated by expression of genes related to degeneration processes (Wobus et al., 2005), and disintegrates during grain development. As displayed in Table 16, several compounds were specifically detected during the prestorage phase in this tissue. The disappearance of individual molecular ions during development reflects the degradation processes that proceed until the end of the storage phase, especially at the dorsal site. Only that part surrounding the main vascular bundle remains (Weschke et al., 2000; Sreenivasulu et al., 2010). The decreasing tendencies of molecular ion concentrations were validated by results from GC-MS analysis. Apolar metabolite extracts from dissected pericarp tissues revealed a steep decline of lipids from 7 to 14 DAP as well (Figures 46 and 47).

4.1.1.5. Photosynthetic activity of developing barley grains

At each developmental stage a cluster highlighting the chlorenchyma layer was observed. This chloroplast containing part of the pericarp is characterized by specific *m/z* values: *m/z* 592.3, 652.9, 870.6 and 909.6. The high specificity of this cluster is explained by the detection of chlorophyll related pigments in this tissue. Chlorophyll *a* was detected as pheophytin *a*, which is the Mg^{2+} released form with an *m/z* of 870.6. A second chlorophyll related metabolite is pheophorbid *a* (pheide *a*), detected with an *m/z* of 592.3. This molecule relates either to be a fragmentation product of chlorophyll *a*, emerging during the measurement by laser excitation (MS/MS measurements revealed a low energy dependent decay of m/z 870.6 generating the pheide *a* fragment), or to be a hydrolyzation product of pheophytin occurring during degradation processes in the chloroplasts (Christ et al., 2012). Both molecules were detected at all investigated developmental stages. The results coincide with the findings from Sreenivasulu et al. (2004), who observed high transcription levels of genes related to photosynthesis between 2 and

10 DAP in barley grains. The presence of photosynthetic pigments during the prestorage stage and the increase of the mitochondrial number in the barley embryo (Norstog, 1972) imply a high demand of energy equivalents. This can relate to massive cellularization processes that require ATP for the progression of the cell cycle (McBride et al., 2006), and to the transient production of starch in the pericarp during the prestorage stage (Weschke et al., 2000). In this study, pyropheide *a* (*m/z* 533.3) was detected at 14 DAP. This molecule is a product of chlorophyll demethylation and decarboxylation occurring during breakdown processes (Suzuki et al., 2006; Suzuki et al., 2009). The detection of a chlorophyll degradation product at 14 DAP indicates a beginning decline of photosynthetic activity. Prior studies revealed the crucial role of seed photosynthesis for the energy supply during grain development (Rolletschek et al., 2004; Rolletschek et al., 2011). To gather more information on the influence of seed photosynthetic activity on early cellularization processes and on storage product accumulation, investigations of mutant lines with impaired photosynthesis would be of interest. The mutant *Albino lemma* that lacks chlorophyll in the pericarp, lemma and palea (Watson and Duffus, 1988) could be useful for such studies.

4.1.2. Developmentally specific differences of molecular ions reflect the progression of barley grain growth

The here presented discovery of developmental stage specific molecular ion abundances, and of differences in the relative signal intensities, reflected a clear relation to the characteristics of grain development: (i) the specificity of tissues being involved in the transport and processing of nutrients increases and (ii) the maternal enclosure diminishes. The latter was concluded as abundances of unique molecular ions in the pericarp were particularly detected at the prestorage stage (Table 16). It is suggested that these compounds are involved in the specific configuration of pericarp cells. Vice versa, several signals that correlated with the endosperm and transfer region appeared with the beginning of storage product accumulation (Table 16) and might represent storage compounds, display intermediate products or belong to specific cellular constitutions. Two of these signals were identified as phospholipids (*m/z* 534.3 – LPC 16:0; *m/z* 679.2 – PC 28:0). In addition to the detection of compounds at particular developmental stages, relative differences of signal intensities during grain development were observed (Table 17). The results clearly reflect the aforementioned findings: decreasing signal intensities were mostly correlated to maternal tissues whereas increasing signal intensities were observed for

molecular ions that are mainly related to the endosperm and transfer tissues during the storage phase. One particular molecule that diminishes was tentatively identified as a hexosyl-ceramide 40:1 (*m/z* 968.6). Identified molecular ions that exhibited increasing values belong to sugar classes (*m/z* 527.2, 543.1, 689.3, 705.2) and to phospholipid classes (496.4, 534.3, 688.4). The molecular ion *m/z* 184.1 was identified as phosphocholine that either represents a precursor molecule of phosphatidylcholines (PCs) or a fragmentation product of PCs. The latter one can result from the decay of PCs caused by laser excitation during the measurement as this was found to be partly induced without any increase of the laser energy by manual MS/MS measurements. The sugar and lipid accumulation patterns are discussed in more detail in the following sections. In summary, MALDI MSI is a highly appropriate technique to display differences in molecular ion signal intensities within one measurement of tissue sections. The strategy using the DHB background signals as an internal standard for the calculation of signal intensity ratios allowed an additional estimation of developmental differences (e.g. between independent MSI runs).

4.1.3. Molecular ion detection from thin tissue sections

The identifications presented in Tables 20 and 21 obviously revealed a high amount of phosphatidylcholines and oligosaccharides. The detection of compounds highly depends on the chosen matrix and on the molecular structure of the target molecules. In pre-experiments the matrix DHB was found to be the best compromise regarding the amount of background signals and the ionization capacity for molecular ions from barley grain sections (Figure 7 and Table 4). In previous studies the DHB matrix was used for MALDI MS analysis of lipid extracts as different lipid classes, such as triacylglycerols (TAGs), diacylglycerols (DAGs), phospholipids (PLs), and galactolipids could be well ionized (Al-Saad et al., 2003; Schiller et al., 2004; Fuchs et al., 2007; Johanson et al., 2007). The majority of lipids detected in the presented MALDI MSI study belong to the phosphatidylcholines (PCs). This is explained by ionization suppression effects of this lipid class in complex lipid mixtures. Quaternary amines in PCs, lysophosphatidylcholines (LPC) and sphingolipids (SL) preform a positive charge that is thought to enhance their detectability in positive ionization mode and to suppress the signals of other PLs that are less cationic (Petković et al., 2001; Johanson et al., 2007; Emerson et al., 2010; Fuchs et al., 2010). The permanent positive charge of the quaternary nitrogen is also responsible for the highly efficiently produced phosphocholine fragment ion (*m/z* 184), which is diagnostic for the PC headgroup (Murphy and Axelsen, 2011). In MALDI MSI experiments a preliminary

exclusion of PCs, LPCs or SLs is not possible. Thus, it has to be kept in mind, that the observed lipid profiles in the mass spectrum don't reflect the *in vivo* lipid concentrations, but rather reflect the ionization capacities of those molecules. Nevertheless, PCs, LPCs and SLs play key roles in living cells and a relative comparison of lipid amounts within the individual lipid classes (such as PCs) was found to be convenient for MALDI MSI experiments compared to other methods (Horn et al., 2012b).

The DHB matrix was also found to be highly suitable for the detection of sugars from barley grain tissue sections. These were mainly detected in form of potassium adducts. This coincides with the findings from Harvey (2011), who reported on the usage of DHB for oligosaccharide measurements. The high affinity of alkali metals to carbohydrates is outlined in Wang et al. (1999). In recent MALDI MSI applications to poplar stem and eggplant oligosaccharides were detected as well by using the DHB matrix (Goto-Inoue et al., 2010; Jung et al., 2010).

4.1.4. Concluding remarks – is an untargeted MALDI MS *Imaging* approach a convenient method to elucidate spatiotemporal distribution patterns of small molecules during plant development?

The before discussed metabolite distribution patterns reflect a correlation to functional units, and characteristic developmental proceedings of barley grains (Figure 48). From the obtained results interesting molecular ions can be extracted as candidate compounds for following targeted analysis as it was carried out in this study for a detailed analysis of oligosaccharide accumulation patterns (4.2.).

In summary, applied for the investigation of barley grain development, the MALDI MSI approach has been proven to exhibit the potential for the elucidation of metabolite distributions in a tissue and developmentally specific manner. In recent plant MSI studies as been summarized in Matros and Mock (2013), functional relations to distribution patterns of metabolites could be observed; e.g. the exploration of "functional food factors" in eggplant (Goto-Inoue et al., 2010), or the characterization of anthocyanin distributions in black rice (Yoshimura et al., 2012). A developmentally depending characterization of metabolite distribution patterns by using the untargeted MALDI MSI approach was carried out for the first time in this study.

4.2. High Accumulation of Oligo Fructans During the Storage Phase in the Nutrient Transition Region is Related to Keep High Import Rates into the Developing Endosperm.

Reallocations of oligosaccharides were found to occur from the prestorage to the storage stage (section 3.3., Figure 34). Higher accumulations were found in the pericarp at 3 DAP but at the transition stage all detected sugars were nearly co-localized. During the storage phase a differentiated pattern was observed: small oligosaccharides of DP 3 and 4 highly accumulated in the region of the emerging cavity whereas sugars of DP 5 - 7 were higher abundant in the central endosperm. These specific distribution patterns were investigated in more detail as a role for processes related to nutrient import and storage production was assumed. Table 28 gives an overview of the obtained key issues discussed in the following sections.

Table 28: Summary of the key issues of studying the distribution patterns of oligosaccharides during barley grain development.

Discussion point	Key issues	Section
Accumulation patterns of fructans	• High quantities of 1-kestose and nystose in the emerging cavity • Decreasing concentration of bifurcose from 7 to 14 DAP	4.2.1.
De novo **biosynthesis in developing barley grains?**	• Tissue and development specific gene expression related to fructan biosynthesis • Detection of enzymes from fructan metabolism	4.2.2.
Tentative functional integration into barley grain development	• Relation of bifurcose to short-term storage functionality • Relation of 1-kestose and nystose accumulation to membrane stability and scavenging of ROS	4.2.3.

4.2.1. Specification of fructan accumulation patterns in barley grain kernels

The oligosaccharides of DP 3 - 7 were mainly distributed in the pericarp during the prestorage stage (Figure 34). Targeted analysis of total kernel extracts from 3 DAP revealed sucrose as the major sugar form, and in addition, high quantities of 1-kestose and bifurcose (Table 25). These findings are in agreement with prior studies on wheat kernel development, where a high fructan partitioning to the outer pericarp was examined until 5 DAP (Housley and Pollock, 1993; Schnyder et al., 1993a). The disintegration of the pericarp was then related to a nearly complete disappearance of all water-soluble carbohydrates (WSC), including fructans, sucrose and hexoses from the pericarp. Also in the present study, a reallocation of oligosaccharides was observed. Sugars of DP 3 and 4 highly concentrated in the region of the emerging cavity between 10 and 14 DAP. Experimental evidences for an accumulation of oligo fructans were obtained by enzyme

assays, performed directly on tissue slices or by using extracted cavity sap. A further quantification of sugars by LC and amperometric detection confirmed these results and additionally exhibited differential patterns for the fructan isomers of DP 4. All determined sugars showed an accumulation in the cavity sap compared to the total kernel amount during the storage stage (Table 25). The concentrations of the hexoses and of sucrose just slightly increased between 7 and 14 DAP in the transfer region/cavity whereas 1-kestose steeply rose. Nystose (DP 4) was nearly exclusively detected in the cavity sap, with a steep incline as well. In contrast, the concentration of bifurcose (the structural isomer of nystose) decreased from 7 to 14 DAP in extracted cavity sap and in total kernels. Figure 50 shows the partition of the determined sugars in the transfer region (7 DAP) and for the extracted cavity sap (10 and 14 DAP). The diagrams clearly display that oligo fructans become the major sugar components during the storage stage in this region.
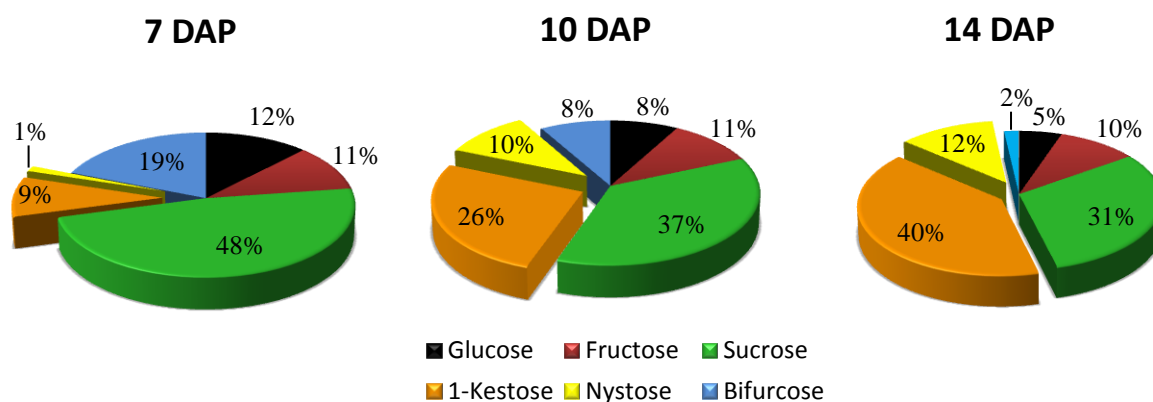
Figure 50: Percentage amounts of quantified sugars (according to µmol/g FW) in separated transfer region (7 DAP) and extracted cavity sap (10 and 14 DAP). Hexose levels were generally low and didn't change extensively. The level of bifurcose steeply declines, whereas the level of nystose becomes larger. The major sugar compound during the storage stage in the cavity is 1-kestose.

In this thesis, the direct visualization of oligosaccharide distributions in tissue slices, and the quantification of the particular fructan molecules during these developmental stages were shown for the first time. The accumulation of fructans in cereals is mainly described for vegetative tissues such as leaves and stems (as described in Pollock and Cairns (1999) and references). The presence of fructans in kernels of barley and wheat was described by Cerning and Guilbot (1973) and Henry and Saini (1989). In the study presented here, the high quantities of oligo fructans were related to the formation of the endospermal cavity (making ≥ 50% of sugars at 14 DAP,

Figure 50). These results coincide with earlier studies, where a fructan accumulation in the cavity of wheat during the late maturation stage (20-27 DAP) was found (Lim and Gifford, 1984; Ugalde and Jenner, 1990a).

Fructans form a complex carbohydrate class and just 10 to 15 % of higher plants exhibit fructan metabolism (Vijn and Smeekens, 1999; Cairns et al., 2000; Van den Ende et al., 2004). Among them the greater proportion of fructan species grows in seasonal habitats. In Hendry (1993) an overview of fructan distribution in the plant kingdom is given. Agronomical important crops containing fructans within the monocots are Poales and Liliales, within the dicots Asterales (Pollock et al., 1996; Vijn and Smeekens, 1999). Different classes of fructans are distinguished according to the position of the sucrose moiety, the kind of linkage between the fructose residues (ß-2,1; ß-2,6 or mixed pattern) and the chain lengths (John, 1992; Pollock and Cairns, 1999) (Cochrane, 2000). The determined oligo fructans 1-kestose and nystose belong to the linear inulin type fructans (having (2-1)-linked ß-d-fructosyl units). Bifurcose displays a mixed levan type of fructans (containing both, (2-1)- and (2-6)-linked ß-d-fructosyl units). Both classes are known to occur in Poales (Vijn and Smeekens, 1999).

The subcellular localization of fructans is generally described to be vacuolar (Darwen and John, 1989; Pollock et al., 1996; Vijn and Smeekens, 1999). Two possible reasons for the here observed apoplastic abundance are suggested: (i) The high concentration in the cavity sap could result from PCD processes of NP cells that release the fructans into the cavity. Similar to this, Ugalde and Jenner (1990a) and Schnyder et al. (1993a) concluded from their results that the biosynthesis of oligo fructans occurs during early development in vacuoles of nucellus cells that are subsequently broken down. (ii) As the highest signal intensities of DP 3 and 4 sugars were found at the surrounding cells of the cavity (Figure 34) the microsomal model that was firstly described by (Kaeser, 1983) is taken into consideration. The co-expression of fructan synthesizing and degrading enzymes (Valluru and Van den Ende, 2008) is hypothesized to be associated to a microsomal differentiation: the vacuole as the major site of storage, but synthesis may occur in small vesicles (Pollock and Cairns, 1999; Cairns et al., 2008). These vesicles could mediate a vesicle-derived-exocytosis of fructans (Valluru and Van den Ende, 2008). An apoplastic abundance of fructans and also of FEH activity was already reported for oat crown tissues and is explained by the microsomal model (Livingston and Henson, 1998; Kawakami et al., 2005).

4.2.2.   Is *de novo* synthesis the source of fructan accumulation?

The temporal differentiated accumulation patterns of fructan oligomers and even of structural isomers such as bifurcose and nystose suggested a *de novo* biosynthesis of fructans in the developing barley grain. The biosynthesis of fructans includes the activity of different fructosyltransferases (FTs) that have been described for several plant species (Vijn and Smeekens, 1999), and is illustrated in Figure 51 according to Livingston et al. (2009).
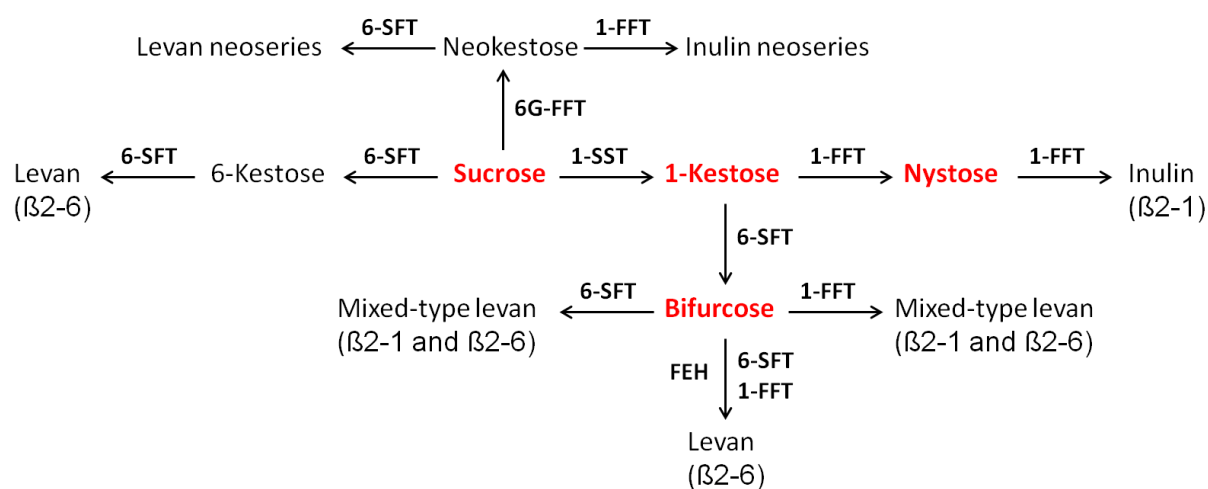
Figure 51: Model for fructan biosynthesis as proposed by Livingston et al. (2009). Synthesis starts in the vacuole with sucrose as both the donor and substrate molecule. Oligo fructans showing specific spatial and temporal accumulations are indicated in red. Neokestose was not detected. Only trace amounts were detected for 6-kestose and therefore this compound is excluded from discussion.

Abbreviations are: 1-FFT, fructan:fructan 1-fructosyltransferase; 1-SST, sucrose:sucrose 1-fructosyl-transferase; 6-SFT, sucrose:fructan 6-fructosyltransferase.

Temporal and spatial differences of expression patterns for genes involved in the biosynthesis and degradation were obtained by qRT PCR analysis (Figure 40). In Figure 52 the patterns of oligo fructan accumulations and of the gene expression data are summarized. The temporal accumulations of the particular sugars correspond to the expression of the genes from fructan metabolism. Between 5 and 7 DAP a high gene expression of 6-SFT in the endosperm was obtained (Figure 40) that nearly stops with the beginning of the storage stage. The presence of this enzyme was further proven by its identification in protein extracts from 7 DAP old grains (Figure 42). 6-SFT catalyzes the elongation of 1-kestose and 6-kestose, forming levan type linkages. It is also capable to synthesize the initial step, thus, producing 6-kestose (Livingston et al., 2009). The expression of this enzyme concurs with the high quantity of bifurcose before onset of storage accumulation. The production of the precursor molecule 1-kestose can be realized by

1-SST that catalyzes the reaction of two sucrose molecules to 1-kestose and glucose, and is also expressed in the endosperm at 5 DAP (but to a less extend).

With transition to storage product accumulation and to cavity formation (7 and 10 DAP) gene expressions of 1-SST, 1-FFT and 1-FEH were found in cells of the NP (Figure 41). The enzyme 1-FFT catalyzes the elongation by transferring a single terminal fructose from an oligosaccharide to another fructan molecule, thus producing inulin type linkages (Livingston et al., 2009). FEHs degrade terminal fructosyl-fructose linkages, releasing fructose monomers. All to date purified plant FEHs are unable to degrade sucrose (Van den Ende et al., 2004). These findings indicate a major biosynthesis of inulin type oligo fructans in the NP. The concerted action of 1-SST (highest expression rate), 1-FFT and 1-FEH suggest a regulation of the chain length as the tri- and tetra oligo fructans (of inulin type) are most abundant in the cavity during the storage stage (Figure 52). By the applied proteomics approach the enzymes 1-SST and 1-FFT couldn't be identified so far. In future experiments, dissected seed material should be used for the protein extraction to increase the proportions of the particular enzymes compared to total grain extracts. Furthermore, the antisera against the particular enzymes have to be purified to decrease the level of cross reactions as observed by different Western blot analyses (data not shown). An expression of vacuolar invertase (WIRVa) was observed for the NP and ETC during early storage stage (10 to 14 DAP, Figure 52). This enzyme could also be involved in the biosynthesis of 1-kestose as acid invertases are generally known to have trans-fructosylation activity (function as 1-SST) depending on the sucrose concentration (Housley and Pollock, 1993; Vijn and Smeekens, 1999).

Up to now, the regulation of chain length is not fully understood and multifunctionality of the involved enzymes (e.g. fructosylation and hydrolyzation capabilities of invertases) complicates a clear description (Pollock and Cairns, 1991; Gupta and Kaur, 2000; Van den Ende et al., 2004; Kawakami et al., 2005; Banguela and Hernández, 2006). It is known that the synthesis in stems and leaves occurs in dependence of the sucrose concentration (Schnyder, 1993b; Wardlaw and Willenbrink, 1994; Cairns et al., 2000). When photosynthesis exceeds demand, critical levels of sucrose in sink tissues are reported to induce fructan biosynthesis (Livingston et al., 2009). The synthesis of fructans occurs *de novo* from sucrose and the energy stored in the sucrose glycosidic bond fuels the process of trans-fructosylation (Pollock and Cairns, 1999).
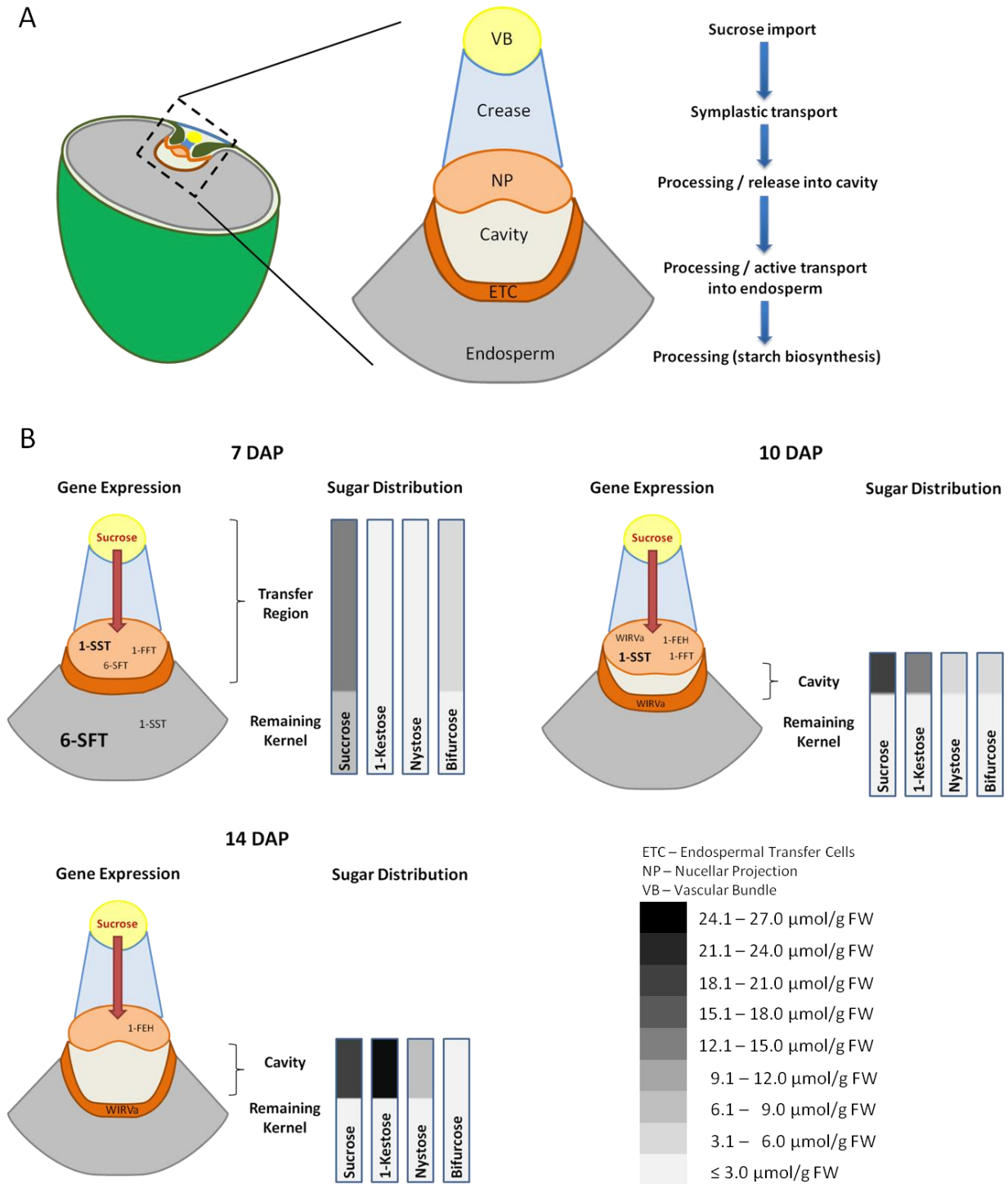
Figure 52: Overview of oligo fructan accumulation patterns and patterns of gene expression of fructan metabolizing enzymes from the transition stage (7 DAP) to the middle storage stage (14 DAP).

A: In several studies the import and processing of sugars were investigated. Sucrose as the major photoassimilate is transported from source organs to sink tissues such as developing seeds. In cereal seeds sucrose is released from the phloem of the vascular bundle into the cells of the pericarp (Lim et al. 2006). Nutrients symplastically move through the pericarp ground tissue (Patrick and Offler 2001), which is in

barley grains the crease region, towards the cells of the NP. Maternal and filial tissues are not symplastically connected (Ho and Gifford 1984). At the maternal/filial interface nutrients are released into the apoplasm, the endospermal cavity in barley and wheat. The cells of the NP are supposed to have regulatory properties controlling efflux of sucrose (Wang an Fisher 1995). The ETCs control the import by activity of specific hexose and sucrose transporters (Weschke et al., 2000). The developmentally depending expression patterns of genes from fructan metabolism gave hints for the processing of sucrose into oligo fructans.

B: Developmentally depending accumulation of oligo fructans, and expression of genes related to fructan metabolism:

7 DAP: Oligosaccharide distributions are slightly shifted to the separated transfer region. From the fructosyl oligomers, bifurcose is most abundant in the kernel. The expression of 6-SFT that is supposed to be involved in bifurcose biosynthesis, was found to be highest in the endosperm part of the grain.

10 DAP: Formation of the cavity has started. In extracted sap, higher concentrations of oligosaccharides compared to the remaining kernels were observed. The expressions of genes from fructan metabolism were exclusively detected in cells of the NP, confirming the accumulation patterns of oligo fructans.

14 DAP: Maximum expansion of the cavity occurs during mid-storage stage. Oligo fructans are the major sugar components in extracted cavity sap. The expression of synthesizing genes has stopped. A slight expression of 1-FEH that is involved in fructan degradation was observed.

The tissue and developmental stage specific analysis of gene expression patterns, and the detection of enzymes involved in fructan synthesis has not yet been described before in cereals. Housley and Daughtry (1987) could demonstrate enzymatic activity of FTs in wheat kernels between 6 and 12 DAP. This was related to the proposed SST/FFT model from Edelman and Jefford (1968), but clear evidences for the identification of both enzymes in wheat kernels were not given. In feeding experiments with $^{14}CO_2$ using 20 DAP old wheat kernels just trace amounts of radioactive fructosyl oligosaccharides were revealed, most of the radioactivity was incorporated into sucrose (Lim and Gifford, 1984). Also Ugalde and Jenner (1990a) who cultured 20 DAP wheat grains on ^{14}C-sucrose for 90 minutes couldn't detect radioactivity in form of oligo fructans but in the endosperm in insoluble form, concluding that at this developmental stage sucrose entering the grain remained mostly in this form during transport processes. In both studies one developmental stage (the late storage phase) was selected, whereas in the present study, the accumulation was found to occur with the beginning of the storage phase. In general, all three enzymes are described to be present and active in barley plants as described by Pollock and Cairns (1999) and references.

Concluding from the obtained fructan distribution and gene expression patterns differential roles of oligo fructan accumulations are assumed. These different roles depend on the developmental stage of grains and the specific localization of fructans inside the grain. The suggested functionalities are covered below.

4.2.3. What functions can be deduced from fructan accumulation patterns?

The spatially and temporally differentiated abundance of inulin and levan type oligo fructans in barley grains are suggested to be related to different functionalities. In general, fructans display a carbohydrate storage form in stems and leaves of temperate cereal crops, such as wheat, rye or barley (Nelson and Spollen, 1987; Schnyder, 1993b) . Synthesis of fructans was also related to regulate the sucrose pool size in terms of keeping the sink strength (Lim and Gifford, 1984; Pollock and Cairns, 1999; Housley, 2000). Further presumed functions are osmoregulation of cellular water potential, adaptation to low-temperature photosynthesis, and the lowering of the freezing point of tissue water upon depolymerization to fructose (Nelson and Spollen, 1987).

In this study, the biosynthesis of levan type fructans is suggested to be related to carbon partition (covered below, 4.2.3.1.); whereas the inulin type oligo fructans are potentially related to stress responses (4.2.3.2.).

4.2.3.1. Short term storage of carbohydrates

The oligo fructan bifurcose was found to be highest abundant in the barley caryopsis prior to onset of massive starch accumulation (Table 25). At 7 DAP the concentration in separated transfer region did not differ from total kernel concentration. From the results of qRT PCR analysis it is even more assumed that this tetrameric isomer higher accumulates in the endosperm than in cells of the NP or ETC. The time point of accumulation coincides with the differentiation of the ETC and the rapid induction of sucrose transporters (*HvSUT1*) from 5 DAP on, while the phase of main starch accumulation in barley is designated between 8/9 and 17/18 DAP (Weschke et al., 2000). Thus, it is suggested that the transient fructan production displays a form of carbohydrate partitioning. The rate of starch accumulation (beginning at 6 DAP) might not be limited by the sucrose supply, but by the activity of starch-synthesizing enzymes (Lim, 1988). Furthermore, the ratio of sucrose to hexose is an additional determinant of development. Similar to acid invertase activity, that has an impact on osmoregulation and cell enlargement (Lim et al., 2006), the 6-SFT activity might influence the hexose to sucrose ratio. Sucrose is split releasing glucose and adding the fructose moiety to 1-kestose forming bifurcose (according to Figure 51). In that way, the hexose to sucrose ratio is kept high and fits with the generally profound effect, that hexoses favor cell division and expansion, whereas sucrose favors differentiation and maturation (Weschke et al., 2003; Koch, 2004). The here observed decrease of bifurcose relates to the transition to main storage product accumulation, and coincides with the findings from

Schnyder et al. (1993a), who also found decreasing amounts of fructan in wheat endosperm when the rapid expansion growth ceases.

To further investigate this issue, the fructan content of isolated tissues during grain development should be determined. Feeding experiments using labeled sucrose (with a labeled fructose moiety) would support the investigations as incorporation of fructose into oligo fructans could be monitored. Such feeding experiments should be carried out at different developmental stages, 5, 7, 10 and 14 DAP.

4.2.3.2. Cell protection during the storage phase

The second accumulation of oligo fructans occurs with onset of massive starch accumulation and upholds until late storage stage (20 DAP). The imaging results indicated the highest concentrations of oligosaccharides in the surrounding cells of the cavity (Figure 34). This cavity is formed between the differentiated ETC and the NP (Figure 52). Part of the NP disintegrates and contributes to the cavity formation (Figure 53, Thiel et al. (2008). Targeted analyses revealed a developmentally depending accumulation of inulin type oligo fructans with 1-kestose and nystose being highly concentrated (Table 25). The present results from qRT PCR analysis indicate that fructan biosynthesis occurs at early storage stage, mainly in the NP, and that the fructan pool is then preserved.

For this observed pattern of oligo fructan accumulation, a function related to a protection of cells surrounding the cavity is supposed. This protection could concern membrane stabilization and/or scavenging of oxidative stress. A transient accumulation in the cavity to keep sink strength is precluded because of the temporal gene expression and the results obtained by Lim and Gifford (1984) and Ugalde and Jenner (1990a), who didn't detect *de novo* biosynthesis at later storage phase in wheat kernels. Furthermore, the turn-over rate of sucrose into starch is rapid and carbohydrate content from the endosperm and the cavity just feeds the demand for a few hours (Ugalde and Jenner, 1990a).

The cells that are involved in the transfer of nutrients have to be kept alive until finishing the grain filling period. In addition, the cells of NP and ETC exhibit transfer cell morphology, which means an enlargement of the cell surface area, a high density of transporter proteins, an extensive ER network and a high number of mitochondria (Ugalde and Jenner, 1990b; Patrick and Offler, 2001; Thiel et al., 2012).

Recent assumptions go for a direct participation of fructans in scavenging of reactive oxygen species (ROS). In barley grains, the high numbers of mitochondria in the ETC and NP are a source of ROS (Marchi et al., 2012). Furthermore, processes of PCD that occur in parts of the NP (Figure 53) are related to ROS as well. In this direction, lipoxygenase driven lipid oxidation and following ß-oxidation generate ROS (Anderson et al., 1999; Bethke et al., 2002; Keunen et al., 2013), that is stated to have a signaling role in PCD (Van Breusegem and Dat, 2006). Transcript studies of the barley NP revealed gene expressions related to a breakdown of macromolecules (e.g. lipoxygenase) and to a remobilization of nutrients (Thiel et al., 2008; Thiel et al., 2012). Additionally, genes from the biosynthetic pathway of ethylene that is involved in mediating PCD (Van Breusegem and Dat, 2006) were found to be up-regulated in NP and ETC (Thiel et al., 2008). The production of ROS scavenging compounds was observed for cells from the NP as well, indicating an improved resistance against oxidative damage and, thereby, an avoidance of senescence; e.g. the production of ascorbate and the expression of catalase and other redox-related genes in the ETC (Thiel et al., 2008). Secondary metabolites such as tannins are also present in cells of the NP (Gubatz and Shewry, 2011). These are declared to have antioxidant capacity (Riedl Ken et al., 2002; Zhao et al., 2011). From the literature data it can be concluded that the generation and scavenge of ROS takes place in those regions, where highest fructan accumulations were observed.
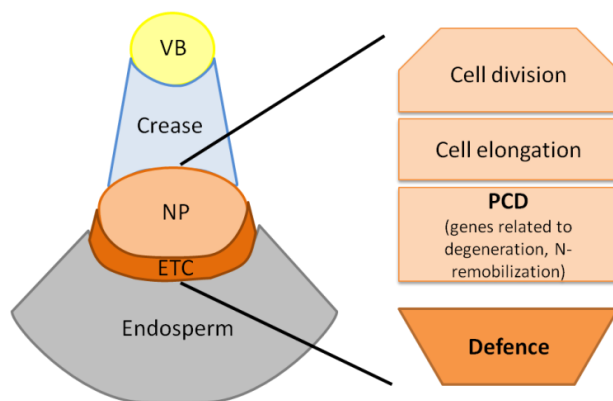
Figure 53: Model of cellular processes in NP and ETC at 8 DAP according to Thiel et al. (2008).

Parts of the NP are characterized to undergo PCD whereas other parts persist until end of nutrient import into the barley grain. Also the ETC keeps alive to sustain the import into the endosperm.

Stress (ROS) related gene expression was found for ETC, indicating a requirement of cell protection.

Sugars act as signaling compounds by inducing gene expressions that are involved in abiotic stress responses (Keunen et al., 2013; Peshev et al., 2013). *In vitro* experiments additionally indicated a direct scavenging capacity of inulin type fructans (Peshev et al., 2013). By reaction with radicals the sugars are partially broken down to mono- and disaccharides. A synergistic

action of phenolic compounds and fructans is proposed to be part of an integrated redox system, especially in tissues with high soluble sugar concentrations; detailed information is outlined in Bolouri-Moghaddam et al. (2010). The reactions of ROS are very fast and occur in direct neighborhood of the positions where OH* radicals are produced, mainly membranes (Van Breusegem and Dat, 2006; Gadjev et al., 2008). Peroxidation of membranes can affect membrane fluidity and functionality (Keunen et al., 2013).

A contribution of oligo fructans to membrane stability was shown by *in vitro* experiments using liposomes and extracted sugars from oat and rye. Especially inulins up to DP 5 showed increased protection against membrane leakage (Hincha et al., 2007). This protection was hypothesized to be determined by the structural flexibility of the sugar rings and glycosidic linkages that facilitate interaction with membrane lipids (Vereyken et al., 2003). In this way inulin type oligo fructans prevent phase transitions of membranes caused by dehydration (Kawakami et al., 2005). Such membrane stabilizing functionalities of fructans are so far discussed in relation to cold and drought stress (Kawakami et al., 2008; Keunen et al., 2013). An apoplastic localization of fructans and FEHs was related to an adaptive response during cold treatments (Livingston and Henson, 1998). A vesicle-mediated transport of these sugars and enzymes to the apoplast was proposed to be involved in this adaption by assisting stabilization of membranes (Valluru and Van den Ende, 2008).

In summary, PCD processes in direct vicinity of the NP and ETC, and the mitochondrial density in these transport active cells might be a source of oxidative stress that has to be quenched. As mentioned above, vitality of both tissues has to be kept until the end of nutrient import. The high accumulations of low DP inulin type fructans are suggested to be related to overcome this abiotic stress and to stabilize plasma membranes.

4.2.4. Concluding remarks to the specific fructan patterns in barley grains

In the here presented study it was shown that the transition stage, which was found to represent a major physiological switch between cellularization and storage product accumulation, also represents a switch in fructan metabolism in the barley kernel. This switch concerns the kind of fructans accumulated as well as their hypothesized specific roles during the prestorage phase and the storage phase. For the first time, a time curve of accumulation of particular oligo fructans, the connection to cells surrounding the cavity and the tissue specific expression patterns of genes from fructan metabolism have been shown.

The outcomes of the presented study encourage for further efforts to unravel the function and the regulation of fructan metabolism in cereal grains. Considering the developmentally and spatially specific distributions of oligo fructans during grain development, further studies have to be carried out regarding the subcellular localization. The physiological relevance of fructan accumulation in the cavity is not yet proven. A general proof of the introduced concepts needs indeed more attention and practical evidences from *in vitro* and *in vivo* experiments. Here, production of RNAi lines repressing fructan synthesis in NP and endosperm (e.g. of 1-SST and 6-SFT) would help to give hints for a functionality of fructans. The capacity of cavity sap to scavenge ROS should be determined *in vitro* by Fenton reactions according to Peshev et al. (2013). In a continuing experiment cell suspension cultures could be exposed to ROS (H_2O_2) monitoring the cell death rate (TUNEL assay) according to different levels of fructans contained in the culture medium.

4.3. Patterns of Lipid Distributions Indicate Divers Tissue and Developmentally Specific Roles

Differing distribution patterns of lipids in a tissue but also in a developmentally specific manner were observed by the MALDI MSI approach. Most of the here identified lipids belong to the phosphatidylcholines (PC) that are mainly known to be part of biological membranes; phospholipids make up ≥50% of lipids in most membranes (Alberts et al., 2002). The individual lipid composition is characteristic for specific membrane types, and directly defines their biophysical properties, as well as the sorting and action of integrated/associated proteins (Al-Saad et al., 2003; Dörmann, 2005; Ham et al., 2005; Heldt and Piechulla, 2011). Besides to this, PCs and LPCs are also known to be surfactants of storage lipid droplets (Krahmer et al., 2011; Barthole et al., 2012), and to be part of the signaling network (Viehweger et al., 2002).

- The observed endosperm specific distribution patterns of PCs and LPCs are suggested to be involved in the formation of association complexes with starch granules (4.3.1.).
- The embryo contains particular lipids that are related to the storage product constitution and to the antioxidant system (4.3.2.).

4.3.1. Phosphatidylcholines are gradually deposited in the endosperm during the storage stage

With the beginning of the storage stage, an increasing abundance of particular PCs and LPCs in the endosperm was observed. Several of them showed an increasing accumulation towards the periphery (*m/z* 520, 558, 783, 821); the others were homogeneously distributed (*m/z* 496, 534, 759, 797, 799, 823). High concentrations of PCs in the barley endosperm are in accordance with the findings from Finnie et al. (2009), but interestingly, clear differences of lipid distribution patterns were observed for rice (Zaima et al., 2010b). In mature rice seeds the PCs *m/z* 797, 799, 821, 823 and 825 were assigned to be higher accumulated in the rice bran (which includes the seed coat and the germ), whereas the same patterns were observed for the LPCs (*m/z* 496, 520, 534).

As phospholipids are major components of the plasma membranes, a specific constitution of the barley endospermal membranes is suggested. The plasma membrane system of this tissue is characterized by the presence of numerous plasmodesmata (Wang et al., 1995b) that facilitate the radial gradient flow of nutrients to the places of storage product biosynthesis, which is near the periphery in the case of starch accumulation (Rolletschek et al., 2004). Furthermore, the ER membrane constitution could be specifically adapted to the formation of prolamin aggregates that is an endosperm specific process (Heldt and Piechulla, 2011).

For the lipids that exhibited a concentration gradient towards the periphery, two possibly functions are suggested. (i) The oil content of barley grains that accounts for 2-4% of seed dry weight (Seefeldt et al., 2011; Barthole et al., 2012) is concentrated in the embryo and in the aleurone layer (Neuberger et al., 2008). There, the lipids are stored in form of oil bodies, which are stabilized by oleosins and phospholipids. A participation of peripheral localized PCs to the formation of these oil bodies would be possible. (ii) Whereas the aleurone and germ contain primarily nonpolar lipids, the flour (endosperm) lipid composition is distinctive different, comprising mainly digalactosyldigylcerol (DGDG), monogalactosyldigylcerol (MGDG) and phospholipids (predominantly PC, LPC and lysophosphatidylethanolamine (LPE) (Finnie et al., 2009; Finnie et al., 2010b). These polar lipids were found to be starch granule bound (Finnie et al., 2010a). Especially LPCs are described to form inclusion complexes with the amylose component of starch granules (Morrison, 1978; Morrison et al., 1993), with palmitic acid (C16:0) and linoleic acid (C18:2) as the major fatty acid moieties (Lee and BeMiller, 2008). Also in the here presented study, the corresponding *m/z* values (*m/z* 496 = LPC 16:0 and *m/z* 520 = LPC

18:2) were found to be accumulated in the endosperm at the storage stage. These associations are speculated to promote helix formation during the synthesis of amylose (a more uniform α-(1-4) glucan chain length and branching) (Becker, 2007). In addition, the polar headgroup might be involved in ordering the helices through electrostatic interactions (Baisted, 1981). During germination a slower hydrolysis of amylose was found for high lipid starches (Baisted, 1981). So far, the positive correlations of amylose and polar lipid content are discussed towards seed quality parameter; e.g. grain hardness and baking quality (Giroux and Morris, 1998; Pasha et al., 2010; Finnie et al., 2010a; Finnie et al., 2010b), and nothing is known about the formation processes. A mutual regulation is suggested for the biosynthetic pathways of starch, lipids and also of proteins that can be part of these association complexes as well. Such attached proteins are described for wheat (Darlington et al., 2001; Beecher et al., 2002; Finnie et al., 2010b). Additionally, a small granule size of starch (B-type granules) was correlated to a higher lipid content (Geera et al., 2006). This granule type was shown to be higher accumulated in peripheral parts of the endosperm (Rolletschek et al., 2004), which would support the assumption that higher abundant PCs in the endosperm periphery are related to starch association complexes (Figure 54).

The obtained gradients of lipids are suggested to reflect a correlation of lipid biosynthesis to the requirement of oxygen and reduction equivalents (NADH/NADPH). Lipids in the endosperm are generated *de novo* from acetate that originates from sucrose degradation (Seefeldt et al., 2011).
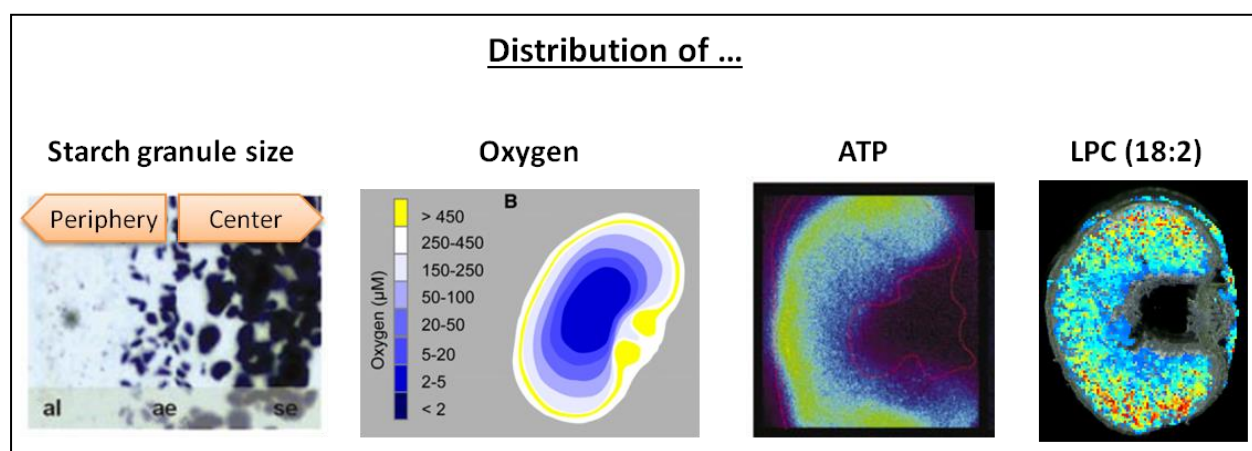
Figure 54: Similar distribution pattern of starch granule size, oxygen supply, ATP and polar lipids (such as LPC 18:2), indicating a common regulatory network. Figures for starch granule size, oxygen and ATP are taken from Rolletschek et al. 2004 and 2011.

In general, the assimilate partition is assumed to be related to the different demands on energy supply, which is highest for lipids, followed by proteins and lowest for starch (Borisjuk et al.,

2004). A favored localization of lipid synthesis in those regions that are better provided with oxygen and ATP would be plausible (Figure 54), analogous to the findings for starch biosynthesis (Rolletschek et al., 2004), and to the declining gradient of protein content from the periphery (aleurone) to the starchy endosperm (Borisjuk et al., 2004; Gubatz and Shewry, 2011).

In summary, the observed patterns of particular PCs and LPCs indicated a relation to the final endosperm constitution that is defined by the interplay of starch, lipid and protein biosynthesis. Factors that determine a specific mutual regulation of all three pathways remain still unclear and have to be further elucidated. Especially a subfractionation of the endosperm into central and peripheral parts for quantitative transcript studies would provide more information regarding a correlation to oxygen and ATP supply.

4.3.2. Lipid accumulation in the developing embryo

Embryo specific distributions of different lipid species were observed by a non-targeted GC-MS analysis of dissected barley seed material. The investigation of three developmental stages revealed an accumulation of α-tocopherol, α-linolenic acid, pentadecanoic acid, squalene and pentacosanol from 7 to 14 DAP in the embryo fraction (Figures 46 and 47). These findings are in accordance to the studies of Banaś et al. (2007) and Moreau (2009), where α-tocopherol and α-linolenic acid have been described to be highly accumulated in the embryo of mature barley kernels. Tocopherols are supposed to serve as antioxidants in relation to changes of the redox status during maturation (Falk et al., 2005). The accumulation of fatty acids and long chain fatty alcohols indicate a relation to the onset of storage product synthesis, as these are parts of the germ oil (Megahad and El Kinawy, 2002; Barthole et al., 2012) that is the major storage site of apolar lipids in the embryo.

4.3.3. Concluding remarks to the potential role of lipids on kernel characteristics

In the presented study different patterns of lipids during the storage stage were observed. PCs and LPCs were found to accumulate in the endosperm either homogeneously or with an increasing gradient towards the periphery. The embryo mainly contains apolar lipids. Both lipid types (polar and apolar) are suggested to be parts of the different storage sites within the barley grain.

In future investigations, the distribution patterns of further lipid classes should be elucidated. For lipids, whose ionizations were suppressed by PCs, other technical solutions are required. In terms of MALDI MSI, the usage of different matrices and/or negative ionization mode could provide an

alternative (e.g. DAHP was found in preliminary experiments to be suited for analysis of sterols). The application of further MS-based techniques like SIMS (Passarelli and Winograd, 2011), or DESI (Dill et al., 2009; Zaima et al., 2010a; Eberlin et al., 2011) has the potential to complement the lipid analysis, together with other high resolution approaches that allow an elucidation of divers lipids at tissue, cell and subcellular level (Horn and Chapman, 2012a).

The contribution of particular PCs to specific endospermal membrane constitutions, and to the formation of associations to starch granules should be investigated. For the examination of the endosperm texture several barley varieties exist that differ in their amylose/amylopectin ratios and/or lipid contents (e.g. *Amo1* mutant, Riso 1506, waxy lines and high amylose varieties). These could be used for analyses of lipid, starch and protein biosynthesis in a spatially and developmentally depending manner, to extrapolate correlations between these three compound classes that are combined and stored in form of complexes.

4.4. Distribution Patterns of CK and ABA Indicate Tissue Specific Functionalities

Phytohormones are key players in the regulation of plant growth and development, and their biological activity is determined by the interplay of various different hormone classes (Wang and Irving, 2011). As related to seed developmental processes, and since the information on phytohormone distributions in cereal grains is lacking, the elucidation of them in dissected barley grain material, and from different developmental stages was addressed. In the presented study, abscisic acid (ABA) and cytokinin (CK) levels were revealed by MRM determination of purified extracts (Figure 44). Minimum amounts of ~20 mg fresh weight were necessary for the sample preparation procedure; in recent publications lowest amounts of 10-100 mg fresh weight per sample were taken for the preparation (Novák et al., 2008; Kojima et al., 2009; Owen and Abrams, 2009; Turečková et al., 2009; Strnad et al., 2011). Tests of recovery rates for auxin, salicylic acid, gibberellic acids and jasmonic acid revealed the chosen extraction method as not appropriate. For those hormones other protocols have to be used.

4.4.1. Decrease of the filial cytokinin level with the transition to the storage stage

Trans-zeatin (tZ), a major biological active form of CK, and its transiently inactivated form *trans*-zeatin riboside (tZR) were determined as the highest abundant forms of CK in the

developing barley grain. The proportions of both types were found to be highest in the embryo and endosperm. From 7 to 14 DAP (Table 26) the total kernel concentrations decreased, and furthermore, also the proportions in the endosperm and embryo compared to the other seed parts declined (Figure 44). This pattern of CK reduction in the filial tissues after the cellularization phase can be related to the general character of CKs to control cell division (Schmülling, 2004; Davies, 2010). The obtained results are in accordance to the published data from Yang et al. (2000) and Yang et al. (2002), who demonstrated a close association of the endospermal cell division rate and the CK level (especially for Z and ZR) in rice. Similar findings were observed for maize kernels (Rijavec et al., 2009). CK activity in plant seeds was also suggested to regulate the sink strength by affecting the expression of genes that encode cell wall invertases and hexose transporters (Werner and Schmülling, 2009; Zalewski et al., 2010). The promotion of cell division by CKs and the metabolism of sucrose are directly linked with each other, as the high rate of cellularization during the early developmental stages requires high rates of energy supply. A correlation of CK signaling and sugar metabolism was found in the study of the Riso 16 mutant (Faix et al., 2012).

4.4.2. ABA and ABA-GE in relation to storage accumulation

The concentration of ABA was found to be similar in all dissected grain parts (Figure 44). Even though the total concentration changes between 7 and 14 DAP, this didn't affect the proportions in the particular grain parts, indicating that the changes occur to similar extends (Table 26). From 7 to 10 DAP a decrease of the total ABA concentration was observed, but increased again between 10 and 14 DAP. This pattern coincides with earlier studies that ABA peaks two times during seed development (Finkelstein et al., 2002; Govind et al., 2011). The first peak is related to the cellularization stage and ceases when the grain enters the transition phase. This early peak of ABA is believed to be of maternal origin, and ABA is then transported to the filial parts. The second accumulation of ABA is associated to the onset of massive storage accumulation. It is supposed to be of filial origin as a gene expression of enzymes involved in the biosynthesis was found in the endosperm and the embryo (Sreenivasulu et al., 2006; Finkelstein, 2010; Seiler et al., 2011). The nearly homogeneous tissue distribution, obtained in this study, is suggested to be related to the general role of ABA during all stages of grain development. It is involved in the regulation of storage product synthesis, in the promotion of seed desiccation tolerance, and it is essential for the induction of dormancy (Finkelstein et al., 2002; Nambara and Marion-Poll,

2003; Gutierrez et al., 2007; Becraft and Yi, 2010). In a recent study, ABA was also proposed to have regulatory influence on the cell differentiation of the ETC and the endosperm (Thiel et al., 2012). In concert with ethylene it promotes PCD processes in the endosperm, and in the embryo it is related to the deposition of oil bodies (Sreenivasulu et al., 2006). As outlined above, the regulatory functions of phytohormones always depend on their combined interplay, and the complex role of ABA is described as follows: high concentration of ABA reduces transport of sucrose into the grains and lowers the ability of grains to synthesize starch, while the appropriate concentration of ABA can enhance SuSy activity and increases the expression of genes related to starch metabolism (Zhu et al., 2011).

ABA homeostasis is simultaneously regulated by biosynthesis and catabolism. Inactivation takes place through two main routes; the hydroxylation pathway, where ABA is converted to phaseic acid and further to dihydrophaseic acid, or by conjugation to glucose, forming the ABA-glycosyl ester (ABA-GE) (Xu et al., 2002). In the present study, ABA-GE was found in much lower concentrations than free ABA but it shows a higher proportion in the endosperm. The specific role of ABA-GE is not yet known. While the hydroxylation pathway is irreversible, ABA-GE can be hydrolyzed back by activity of a beta-glucosidase (BG). Thus, it could serve as a transport or a storage form (Hartung et al., 2002; Xu et al., 2002; Priest et al., 2006; Jiang and Hartung, 2008). In addition, a relation to stress responses was shown as well, and the expression of BG at high levels in the endosperm and embryo of barley grains (Seiler et al., 2011) coincides with the here observed pattern of ABA-GE.

An evidence of ABA-GE biosynthesis in barley grains was never supplied. In this study, first indications were gathered by Western blot experiments. As the gene sequence of a barley ABA-glycosyltransferase (ABA-GT) is not yet annotated, the Arabidopsis ABA-GT (UGT71B6) was recombinantly expressed for antibody production. This enzyme was characterized to recognize the naturally occurring enantiomer of ABA and to massively increase the ABA-GE level in transgenic plants of *A. thaliana* (Priest et al., 2006). The purified antiserum was applied for the detection of ABA-GT on Western blots of separated barley seed protein extracts from the different developmental stages (data not shown). Clear signals could were revealed in 1-D and 2-D experiments. The observed patterns corresponded to the protein size of 53.8 kDa for UGT71B6 (http://www.uniprot.org/uniprot/Q9LSY6). From 7 to 14 DAP a reduction of band (1-D) and spot (2-D) intensity at ~50 kDa was observed. This correlates to the obtained ABA-GE concentrations that decreased from 7 to 14 DAP as well. As glycosyltransferases share homolog

sequences, cross reactions are not excluded. A phylogenetic tree of glycosyltransferases (http://www.p450.kvl.dk/ugt_all_030802_tree.pdf) showing their high homology was provided by Søren Bak and Suzanne Paquette. In future experiments, the activity of this enzyme in barley kernels has to be confirmed.

In summary, during the storage stage ABA is involved in several processes of barley grain development, especially those that are related to the endosperm formation and storage production. The accumulation of the biologically less active form, the ABA-GE, in the endosperm is suggested to a tight regulation of the ABA levels according to short term demands by a transient interconversion.

4.4.3.   Concluding remarks to phytohormone distributions

For the first time, the concentrations of two hormone classes (ABA and CK) could be determined for the particular grain parts in terms of seed development. The observed patterns could be related to developmental proceedings, but it has to be kept in mind that the patterns for ABA and CK can just be seen as a part of a complex regulatory network as the actions of phytohormones depend on their relative ratios to each other (synergistic and antagonistic effects). Further experiments should elucidate the levels of the other hormones. Especially auxin, a key regulator of cell specification in cross-talk with CK (Su et al., 2011), would be of high interest. In this regard, Becraft and Yi (2010) hypothesized the regulation of aleurone differentiation by an auxin-CK interplay. Action of ethylene was proposed rather antagonistically to ABA in glucose sensing, mediating PCD, and during germination (Eckardt, 2002; Finkelstein et al., 2002; León and Sheen, 2003; Sreenivasulu et al., 2006). Special attention is needed regarding the question how local phytohormone levels are regulated during development. To get access to such local hormone concentrations more sensitive detection methods are necessary to downscale the tissue amounts needed for the detection.

5.   Summary

To deepen the knowledge about the physiological processes that occur in a developing seed is in the focus of this thesis. Processes of cellularization and storage accumulation are subjected to a complex regulatory network. Actually, we are still away from knowing how the decisions are made to switch from cell proliferation to the biosynthesis of storage products, which are crucial for the fate of the imported nutrients. The presented work constitutes new insights into grain development. The key findings of this study comprise the tissue and developmentally depending distribution patterns of particular metabolites, including: (i) characteristic phospholipid patterns in the endosperm, (ii) an integrated study of oligo fructan accumulations at the transcript, the protein and the metabolite level, and (iii) particular distribution patterns of the phytohormones ABA and CK.

i.   The accumulation of PCs and LPCs in the endosperm of cereal grains is already known. In this thesis, gradually differential patterns for individual PCs and LPCs could be shown. Furthermore, the accumulation of lipids in the endosperm was related to the early storage stage. Particular lipids are suggested to be involved in the formation of association complexes with starch granules, and thus, having an impact on the final grain quality.

ii.   Oligo fructans of the inulin type were found to highly accumulate in the forming endospermal cavity, whereas bifurcose, a mixed levan type fructan, steeply decreased with the onset of storage production. The results from gene expression and protein analyses supported the hypothesis of a fructan *de novo* biosynthesis. Here, the spatial and temporal patterns of expressed genes, related to the biosynthesis of the particular fructan types, corresponded to the observed sugar distributions. Discrete functions during grain development are suggested to the differential patterns of oligo fructans. First, synthesis of the branched form (bifurcose) is related to short term storage, possibly involved in keeping sink strength prior to starch accumulation and/or in osmoregulation. Second, the accumulation related to the emergence of the cavity is assumed to be related to the protection of living cells around the cavity (membrane stabilization and/or ROS scavenging). A summarizing scheme is presented in Figure 55.
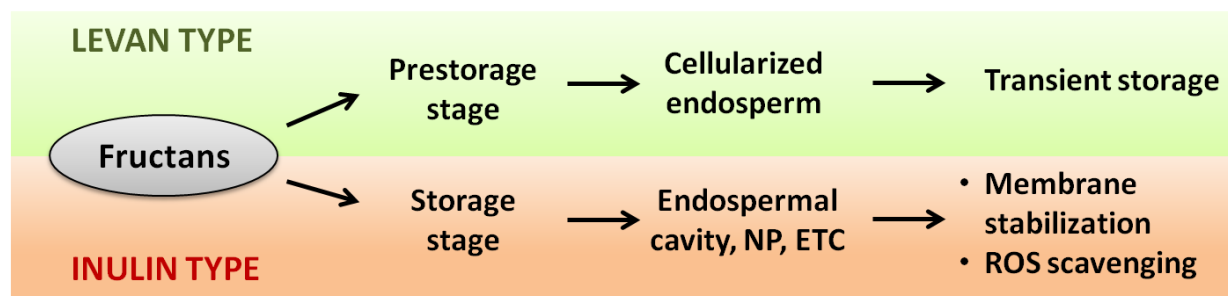
Figure 55: Differential distribution patterns of oligo fructans in the developing barley grain are hypothesized to be related to different functionalities. These are deduced from the obtained results in this study and from the literature. The proof of this concept is in the focus of further investigations. NP, nucellar projection; ETC, endospermal transfer cells; ROS, reactive oxygen species.

iii.   For ABA and CK development- and tissue-specific concentrations were observed. Both phytohormones have important effects on the final grain composition. A relation of CK to cellularization processes is suggested as the highest proportions were found in filial parts of the developing grain. Thus, cell cycle control by CK could be related to cell number and by this to the final grain composition.

A broad range of different metabolite distributions was gained in this presented study. The MALDI MSI approach revealed candidate compounds that are suggested to have an impact on the final grain composition. These candidates will be included into further integrated approaches to deepen the knowledge of developmental processes. In this regard the analysis of the formation of starch-lipid complexes would exhibit information about carbon partitioning that would be useful for the influence on grain quality parameters. The here hypothesized roles of oligo fructans for membrane stabilization and ROS scavenging have to be evaluated by *in vivo* experiments as a function related to maintaining the vitality of nutrient transfer cell would be of highest importance for the grain filling. The patterns of ABA and CK have to be integrated into an entire network of phytohormone distributions within the barley grain. Further efforts should go for the elucidation of the remaining hormone classes.

6. References

Al-Saad KA, Zabrouskov V, Siems WF, Knowles NR, Hannan RM, Hill HH (2003) Matrix-assisted laser desorption/ionization time-of-flight mass spectrometry of lipids: ionization and prompt fragmentation patterns. Rapid Communications in Mass Spectrometry **17:** 87-96

Alberts B, Johnson A, Lewis J, Raff M, Roberts K, Walter P (2002) Molecular Biology of the Cell, Ed 4. Garland Science, New York, USA

Amiard V, Morvan-Bertrand A, Billard J-P, Huault C, Keller F, Prud'homme M-P (2003) Fructans, But Not the Sucrosyl-Galactosides, Raffinose and Loliose, Are Affected by Drought Stress in Perennial Ryegrass. Plant Physiology **132:** 2218-2229

Amme S, Rutten T, Melzer M, Sonsmann G, Vissers JPC, Schlesier B, Mock H-P (2005) A proteome approach defines protective functions of tobacco leaf trichomes. Proteomics **5:** 2508-2518

Anderson KM, Seed T, Ou D, Harris JE (1999) Free radicals and reactive oxygen species in programmed cell death. Medical Hypotheses **52:** 451-463

Baisted DJ (1981) Turnover of starch-bound lysophosphatidylcholine in germinating barley. Phytochemistry **20:** 985-988

Banaś A, Debski H, Banaś W, Heneen WK, Dahlqvist A, Bafor M, Gummeson P-O, Marttila S, Ekman Å, Carlsson AS, Stymne S (2007) Lipids in grain tissues of oat (Avena sativa): differences in content, time of deposition, and fatty acid composition. Journal of Experimental Botany **58:** 2463-2470

Banguela A, Hernández L (2006) S223-248. Biotecnología Aplicada **23:** 202-210

Barthole G, Lepiniec L, Rogowsky PM, Baud S (2012) Controlling lipid accumulation in cereal grains. Plant Science **185–186:** 33-39

Becker R (2007) Fatty acids in food cereal grains and grain products. *In* CK Chow, ed, Fatty acids in foods and their health implications. CRC Press, Boca Roaton, USA, pp 271-284

Becraft PW, Yi G (2010) Regulation of aleurone development in cereal grains. Journal of Experimental Botany

Beecher B, Bowman J, Martin JM, Bettge AD, Morris CF, Blake TK, Giroux MJ (2002) Hordoindolines are associated with a major endosperm-texture QTL in Barley (Hordeum vulgare). Genome **45:** 584-591

Berit E, Daniela Z, Alexander E, Ines F, Jürgen H, Annette N, Joachim K, Joachim F (2010) Metabolic profiling of Arabidopsis thaliana epidermal cells. Journal of Experimental Botany **61:** 1321-1335

Bethke P, Fath A, Spiegel Y, Hwang Y-s, Jones R (2002) Abscisic acid, gibberellin and cell viability in cereal aleurone. Euphytica **126:** 3-11

Bethke PC, Jacobsen JV, Jones RL (2000) Barley Biotechnology *In* M Black, JD Bewley, eds, Seed technology and its biological basis. CRC Press, Boca Raton, USA, pp 184-226

Bewley JD, Bradford KJ, Hilhors HWM, Nonogaki H (2013) Seeds - Physiology of Development, Germination and Dormancy, Ed 3. Springer, New York, USA

Black MJ, Bewley JD, Halmer P (2006) The Encyclopedia of Seeds. CABI

Blackig M, Corbineau F, Grzesikit M, Guyi P, Côme D (1996) Carbohydrate metabolism in the developing and maturing wheat embryo in relation to its desiccation tolerance. Journal of Experimental Botany **47:** 161-169

Bolouri-Moghaddam MR, Le Roy K, Xiang L, Rolland F, Van den Ende W (2010) Sugar signalling and antioxidant network connections in plant cells. FEBS Journal **277:** 2022-2037

Borisjuk L, Rolletschek H, Radchuk R, Weschke W, Wobus U, Weber H (2004) Seed Development and Differentiation: A Role for Metabolic Regulation. Plant Biology **6:** 375-386

Bradford M (1976) A rapid and sensitive method for the quantitation of icrogram quantities of protein utilizing the principle of protein-dye binding. Anal Biochem **7:** 248-254

Burrell MM, Earnshaw CJ, Clench MR (2007) Imaging Matrix Assisted Laser Desorption Ionization Mass Spectrometry: a technique to map plant metabolites within tissues at high spatial resolution. J. Exp. Bot. **58:** 757-763

Byung-Kee B, Newman CW, Newman RK (2011) Food Uses of Barley. *In* SE Ullrich, ed, Barley: Production, Improvement, and Uses. Wiley-Blackwell, Chichester, West Sussex, UK, pp 532-562

Cairns AJ, J. PC, Gallagher JA, Harrison J (2000) Fructans: Synthesis and Regulation. *In* RC Leegood, TD Sharkey, S von Caemmerer, eds, Photosynthesis: Physiology and Metabolism. Kluwer Academic Publishers, pp 301-320

Cairns AJ, Turner LB, Gallagher JA (2008) Ryegrass leaf fructan synthesis is oxygen dependent and abolished by endomembrane inhibitors. New Phytologist **180:** 832-840

Cerning J, Guilbot A (1973) Changes in the carbohydrate composition during development and maturation of the wheat and barley kernel. Cereal Chemistry **50:** 220-231

Cha S, Yeung ES (2007) Colloidal Graphite-Assisted Laser Desorption/Ionization Mass Spectrometry and MSn of Small Molecules. 1. Imaging of Cerebrosides Directly from Rat Brain Tissue. Analytical Chemistry **79:** 2373-2385

Chaudhuri B, Hörmann F, Frommer WB (2011) Dynamic imaging of glucose flux impedance using FRET sensors in wild-type Arabidopsis plants. Journal of Experimental Botany

Chaudhuri B, Hörmann F, Lalonde S, Brady SM, Orlando DA, Benfey P, Frommer WB (2008) Protonophore- and pH-insensitive glucose and sucrose accumulation detected by FRET nanosensors in Arabidopsis root tips. The Plant Journal **56:** 948-962

Chaurand P, Sanders ME, Jensen RA, Caprioli RM (2004) Proteomics in Diagnostic Pathology: Profiling and Imaging Proteins Directly in Tissue Sections. The American Journal of Pathology **165:** 1057-1068

Christ B, Schelbert S, Aubry S, Süssenbacher I, Müller T, Kräutler B, Hörtensteiner S (2012) MES16, a Member of the Methylesterase Protein Family, Specifically Demethylates Fluorescent Chlorophyll Catabolites during Chlorophyll Breakdown in Arabidopsis. Plant Physiology **158:** 628-641

Cochrane MP (2000) Seed Carbohydrates. *In* M Black, JD Bewley, eds, Seed technology and its biological basis. CRC Press, Boca Raton, USA, pp 85-120

Cohen L, Gusev A (2002) Small molecule analysis by MALDI mass spectrometry. Analytical and Bioanalytical Chemistry **373:** 571-586

Consortium TIBGS (2012) A physical, genetic and functional sequence assembly of the barley genome. Nature **491:** 711-716

Cornett DS, Mobley JA, Dias EC, Andersson M, Arteaga CL, Sanders ME, Caprioli RM (2006) A novel histology-directed strategy for MALDI-MS tissue profiling that improves throughput and cellular specificity in human breast cancer. Mol. Cell. Proteomics **5:** 1975-1983

Darlington HF, Rouster J, Hoffmann L, Halford NG, Shewry PR, Simpson DJ (2001) Identification and molecular characterisation of hordoindolines from barley grain. Plant Molecular Biology **47:** 785-794

Darwen CWE, John P (1989) Localization of the Enzymes of Fructan Metabolism in Vacuoles Isolated by a Mechanical Method from Tubers of Jerusalem Artichoke (Helianthus tuberosus L.). Plant Physiology **89:** 658-663

Davies PJ (2010) The Plant Hormones: Their Nature, Occurrence, and Functions. *In* PJ Davies, ed, Plant Hormones - Biosynthesis, Signal Transduction, Action!, Ed 3rd. Springer, pp 1-35

Devaiah SP, Roth MR, Baughman E, Li MY, Tamura P, Jeannotte R, Welti R, Wang XM (2006) Quantitative profiling of polar glycerolipid species from organs of wild-type Arabidopsis and a phospholipase D alpha 1 knockout mutant. Phytochemistry **67:** 1907-1924

Dill AL, Ifa DR, Manicke NE, Ouyang Z, Cooks RG (2009) Mass spectrometric imaging of lipids using desorption electrospray ionization. Journal of Chromatography B **877:** 2883-2889

Dörmann P (2005) Membrane Lipids. *In* DJ Murphy, ed, Plant Lipids, Biology, Utilisation and Manipulation CRC Press, Boca Raton, USA, pp 123-161

Eberlin LS, Ferreira CR, Dill AL, Ifa DR, Cooks RG (2011) Desorption electrospray ionization mass spectrometry for lipid characterization and biological tissue imaging. Biochimica et Biophysica Acta (BBA) - Molecular and Cell Biology of Lipids **1811:** 946-960

Eckardt NA (2002) Abscisic Acid Biosynthesis Gene Underscores the Complexity of Sugar, Stress, and Hormone Interactions. The Plant Cell Online **14:** 2645-2649

Edelman J, Jefford TG (1968) The mechanism of fructosan metabolism in higher plants as exemplified in Helianthus tuberosus. New Phytologist **67:** 517–531

Emerson B, Gidden J, Lay JO, Durham B (2010) A rapid separation technique for overcoming suppression of triacylglycerols by phosphatidylcholine using MALDI-TOF MS. Journal of Lipid Research **51:** 2428-2434

Engell K (1989) Embryology of barley: Time course and analysis of controlled fertilization and early embryo formation based on serial sections. Nordic Journal of Botany **9:** 265-280

Enomoto H, Sugiura Y, Setou M, Zaima N (2011) Visualization of phosphatidylcholine, lysophosphatidylcholine and sphingomyelin in mouse tongue body by matrix-assisted laser desorption/ionization imaging mass spectrometry. Analytical and Bioanalytical Chemistry **400:** 1913-1921

Faix B, Radchuk V, Nerlich A, Hümmer C, Radchuk R, Emery RJN, Keller H, Götz K-P, Weschke W, Geigenberger P, Weber H (2012) Barley grains, deficient in cytosolic small subunit of ADP-glucose pyrophosphorylase, reveal coordinate adjustment of C:N metabolism mediated by an overlapping metabolic-hormonal control. The Plant Journal **69:** 1077-1093

Falk J, Brosch M, Schäfer A, Braun S, Krupinska K (2005) Characterization of transplastomic tobacco plants with a plastid localized barley 4-hydroxyphenyl-pyruvate dioxygenase. Journal of Plant Physiology **162:** 738-742

Finkelstein RR (2010) The Role of Hormones during Seed Development and Germination. *In* PJ Davies, ed, Plant Hormones - Biosynthesis, Signal Transduction, Action!, Ed 3rd. Springer, pp 549-573

Finkelstein RR, Gampala SSL, Rock CD (2002) Abscisic Acid Signaling in Seeds and Seedlings. The Plant Cell Online **14:** S15-S45

Finnie SM, Jeannotte R, Faubion JM (2009) Quantitative Characterization of Polar Lipids from Wheat Whole Meal, Flour, and Starch. Cereal Chemistry Journal **86:** 637-645

Finnie SM, Jeannotte R, Morris CF, Faubion JM (2010b) Variation in polar lipid composition among near-isogenic wheat lines possessing different puroindoline haplotypes. Journal of Cereal Science **51:** 66-72

Finnie SM, Jeannotte R, Morris CF, Giroux MJ, Faubion JM (2010a) Variation in polar lipids located on the surface of wheat starch. Journal of Cereal Science **51:** 73-80

Fisher DB, Gifford RM (1987) Accumulation and Conversion of Sugars by Developing Wheat Grains: VII. Effect of Changes in Sieve Tube and Endosperm Cavity Sap Concentrations on the Grain Filling Rate. Plant Physiology **84:** 341-347

Frederick CF, David MP, Oliver EN (1984) Development of tannin vacuoles in chalaza and seed coat of barley in relation to early chalazal necrosis in the seg1 mutant. Planta

Frey A, Godin B, Bonnet M, Sotta B, Marion-Poll A (2004) Maternal synthesis of abscisic acid controls seed development and yield in Nicotiana plumbaginifolia. Planta **218:** 958-964

Fuchs B, Schiller J, Süß R, Schürenberg M, Suckau D (2007) A direct and simple method of coupling matrix-assisted laser desorption and ionization time-of-flight mass spectrometry (MALDI-TOF MS) to thin-layer chromatography (TLC) for the analysis of phospholipids from egg yolk. Analytical and Bioanalytical Chemistry **389:** 827-834

Fuchs B, Süss R, Schiller J (2010) An update of MALDI-TOF mass spectrometry in lipid research. Progress in lipid research **49:** 450-475

Gadjev I, Stone JM, Gechev TS (2008) Chapter 3: Programmed Cell Death in Plants: New Insights into Redox Regulation and the Role of Hydrogen Peroxide. *In* WJ Kwang, ed, International Review of Cell and Molecular Biology, Vol Volume 270. Academic Press, pp 87-144

Geera BP, Nelson JE, Souza E, Huber KC (2006) Composition and Properties of A- and B-type Starch Granules of Wild-Type, Partial Waxy, and Waxy Soft Wheat. Cereal Chemistry Journal **83:** 551-557

Giroux MJ, Morris CF (1998) Wheat grain hardness results from highly conserved mutations in the friabilin components puroindoline a and b. Proceedings of the National Academy of Sciences **95:** 6262-6266

Golovina EA, Hoekstra FA (2003) Acquisition of desiccation tolerance in developing wheat embryos correlates with appearance of a fluid phase in membranes. Plant, Cell & Environment **26:** 1815-1826

Goto-Inoue N, Setou M, Zaima N (2010) Visualization of Spatial Distribution of gamma-Aminobutyric Acid in Eggplant (Solanum melongena) by Matrix-assisted Laser Desorption/Ionization Imaging Mass Spectrometry. Anal. Sci. **26:** 821-825

Govind G, Seiler C, Wobus U, Sreenivasulu N (2011) Importance of ABA homeostasis under terminal drought stress in regulating grain filling events. Plant Signaling & Behavior **6:** 1228-1231

Gross JH (2011) Mass Spectrometry, A Textbook, Ed 2. Springer, Heidelberg, Germany

Gubatz S, Shewry PR (2011) The Development, Structure, and Composition of the Barley Grain. *In* SE Ullrich, ed, Barley: Production, Improvement, and Uses. Wiley-Blackwell, Chichester, West Sussex, UK, pp 391-448

Gupta AK, Kaur N (2000) Fructan metabolism in Jerusalem artichoke and chicory *In* AK Gupta, N Kaur, eds, Carbohydrate Reserves in Plants (Synthesis and Regulation). Elsevier, Amsterdam, The Netherlands, pp S223-248

Gutierrez L, Van Wuytswinkel O, Castelain M, Bellini C (2007) Combined networks regulating seed maturation. Trends in Plant Science **12:** 294-300

Ham BM, Jacob JT, Cole RB (2005) MALDI-TOF MS of Phosphorylated Lipids in Biological Fluids Using Immobilized Metal Affinity Chromatography and a Solid Ionic Crystal Matrix. Analytical Chemistry **77:** 4439-4447

Hartung W, Sauter A, Hose E (2002) Abscisic acid in the xylem: where does it come from, where does it go to? Journal of Experimental Botany **53:** 27-32

Harvey DJ (2011) Analysis of carbohydrates and glycoconjugates by matrix-assisted laser desorption/ionization mass spectrometry: An update for the period 2005–2006. Mass Spectrometry Reviews **30:** 1-100

Heinig U, Gutensohn M, Dudareva N, Aharoni A (2013) The challenges of cellular compartmentalization in plant metabolic engineering. Current Opinion in Biotechnology **24:** 239-246

Heldt H-W, Piechulla B (2011) Plant Biochemistry Ed 4. Academic Press, San Diego, USA

Hendry GAFaW, Rebecca K. (1993) The origin, distribution, and evolutionary significance of fructans. *In* MaCNJ Sizuki, ed, Science and technology of fructans. CRC Press, Boca Raton, Florida, USA, pp 119-139

Henry R, Saini H (1989) Characterization of Cereal Sugars and Oligosaccharides. Cereal Chemistry **66(5):** 362-365

Hincha DK, Livingston Iii DP, Premakumar R, Zuther E, Obel N, Cacela C, Heyer AG (2007) Fructans from oat and rye: Composition and effects on membrane stability during drying. Biochimica et Biophysica Acta (BBA) - Biomembranes **1768:** 1611-1619

Horn PJ, Chapman KD (2012a) Lipidomics in tissues, cells and subcellular compartments. The Plant Journal **70:** 69-80

Horn PJ, Korte AR, Neogi PB, Love E, Fuchs J, Strupat K, Borisjuk L, Shulaev V, Lee Y-J, Chapman KD (2012b) Spatial Mapping of Lipids at Cellular Resolution in Embryos of Cotton. The Plant Cell Online **24:** 622-636

Housley TL (2000) Role of fructans redistributed from vegetative tissues in grain filling of wheat and barley. *In* AK Gupta, N Knaur, eds, Carbohydrate Reserves in Plants - Synthesis and Regulation. Elsevier Science, Amsterdam, The Netherlands, pp 207 - 221

Housley TL, Daughtry CST (1987) Fructan Content and Fructosyltransferase Activity during Wheat Seed Growth. Plant Physiology **83:** 4-7

Housley TL, Pollock CJ (1993) The metabolism of fructan in higher plants. *In* M Suzuki, NJ Chatterton, eds, Science and technology of fructans. CRC Press, Boca Raton, Florida, USA, pp 191-225

Ingram J, Bartels D (1996) The Molecular Basis of Dehydration Tolerance in Plants. Annual Review of Plant Physiology and Plant Molecular Biology **47:** 377-403

Jiang F, Hartung W (2008) Long-distance signalling of abscisic acid (ABA): the factors regulating the intensity of the ABA signal. Journal of Experimental Botany **59:** 37-43

Johanson RA, Buccafusca R, Quong JN, Shaw MA, Berry GT (2007) Phosphatidylcholine removal from brain lipid extracts expands lipid detection and enhances phosphoinositide quantification by matrix-assisted laser desorption/ionization time-of-flight (MALDI-TOF) mass spectrometry. Analytical Biochemistry **362:** 155-167

John P (1992) Biosynthesis of the Major Crop Products. Wiley & Sons, Chichester, West Sussex, UK

Jones RJ, Roessler J, Ouattar S (1985) Thermal Environment During Endosperm Cell Division in Maize: Effects on Number of Endosperm Cells and Starch Granules1. Crop Sci. **25:** 830-834

Jung S, Chen Y, Sullards MC, Ragauskas AJ (2010) Direct analysis of cellulose in poplar stem by matrix-assisted laser desorption/ionization imaging mass spectrometry. Rapid Communications in Mass Spectrometry **24:** 3230-3236

Kaeser W (1983) Ultrastructure of Storage Cells in Jerusalem Artichoke Tubers (Helianthus tuberosus L.) Vesicle Formation During Inulin Synthesis. Zeitschrift für Pflanzenphysiologie **111:** 253-260

Kang DH, Gho YS, Suh MK, Kang CH (2002) Highly sensitive and fast protein detection with coomassie brilliant blue in sodium dodecyl sulfate-polyacrylamide gel electrophoresis. Bull. Korean Chem. Soc. **23:** 1511-1512

Kaspar S, Peukert M, Svatos A, Matros A, Mock HP (2011) MALDI-Imaging mass spectrometry – an emerging technique in plant biology. Proteomics **11:** 1840-1850

Kawakami A, Sato Y, Yoshida M (2008) Genetic engineering of rice capable of synthesizing fructans and enhancing chilling tolerance. Journal of Experimental Botany **59:** 793-802

Kawakami A, Yoshida M, Van den Ende W (2005) Molecular cloning and functional analysis of a novel 6&1-FEH from wheat (Triticum aestivum L.) preferentially degrading small graminans like bifurcose. Gene **358:** 93-101

Keunen ELS, Peshev D, Vangronsveld J, Van Den Ende WIM, Cuypers ANN (2013) Plant sugars are crucial players in the oxidative challenge during abiotic stress: extending the traditional concept. Plant, Cell & Environment**:** n/a-n/a

Klie S, Krueger S, Krall L, Giavalisco P, Flügge U-I, Willmitzer L, Steinhauser D (2011) Analysis of the compartmentalized metabolome – a validation of the non-aqueous fractionation technique. Frontiers in Plant Science **2**

Koch K (2004) Sucrose metabolism: regulatory mechanisms and pivotal roles in sugar sensing and plant development. Current Opinion in Plant Biology **7:** 235-246

Kojima M, Kamada-Nobusada T, Komatsu H, Takei K, Kuroha T, Mizutani M, Ashikari M, Ueguchi-Tanaka M, Matsuoka M, Suzuki K, Sakakibara H (2009) Highly Sensitive and High-Throughput Analysis of Plant Hormones Using MS-Probe Modification and Liquid ChromatographyTandem Mass Spectrometry: An Application for Hormone Profiling in Oryza sativa. Plant and Cell Physiology **50:** 1201-1214

Krahmer N, Guo Y, Wilfling F, Hilger M, Lingrell S, Heger K, Newman Heather W, Schmidt-Supprian M, Vance Dennis E, Mann M, Farese Jr Robert V, Walther Tobias C (2011) Phosphatidylcholine Synthesis for Lipid Droplet Expansion Is Mediated by Localized Activation of CTP:Phosphocholine Cytidylyltransferase. Cell Metabolism **14:** 504-515

Kubo A, Fujita N, Harada K, Matsuda T, Satoh H, Nakamura Y (1999) The Starch-Debranching Enzymes Isoamylase and Pullulanase Are Both Involved in Amylopectin Biosynthesis in Rice Endosperm. Plant Physiology **121:** 399-410

Kueger S, Steinhauser D, Willmitzer L, Giavalisco P (2012) High-resolution plant metabolomics: from mass spectral features to metabolites and from whole-cell analysis to subcellular metabolite distributions. The Plant Journal **70:** 39-50

Lee S-H, BeMiller JN (2008) Lysophosphatidylcholine Identified as Channel-Associated Phospholipid of Maize Starch Granules. Cereal Chemistry **85:** 776-779

León P, Sheen J (2003) Sugar and hormone connections. Trends in plant science **8:** 110-116

Leung J, Giraudat J (1998) Abscisic Acid Signal Transduction. Annual Review of Plant Physiology and Plant Molecular Biology **49:** 199-222

Lim HC (1988) Metabolism and Compartmentation of Imported Sugars in Sink Organs in Relation to Sink Strength. Annual Review of Plant Physiology and Plant Molecular Biology **39:** 355-378

Lim HC, Gifford RM (1984) Accumulation and Conversion of Sugars by Developing Wheat Grains: V. The Endosperm Apoplast and Apoplastic Transport. Journal of Experimental Botany **35:** 58-73

Lim JD, Cho J-I, Park Y-I, Hahn T-R, Choi S-B, Jeon J-S (2006) Sucrose transport from source to sink seeds in rice. Physiologia Plantarum **126:** 572-584

Lippmann R, Kaspar S, Rutten T, Melzer M, Kumlehn J, Matros A, Mock H-P (2009) Protein and Metabolite Analysis Reveals Permanent Induction of Stress Defense and Cell Regeneration Processes in a Tobacco Cell Suspension Culture. International Journal of Molecular Sciences **10:** 3012-3032

Lisec J, Schauer N, Kopka J, Willmitzer L, Fernie AR (2006) Gas chromatography mass spectrometry-based metabolite profiling in plants. Nat. Protocols **1:** 387-396

Liu K (2011) Comparison of Lipid Content and Fatty Acid Composition and Their Distribution within Seeds of 5 Small Grain Species. Journal of Food Science **76:** C334-C342

Livingston D, Hincha D, Heyer A (2009) Fructan and its relationship to abiotic stress tolerance in plants. Cellular and Molecular Life Sciences **66:** 2007-2023

Livingston DP, Henson CA (1998) Apoplastic Sugars, Fructans, Fructan Exohydrolase, and Invertase in Winter Oat: Responses to Second-Phase Cold Hardening. Plant Physiology **116:** 403-408

Marchi S, Giorgi C, Suski JM (2012) Mitochondria-Ros Crosstalk in the Control of Cell Death and Aging. Journal of Signal Transduction **2012**

Martina S, Rajsree M, Oliver F, Julia K (2005) Metabolic profiling of laser microdissected vascular bundles of Arabidopsis thaliana. Plant Methods **1:** 2-2

Martinetz T, Schulten K (1991) A Neural-Gas Network Learns Topologies. *In* Artificial Neural Networks. Elsevier Science Amsterdam, The Netherlands, pp 397-402

Matros A, Mock H-P (2013) Mass spectrometry based imaging techniques for spatially resolved analysis of molecules. Frontiers in Plant Science **4**

McBride HM, Neuspiel M, Wasiak S (2006) Mitochondria: More Than Just a Powerhouse. Current biology : CB **16:** R551-R560

Megahad OA, El Kinawy OS (2002) Studies on the extraction of wheat germ oil by commercial hexane. Grasas y Aceites **53:** 414-418

Minorsky PV (2003) The hot and the classic. Plant Physiology **132:** 1779-1780

Moreau RA (2009) Barley Oil. *In* RA Moreau, Kamal-Edin, eds, Gourmet and Health-Promoting Specialty Oils. AOCS Press, Illinois, USA, pp 455-478

Morrison WR (1978) Wheat Lipid Composition. Cereal Chemistry **55:** 548 - 558

Morrison WR, Tester RF, Snape CE, Law R, Gidley MJ (1993) Swelling and Gelatinization of Cereal Starches. IV. Some Effects of Lipid-Complexed Amylose and Free Amylose in Waxy and Normal Barley Starches. Cereal Chemistry **70:** 385-391

Müller T, Oradu S, Ifa DR, Cooks RG, Kräutler B (2011) Direct Plant Tissue Analysis and Imprint Imaging by Desorption Electrospray Ionization Mass Spectrometry. Analytical Chemistry **83:** 5754-5761

Murphy RC, Axelsen PH (2011) Mass spectrometric analysis of long-chain lipids. Mass Spectrometry Reviews **30:** 579-599

Murphy RC, Hankin JA, Barkley RM, Zemski Berry KA (2011) MALDI imaging of lipids after matrix sublimation/deposition. Biochim Biophys Acta **1811:** 970-975

Nambara E, Marion-Poll A (2003) ABA action and interactions in seeds. Trends in Plant Science **8:** 213-217

Nedeva D, Nikolova A (1997) Desiccation Tolerance in Developing Seeds. Bulg. J. Plant Physiol **23:** 100-113

Nelson CJ, Spollen WG (1987) Fructans. Physiologia Plantarum **71:** 512-516

Neuberger T, Sreenivasulu N, Rokitta M, Rolletschek H, Göbel C, Rutten T, Radchuk V, Feussner I, Wobus U, Jakob P, Webb A, Borisjuk L (2008) Quantitative imaging of oil storage in developing crop seeds. Plant Biotechnology Journal **6:** 31-45

Nguyen HN, Sabelli PA, Larkins BA (2007) Endoreduplication and Programmed Cell Death in the Cereal Endosperm. *In* O-A Olsen, ed, Endosperm, Vol 8. Springer Berlin Heidelberg, pp 21-43

Niemüller D, Reimann A, Ober D (2012) Distinct Cell-Specific Expression of Homospermidine Synthase Involved in Pyrrolizidine Alkaloid Biosynthesis in Three Species of the Boraginales. Plant Physiology **159:** 920-929

Nilsson U, Öste R, Jägerstad M (1987) Cereal fructans: Hydrolysis by yeast invertase, in vitro and during fermentation. Journal of Cereal Science **6:** 53-60

Norstog K (1972) Early Development of the Barley Embryo: Fine Structure American Journal of Botany **59 (2):** 123-132

Novák O, Hauserová E, Amakorová P, Doležal K, Strnad M (2008) Cytokinin profiling in plant tissues using ultra-performance liquid chromatography–electrospray tandem mass spectrometry. Phytochemistry **69:** 2214-2224

Olsen O-A (2001) ENDOSPERM DEVELOPMENT: Cellularization and Cell Fate Specification. Annu. Rev. Plant Physiol. Plant Mol. Biol. **52:** 233–267

Owen SJ, Abrams SR (2009) Measurement of plant hormones by liquid chromatography-mass spectrometry. Methods Mol Biol **495:** 39-51

Pasha I, Anjum FM, Morris CF (2010) Grain Hardness: A Major Determinant of Wheat Quality. Food Science and Technology International **16:** 511-522

Passarelli MK, Winograd N (2011) Lipid imaging with time-of-flight secondary ion mass spectrometry (ToF-SIMS). Biochimica et Biophysica Acta (BBA) - Molecular and Cell Biology of Lipids **1811:** 976-990

Patrick JW, Offler CE (2001) Compartmentation of transport and transfer events in developing seeds. Journal of Experimental Botany **52:** 551-564

Peshev D, Vergauwen R, Moglia A, Hideg É, Van den Ende W (2013) Towards understanding vacuolar antioxidant mechanisms: a role for fructans? Journal of Experimental Botany **64:** 1025-1038

Petković M, Schiller J, Müller M, Benard S, Reichl S, Arnold K, Arnhold J (2001) Detection of Individual Phospholipids in Lipid Mixtures by Matrix-Assisted Laser Desorption/Ionization Time-of-Flight Mass Spectrometry: Phosphatidylcholine Prevents the Detection of Further Species. Analytical Biochemistry **289:** 202-216

Peukert M, Matros A, Lattanzio G, Kaspar S, Abadía J, Mock H-P (2012) Spatially resolved analysis of small molecules by matrix-assisted laser desorption/ionization mass spectrometric imaging (MALDI-MSI). New Phytologist **193:** 806-815

Pollock CJ, Cairns AJ (1991) Fructan Metabolism in Grasses and Cereals. Annual Review of Plant Physiology and Plant Molecular Biology **42:** 77-101

Pollock CJ, Cairns AJ (1999) The integration of sucrose and fructan metabolism in temperate grasses and cereals. *In* NJ Kruger, SA Hill, RG Ratcliffe, eds, Regulation of Primary Metabolic Pathways in Plants. Kluwer Academic Publisher, pp 195-226

Pollock CJ, Cairns AJ, Sims IM, Housley TL (1996) Fructans as reserve carbohydrates in crop plants *In* E Zamski, AA Shaffer, eds, Photoassimilate Distribution in Plants and Crops: Source-Sink Relationships. Marcel Dekker NY, USA, pp 97-114

Priest DM, Ambrose SJ, Vaistij FE, Elias L, Higgins GS, Ross ARS, Abrams SR, Bowles DJ (2006) Use of the glucosyltransferase UGT71B6 to disturb abscisic acid homeostasis in Arabidopsis thaliana. The Plant Journal **46:** 492-502

Rademaker GJ, Pergantis SA, Blok-Tip L, Langridge JI, Kleen A, Thomas-Oates JE (1998) Mass Spectrometric Determination of the Sites of O-Glycan Attachment with Low Picomolar Sensitivity. Analytical Biochemistry **257:** 149-160

Riedl Ken M, Carando S, Alessio Helaine M, McCarthy M, Hagerman Ann E (2002) Antioxidant Activity of Tannins and Tannin-Protein Complexes: Assessment In Vitro and In Vivo. *In* Free Radicals in Food, Vol 807. American Chemical Society, pp 188-200

Rijavec T, Kovač M, Kladnik A, Chourey PS, Dermastia M (2009) A Comparative Study on the Role of Cytokinins in Caryopsis Development in the Maize miniature1 Seed Mutant and Its Wild Type. Journal of Integrative Plant Biology **51:** 840-849

Rolletschek H, Melkus G, Grafahrend-Belau E, Fuchs J, Heinzel N, Schreiber F, Jakob PM, Borisjuk L (2011) Combined Noninvasive Imaging and Modeling Approaches Reveal Metabolic Compartmentation in the Barley Endosperm. The Plant Cell Online **23:** 3041-3054

Rolletschek H, Weschke W, Weber H, Wobus U, Borisjuk L (2004) Energy state and its control on seed development: starch accumulation is associated with high ATP and steep oxygen gradients within barley grains. Journal of Experimental Botany **55:** 1351-1359

Sabelli PA, Larkins BA (2009) The Development of Endosperm in Grasses. Plant Physiology **149:** 14-26

Sakakibara H (2006) CYTOKININS: Activity, Biosynthesis, and Translocation. Annual Review of Plant Biology **57:** 431-449

Sauter A, Dietz KJ, Hartung W (2002) A possible stress physiological role of abscisic acid conjugates in root-to-shoot signalling. Plant, Cell & Environment **25:** 223-228

Schiller J, Süss R, Arnhold J, Fuchs B, Lessig J, Müller M, Petković M, Spalteholz H, Zschörnig O, Arnold K (2004) Matrix-assisted laser desorption and ionization time-of-flight (MALDI-TOF) mass spectrometry in lipid and phospholipid research. Progress in lipid research **43:** 449-488

Schlesier B, Mock H-P (2006) Protein Isolation and Second-Dimension Electrophoretic Separation. *In*, Vol 323, pp 381-391

Schmülling T (2004) Cytokinin. *In* W Lennarz, MD Lane, eds, Encyclopedia of Biological Chemistry. Academic Press/Elsevier Science

Schnyder H (1993b) The role of carbohydrate storage and redistribution in the source-sink relations of wheat and barley during grain filling — a review. New Phytologist **123:** 233-245

Schnyder H, Gillenberg C, Hinz J (1993a) Fructan contents and dry matter deposition in different tissues of the wheat grain during development. Plant, Cell & Environment **16:** 179-187

Schwartz SA, Weil RJ, Thompson RC, Shyr Y, Moore JH, Toms SA, Johnson MD, Caprioli RM (2005) Proteomic-based prognosis of brain tumor patients using direct-tissue matrix-assisted laser desorption ionization mass spectrometry. Cancer Res. **65:** 7674-7681

Seefeldt HF, Larsen FH, Viereck N, Petersen MA, Engelsen SB (2011) Lipid composition and deposition during grain filling in intact barley (Hordeum vulgare) mutant grains as studied by 1H HR MAS NMR. Journal of Cereal Science **54:** 442-449

Seiler C, Harshavardhan VT, Rajesh K, Reddy PS, Strickert M, Rolletschek H, Scholz U, Wobus U, Sreenivasulu N (2011) ABA biosynthesis and degradation contributing to ABA homeostasis during barley seed development under control and terminal drought-stress conditions. Journal of Experimental Botany **62:** 2615-2632

Shroff R, Svatoš A (2009) Proton Sponge: A Novel and Versatile MALDI Matrix for the Analysis of Metabolites Using Mass Spectrometry. Analytical Chemistry **81:** 7954-7959

Shroff R, Vergara F, Muck A, Svatos A, Gershenzon J (2008) Nonuniform distribution of glucosinolates in Arabidopsis thaliana leaves has important consequences for plant defense. PNAS **105:** 6196-6201

Spencer MT, Furutani H, Oldenburg SJ, Darlington TK, Prather KA (2008) Gold Nanoparticles as a Matrix for Visible-Wavelength Single-Particle Matrix-Assisted Laser Desorption/Ionization Mass Spectrometry of Small Biomolecules. The Journal of Physical Chemistry C **112:** 4083-4090

Sreenivasulu N, Altschmied L, Radchuk V, Gubatz S, Wobus U, Weschke W (2004) Transcript profiles and deduced changes of metabolic pathways in maternal and filial tissues of developing barley grains. The Plant Journal **37:** 539-553

Sreenivasulu N, Borisjuk L, Junker BH, Mock HP, Rolletschek H, Seiffert U, Weschke W, Wobus U (2010) Barley Grain Development: toward an Integrative View. *In* International Review of Cell and Molecular Biology, Vol 281, Vol 281. Elsevier Academic Press Inc, San Diego, pp 49-89

Sreenivasulu N, Radchuk V, Strickert M, Miersch O, Weschke W, Wobus U (2006) Gene expression patterns reveal tissue-specific signaling networks controlling programmed cell death and ABA- regulated maturation in developing barley seeds. The Plant journal : for cell and molecular biology **47:** 310-327

Strnad M, Novak O, Rolcik J, Tarkowska D, Gruz J, Dolezal K (2011) Phytohormone targeting in plant tissues. BMC Proceedings **5:** 1-1

Su Y-H, Liu Y-B, Zhang X-S (2011) Auxin–Cytokinin Interaction Regulates Meristem Development. Molecular Plant **4:** 616-625

Sumner LW, Yang DS, Bench BJ, Watson BS, Li C, Jones AD (2011) Spatially Resolved Plant Metabolomics. *In* Annual Plant Reviews Volume 43. Wiley-Blackwell, pp 343-366

Suzuki T, Midonoya H, Shioi Y (2009) Analysis of chlorophylls and their derivatives by matrix-assisted laser desorption/ionization–time-of-flight mass spectrometry. Analytical Biochemistry **390:** 57-62

Suzuki Y, Amano T, Shioi Y (2006) Characterization and Cloning of the Chlorophyll-Degrading Enzyme Pheophorbidase from Cotyledons of Radish. Plant Physiology **140:** 716-725

Tanaka K, Yamada M, Tamiya-Koizumi K, Kannagi R, Aoyama T, Hara A, Kyogashima M (2011) Systematic analyses of free ceramide species and ceramide species comprising neutral glycosphingolipids by MALDI-TOF MS with high-energy CID. Glycoconjugate Journal **28:** 67-87

Thiel J, Hollmann J, Rutten T, Weber H, Scholz U, Weschke W (2012) 454 Transcriptome Sequencing Suggests a Role for Two-Component Signalling in Cellularization and Differentiation of Barley Endosperm Transfer Cells. PLoS ONE **7:** e41867

Thiel J, Müller M, Weschke W, Weber H (2009) Amino acid metabolism at the maternal–filial boundary of young barley seeds: a microdissection-based study. Planta **230:** 205-213

Thiel J, Riewe D, Rutten T, Melzer M, Friedel S, Bollenbeck F, Weschke W, Weber H (2012) Differentiation of endosperm transfer cells of barley: a comprehensive analysis at the micro-scale. The Plant Journal **71:** 639-655

Thiel J, Weier D, Sreenivasulu N, Strickert M, Weichert N, Melzer M, Czauderna T, Wobus U, Weber H, Weschke W (2008) Different Hormonal Regulation of Cellular Differentiation and Function in Nucellar Projection and Endosperm Transfer Cells: A Microdissection-Based Transcriptome Study of Young Barley Grains. Plant Physiology **148:** 1436-1452

Thitisaksakul M, Jiménez RC, Arias MC, Beckles DM (2012) Effects of environmental factors on cereal starch biosynthesis and composition. Journal of Cereal Science **56:** 67-80

Tohge T, Ramos MS, Nunes-Nesi A, Mutwil M, Giavalisco P, Steinhauser D, Schellenberg M, Willmitzer L, Persson S, Martinoia E, Fernie AR (2011) Towards the storage metabolome: profiling the barley vacuole. Plant Physiology

Turečková V, Novák O, Strnad M (2009) Profiling ABA metabolites in Nicotiana tabacum L. leaves by ultra-performance liquid chromatography–electrospray tandem mass spectrometry. Talanta **80:** 390-399

Ugalde T, Jenner C (1990a) Substrate Gradients and Regional Patterns of Dry Matter Deposition Within Developing Wheat Endosperm. I. Carbohydrates. Functional Plant Biology **17:** 377-394

Ugalde T, Jenner C (1990b) Route of Substrate Movement Into Wheat Endosperm. I. Carbohydrates. Functional Plant Biology **17:** 693-704

Ullrich SE (2011) Significance, Adaption, Production, and Trade of Barley. *In* SE Ullrich, ed, Barley: Production, Improvement, and Uses. Wiley-Blackwell, Chichester, West Sussex, UK, pp 3-13

Ulmer L, Mattay J, Torres-Garcia HG, Luftmann H (2000) Letter: The use of 2- (2E)-3-(4-tert-butylphenyl)-2-methylprop-2-enylidene malononitrile as a matrix for matrix-assisted laser desorption/ionization mass spectrometry. European Journal of Mass Spectrometry **6:** 49-52

Valluru R, Van den Ende W (2008) Plant fructans in stress environments: emerging concepts and future prospects. Journal of Experimental Botany **59:** 2905-2916

Van Breusegem F, Dat JF (2006) Reactive Oxygen Species in Plant Cell Death. Plant Physiology **141:** 384-390

Van den Ende W, De Coninck B, Van Laere A (2004) Plant fructan exohydrolases: a role in signaling and defense? Trends in plant science **9:** 523-528

Van den Ende W, Van Laere A (1996) Fructan synthesizing and degrading activities in chicory roots (Cichorium intybus L.) during field-growth, storage and forcing. Journal of Plant Physiology **149:** 43-50

Veloso A, Fernández R, Astigarraga E, Barreda-Gómez G, Manuel I, Giralt MT, Ferrer I, Ochoa B, Rodríguez-Puertas R, Fernández J (2011) Distribution of lipids in human brain. Analytical and Bioanalytical Chemistry **401:** 89-101

Vereyken IJ, Albert van Kuik J, Evers TH, Rijken PJ, de Kruijff B (2003) Structural Requirements of the Fructan-Lipid Interaction. Biophysical journal **84:** 3147-3154

Viehweger K, Dordschbal B, Roos W (2002) Elicitor-Activated Phospholipase A2 Generates Lysophosphatidylcholines That Mobilize the Vacuolar H+ Pool for pH Signaling via the Activation of Na+-Dependent Proton Fluxes. The Plant Cell Online **14:** 1509-1525

Vieler A, Wilhelm C, Goss R, Süß R, Schiller J (2007) The lipid composition of the unicellular green alga Chlamydomonas reinhardtii and the diatom Cyclotella meneghiniana investigated by MALDI-TOF MS and TLC. Chemistry and Physics of Lipids **150:** 143-155

Vijn I, Smeekens S (1999) Fructan: More Than a Reserve Carbohydrate? Annu Rev Plant Physiol **120:** 351-360

Wang HL, Offler CE, Patrick JW (1995a) The cellular pathway of photosynthate transfer in the developing wheat grain. II. A structural analysis and histochemical studies of the pathway from the crease phloem to the endosperm cavity. Plant, Cell & Environment **18:** 373-388

Wang HL, Patrick JW, Offler CE, Wang XD (1995b) The cellular pathway of photosynthate transfer in the developing wheat grain. III. A structural analysis and physiological studies of the pathway from the endosperm cavity to the starchy endosperm. Plant, Cell & Environment **18:** 389-407

Wang J, Sporns P, Low NH (1999) Analysis of Food Oligosaccharides Using MALDI-MS: Quantification of Fructooligosaccharides. Journal of Agricultural and Food Chemistry **47:** 1549-1557

Wang N, Fisher DB (1995c) Sucrose Release into the Endosperm Cavity of Wheat Grains Apparently Occurs by Facilitated Diffusion across the Nucellar Cell Membranes. Plant Physiology **109:** 579-585

Wang YH, Irving HR (2011) Developing a model of plant hormone interactions. *In* Plant Signaling & Behavior, Vol 6, pp 494-500

Wardlaw I, Willenbrink J (1994) Carbohydrate Storage and Mobilisation by the Culm of Wheat Between Heading and Grain Maturity: the Relation to Sucrose Synthase and Sucrose-Phosphate Synthase. Functional Plant Biology **21:** 255-271

Watson PA, Duffus CM (1988) Carbon Dioxide Fixation by Detached Cereal Caryopses. Plant Physiology **87:** 504-509

Wenzel T, Sparbier K, Mieruch T, Kostrzewa M (2006) 2,5-Dihydroxyacetophenone: a matrix for highly sensitive matrix-assisted laser desorption/ionization time-of-flight mass spectrometric analysis of proteins using manual and automated preparation techniques. Rapid Communications in Mass Spectrometry **20:** 785-789

Werner T, Schmülling T (2009) Cytokinin action in plant development. Current Opinion in Plant Biology **12:** 527-538

Weschke W, Panitz R, Gubatz S, Wang Q, Radchuk R, Weber H, Wobus U (2003) The role of invertases and hexose transporters in controlling sugar ratios in maternal and filial tissues of barley caryopses during early development. The Plant Journal **33:** 395-411

Weschke W, Panitz R, Sauer N, Wang Q, Neubohn B, Weber H, Wobus U (2000) Sucrose transport into barley seeds: molecular characterization of two transporters and implications for seed development and starch accumulation. Plant Journal **21:** 455-467

Witzel K, Surabhi G-K, Jyothsnakumari G, Sudhakar C, Matros A, Mock H-P (2007) Quantitative Proteome Analysis of Barley Seeds Using Ruthenium(II)-tris-(bathophenanthroline-disulphonate) Staining. Journal of Proteome Research **6:** 1325-1333

Wobus U, Sreenivasulu N, Borisjuk L, Rolletschek H, Panitz R, Gubatz S, Weschke W (2005) Molecular physiology and genomics of of developing barley grains. Recent Res. Devel. Plant Mol. Biol. **2:** 1–29

Wolswinkel P (1992) Transport of nutrients into developing seeds: a review of physiological mechanisms. Seed Science Research **2:** 59-73

Xu Z-J, Nakajima M, Suzuki Y, Yamaguchi I (2002) Cloning and Characterization of the Abscisic Acid-Specific Glucosyltransferase Gene from Adzuki Bean Seedlings. Plant Physiology **129:** 1285-1295

Yang J, Peng S, Visperas R, Sanico A, Zhu Q, Gu S (2000) Grain filling pattern and cytokinin content in the grains and roots of rice plants. Plant Growth Regulation **30:** 261-270

Yang J, Zhang J, Huang Z, Wang Z, Zhu Q, Liu L (2002) Correlation of Cytokinin Levels in the Endosperms and Roots with Cell Number and Cell Division Activity during Endosperm Development in Rice. Annals of Botany **90:** 369-377

Yang J, Zhang J, Wang Z, Xu G, Zhu Q (2004) Activities of Key Enzymes in Sucrose-to-Starch Conversion in Wheat Grains Subjected to Water Deficit during Grain Filling. Plant Physiology **135:** 1621-1629

Yoshimura Y, Zaima N, Moriyama T, Kawamura Y (2012) Different Localization Patterns of Anthocyanin Species in the Pericarp of Black Rice Revealed by Imaging Mass Spectrometry. PLoS ONE **7:** e31285

Zaima N, Goto-Inoue N, Hayasaka T, Setou M (2010b) Application of imaging mass spectrometry for the analysis of Oryza sativa rice. Rapid Commun. Mass Spectrom. **24:** 2723-2729

Zaima N, Hayasaka T, Goto-Inoue N, Setou M (2010a) Matrix-Assisted Laser Desorption/Ionization Imaging Mass Spectrometry. Int. J. Mol. Sci. **11:** 5040-5055

Zalewski W, Galuszka P, Gasparis S, Orczyk W, Nadolska-Orczyk A (2010) Silencing of the HvCKX1 gene decreases the cytokinin oxidase/dehydrogenase level in barley and leads to higher plant productivity. Journal of Experimental Botany **61:** 1839-1851

Zhang J, Zenobi R (2004) Matrix-dependent cationization in MALDI mass spectrometry. Journal of mass spectrometry : JMS **39:** 808-816

Zhang W-H, Zhou Y, Dibley KE, Tyerman SD, Furbank RT, Patrick JW (2007) Nutrient loading of developing seeds. Functional Plant Biology **34:** 314-331

Zhao S, Liu JY, Chen SY, Shi LL, Liu YJ, Ma C (2011) Antioxidant Potential of Polyphenols and Tannins from Burs of Castanea mollissima Blume. Molecules **16:** 8590-8600

Zhu G, Ye N, Yang J, Peng X, Zhang J (2011) Regulation of expression of starch synthesis genes by ethylene and ABA in relation to the development of rice inferior and superior spikelets. Journal of Experimental Botany

7.   Abbreviations

1-FEH	fructosyl 1-exohydrolase
1-FFT	fructan:fructan 1-fructosyltransferase
1-SST	sucrose:sucrose 1-fructosyltransferase
2-DE	two-dimensional gel electrophoresis
6-FEH	fructosyl 6-exohydrolase
6-SFT	sucrose:fructan 6-fructosyltransferase
ABA	abscisic acid
ABA-GE	abscisic acid-glycosyl ester
ABA-GT	abscisic acid-glycosyltransferase
ACN	acetonitrile
BG	ß-glucosidase
BSA	bovine serum albumin
cCBB	colloidal Coomassie Brilliant Blue
CHAPS	3-[(3-cholamidopropyl) dimethylamonio]-1-propanesulfonate
CHCA	α-Cyano-4-hydroxycinnamic acid
CK	cytokinin
CPT	ClinProTools
Da	Dalton
DAP	days after pollination
DAHP	2,5-Dihydroxyacetophenone
DESI	desorption electrospray ionization
DHB	2,5-dihydroxybenzoic acid
DP	degree of polymerization
DMAN	1,8-Bis-(dimethylamino)-naphthalene
DTT	dithiothreitol
ESI	electrospray ionization
EST	expressed sequence tag
ETC	endosperm transfer cells
FW	fresh weight
GC	gas chromatography
GNP	gold nanoparticle
HPLC	high performance liquid chromatography
Hv	Hordeum vulgare
IEF	isoelectric focussing
IPG	immobilized pH gradient
ITO	indium tin oxide
LC	liquid chromatography
LMD	laser micro-dissection
LMPC	laser capture micro-dissection combined with pressure catapulting
LPC	lysophosphatidylcholine
MALDI	matrix-assisted laser desorption/ionization
MeOH	methanol
MS	mass spectrometry
Mw	molecular weight
m/z	mass-to-charge

NG	Neural Gas
NP	nucellar projection
O.C.T.	optimal cutting temperature compound
PC	phosphatidylcholine
PCA	principal component analyses
PCD	programmed cell death
PEG	polyethylene glycol
p*I*	isoelectric point
PMF	peptide mass fingerprints
RI	retention time index
RNAi	RNA interference
ROI	region of interest
ROS	reactive oxygen species
RT	retention time
SA	sinapinic acid
SIMS	secondary ion mass spectrometry
SDS-Page	sodium dodecyl polyacrylamide gel electrophoresis
SuSy	sucrose synthase
TCA	trichloroacetic acid
TFA	trifluoroacetic acid
TIC	total ion chromatogram
TOF	time-of-flight
*t*Z	*trans*-zeatin
*t*ZR	*trans*-zeatin riboside
v/v	volume-to-volume ratio
w/v	weight-to-volume ratio
w/w	weight-to-weight ratio
x*g*	gravitation force

8. Curriculum Vitae

Name: Manuela Peukert

Date of Birth: 02.01.1982

Place of Birth: Aschersleben

Nationality: German

EDUCATION / SCIENTIFIC CAREER

1/2010 -	PhD student	Leibniz Institute of Plant Genetics and Crop Plant Research Gatersleben, Dept. Physiology and Cell Biology, Applied Biochemistry Group
		PhD thesis: "Spatiotemporal Distributions of Metabolites Involved in Barley Grain Development with Emphasis on Endosperm Formation"
9/2009 – 12/2009	Graduate Research Assistant	Leibniz Institute of Plant Genetics and Crop Plant Research Gatersleben, Dept. Molecular Cell Biology, Applied Biochemistry Group
6/2009 – 8/2009	Graduate Research Assistant	Leibniz Institute of Plant Genetics and Crop Plant Research Gatersleben, Dept. Gene and Genome Mapping, Gene and Genome Mapping Group
9/2008 – 5/2009	Undergraduate Research Assistant	Leibniz Institute of Plant Genetics and Crop Plant Research Gatersleben, Dept. Gene and Genome Mapping, Gene and Genome Mapping Group
		Diploma thesis: „Haplotypendiversität in Genen des Phenylpropanoid-Stoffwechsels in *Hordeum vulgare* und Entwicklung molekularer Marker"
2005 – 2009		Study of Biology, Freie Universität Berlin, Germany, Institute of Biology
2000 - 2005		Study of the Special Education for Speech- and Hearing-Impaired, Humboldt-Universität zu Berlin, Dept. Rehabilitation Sciences
2000		Final secondary-school examinations, Gymnasium Stephaneum zu Aschersleben

PUBLICATIONS

Kaspar S, Peukert M, Svatos A, Matros A, Mock HP (2011) MALDI-Imaging mass spectrometry – an emerging technique in plant biology. Proteomics **11:** 1840-1850

Peukert M, Matros A, Lattanzio G, Kaspar S, Abadía J, Mock H-P (2012) Spatially resolved analysis of small molecules by matrix-assisted laser desorption/ionization mass spectrometric imaging (MALDI-MSI). New Phytologist **193:** 806-815

Peukert M, Matros A, Dittbrenner A, Seiffert U, Mock H-P (2012) Mass Spectrometry based Imaging in Plant Science: Current Status and Perspectives. Frontiers in Agriculture Proteome Research: 3-6

Peukert M, Becker M, Matros A, Mock H-P (2013) Mass spectrometry based imaging of metabolites and proteins. *In* JV Jorrin-Novo, S Komatsu, W Weckwerth, S Wienkoop, eds, Plant Proteomics, Methods and Protocols, Methods in Molecular Biology, Vol. 1072

ORAL PRESENTATIONS

M Peukert, H-P Mock. MALDI-*Imaging* for Spatial Protein and Metabolite Profiling During Barley Grain Development. Bruker Daltonic, Operators Meeting. Kassel, 20.-21.03.2011

M Peukert, A Matros, H-P Mock. Mass Spectrometric Analysis of Spatial Metabolite Distribution Pattern during Barley Grain Development. DGMS (German Association for Mass Spectrometry), 45th Annual Meeting. Poznan, Poland, 03.-07.03.2012

M Peukert, A Matros, H-P Mock. Mass Spectrometric Imaging Revealed Metabolic Compartmentation Related to Endosperm Development during Storage Phase of Barley Grains. Plant Science Students Conference, IPK. Gatersleben, 04.-07.06.2012

M Peukert, H-P Mock. Metabolite Distribution Pattern by MALDI-MS *Imaging*. KWS In-house training. Einbeck, 02.06.2012

M Peukert, A Matros, A Svatos, H-P Mock. Spatial Resolution of Metabolites During Barley Grain Development by Imaging Mass Spectrometric Analysis. IMSC (International Mass Spectrometry Conference), 19th Meeting. Kyoto, Japan, 15.-21.09.2012

POSTER PRESENTATIONS

M Peukert, A Matros, H-P Mock. MALDI-imaging: A tool for direct analysis of intact tissue sections. Plant Science Students Conference, IPK. Gatersleben, 15.-18.06.2010

M Peukert, S Kaspar, A Matros, W Weschke, H-P Mock. MALDI-*Imaging* and LC-MS for Spatial Protein and Metabolite Profiling During Barley Grain Development. Institut's Day IPK. Gatersleben, 04.-06.10.2010

M Peukert, A Matros, H-P Mock. MALDI-MS Imaging – A Tool for Characterization of Tissue Specific Distribution Patterns of Small Molecules during Barley Grain Development. Botanikertagung. Berlin, 18.-23.09. 2011

M Peukert, A Matros, W Weschke, H Weber, H-P Mock. Metabolite pattern related to endosperm development in barley as revealed by means of MALDI-MS *Imaging*. Institut's Day IPK. Gatersleben, 01.-03.10.2012

M Peukert, A Matros, H-P Mock. Integration of MALDI MSI into Plant Physiological Questions – Metabolite Distributions during Grain Development in Barley. DGMS (German Association for Mass Spectrometry), 46th Annual Meeting. Berlin, 10.-13.03.2013

9.   Acknowledgements

# 10.	Affirmation

Hereby, I declare that all the work presented in this dissertation is my own, carried out solely with the help of the literature and aids cited.

Hiermit erkläre ich, dass ich mich mit der vorliegenden wissenschaftlichen Arbeit erstmals um die Erlangung des Doktorgrades bewerbe.
Ich erkläre, dass ich die Arbeit selbständig und ohne fremde Hilfe verfasst, nur die von mir angegebenen Quellen und Hilfsmittel benutzt und die den benutzten Werken wörtlich oder inhaltlich entnommenen Stellen als solche kenntlich gemacht habe.

Gatersleben, May 2013

11. Appendix

Appendix 1: List of mean signal intensities from independent MALDI MSI experiments of 3 DAP barley grains according to the selected regions of interest (ROIs). Mean signal intensities are in arbitrary units as obtained by ClinProTools v.2.2 software (Bruker Daltonics). The cluster numbers correspond to the outcomes from the Neural Gas (NG) cluster analysis. Colors represent identical cluster revealed for all three experiments; 1 – chlorenchyma layer, 2 – embryo sac, 3 – maternal enclosure. Abbreviations are: Exp., experiment; Emb.sac, embryo sac; Ch, chlorenchyma layer; P,basal, pericarp-basal; P,scar, pericarp-scar; P, mid, pericarp-middle.

		Cluster sorting			Mean Signal intensities in Selected ROIs														
					Experiment 1					Experiment 1					Experiment 1				
Index	m/z	Exp. 1	Exp. 2	Exp.3	Emb. Sac	Chlor.	P, basal	P, scar	P, mid	Emb. Sac	Chlor.	P, basal	P, scar	P, mid	Emb. Sac	Chlor.	P, basal	P, scar	P, mid
1	86,11	3	2	3	1,11	0,93	1,22	1,5	1,19	3,82	1,95	1,51	2,41	1,51	1,04	0,93	0,96	1,06	0,95
2	90,03	2	2	2	1,72	1,29	1,27	0,99	1,28	2,93	1,42	1,43	1,49	1,49	1,82	1,41	0,73	0,95	1,16
3	94,09	3	3	3	2,34	2,54	3,36	17,98	5,84	3,99	4,02	3,23	17,7	6,63	0,76	1,24	0,95	2,46	1,54
4	104,13	3	2	3	62,19	53,62	52,92	61,66	76,67	142,51	88,29	65,95	116,68	88,15	43,44	44,78	16,52	38,55	45,47
5	116,1	2	2	2	1,77	1,35	1,42	1,01	1,33	2,7	1,58	1,53	1,62	1,8	1,87	1,53	1,04	1,07	1,35
6	118,08	3	3	3	15,85	13,27	14,94	27,02	18,71	31,11	21,35	13,64	50,57	27,16	13,38	15,54	4,97	19,44	16,78
7	130,11	3	2	3	1,72	1,38	1,51	1,52	1,7	3,29	1,92	1,74	2,5	2,24	1,57	1,39	0,86	1,23	1,49
8	136,05	3	3	2	2,63	1,85	3,15	2,45	2,66	5,02	3,38	2,63	4,82	4,35	2,72	2,58	1,57	1,82	2,2
9	140,12	3	3	3	2,97	2,78	3,66	6,38	4,03	5,91	4,61	3,61	13,37	6,45	2,24	2,35	1,42	3,3	2,51
10	147,08	2	2	2	6,47	4,33	4,47	3,86	5,1	12,58	6,23	5,07	6,57	7,03	10,44	8,97	3,57	5,26	7,57
11	148,07	2	2	2	1,82	1,39	1,48	1,06	1,43	5,38	2,71	2,42	2,69	2,94	2,86	2,54	1,23	1,59	2,18
12	152,13	3	3	3	0,89	0,85	0,97	1,16	0,91	1,34	0,99	0,91	1,17	1,04	0,74	0,81	0,69	0,72	0,81
13	156,11	3	3	3	44,49	36,6	44,12	54,01	51,21	86,77	57,77	45,75	95,26	70	40,79	36,54	15,32	42,03	38,39
14	158,09	3	3	3	3,36	2,96	3,08	4,12	3,84	6,45	4,77	3,71	8,47	5,64	3,44	3,56	1,72	4,75	3,98
15	164,11	3	2	3	1,55	1,5	1,34	1,22	1,51	5,85	4,29	3,4	3,47	3,83	2,68	3,38	1,68	2,33	2,87
16	166,14	3	3	3	0,93	0,86	0,86	1,17	1,01	1,53	1,12	1,04	2,07	1,49	1,35	1,33	0,84	1,49	1,71
17	184,14	3	2	2	3,18	1,91	5,17	4,71	3,33	17,9	9,79	7,5	11,15	8,89	6,13	4,45	4,91	3,55	3,48
18	192,04	3	3	3	13,82	10,18	14,69	14,55	16,51	45,34	30,94	28,84	37,11	36,4	17,09	17,38	10,42	15,42	17,64
19	193,03	3	3	3	52,49	38,05	54,09	47,94	58,45	106,86	73,13	68,25	89,79	88,84	51,48	51,16	31,28	43,12	52,06
20	195,02	3	3	3	5,32	3,89	5,36	5,15	6,05	14,61	10,26	10,51	12,07	12,22	6,92	7,46	4,64	6,42	7,33

#																			
21	205,18	2	2	2	1,17	0,87	0,84	0,79	0,78	1,81	0,9	0,88	0,99	0,98	1,35	0,98	0,76	1,01	1,18
22	221,26	3	3	3	6,77	6,38	4,27	5,63	7,13	13,44	9,37	6,65	13,05	10,91	6,68	6,85	2,76	8,09	7,56
23	222,09	3	2	3	2,23	2,05	1,96	1,99	2,33	11,24	8,04	6,68	6,81	7,35	3,07	3,23	2,17	2,93	3,2
24	229,99	3	2	3	5,19	4,22	5,44	4,8	6,16	17,91	13,02	13,67	12,96	14,47	5,99	6,13	4,04	6,61	7,09
25	230,99	3	2	3	20,29	16,16	21,57	21,92	24,88	65,15	46,41	48,79	49,05	53,17	22,35	22,76	15,06	24,25	26,13
26	233,01	3	3	3	3,81	3,11	3,83	3,72	4,49	11,89	8,89	9,44	9,02	10,18	4,54	4,59	3,34	5,03	5,29
27	240,23	3	2	3	1,24	1,08	1,32	1,64	1,31	2,02	1,24	1,21	1,71	1,46	0,97	0,85	0,7	0,92	0,92
28	241,25	3	3	3	1,71	2,17	1,91	5,36	3,29	2,02	2,28	1,94	6,75	4,18	0,83	0,98	0,7	1,93	1,39
29	246,11	3	3	2	1,91	1,51	2,09	2,98	2,1	3,96	2,19	2,6	4,21	3,43	2,61	1,7	1,6	1,84	1,72
30	254,17	3	3	3	1,59	1,48	1,56	2,33	1,89	1,87	1,55	1,34	2,87	2,14	1,16	1,18	0,84	1,68	1,37
31	258,17	3	3	3	1,73	1,71	2,11	3,58	2,48	2,22	1,85	1,68	4,67	3,06	1,4	1,33	1,13	1,81	1,52
32	284,19	3	3	3	1,74	1,66	1,94	1,63	2,42	2,9	2,78	3,63	2,77	3,66	1,38	1,36	1,36	1,23	1,55
33	292,15	3	3	2	2,88	2,08	3,16	2,92	2,68	3,93	2,19	3,15	3,87	3,43	4,81	2,74	2,45	2,48	2,43
34	293,2	3	3	3	1,85	1,85	2,49	4,77	2,74	2,09	1,56	1,93	4,74	2,88	2,1	1,44	1,27	2,63	1,77
35	294,16	3	3	3	1,39	1,36	1,68	3,03	1,92	1,45	1,42	1,45	4,14	2,65	1,16	1,07	0,89	1,99	1,41
36	296,18	3	3	3	1,59	1,66	1,68	2,46	2,24	1,99	1,65	1,5	3,2	2,4	1,07	1,16	0,91	1,49	1,42
37	308,14	3	3	2	1,83	1,46	2,04	1,75	1,75	2,4	1,54	2,25	2,44	2,32	2,44	1,51	1,55	1,48	1,55
38	319,16	3	3	3	1,63	1,61	1,82	1,62	2,36	2,22	2,33	2,81	2,32	3,24	1,31	1,32	1,33	1,32	1,54
39	337,36	3	3	3	1,04	1,02	1,55	1,44	1,2	1,07	1,14	1,48	1,79	1,52	0,85	0,91	0,97	1,2	1,06
40	350,13	3	3	3	1,54	1,32	1,39	1,45	1,6	2,09	1,7	1,64	2,05	2,68	1,39	1,33	1,33	1,24	1,51
41	358,19	3	3	3	1,38	1,23	1,58	1,1	1,03	1,62	1,21	1,44	1,29	1,38	1,33	1,07	1,94	1,03	1,06
42	379,94	3	3	3	1,62	1,5	1,49	2,17	2,51	1,68	1,5	1,27	2,6	2,97	1,5	1,52	1,43	2,01	2,25
43	381,23	3	2	2	5,66	4,46	6,74	3,55	5	14,93	9,03	13,25	8,31	9,34	7,1	5,88	8,36	4,07	5,31
44	399,27	3	3	3	3,77	3,78	4,46	3,3	6,54	9,25	9,87	11,17	8,24	13,15	2,88	2,92	3,26	2,15	3,24
45	412,34	3	3	3	1,13	1,07	1,72	2,56	1,46	0,7	0,79	1,36	5,85	2,02	0,98	0,92	1,6	4,17	1,46
46	419,08	3	3	3	1,29	1,15	1,18	1,13	1,32	1,7	1,41	1,83	1,64	2,04	1,34	1,4	1,69	1,43	1,61
47	423,06	3	2	3	4,03	3,52	3,65	2,64	4,14	9,62	7,32	9,34	5,97	8,3	6,04	5,73	4,58	5,49	6,28
48	448,29	3	3	3	1,36	1,32	1,27	2,55	1,77	2,54	2,27	4,12	8,35	4,76	2,25	1,88	3,7	4,64	3,11
49	460,25	2	2	2	2,64	2,27	3,78	1,59	1,61	4,67	3,01	3,38	2,68	3,02	3,4	2,47	5,15	1,76	1,71

50	466,18	3	3	3	1,47	1,38	1,54	1,51	1,83	1,97	1,79	2,31	1,8	2,06	1,72	1,5	1,87	1,48	1,66
51	479,05	3	3	3	1,79	1,46	1,94	1,36	1,67	3,95	3,04	4,69	2,86	3,3	2,34	1,87	2,87	2,19	2,21
52	481,06	3	3	3	1,52	1,27	1,54	1,25	1,47	2,76	2,11	3,42	2,24	2,54	1,96	1,74	2,32	1,92	2,04
53	489,27	3	3	3	1,43	1,48	1,78	1,74	2,05	1,41	1,72	2,28	1,74	2,03	1,43	1,44	1,84	1,46	1,71
54	496,52	2	2	3	1,35	1,14	1,02	1	0,99	1,62	1,36	1,3	1,06	0,9	1,49	1,57	1,77	1,16	1,24
55	511,18	3	3	3	1,31	1,28	3,34	1,72	1,69	1,25	1,16	1,65	1,07	1,24	1,13	1,22	1,59	1,72	1,4
56	518,47	3	2	3	1,22	1,08	3,24	1,11	1,22	1,33	0,94	1,27	0,99	0,94	1,64	1,25	1,92	1,26	1,52
57	520,45	3	3	3	1,81	1,72	13,5	4,16	3,77	1,86	2,03	2,77	2,59	1,86	1,91	2,57	5,37	4,91	3,67
58	543,28	3	3	3	7,28	6,69	9,6	5,59	8,93	16,12	12,04	19,1	12,54	15,42	8,88	7,92	10,71	7,33	8,89
59	558,37	3	3	3	1,55	1,65	13,64	3,83	4,05	1,57	1,75	3,27	2,63	1,99	1,46	1,85	3,62	4,56	3,01
60	560,43	3	3	3	1,38	1,35	5,58	1,92	2,4	1,37	1,62	1,84	1,71	1,58	1,48	1,52	2,02	2,02	2,05
61	573,67	3	2	2	1,32	1,15	1,19	1,1	1,13	3,34	1,78	1,97	1,48	1,78	2,03	1,4	1,56	1,2	1,31
62	575,63	3	3	3	1,6	1,5	1,87	2,32	1,95	3,5	3,57	4,1	4,29	4,68	1,84	2,26	2,9	2,33	2,21
63	576,61	3	3	3	2,46	2,26	3,11	2,75	3,35	3,06	2,8	3,93	3,39	3,69	2,18	2,24	3,26	2,48	2,69
64	580,17	3	3	3	1,7	1,65	2,02	1,88	2,5	2,57	2,76	3,52	2,62	3,3	1,57	1,81	2,49	1,73	2,08
65	592,41	1	1	1	1,02	2,64	1,1	1,06	1,12	0,84	6,79	1,88	1,4	2,18	1,06	3,29	1,2	1,03	1,19
66	597,64	3	2	3	1,31	1,41	1,3	1,3	1,23	3,05	2,41	2,49	1,96	2,19	1,82	2,12	1,97	1,46	1,5
67	599,63	3	1	1	1,73	3,55	1,76	2,75	1,91	4,82	9,59	4,4	4,27	4,79	2,4	7,77	3,09	2,33	2,22
68	602,39	3	2	3	1,33	1,65	1,28	1,3	1,23	2,58	3,4	2,14	1,55	1,82	2,06	2,11	2,56	2,17	2,22
69	604,39	3	3	3	1,51	1,54	1,97	1,65	1,77	2,02	2,13	2,35	1,84	2,05	1,83	2,08	2,52	1,65	1,93
70	615,11	3	3	3	1,84	1,67	1,66	1,41	1,96	3,39	2,93	3,34	2,84	3,72	2,71	2,32	2,57	2,66	2,75
71	616,37	2	2	2	3,09	1,99	2,42	2,16	1,87	14,34	4,86	7,24	7,31	6,22	10,59	4,09	4,44	3,68	3,1
72	618,28	3	2	2	2,17	1,78	2,25	2,11	2,88	5,4	2,15	3,55	3,04	2,82	4,56	2,24	2,82	2,33	2,34
73	646,39	3	3	3	1,54	1,56	1,69	1,44	2,05	2,15	2,41	1,88	2,17	2,88	1,79	1,88	1,91	2,15	2,32
74	650,55	2	2	2	1,72	1,15	1,37	1,2	1,32	2,06	1,19	1,21	1,29	1,27	3,39	1,41	2,07	1,68	1,54
75	653,02	1	1	1	1,39	9,15	1,49	1,34	1,67	1,73	14,43	3,7	2,29	4,16	1,68	7,66	2,55	1,6	1,91
76	664,29	3	3	3	1,42	1,39	1,55	1,37	1,76	2,16	2,1	2,19	1,98	2,4	1,81	1,96	2,83	1,89	2,08
77	684,31	3	3	3	1,49	1,44	1,54	1,21	1,65	1,99	2,05	2,11	1,7	2,41	1,57	1,58	1,74	1,79	2,01
78	689,39	3	3	3	2,43	2,39	4,67	2,14	3,01	3,18	3,3	4,82	4,02	4,39	2,82	2,57	4,9	2,5	2,82

79	705,3	3	3	3	14,18	13,63	20,64	10,3	18,59	21,89	19,35	30,38	20,85	26,95	16,69	16,42	22,82	15,12	18,78
80	711,55	3	3	3	1,21	1,36	1,49	1,4	1,57	1,43	2,19	2,27	2,03	2,57	1,29	1,62	2	1,89	2,1
81	738,22	3	3	3	2,97	2,73	3,69	2,6	4,1	3,02	2,78	4,65	3,19	3,98	2,69	2,58	3,67	3,02	3,24
82	743,5	3	3	3	1,1	1,08	1,11	1,78	1,13	1,02	0,88	0,94	1,33	1,24	1,46	1,5	1,5	13,53	4,24
83	747,13	2	2	3	1,5	1,41	1,21	1,02	1,17	4,11	2,16	2,18	1,16	1,46	1,92	1,65	1,83	1,53	1,46
84	749,22	3	2	3	2,06	2	2,24	1,98	2,2	5,39	5,52	5,65	3,67	4,32	2,1	3,06	3,71	2,86	2,73
85	749,43	3	3	3	1,42	1,88	1,67	1,72	1,94	2,26	3,94	3,61	2,74	3,64	1,33	2,16	2,51	2,38	2,57
86	754,68	3	2	3	1,48	1,43	1,43	1,21	1,41	3,97	3,46	3,61	2,07	3,12	1,9	1,99	2,22	1,55	1,71
87	756,79	2	2	2	3,83	2,19	2,22	1,3	1,66	15,46	6,7	6,34	2,55	4,06	7,78	4,42	5,33	2,07	2,48
88	758,76	3	2	3	6,54	5,38	7,28	5,4	6,01	18,58	17,39	16,95	12,51	15,25	8,3	11,12	14,53	6,84	6,69
89	760,73	2	2	2	4,15	2,61	2,86	1,73	2,22	12,06	7,08	6,28	2,98	4,5	6,37	4,66	5,54	3,03	2,95
90	773,03	3	2	3	2,27	1,84	2,12	2,02	1,95	7,39	5,17	5,39	3,9	4,17	3,48	3,15	3,9	3,56	2,43
91	773,6	3	3	3	1,78	2,06	1,83	6,45	2,2	3,52	5,68	4,85	6,48	6,33	2,84	4,76	6,81	32,1	12,11
92	778,72	2	2	2	2,69	1,66	1,54	1,22	1,44	11,85	5,11	4,85	2,42	3,62	7,6	2,98	3,69	2,07	2,19
93	780,72	2	2	2	5,1	2,85	3,13	1,65	2,19	20,56	9,39	9,41	4,81	6,54	11,75	6,05	7,92	2,69	3,17
94	782,72	2	2	2	7,8	5,23	6,82	4,98	5,1	26,74	16,67	16,23	12,93	14,49	16,58	11,76	15,31	7,39	6,44
95	784,72	2	2	2	6,4	3,49	3,61	1,86	2,63	19,76	9,66	8,52	3,95	5,76	11,97	7,09	8,15	2,75	3,64
96	786,72	2	2	2	3,18	1,87	1,68	1,42	1,56	9,21	4,25	3,42	2,05	2,74	7,23	3,27	3,73	1,95	2,31
97	794,62	2	2	2	3,82	2,23	2,17	1,21	1,66	17,72	8,27	7,89	2,65	4,52	5,45	3,93	4,15	1,91	2,43
98	796,64	3	2	3	6,83	5,77	7,37	4,87	6,47	23,29	22,88	23,18	13,72	18,35	6,54	10,51	12,38	7,95	7,5
99	798,65	2	2	2	4,87	3,19	3,67	2,13	3,05	16,44	11,26	10,64	4,76	7,3	5,33	5,41	5,73	3,05	3,6
100	800,68	2	2	2	1,82	1,36	1,49	1,2	1,32	4,47	2,87	2,72	1,52	1,95	2,25	1,81	1,9	1,66	1,58
101	804,58	3	2	3	1,45	1,39	1,54	1,6	1,46	3,37	2,71	2,87	2,2	2,36	1,81	1,79	2,53	2,43	1,81
102	808,35	2	2	2	1,77	1,42	1,42	1,23	1,36	4,21	1,92	2,52	1,88	2,05	2,91	1,98	2,07	1,76	1,82
103	813,59	3	1	3	1,42	2,37	1,53	1,38	1,47	2,81	6,37	2,92	1,77	2,91	1,83	3,18	2,23	2,47	1,98
104	814,61	3	2	3	1,53	1,8	1,83	1,32	1,46	3,28	4,18	2,61	1,69	2,39	2,07	2,45	2,09	1,8	1,67
105	816,65	2	2	2	2,4	1,68	1,58	1,19	1,55	10,32	4,31	3,86	1,93	2,88	5,03	2,69	2,83	1,72	2,11
106	818,7	2	2	2	4,35	2,47	2,38	1,32	1,8	20,86	9,22	9	3,69	5,49	7,8	4,85	5,38	2,42	2,74
107	820,74	2	2	2	7,2	5,39	6,41	4,1	5,08	30,35	20,3	20,23	13,08	15,94	12,33	10,86	12,25	7,31	6,5

108	822,65	2	2	2	6,5	3,9	3,8	2	3,03	24,33	13,14	11,76	5	7,65	9,22	7,17	7,24	3,3	4,11
109	824,7	2	2	2	3,49	2,22	1,83	1,37	1,64	12,31	5,93	4,61	2,12	3,17	5,99	3,56	3,3	2,05	2,43
110	839,73	3	1	3	1,21	2,03	1,24	1,03	1,12	1,25	4,58	1,83	1,36	2,01	1,3	2,4	1,41	1,36	1,39
111	851,46	3	3	3	2,93	2,86	4,68	2,27	3,51	3,46	3,58	5,53	4,54	5,29	2,76	2,7	4,96	2,75	2,97
112	867,48	3	3	3	18,52	18,75	25,81	12,77	25,75	24,52	23,94	37,72	24,91	35,36	17,89	19,19	24,82	19,3	23,56
113	870,8	1	1	1	2,03	18,49	2,62	1,84	2,98	1,92	39,44	8,27	4,29	11,02	2,26	16,51	3,91	2,31	3,06
114	884,72	1	1	1	1,49	4,16	1,51	1,37	1,43	1,96	12,01	2,8	1,88	3,1	1,75	4,36	2,74	1,58	1,76
115	899,98	3	3	3	2,1	2,09	2,52	2,18	2,91	1,89	2,15	2,74	2,48	2,75	2,03	2,25	2,98	2,59	2,67
116	909,66	1	1	1	1,46	15,48	1,59	1,26	1,85	2,5	38,06	7,67	3,21	8,39	1,6	12,26	2,57	1,75	2,18
117	917,84	3	3	3	1,25	1,52	1,28	2,83	1,73	1,07	1,71	1,44	2,84	1,48	1,26	1,7	1,56	2,28	1,92
118	923,73	1	1	1	1,24	3,35	1,25	1,18	1,23	1,21	11,69	2,39	1,55	2,54	1,29	3,29	1,67	1,49	1,52
119	950,79	3	3	3	1,61	1,4	2,56	1,7	2,14	1,99	2,22	2,92	2,86	3,69	1,78	1,84	2,43	2,08	2,16
120	953,78	3	3	3	1,3	1,43	1,44	1,15	1,37	1,82	2,92	2,3	1,88	2,56	1,46	1,85	1,99	1,53	1,68
121	955,68	3	3	3	1,22	1,42	1,29	1,42	1,44	1,59	2,86	2,62	3,06	3,32	1,24	1,66	1,97	2,16	2,01
122	968,83	3	3	3	2,23	1,36	2,82	1,37	1,83	2,17	2,36	2,82	2,03	2,86	1,82	2,05	2,15	1,58	1,7
123	975,68	3	1	3	1,52	2,78	1,46	1,32	1,69	3,49	8,46	4,16	2,65	4,39	1,79	3,38	2,53	1,81	2,02
124	977,76	3	3	3	1,33	1,78	1,35	1,35	1,53	2,25	4,66	3,21	2,98	3,74	1,45	2,11	2,09	2,21	1,96
125	981,75	3	3	3	1,33	1,66	1,52	1,43	1,5	1,39	2,95	2,31	2,54	2,64	1,35	1,89	1,86	2,02	1,8
126	1006,73	3	3	3	1,98	1,43	2,15	1,32	1,64	2,45	2,63	3,05	2	2,7	1,62	1,95	2,41	1,57	1,72
127	1008,67	2	3	3	1,94	1,8	1,75	1,25	1,59	2,22	2,92	2,46	1,63	2,35	1,51	2,15	2,07	1,43	1,59
128	1009,81	3	3	3	1,56	1,99	1,47	1,2	1,4	1,57	3,29	2,09	1,49	2,1	1,28	2,18	1,8	1,37	1,52
129	1013,55	3	3	3	2,09	2,19	3,15	2,08	2,69	1,96	2,21	2,81	3,28	3,63	1,87	2,03	3,36	2,25	2,39
130	1029,55	3	3	3	10,68	11,57	16,04	10,08	17,23	11,09	12,09	16,11	16,76	20,85	10,23	11,82	14,87	13,11	14,71
131	1061,77	3	3	3	1,79	1,88	2,21	2,05	2,5	1,4	1,93	2,12	2,18	2,36	1,67	1,85	2,46	2,41	2,3
132	1080,67	2	2	3	1,94	1,58	1,48	1,15	1,54	3,29	3,17	2,59	1,5	3,66	1,36	1,69	1,93	1,47	1,81
133	1110,61	2	3	3	1,91	1,59	1,51	1,17	1,74	2,48	2,42	2,14	1,56	3,03	1,25	1,56	1,8	1,44	1,68
134	1173,65	3	3	3	1,36	1,41	1,61	1,87	1,87	1,05	1,15	1,28	1,56	1,72	1,21	1,24	1,8	1,73	1,57
135	1175,75	3	3	3	1,9	1,97	2,73	2,07	2,61	1,52	1,77	2,15	2,84	2,94	1,62	1,75	2,85	2,14	2,11
136	1191,58	3	3	3	8,11	9,47	12,35	9,69	15,34	6,99	8,26	10,11	13,47	15,44	6,72	8,24	10,45	9,97	10,67

137	1212,66	2	3	3	1,77	1,43	1,24	1,1	1,42	2,33	2,3	1,95	1,27	2,63	1,27	1,48	1,71	1,35	1,62
138	1223,73	3	3	3	1,61	1,67	1,91	2,04	2,38	1,38	1,41	1,61	1,81	1,91	1,57	1,63	2,23	2,22	2,09
139	1242,75	2	2	3	2,52	1,96	1,54	1,15	1,97	3,76	3,59	2,74	1,7	4,41	1,34	1,69	1,83	1,42	1,79
140	1272,85	3	3	3	2,03	1,78	1,75	1,33	2,19	2,26	2,48	2,25	1,81	3,3	1,27	1,54	1,76	1,45	1,73

Appendix 2: Mean signal intensities from selected regions of interest (ROIs) of 7 DAP barley grain MALDI MSI experiments. Mean signal intensities are in arbitrary units as obtained by ClinProTools v.2.2 software (Bruker Daltonics). The cluster numbers correspond to the outcomes from the Neural Gas (NG) cluster analysis. Colors represent identical cluster revealed for all three experiments; 1 – embryo, 2 – maternal enclosure, 3 – chlorenchyma layer, 4 – co-localization. Abbreviations are: Tra, transfer region; En, endosperm; Emb, embryo; Ch, chlorenchyma layer; P-Ve, pericarp-ventral; P-Do, pericarp-dorsal.

Index	m/z	Cluster	Mean signal intensities in selected ROIs of experiment 1						
			Tra	En	Emb	Ch	P-Ve	P-Do	Scar
1	86.1	1	1.58	2.08	4.79	1.71	1.61	1.18	1.09
2	90.0	3	1.59	1.84	1.68	1.49	1.19	1.66	0.96
3	94.1	2	2.96	2.41	6.88	5.16	5.92	3.11	14.11
4	104.1	3	51.28	60.23	60.27	39.66	28.25	60.39	48.96
5	116.1	3	2.23	3.95	4.13	2.15	1.39	3.68	1.4
6	118.1	2	5.01	7.82	12.73	5.88	5.51	8.54	14.3
7	130.1	3	1.04	1.11	1.13	1.03	0.96	1.04	1.11
8	136.0	3	3.51	2.73	2.81	4.49	4.81	3.74	4.48
9	140.1	2	2.6	2.54	4	2.65	3.38	3.26	6.02
10	147.1	3	1.91	2.16	3.38	3.03	3.62	2.61	3.16
11	148.1	3	1.2	1.47	1.5	1.14	1.22	1.48	1.09
12	158.1	3	2.04	1.75	2.54	1.51	1.22	1.84	1.53
13	164.1	3	1.16	1.03	0.93	1.11	0.98	0.96	1.19
14	175.1	2	3.66	3.42	4.1	6.05	6.35	4.44	6.81
15	182.1	2	1.02	1.66	2.35	1.69	2.76	1.44	3.68
16	184.1	3	2.72	5.17	11.49	5.47	9.57	4.25	4.57
17	192.0	3	8.22	11.34	12.85	11.35	15.66	15.96	9.22
18	193.0	3	25.8	31.68	38.87	38.46	48.09	51.07	29.86
19	195.0	3	3.18	3.78	4.5	4.14	5.5	5.64	3.22
20	221.2	3	2.36	2.91	3.68	1.66	1.89	3.05	2.89
21	222.1	3	2.38	1.72	2.09	2.26	1.98	1.73	1.41
22	230.0	3	4.92	3.38	4.51	4.19	3.73	4.44	1.91
23	231.0	3	17.78	11.76	16.72	15.2	12.9	16.54	7.57
24	233.0	3	3.53	2.49	3.26	2.97	2.57	3.2	1.51
25	240.1	3	1.19	1.48	1.74	1.09	1.21	1.1	1.51
26	241.2	2	1.36	1.43	2.23	1.43	1.37	1.41	3.98
27	254.1	3	1.26	1.26	1.31	1.01	0.94	1.1	1.32
28	258.1	2	1.32	1.6	1.55	1.45	2.15	1.72	3.2
29	268.2	3	1.22	1.2	1.11	1.26	0.99	1.16	1.57
30	284.2	3	1.12	1.23	1.12	1.08	1.23	1.34	1.18
31	294.1	2	1.34	1.17	1.53	1.39	1.83	1.3	2.98
32	308.1	3	1.15	1.42	1.74	1.19	1.8	1.6	2.04
33	348.1	3	1.55	4.16	2.28	1.62	3.21	4.44	3.71
34	381.1	3	8.17	6.43	8.18	7.32	7.64	7.96	4.54
35	399.2	3	1.29	1.7	1.61	1.38	1.97	2.32	1.56
36	407.0	3	1.99	1.58	1.63	1.64	1.58	1.79	1.1
37	422.9	3	3.03	2.22	2.68	2.42	1.97	2.48	1.22

38	428.1	3	1.42	3.71	2.25	1.54	3.01	3.9	1.71
39	448.2	2	1.23	1.3	0.97	1.46	1.39	1.71	2.5
40	460.2	3	1.33	1.28	1.3	1.4	2.65	1.11	1.28
41	466.0	3	1.29	1.64	1.22	1.19	1.47	1.81	1.04
42	489.3	3	1.22	1.31	1.1	1.4	1.51	1.55	1.17
43	508.0	3	1.18	1.37	1.01	0.99	1.61	1.24	1.02
44	518.3	3	1.17	1.35	2.49	1.43	4.01	1.01	1.12
45	520.3	3	1.21	2.43	2.21	2.25	10.28	2.34	3.23
46	522.3	3	1.08	1.22	0.99	1.11	4.52	1.42	1.48
47	527.2	3	4.25	2.56	2.03	3.91	3.81	3.3	2.33
48	543.1	3	18.05	7.65	6.73	14.12	10.12	8.85	4.91
49	558.3	3	1.27	1.82	1.71	1.69	6.05	1.67	1.63
50	560.4	3	2.26	1.7	1.3	1.92	3.68	1.82	1.47
51	573.6	3	1.22	1.25	2.69	1.2	1.55	1.48	1.28
52	575.5	3	1.46	1.95	2.25	1.58	2.43	2.94	2.24
53	576.5	3	5.49	3.27	2.85	4.05	3.87	3.82	2.42
54	580.1	3	1.37	1.39	1.18	1.35	1.79	1.93	1.11
55	592.3	4	1.11	0.96	0.91	3.29	1.42	1.57	1.36
56	599.5	3	1.31	1.68	1.93	3.68	1.69	2.43	1.97
57	615.1	3	1.49	1.23	1.34	1.3	1.08	1.27	1.15
58	616.3	1	1.66	2.58	7.37	2.45	1.33	1.93	3.44
59	618.2	3	1.57	1.74	2.79	1.65	1.67	1.97	1.86
60	652.9	4	1.66	1.11	1.17	8.87	2.3	3.19	2.31
61	664.2	3	1.19	1.41	1.01	1.24	1.94	1.93	1.15
62	688.4	3	1.3	1.23	1.09	1.43	5.19	1.35	1.37
63	689.3	3	7.57	4.37	2.92	6.82	8.54	5.75	4.28
64	705.2	3	32.98	16.73	12.81	27.31	22.82	19.61	10.87
65	738.1	3	4.37	3.16	2.38	3.12	3.12	3.43	2.1
66	744.4	2	1.16	1.08	0.99	1.3	2.73	1.61	2.44
67	747.0	1	1.49	1.52	5.91	1.57	1.33	1.31	1.24
68	749.1	1	2.23	3.26	4.78	2.57	2.18	2.39	1.48
69	751.0	3	1.73	2.22	2.03	1.62	1.32	1.54	1.15
70	752.5	3	1.34	1.31	2	1.26	1.1	1.17	1.02
71	754.5	3	1.39	1.47	1.95	1.38	1.32	1.41	1.14
72	756.6	1	2.31	3.69	19.78	3.81	3.96	2.89	2.71
73	758.7	3	4.51	11.23	15.07	8.97	11.54	12.95	9.93
74	760.7	3	2.97	6.31	5	4.05	4.33	5.28	4.47
75	771.0	1	1.38	1.32	3.57	1.44	1.12	1.19	1.11
76	773.0	2	1.58	2.14	3.24	2.13	1.5	1.72	4.45
77	773.4	2	1.48	1.52	2.03	1.64	1.62	1.85	9.15
78	778.5	1	1.63	1.94	11.59	2.06	1.84	1.81	1.35
79	780.7	1	2.36	4.09	13.07	4.5	3.9	3.67	2.96
80	782.7	3	2.81	7.17	10.11	7.31	6.56	7.93	6.71
81	784.6	3	2.15	4.67	4.49	4.85	3.32	4.55	4.45
82	786.7	3	1.59	2.62	2.15	2.61	1.97	2.86	3.04

Index	m/z	Cluster							
83	794.6	1	2.55	3	19.14	3.39	2.45	2.06	1.4
84	796.6	1	5.4	9.83	16.1	8.21	7.4	8.15	3.88
85	798.6	3	3.76	5.99	5.99	4.11	3.58	4.16	2.24
86	800.6	3	1.57	1.88	2.41	1.51	1.44	1.41	1.28
87	813.6	3	1.25	1.19	1.32	2.24	1.69	1.49	1.33
88	816.5	1	1.42	1.51	8.24	1.7	1.52	1.33	1.09
89	818.5	1	1.88	2.57	10.68	3.2	1.83	1.69	1.29
90	820.6	1	2.93	5.79	9.46	6.17	3.82	4.59	2.62
91	822.6	3	2.65	4.38	4.74	4.41	2.51	3.21	2.12
92	824.6	3	1.71	2.47	2.16	2.58	1.54	2.01	1.56
93	851.3	3	4.93	4.4	2.85	4.44	6.35	5.79	4.41
94	867.4	3	21.55	16.74	12.57	17.85	19.78	21.97	12.24
95	870.6	4	2.53	1.72	1.87	16.37	4.31	6.63	4.17
96	884.7	3	1.39	1.33	1.22	2.58	1.69	1.5	1.28
97	899.9	3	3.58	2.75	2.16	2.83	2.76	2.81	1.97
98	906.4	3	1.28	1.26	1.47	1.45	1.9	3.18	1.66
99	909.6	4	1.68	1.16	1.75	8.96	2.07	2.86	1.66
100	923.6	3	1.23	1.04	1.18	1.9	1.16	1.2	1.11
101	926.7	3	1.22	1.09	1.1	1.46	2.28	1.43	1.25
102	944.6	3	1.29	1.08	1.15	1.37	2.42	1.64	1.34
103	950.7	3	1.22	1.35	1.49	1.36	1.71	1.46	1.34
104	968.6	3	1.2	1.18	1.41	1.68	1.7	1.36	1.19
105	975.6	3	1.4	1.41	1.64	2.05	1.47	1.66	1.31
106	1013.5	3	4.15	4.01	2.52	3.97	5.79	5.09	4.4
107	1029.3	3	17.93	15.46	10.4	16.14	19.25	18.57	12.53
108	1061.7	3	2.88	2.42	1.8	2.42	2.52	2.5	1.99
109	1068.5	3	1.25	1.4	1.75	1.47	2.91	5.3	2.53
110	1175.5	3	3.59	3.67	2.25	3.72	5.45	4.5	4.69
111	1191.4	3	14.65	13.31	8.88	13.33	17.1	15.84	13.2
112	1214.7	3	1.29	1.3	1.47	1.31	2.14	4.22	1.66
113	1223.6	3	2.58	2.23	1.77	2.23	2.38	2.21	2.05
114	1230.6	3	1.41	2.12	3.46	1.89	5.6	14.16	3.77

Index	m/z	Cluster	Mean signal intensities in selected ROIs of experiment 2						
			Tra	Endo	Embryo	Chlor	P-Ve	P-Do	Scar
1	86.1	3	1.43	2.31	2.23	1.59	1.63	1.47	1.33
2	90.0	3	1.6	2.16	1.73	1	1.17	1.43	0.88
3	94.1	2	2.18	3.01	2.37	9.73	4.29	4.7	8.79
4	104.1	3	42.51	83.82	63.18	48.45	45.24	84.92	64.05
5	116.1	1	4.01	6.49	7.58	2.25	1.8	5.46	1.17
6	118.1	3	10.88	15.79	16.29	11.12	13.14	15.27	19.95
7	130.1	3	1.5	1.78	1.54	1.14	1.9	1.36	1.63
8	136.0	3	3.47	3.97	4.53	3.97	3.54	3.43	3.85
9	140.1	2	2.26	3.13	3.67	3.16	3.2	3.71	4.78
10	147.1	3	6.67	10.23	8.36	5.22	8.12	6.27	6.38

11	148.1	3	2.67	3.94	3.45	1.87	2.66	2.34	1.7
12	158.1	3	2.61	3.82	3.26	2.49	2.71	3.31	2.54
13	164.1	3	2.97	3.84	2.88	2.82	2.38	3.07	2.1
14	175.1	3	7.97	9.98	9.58	10.98	12.25	7.6	10.2
15	182.1	3	3.73	2.27	3.27	5.87	3.96	3.67	4.72
16	184.1	3	5.87	9.22	9.55	7.62	10.31	5.04	5.26
17	192.0	3	16.37	23.29	18.31	22.32	22.84	23.24	14.01
18	193.0	3	49.89	69.34	54.77	63.12	65.33	68.13	44.61
19	195.0	3	5.96	7.99	6.26	7.85	7.91	8.05	5.21
20	221.2	3	3.72	6.22	5.07	2.8	3.21	4.46	5.11
21	222.1	3	5.25	7.1	4.08	6	6.36	4.71	2.6
22	230.0	3	6.31	10	5.81	9.59	7.99	8.35	3.78
23	231.0	3	23.56	38.12	21.55	34.81	29.69	31.97	13.33
24	233.0	3	4.56	6.98	4.09	6.55	5.48	5.78	3.03
25	240.1	3	1.1	1.14	1.24	0.8	1.01	1.12	1.14
26	241.2	2	1.42	1.34	1.09	1.91	1.34	1.79	3.25
27	254.1	3	1.24	1.29	1.22	0.95	1.11	1.14	1.33
28	258.1	3	1.75	2.04	1.85	1.93	2.35	1.89	2.5
29	268.2	3	5.69	4.28	1.22	3.18	1.05	1.04	1.26
30	284.2	3	1.76	1.82	2.13	2.8	2.48	2.28	1.88
31	294.1	2	1.25	1.3	1.34	1.4	1.62	1.41	2.31
32	308.1	3	1.82	2.1	2.45	1.42	2.7	1.76	2.19
33	348.1	2	2.26	2.92	3.15	2.81	3.59	2.49	4.5
34	381.1	3	6.96	10.18	10.42	5.96	7.66	8.92	4.98
35	399.2	3	3.03	3.45	5.43	7.57	6.39	5.6	3.94
36	407.0	3	1.72	2.16	2.07	1.49	1.77	2.2	1.4
37	422.9	3	4.76	6.69	3.58	5.53	4.86	4.58	2.19
38	428.1	3	1.71	2.53	4.7	2.51	3	2.77	2.12
39	448.2	2	1.59	1.51	1.16	1.87	1.93	2.41	7.19
40	460.2	2	1.51	2.23	3.09	1.9	3.88	4.51	5.86
41	466.0	3	1.42	1.53	1.7	2.14	1.78	2.08	1.41
42	489.3	3	1.51	1.22	1.3	3.16	2	2.19	1.41
43	508.0	3	1.08	1.12	1.46	1.14	1.43	1.31	1.17
44	518.3	3	1.12	0.99	1.24	0.85	2.29	1.07	1.08
45	520.3	3	1.3	1.04	1.04	1.49	10.03	2.2	3.23
46	522.3	3	1.03	0.83	0.79	0.8	4.36	1.04	1.23
47	527.2	3	1.98	2.32	1.99	3.21	2.41	2.69	1.86
48	543.1	3	9.46	16.15	7.6	7.58	8.34	10.94	4.83
49	558.3	3	1.34	1.03	0.94	1.19	9.21	2.37	2.26
50	560.4	3	1.16	1.11	1.12	1.25	4.95	1.53	1.47
51	573.6	1	1.62	2.02	2.94	1.05	1.12	1.22	1.14
52	575.5	3	1.94	1.49	1.65	1.46	2.18	1.54	2.02
53	576.5	3	2.43	3.28	2.53	2.36	3.41	2.94	2.36
54	580.1	3	1.73	1.45	1.57	3.84	2.37	2.57	1.49
55	592.3	4	1.16	0.88	0.87	5.41	1.62	1.35	1.43

56	599.5	4	1.84	1.61	1.48	4.75	1.8	1.42	1.83
57	615.1	3	2.18	2.17	1.56	1.65	1.55	1.88	1.32
58	616.3	1	13.19	5.03	9.75	2.1	2.9	2.27	3.22
59	618.2	3	5.45	2.73	4.12	6.16	3.41	2.93	1.99
60	652.9	4	1.45	1.18	1.05	13.16	2.81	2.1	2.16
61	664.2	3	1.37	1.24	1.66	1.66	1.56	1.77	1.4
62	688.4	3	1.2	0.99	1.03	0.98	2.99	1.48	1.3
63	689.3	3	2.24	2.83	2.87	2.2	3.69	3.35	2.65
64	705.2	3	16.76	26.31	17.26	17.29	23.64	21.43	11.23
65	738.1	3	2	2.78	2.44	2.35	3.07	3.11	2.29
66	744.4	3	1.07	0.95	1.11	1.18	1.67	2.09	1.83
67	747.0	1	2	3.22	3.55	1.46	1.1	1.37	1.11
68	749.1	3	2.69	3.07	2.07	3.41	2.75	1.9	1.7
69	751.0	3	1.62	2.15	1.16	1.56	1.46	1.36	1.17
70	752.5	3	1.42	2.06	2.05	1	0.98	1.2	1
71	754.5	3	1.6	1.55	1.44	1.28	1.3	1.25	1.13
72	756.6	1	5.98	8.63	14.51	3.91	2.23	2.87	1.72
73	758.7	3	7.95	7.34	6.44	10.78	9.11	4.3	5.81
74	760.7	3	3.45	4.66	2.54	3.35	2.94	2.22	1.97
75	771.0	1	2.19	3.11	3.78	1.59	1.18	1.42	1.18
76	773.0	2	2.82	3.21	2.4	3.38	2.51	1.89	4.06
77	773.4	2	1.86	1.56	1.15	2.02	1.79	1.75	6.38
78	778.5	1	3.26	5.07	13.79	1.99	1.44	2.19	1.32
79	780.7	1	6.63	8.6	14.76	5.36	3.11	3.2	2.15
80	782.7	3	8.27	7.88	7.63	10.65	8.03	4.14	5.25
81	784.6	3	4.51	4.77	3.18	4.47	3.8	2.35	2.06
82	786.7	3	1.87	2.15	1.48	1.69	1.76	1.57	1.45
83	794.6	1	6.32	10.77	12.28	4.27	2.15	3.12	1.49
84	796.6	3	9.37	10.2	6.65	12.7	9.22	5.12	4.3
85	798.6	3	4.69	6.72	2.78	5.08	4	2.93	2.1
86	800.6	3	1.64	2.01	1.96	1.42	1.3	1.26	1.13
87	813.6	4	1.46	1.3	1.15	3.57	1.75	1.46	1.37
88	816.5	1	2.77	4.97	10.18	1.94	1.41	1.89	1.19
89	818.5	1	6.41	9.8	12.29	4.99	2.45	2.81	1.52
90	820.6	3	9.06	9.97	7.11	11.64	7.62	4.38	3.6
91	822.6	3	5.32	6.49	3.08	5.77	4.18	2.75	1.83
92	824.6	3	2.21	2.87	1.37	2.35	1.86	1.76	1.25
93	851.3	3	1.69	2.06	2.46	1.81	2.64	2.97	2.64
94	867.4	3	10.9	17.24	14.21	14.33	20.12	19.89	11.94
95	870.6	4	2	1.4	1.48	28.04	6.2	4.84	3.76
96	884.7	4	1.83	1.34	1.35	5.53	1.97	1.46	1.49
97	899.9	3	1.68	1.86	2.06	2.29	2.57	2.27	1.98
98	906.4	3	1.15	1.1	2.02	1.14	1.1	3.97	1.13
99	909.6	4	1.84	1.36	1.36	21.4	3.82	3.43	2.32
100	923.6	4	1.3	0.98	1	3.85	1.37	1.23	1.23

101	926.7	3	1.15	0.92	0.89	1.94	2.28	1.22	1.35
102	944.6	3	1.15	0.94	1.06	1.14	2.21	1.37	1.37
103	950.7	3	1.28	1.09	1.11	1.27	2.26	1.27	1.54
104	968.6	3	1.21	1.02	1.5	1.58	2.37	1.3	1.33
105	975.6	3	1.56	1.64	1.3	3.13	1.56	1.64	1.48
106	1013.5	3	1.47	1.36	1.89	1.66	2.19	2.29	2.38
107	1029.3	3	6.99	8.38	10.54	10.86	15.19	12.63	10.09
108	1061.7	3	1.39	1.31	1.57	1.74	2	1.85	1.8
109	1068.5	3	1.15	1.09	1.83	0.98	1	4.36	1.22
110	1175.5	3	1.31	1.12	1.61	1.49	1.8	1.94	2.17
111	1191.4	3	4.86	4.84	7.41	8.27	11.12	9.54	8.57
112	1214.7	3	1.04	0.88	1.18	0.78	0.81	2.46	1.09
113	1223.6	3	1.3	1.18	1.49	1.42	1.69	1.66	1.63
114	1230.6	3	1.24	1.15	2.78	0.99	1.05	8.01	1.21

Index	m/z	Cluster	Mean signal intensities in selected ROIs of experiment 3						
			Tra	Endo	Embryo	Chlor	P-Ve	P-Do	Scar
1	86.1	3	1.11	1.08	1.06	0.95	1.09	0.97	0.93
2	90.0	3	1.85	1.44	1.31	1.2	1.19	1.15	0.93
3	94.1	2	1.48	1.43	1.99	2.41	2.45	1.93	7.07
4	104.1	3	17.79	20.72	35.51	23.23	19	21.12	18.46
5	116.1	3	2.98	3.12	4	2.15	1.38	2.71	1.06
6	118.1	2	4.71	4.94	9.68	6.4	4.47	5.6	12.69
7	130.1	3	1.42	1.26	1.32	1.18	1.35	1.34	1.23
8	136.0	3	1.65	1.7	2.74	1.79	1.89	1.92	2.32
9	140.1	2	1.66	1.86	2.84	2.17	2.22	2.22	5.94
10	147.1	2	2.76	2.56	4.51	3.16	3.4	3.21	4.89
11	148.1	3	1.65	1.43	1.78	1.38	1.42	1.32	1.22
12	158.1	3	2.04	2.03	2.91	2.09	1.72	1.75	2.05
13	164.1	3	2.22	2.31	4.14	2.68	1.87	2.33	1.62
14	175.1	2	2.55	2.37	7.24	6.2	5.13	3.66	6.48
15	182.1	2	1.28	1.13	1.54	2.03	2.13	1.57	2.72
16	184.1	3	1.74	2.05	3.6	2.23	2.49	1.97	2.15
17	192.0	3	5.88	7.31	11.64	7.99	6.95	8.17	4.75
18	193.0	3	20.34	23.85	39.59	28.24	24.28	29.52	16.01
19	195.0	3	2.96	3.21	4.79	3.37	3.24	3.74	2.29
20	221.2	2	2.81	3.02	4.63	2.93	2.38	2.2	4.8
21	222.1	3	1.92	1.76	1.95	2.05	1.95	1.54	1.7
22	230.0	3	3.8	4.02	5.09	4.33	3.66	3.72	1.66
23	231.0	3	11.87	13.25	18.23	14.91	12.17	12.79	8.87
24	233.0	3	2.9	3.06	3.67	3.14	2.91	2.88	1.56
25	240.1	2	1.22	1.23	1.08	1.03	1.2	1.16	1.84
26	241.2	2	1.55	1.61	1.92	2.15	1.93	1.73	4.72
27	254.1	3	1.22	1.17	1.21	1.1	1.09	1.11	1.42
28	258.1	2	1.37	1.31	1.54	1.43	1.51	1.43	2.38

29	268.2	3	1.75	1.13	0.89	1.06	1.19	1.02	1.23
30	284.2	3	1.31	1.3	1.42	1.43	1.39	1.4	1.22
31	294.1	2	1.42	1.46	1.83	1.83	1.89	1.73	4.67
32	308.1	3	1.58	1.72	2.64	1.37	1.58	1.49	2.05
33	348.1	3	1.63	1.74	2.11	2.24	3.05	1.74	2.8
34	381.1	3	4.03	4.6	8.93	5.69	4.78	5.04	3.52
35	399.2	3	1.35	1.51	2.23	2.11	1.88	1.96	1.44
36	407.0	3	1.65	1.83	1.97	1.45	1.56	1.79	1.25
37	422.9	3	4.15	4.32	4.56	3.9	3.37	3.04	1.43
38	428.1	3	1.6	2.11	3.2	2.1	1.81	2.14	1.82
39	448.2	2	1.42	1.27	1.11	1.35	1.42	1.65	2.17
40	460.2	3	1.5	1.58	1.86	1.48	1.63	1.63	1.89
41	466.0	3	1.43	1.54	1.79	1.71	1.49	1.63	1.19
42	489.3	3	1.34	1.34	1.6	2.08	1.79	1.74	1.39
43	508.0	3	1.19	1.33	1.44	1.21	1.24	1.3	1.18
44	518.3	3	1.26	1.25	1.21	1.14	1.82	1.37	1.19
45	520.3	2	1.34	1.35	1.29	1.45	3.1	2.74	2.9
46	522.3	3	1.22	1.18	1.07	1.11	2	1.34	1.32
47	527.2	3	1.7	1.91	2.03	1.86	1.85	2.21	1.72
48	543.1	3	8.79	8.28	7.96	6.46	5.38	6.97	3.17
49	558.3	3	1.37	1.3	1.19	1.37	3.07	2.5	1.68
50	560.4	3	1.33	1.37	1.24	1.37	2.2	1.71	1.36
51	573.6	3	1.55	1.59	2.49	1.31	1.39	1.42	1.36
52	575.5	3	1.68	1.76	1.9	1.56	1.94	1.81	1.98
53	576.5	3	2.27	2.49	2.46	2.25	2.32	2.66	1.82
54	580.1	3	1.38	1.53	1.9	2.22	1.9	1.99	1.39
55	592.3	4	1.2	1.16	1.02	3.37	1.25	1.37	1.29
56	599.5	3	1.41	1.58	1.74	2.75	1.75	1.51	1.76
57	615.1	3	1.94	1.92	1.94	1.83	1.65	1.81	1.36
58	616.3	1	4.56	2.57	5.28	2.37	1.92	1.69	2.96
59	618.2	3	2.32	1.83	2.87	2.65	2.13	2.1	1.67
60	652.9	4	1.39	1.53	1.57	7.74	1.63	2.07	1.78
61	664.2	3	1.33	1.44	1.77	1.78	1.76	2.04	1.53
62	688.4	3	1.41	1.47	1.36	1.38	2.31	1.83	1.47
63	689.3	3	2.2	3.02	2.59	2.15	2.64	3.82	2.59
64	705.2	3	13.73	18.29	15.6	13.27	12.04	17.42	6.57
65	738.1	3	1.79	2.36	2.12	2.22	2.25	2.67	1.67
66	744.4	2	1.38	1.39	1.52	1.53	1.82	2.23	3.37
67	747.0	1	1.75	1.99	3.47	1.76	1.46	1.58	1.34
68	749.1	3	2.14	3.08	3.14	2.99	2.36	2.12	1.51
69	751.0	3	1.85	2.41	2.15	1.8	1.73	1.78	1.34
70	752.5	3	1.54	1.67	2.27	1.32	1.34	1.37	1.13
71	754.5	3	1.6	1.7	1.9	1.5	1.6	1.52	1.3
72	756.6	1	3.29	4.47	13.2	2.86	2.22	2.48	1.95
73	758.7	3	4.66	7.85	10.36	6.96	6.4	5.47	5.32

74	760.7	3	3.04	4.72	5.39	2.73	2.65	2.87	2.44
75	771.0	3	1.7	1.97	2.98	1.72	1.55	1.56	1.71
76	773.0	3	1.8	2.55	2.73	2.66	2.37	1.86	2.38
77	773.4	2	1.66	1.68	2.12	1.87	2.11	1.71	12.09
78	778.5	1	2.03	2.35	7.38	1.86	1.74	1.7	1.56
79	780.7	1	2.97	4.57	10.87	3.42	2.88	2.66	2.31
80	782.7	3	3.61	6.09	8.94	6.17	5.7	4.27	5.12
81	784.6	3	2.84	4.13	5.24	3.54	3.16	2.88	2.69
82	786.7	3	1.82	2.3	2.63	2.06	1.85	2.25	2.05
83	794.6	1	3.58	4.59	11.86	3.2	2.12	2.22	1.45
84	796.6	3	5.47	8.77	10.64	8.37	6.35	5.32	2.84
85	798.6	3	3.72	5.77	6.26	3.96	3.09	3.09	1.77
86	800.6	3	1.64	2.09	2.09	1.59	1.54	1.52	1.91
87	813.6	3	1.42	1.56	1.66	2.71	1.73	1.77	1.53
88	816.5	1	1.74	2.16	5.29	1.93	1.71	1.63	1.36
89	818.5	1	3.08	4.27	9.36	3.38	2.39	2.03	1.52
90	820.6	3	3.97	6.5	8.36	7.09	5.51	3.78	2.58
91	822.6	3	3.21	4.88	5.46	4.51	3.51	2.88	1.76
92	824.6	3	2.03	2.72	2.79	2.53	1.97	2.22	1.49
93	851.3	3	1.67	2.53	2.28	1.98	2.21	3.5	2.59
94	867.4	3	6.94	15.07	12.57	12.24	11.92	17.11	7.1
95	870.6	4	1.67	2.05	2.04	18.46	2.2	3.64	2.96
96	884.7	4	1.58	1.62	1.74	4.24	1.87	1.73	1.5
97	899.9	3	1.56	2.09	1.82	2.07	2.14	2.37	1.64
98	906.4	3	1.4	1.55	2.57	1.78	1.58	3.71	1.31
99	909.6	4	1.41	1.47	1.96	12.01	1.69	2.4	1.75
100	923.6	3	1.33	1.34	1.22	2.92	1.43	1.45	1.28
101	926.7	3	1.38	1.37	1.25	2.04	2.09	1.72	1.58
102	944.6	3	1.29	1.25	1.2	1.45	1.95	1.6	1.44
103	950.7	3	1.33	1.39	1.44	1.46	2.04	1.69	1.53
104	968.6	3	1.32	1.42	1.48	1.67	1.91	1.58	1.53
105	975.6	3	1.49	1.6	1.9	2.44	1.65	1.81	1.37
106	1013.5	3	1.5	2.03	1.73	1.76	2.03	3.05	2.37
107	1029.3	3	4.37	9.62	8.01	9.25	9.8	13.48	6.08
108	1061.7	3	1.41	1.73	1.58	1.81	1.93	2.08	1.55
109	1068.5	3	1.32	1.53	2.75	1.72	1.46	4.84	1.21
110	1175.5	3	1.35	1.64	1.5	1.54	1.82	2.42	2.14
111	1191.4	3	2.53	5.79	5.46	6.23	7.22	9.5	5.37
112	1214.7	3	1.33	1.36	1.95	1.32	1.32	2.63	1.23
113	1223.6	3	1.32	1.59	1.5	1.62	1.82	1.98	1.48
114	1230.6	3	1.33	1.55	4.72	2.08	1.51	7.54	1.25

Appendix 3: Mean signal intensities from selected regions of interest (ROIs) of 10 DAP barley grain MALDI MSI experiments. Mean signal intensities are in arbitrary units as obtained by ClinProTools v.2.2 software (Bruker Daltonics). The cluster numbers correspond to the outcomes from the Neural Gas (NG) cluster analysis. Colors represent identical cluster revealed for all three experiments; 1 – embryo, 2 – chlorenchyma layer, 3 – transfer region, 4 – endosperm, 5 – maternal enclosure. Abbreviations are: P-V, vascular tissue; NP-C, nucellar projection/cavity; ET-C, endospermal transfer cells/cavity; Emb, embryo; P, outer pericarp-ventral; Ch, chlorenchyma layer; Scar, pericarp-scar.

Index	m/z	Cluster	Mean signal intensities in selected ROIs of experiment 1								
			P-V	NP-C	ET-C	En-C	En-P	Emb	P	Ch	Scar
1	86.1	4	1.41	1.78	1.69	3.26	2.25	2.16	2.01	1.86	1.53
2	90.0	3	2.07	3.99	3.51	3.73	2.31	2.35	1.57	1.99	1.09
3	94.1	5	7.63	3.08	2.13	2.28	1.26	9.91	5.33	5.03	11.69
4	104.1	3	53.05	62.79	60.95	48.76	42.67	67.61	39.7	34.76	46.06
5	116.1	1	0.83	1.16	1.32	1.62	1.4	7.39	0.63	0.79	0.96
6	118.1	1	6.23	5	5.11	7.54	4.82	35.21	5.4	4.12	13
7	130.1	3	1.48	1.37	1.21	1.17	1.07	1.35	1.47	1.06	1.55
8	136.0	5	7.39	2.55	2.03	3.38	2.19	3.4	6	3.51	11.89
9	140.1	1	3.68	2.18	1.8	2.01	1.63	5.96	3.1	2.24	5.83
10	146.1	1	1.07	1.08	1.33	1.47	1.19	2.35	0.98	0.91	0.97
11	147.1	5	8.21	8.69	4.68	3.96	4.31	7.66	8.86	6.34	9.63
12	148.1	4	1.63	2.31	2.24	3.08	2.11	2.51	1.49	1.38	1.53
13	158.1	1	1.48	1.8	1.93	2.07	1.7	5.55	1.42	1.26	2.04
14	184.1	5	6.33	7.45	5.56	11.22	6.24	7.59	11.92	7.02	6.41
15	192.0	3	20.18	19.81	15.55	17.6	11.26	15.86	22.56	16.13	11.63
16	193.0	3	49.01	53.81	39.98	43.71	26.99	38.72	57.88	39.4	32.02
17	195.0	3	7.13	6.84	5.33	6.15	4.07	5.53	7.52	5.61	4.03
18	205.1	5	1.93	0.91	0.93	0.86	1.01	1.38	3.02	1.03	2.53
19	221.2	1	1.82	1.85	2.28	2.58	2.36	12.01	1.46	1.2	2.51
20	222.1	3	2.9	5.92	4.2	3.05	1.6	2.54	2.83	3.52	1.72
21	230.0	3	5.65	8.52	8.28	7.15	5.25	4.56	6.48	5.56	2.77
22	231.0	3	19.67	30.43	29.03	25.18	17.42	16.45	23.94	19.25	9.56
23	233.0	3	4.06	5.88	5.72	5.06	3.89	3.32	4.54	3.97	2.14
24	240.1	3	1.2	1.19	1.33	1.58	1.34	1.47	1.12	0.93	1.32
25	241.1	1	2.11	1.42	1.28	1.14	1.05	4.03	1.13	1.36	2.61
26	254.1	1	0.87	0.97	1.04	0.99	1.05	2.3	0.73	0.8	1.12
27	294.1	3	2.89	1.76	1.27	1.21	1.17	2.71	1.99	1.97	2.61
28	299.1	3	1.79	1.63	1.36	1.41	1.28	1.48	1.68	1.26	1.62
29	321.2	3	2.62	4.18	4.24	3.12	2.29	1.98	2.49	2.44	2.02
30	337.3	5	1.35	0.98	1.23	1.32	1.68	1.21	1.98	0.97	1.36
31	348.1	5	7.75	1.7	1.82	4.18	2.35	3.78	5.64	2.95	2.88
32	381.1	3	8.02	11.6	7.58	6.41	4.54	7.21	9.25	7.07	5.03
33	399.2	3	4.21	1.29	1.24	2.12	1.41	2.9	2.18	2.79	1.67
34	422.9	3	2.78	4.94	5.24	4.14	3.5	2.33	3	2.92	1.54
35	428.1	4	3.65	1.49	1.98	5.61	2.37	4.17	2.22	2.49	1.52
36	448.2	5	4.7	2.28	1.24	1.14	1.28	1.23	2.98	3.3	2.82
37	496.4	4	1.24	1.56	1.99	7.97	5.75	1.89	1.19	1.16	1.15

38	508.0	4	1.39	0.99	1.19	2.39	1.36	1.31	1.43	1.28	1.02
39	518.3	5	1.37	1.1	1.22	2.25	1.77	1.34	4.72	1.07	1.26
40	520.3	5	2.48	1.28	1.6	4.59	5.68	1.95	16.03	1.65	2.83
41	527.2	3	3.04	5.28	3.61	2.34	1.42	1.6	2.6	3.02	1.65
42	534.3	4	1.14	1.29	1.71	5.68	4.07	1.23	2.47	1.67	1.17
43	543.1	3	7.77	38.78	28.54	14.84	3.57	7.16	9.14	13.36	3.31
44	558.3	5	1.77	1.24	1.51	3.75	4.44	1.51	11.03	1.25	1.59
45	560.4	5	1.17	1.63	1.47	1.8	1.7	1.04	4.37	1.26	1.2
46	562.3	3	1.53	4.27	3.36	2.58	1.31	1.18	1.79	2.03	1.18
47	573.6	3	1.73	1.33	1.79	2.03	1.55	1.97	1.46	1.39	1.44
48	575.5	4	2.57	2.19	3.39	3.87	3.93	2.9	2.56	1.88	2.21
49	576.5	3	2.52	6.58	5.69	3.78	2.8	2.78	3.13	2.86	1.99
50	592.3	5	1.81	1	1	0.85	1.28	0.88	2.5	4.85	2.06
51	599.5	3	2.45	1.25	1.96	2.22	3.38	1.99	1.92	3.86	1.97
52	616.3	1	4.48	2.54	2.91	4.19	3.69	6.18	2.5	2.91	3.97
53	618.2	3	4.37	1.77	1.83	3.11	2.15	2.68	1.85	2.74	2
54	628.2	4	1.82	1.45	1.89	2.15	1.98	1.65	1.45	1.47	1.47
55	650.5	3	1.18	2.16	1.61	1.79	1.5	1.57	1.68	1.5	1.48
56	652.9	2	3.64	1.37	1.37	1.13	1.89	1.04	5.38	13.99	4.02
57	688.4	5	1.58	1.71	1.56	1.56	1.38	1.25	4.38	1.19	1.65
58	689.3	3	2.64	8.14	5.13	2.43	1.68	1.87	4.22	3.48	2.16
59	705.2	3	12.68	54.02	40.32	21.35	6.31	11.81	16.87	19.96	5.85
60	738.1	3	2.28	2.32	2.75	2.74	2.1	2.96	3.28	1.96	1.77
61	743.5	5	1.23	1.1	1.17	1	1.13	0.97	1.37	1.1	12.17
62	747.0	4	1.53	1.72	1.92	2.78	1.64	2.64	1.39	1.83	1.44
63	749.1	4	2.28	3.3	4.29	7.95	6.55	4.71	2.4	3.19	1.76
64	751.0	4	1.31	2.06	2.57	4.32	2.76	1.83	1.24	1.54	1.27
65	754.5	4	1.37	1.65	2.51	2.93	2.18	1.93	1.22	1.37	1.21
66	756.6	1	4.59	4	4.15	7.49	3.05	9.92	3.09	5.19	2.72
67	758.7	4	8.78	9.32	9.69	20.12	14.43	16.88	8.34	10.2	7.57
68	760.7	4	2.72	4.34	4.97	9.85	4.49	4.8	2.3	2.91	2.63
69	771.0	3	1.65	1.35	1.71	1.75	1.57	2.36	1.17	1.89	1.4
70	773.0	4	2.27	1.86	2.4	3.23	3.96	3.15	1.69	2.91	3.1
71	773.4	5	1.99	1.48	2.09	2.14	2.49	1.93	1.99	2.02	12.32
72	775.0	4	1.52	1.74	2.25	3.12	2.22	1.64	1.41	1.87	2.83
73	778.5	1	2.5	1.79	2.67	2.96	2.53	3.67	1.62	2.67	1.57
74	780.7	1	5.97	3.16	3.87	5.23	4.03	9.4	3.1	6.58	3.17
75	782.7	1	8.54	4.31	5.43	8.45	9.11	11.58	5.62	9.89	6.37
76	784.6	4	3.8	3.58	4.43	7.17	3.67	4.25	2.4	5	3.26
77	786.7	4	2.03	3.28	4.13	7.57	2.23	1.97	1.59	2.54	2.12
78	794.6	1	3.51	4.02	4.69	7.96	3.33	8.03	2.47	4.76	1.67
79	796.6	4	6.9	10.13	12.43	22.89	17.11	14.88	6.68	10.12	4.08
80	798.6	4	2.79	5.38	6.86	12.67	6.61	5.16	2.58	3.74	1.96
81	813.6	3	1.83	1.38	1.43	1.38	1.44	1.21	1.9	4.24	1.72
82	816.5	3	1.72	1.57	2.07	2.34	2.08	2.46	1.46	2.32	1.24

83	818.5	1	3.75	2.42	3.35	4.43	3.3	6.58	1.91	4.94	1.57
84	820.6	4	6.04	4.08	5.98	8.76	9.9	9.26	4.13	8.79	3.05
85	822.6	4	3.18	3.59	5.17	8.05	4.63	3.91	2.27	5.01	2.08
86	824.6	4	2.77	3.2	4.48	8.45	2.44	1.68	1.74	3.36	1.63
87	839.6	5	1.73	1.11	1.17	0.98	1.23	0.94	2.33	2.74	1.6
88	851.3	5	2.42	2.29	2.22	1.94	1.85	2.16	3.56	1.99	2.42
89	867.4	3	13.35	14.56	15.82	15.07	8.65	16.67	19.26	10.85	7.87
90	870.6	2	7.26	1.79	1.81	1.67	2.63	1.8	9.45	24.03	7.31
91	899.9	5	2.63	1.92	2.35	2.85	2.21	1.98	3.89	2.51	1.99
92	909.6	2	4.14	1.26	1.36	1.29	1.99	1.14	5.14	17.14	3.11
93	917.7	4	0.99	1.01	1.11	0.95	2.06	1.12	1.09	1.28	1.07
94	919.7	4	1.04	1.01	1.07	0.92	2.16	1.12	1.14	1.1	1.17
95	923.6	3	1.37	1.08	1.13	0.97	1.54	0.95	1.39	2.69	1.28
96	926.7	5	1.37	1.37	1.17	1.04	1.24	1.1	2.1	1.86	1.96
97	934.5	3	1.52	1.25	1.49	1.89	1.78	1.8	1.99	1.54	1.49
98	953.7	3	1.6	1.19	1.47	1.85	1.38	1.37	1.74	2.75	1.34
99	955.6	4	1.48	1.24	1.45	2.37	1.96	1.5	1.91	1.94	1.32
100	975.6	3	1.94	1.26	1.33	1.41	1.65	1.54	2	4.28	1.49
101	977.7	3	1.4	1.16	1.36	1.8	1.87	1.6	1.53	2.29	1.26
102	979.6	4	1.26	1.19	1.36	2.08	2.51	1.56	1.41	2.07	1.28
103	1013.5	5	2.64	1.78	1.83	1.73	1.83	1.6	4.03	2.19	2.67
104	1025.7	5	1.56	0.97	1.02	0.89	1.18	0.93	1.72	2.82	1.78
105	1029.3	5	13.77	9.22	11.23	14.17	8.24	9.54	21.39	10.98	8.88
106	1061.7	5	2.38	1.4	1.95	2.65	1.99	1.82	3.74	2.18	1.97
107	1068.5	3	1.32	1	1.12	0.99	1.29	1.24	1.47	1.17	1.13
108	1101.5	3	1.64	1.11	1.1	1.19	1.41	1.1	1.35	1.69	1.35
109	1173.6	5	1.95	1.11	1.25	1.32	1.38	1.17	2.54	1.59	1.71
110	1175.5	5	2.6	1.28	1.59	1.66	1.67	1.59	3.98	2.24	2.73
111	1191.4	5	12.87	4.48	8.52	13.72	7.85	8.65	21.22	10.41	8.91
112	1214.7	3	1.4	1.2	1.09	0.96	1.16	1	1.02	1.27	1.18
113	1223.6	5	2.13	1.27	1.57	2.22	1.79	1.56	3.39	1.99	1.78
114	1230.6	3	1.34	1.12	1.18	1.07	1.37	1.31	1.33	1.31	1.16

Index	m/z	Cluster	Mean signal intensities in selected ROIs of experiment 2								
			P-V	NP-C	ET-C	En-C	En-P	Emb	P	Ch	Scar
1	86.1	4	2.25	2.8	5.66	7.08	6.57	5.45	3.34	2.34	2.29
2	90.0	4	0.97	3.25	4.02	3.31	2.88	1.87	0.97	1.68	0.98
3	94.1	1	9.27	5.45	3.89	3.54	2.63	12.56	6.3	8.94	6.15
4	104.1	3	26.87	86.52	68.03	65.89	75.6	69.55	41.72	40.91	41.26
5	116.1	4	0.9	3.38	4.45	5.08	4.55	3.25	0.68	1.42	1.11
6	118.1	1	7.98	13.91	13.11	14.25	15.2	31.31	14.03	10.69	12.13
7	130.1	5	5.51	2.91	2.38	2.02	2.28	2.25	3.38	3.41	4.02
8	136.0	3	4.4	2.96	3.15	3.67	3.91	3.5	5.37	5.26	2.98
9	140.1	1	5.58	3.7	3.2	2.95	3.1	7.46	3.89	3.94	3.63
10	146.1	3	0.77	1.38	1.3	1.2	1.33	1.3	0.83	0.97	0.85

11	147.1	3	3.15	5.96	4.52	2.37	4.94	6.82	7.41	5.22	3.71
12	148.1	4	1.03	2.56	2.97	2.93	3.08	2.93	2.42	1.64	1.12
13	158.1	1	1.29	3.24	2.9	2.38	2.2	4.76	2.14	1.76	1.38
14	184.1	4	15.6	10.49	19.03	25.09	26.18	20.08	19.42	11.93	12.34
15	192.0	3	12.73	20.17	17.29	16.34	17.48	20.07	19.91	18.45	6.92
16	193.0	3	34.39	56.36	44.97	42.1	45.29	51.45	51.67	48.68	19.76
17	195.0	3	4.24	6.54	5.54	5.29	5.66	6.36	6.45	5.99	2.68
18	205.1	5	17.79	3.04	1.25	1.14	1.43	1.42	7.5	7.92	10.55
19	221.2	1	2.14	2.97	2.98	3.01	3.13	5.11	2.07	1.75	1.97
20	222.1	3	1.48	6.06	4.67	2.67	2.58	2.56	3.72	3.53	1.21
21	230.0	3	2.3	9.06	7.56	5.26	4.82	6.41	5.43	4.91	1.43
22	231.0	3	9.22	34.11	28.12	19.63	18.23	23.97	20.02	18.4	4.05
23	233.0	3	1.76	6.27	5.26	3.61	3.38	4.42	3.88	3.47	1.37
24	240.1	4	1.04	1.16	1.47	1.77	1.63	1.38	1.06	0.94	1.02
25	241.1	1	1.3	1.58	1.2	1.11	1.02	2.39	1.07	1.38	1.54
26	254.1	1	0.63	1.13	0.99	0.94	0.89	1.49	0.91	0.8	0.94
27	294.1	1	2.42	1.27	1	1.03	1.03	4.16	1.61	1.74	1.87
28	299.1	3	2.18	1.63	2.02	1.99	2.07	2.05	1.78	1.42	2
29	321.2	3	0.81	1.31	1.01	0.93	0.81	1.3	1.68	0.91	0.95
30	337.3	5	1.28	0.98	1.2	1.39	1.8	1.25	1.84	0.95	1.44
31	348.1	5	4.07	1.67	3.16	4.38	3.2	2.47	6.04	2.35	2.65
32	381.1	3	5.27	13.12	12.35	9.79	8.65	11.97	8.93	5.67	4.26
33	399.2	4	2.1	1.77	2.25	2.91	3.49	2.32	3.24	2.93	1.26
34	422.9	3	1.57	4.36	3.61	2.35	2.72	2.91	2.22	2.48	1.35
35	428.1	4	3.13	1.89	3.39	5.05	4.58	3.57	4.13	3.12	1.81
36	448.2	5	3.61	2.15	0.95	0.79	1.33	0.86	1.81	3.4	4.07
37	496.4	4	1.8	1.76	3.71	7.33	5.97	1.78	1.32	1.08	1.33
38	508.0	4	1.63	0.98	1.23	1.96	1.88	1.46	1.84	1.37	1.2
39	518.3	5	1.72	0.97	1.3	2.09	1.57	1.09	3.12	1.15	1.28
40	520.3	5	5.05	1.26	2.42	6.01	6.31	1.49	10.07	2.23	5.18
41	527.2	3	3.73	4.89	3.7	1.69	1.58	1.78	2.54	2.76	2.32
42	534.3	4	1.48	1.29	2.3	3.56	2.46	1	1.76	1.96	1.13
43	543.1	3	8.81	31.97	24.83	8.89	7.51	10.2	7.86	10.8	4.66
44	558.3	5	1.98	1.2	1.87	3.52	3.19	1.12	6.6	1.33	1.97
45	560.4	5	2.41	1.69	1.64	1.6	1.54	1.11	3.11	1.52	1.73
46	562.3	3	1.58	3.22	2.68	1.49	2	1.23	1.52	1.81	1.32
47	573.6	1	1.77	1.69	2.38	2.3	2.18	3.45	1.53	1.51	1.37
48	575.5	4	3.62	2.93	4.45	4.75	5.65	4.48	3.61	2.02	2.95
49	576.5	3	4.95	6.86	6.82	4.65	4.94	4.86	4.11	3.34	3.27
50	592.3	2	3.77	0.91	0.72	0.77	1.08	0.69	1.2	7.56	1.89
51	599.5	3	3.72	1.85	2.52	2.85	4.06	3.64	3.04	6.48	2.6
52	616.3	1	3.65	6.89	4.97	4.23	5.95	8.39	5.68	2.73	5.81
53	618.2	3	1.98	3.18	2.58	2.2	2.75	3.26	2.99	2.23	2.72
54	628.2	4	1.73	1.69	2.22	2.59	3.21	2.03	1.9	1.4	1.78
55	650.5	4	12.4	2.62	4.35	8.84	8.42	5.61	6.54	3.72	4.5

56	652.9	2	8.41	1.28	1.25	1.73	1.65	1.27	1.98	18.55	4.16
57	688.4	5	3.39	2.02	2.29	3.04	2.46	2.07	4.83	1.71	1.96
58	689.3	3	9.53	7.42	5.76	3.02	3.06	3.25	4.41	3.67	4.49
59	705.2	3	25.55	48	38.6	19.39	17.95	23.09	18.77	19.87	11.4
60	738.1	3	4.21	4.83	6.23	4.47	3.6	3.71	3.56	2.64	2.61
61	743.5	5	0.91	0.99	0.87	0.99	0.92	0.76	1.28	0.86	3.71
62	747.0	1	1.37	2.23	3.83	3.25	2.08	5.17	1.37	1.57	1.26
63	749.1	4	3.09	5.4	10.64	11.08	9.49	7.45	3.88	3.07	2.05
64	751.0	4	1.24	2.46	4.71	4.79	3.93	3.33	1.68	1.37	1.23
65	754.5	4	1.42	2.5	3.22	2.8	2.5	2.65	1.64	1.33	1.2
66	756.6	1	7.23	5.51	10.7	11.05	8.75	18.15	4.38	6.01	3.31
67	758.7	4	21.57	13.53	24.72	31.62	34.83	23.68	15.68	12.58	14.14
68	760.7	4	5.34	4.52	9.97	13.41	13.65	9.42	4.94	3.76	4.58
69	771.0	1	1.22	1.85	2.98	2.75	2.1	4.17	1.41	1.56	1.21
70	773.0	4	2.32	2.82	5.55	6.73	6.96	5.19	3.32	2.63	5.64
71	773.4	5	1.81	2.02	2.58	2.78	2.83	2.26	3.15	1.67	7.97
72	775.0	4	1.72	2	3.72	4.17	3.86	3.15	2.11	1.72	2.5
73	778.5	1	2.75	2.96	4.46	4.04	3.74	8.55	2.25	2.56	1.57
74	780.7	1	8.67	5.68	10.2	10.69	11.06	15.42	5.75	6.99	4.28
75	782.7	4	15.15	7.08	14.27	20.55	27.53	17.18	12.93	10.83	11.68
76	784.6	4	5.1	3.47	7.79	11.03	12.77	8.94	5.91	5.36	5.13
77	786.7	4	2.15	1.97	4.23	5.85	5.53	3.53	2.39	2.31	2.79
78	794.6	1	3.32	5.72	11.41	9.7	6.35	16.12	3.14	4.37	1.52
79	796.6	4	9.92	15.58	28.82	29.79	27.5	22.96	12.14	9.88	4.95
80	798.6	4	3.96	6.49	13.63	14.58	12.54	10.26	5.06	3.85	2.62
81	813.6	3	2.53	1.24	1.42	1.61	1.49	1.44	1.69	4.01	1.52
82	816.5	1	1.74	2.15	3.26	2.77	2.31	6.01	1.74	1.91	1.27
83	818.5	1	3.01	4.4	8.43	7.89	6.62	12.38	3.33	4.43	1.57
84	820.6	4	6.38	7.48	15.76	18.67	20.5	15.43	9.23	7.91	4.03
85	822.6	4	2.81	4.3	9.51	10.94	10.68	8.51	5.1	4.38	2.37
86	824.6	4	1.66	2.3	4.96	5.58	4.47	3.37	2.05	2.62	1.61
87	839.6	3	2.17	0.95	0.91	1.04	1.03	0.83	1.22	3.56	1.48
88	851.3	3	7.95	4.03	4.41	3.07	3.11	2.88	3.45	2.49	4.27
89	867.4	3	24	27.76	32.32	24.37	20.9	21.62	19.47	14.23	11.93
90	870.6	2	15.17	2.38	2.7	2.16	1.92	1.92	3.11	29.96	5.88
91	899.9	3	3.95	4.07	5.03	4.28	3.37	3.16	3.39	2.92	2.46
92	909.6	2	4.74	1.33	1.29	1.15	0.98	1.26	1.53	15.74	2.01
93	917.7	1	0.92	1.06	0.94	0.88	1.16	1.73	0.9	1.13	1.09
94	919.7	3	1.06	1.04	0.97	0.92	1.22	1.69	1.09	0.96	1.17
95	923.6	3	1.25	1.01	0.91	0.89	0.98	1.03	1.15	2.38	1.12
96	926.7	5	2.03	0.99	0.9	0.97	1.18	0.87	2.23	1.7	1.39
97	934.5	3	1.75	1.72	2.2	2.17	2.13	1.95	1.62	1.53	1.63
98	953.7	3	1.71	1.17	1.78	1.73	1.56	2.04	1.63	2.11	1.31
99	955.6	3	1.85	1.08	1.71	1.96	1.99	2	2.22	1.62	1.32
100	975.6	3	2.13	1.36	1.81	1.79	1.94	2.52	1.66	3.27	1.65

Index	m/z	Cluster									
101	977.7	4	1.34	1.19	1.86	2.22	2.28	2.8	1.53	1.69	1.32
102	979.6	4	1.75	1.08	1.73	2.31	2.7	2.55	1.88	1.96	1.44
103	1013.5	3	6.65	3.3	3.56	2.85	2.76	2.39	3.26	2.4	4.02
104	1025.7	3	1.69	0.9	0.83	0.78	0.74	0.79	0.86	2.76	1.26
105	1029.3	3	19.99	21.61	25.87	22.36	18.53	16.78	18.17	12.73	10.63
106	1061.7	3	3.06	2.92	4.01	3.64	2.81	2.29	2.93	2.07	2.17
107	1068.5	5	1.5	1.05	0.91	0.89	1.05	1.04	2.57	1.34	1.37
108	1101.5	5	2.03	1.28	0.88	0.89	0.93	1	2.01	1.58	2.23
109	1173.6	3	1.79	1.26	1.32	1.51	1.4	1.2	1.79	1.13	1.53
110	1175.5	3	5.28	2.59	3.02	2.63	2.46	2.04	3.03	2.02	3.49
111	1191.4	3	16	15.75	22.22	20.67	16.5	13.24	15.45	9.69	9.33
112	1214.7	5	0.98	1.31	0.88	0.82	0.81	0.94	2.08	1.13	2.19
113	1223.6	3	2.61	2.42	3.23	3.27	2.66	1.99	2.59	1.67	1.96
114	1230.6	5	1.75	1.1	0.87	0.89	1.18	1.59	5.85	1.85	1.49

Index	m/z	Cluster	Mean signal intensities in selected ROIs of experiment 3								
			P-V	NP-C	ET-C	En-C	En-P	Emb	P	Ch	Scar
1	86.1	4	13.13	12.48	19.06	28.63	33.3	22.4	14.05	13.83	5.65
2	90.0	4	2.01	2.46	4.05	3.76	2.99	1.89	0.95	1.52	1.11
3	94.1	1	14.38	10.19	9.37	6.14	5.39	39.57	9.91	14.32	13.94
4	104.1	3	143.61	142.18	107.54	92.98	126.47	118.81	92.55	72.7	79.36
5	116.1	1	1.02	1.35	3.54	5.1	4.15	18.04	0.86	0.72	1
6	118.1	1	12.39	7.44	10.14	14.09	12.84	35.72	8.48	6.09	14.22
7	130.1	1	1.93	1.4	1.58	1.41	1.41	2.72	1.21	0.88	3.53
8	136.0	5	7.49	2.89	3.61	5.38	5.38	4.33	6.78	6.93	4.22
9	140.1	1	3.74	2.55	2.4	2.43	2.42	7.92	3.75	3.14	4.03
10	146.1	1	1.08	0.96	1.23	1.27	1.48	1.92	0.84	0.72	0.97
11	147.1	3	7.52	5.96	5.83	2.15	2.81	4.16	4.71	4.83	3.35
12	148.1	4	2.4	1.75	2.6	3.23	3.15	2.58	1.52	1.24	1.23
13	158.1	1	2.69	2.58	2.43	1.93	1.63	6.19	1.21	1.18	1.51
14	184.1	4	26.8	24.35	40.2	60.55	70.37	40.25	41.28	33.04	17.18
15	192.0	3	19.89	12.81	12.03	11.69	12.26	15.82	12.86	14.52	4.36
16	193.0	3	49.5	33.67	31.11	30.2	31	39.99	35.13	37.41	11.72
17	195.0	3	5.57	3.92	3.59	3.65	3.8	4.6	3.87	4.2	1.77
18	205.1	5	2.05	0.84	0.84	0.85	0.77	2.38	1.02	0.68	7.68
19	221.2	1	2.67	1.88	1.66	1.99	2.34	6.24	1.35	1.02	2.17
20	222.1	3	11.86	15.52	9.33	4.31	3.47	4.16	2.37	6.59	1.83
21	230.0	3	10.55	9.31	7.3	4.25	3.91	7.39	3.27	5.94	1.48
22	231.0	3	40.83	35.83	27.75	16.03	14.66	29.13	11.66	22.82	3.67
23	233.0	3	7.18	6.16	4.82	2.91	2.74	4.99	2.97	4.07	1.39
24	240.1	4	1.81	1.54	1.69	2.57	2.84	1.94	1.53	1.13	1.49
25	241.1	1	2.3	1.78	1.33	1.14	1.27	3.41	1.2	1.31	2.21
26	254.1	1	1.06	1.01	1.02	0.96	0.84	2.04	0.74	0.63	1.24
27	294.1	1	1.13	0.95	1.01	0.89	0.92	2.52	1.11	0.97	1.71
28	299.1	4	1.41	1.26	1.84	2.29	2.19	1.7	2.17	1.2	2.2

29	321.2	3	1.89	2.1	2.38	1.87	1.41	2.39	2.06	1.87	1.26
30	337.3	4	0.97	0.83	0.97	1.4	2.06	0.84	1.24	0.78	1.32
31	348.1	4	5.41	1.62	2.53	5.24	5.01	2.23	2.84	2.27	3.2
32	381.1	3	14.51	9.02	10	8.46	6.45	10.74	10.03	5.6	3.26
33	399.2	3	4.25	1.76	1.86	2.73	2.55	2.25	2.42	3.28	1.43
34	422.9	3	3.35	3.18	2.49	1.5	1.36	2.35	1.3	1.74	1.17
35	428.1	4	2.84	1.42	2.12	4.92	3.97	2.52	2.18	2.33	1.51
36	448.2	5	5.59	2.68	0.86	0.65	0.82	0.7	3.74	4.28	4.17
37	496.4	4	1.05	1.32	2.16	5.89	4.49	1.65	1.36	0.97	1.21
38	508.0	4	1.18	0.9	0.98	1.69	1.51	1.07	1.25	1.18	1.38
39	518.3	5	0.78	0.96	0.97	1.4	1.09	1.15	1.89	1.02	1.3
40	520.3	5	1.02	1.04	1.39	3.74	4.03	1.27	5.36	2.16	4.35
41	527.2	3	5.21	6.88	4.37	1.76	1.38	1.62	6.39	5.26	2.74
42	534.3	4	0.92	1.12	1.39	2.79	1.83	1.08	1.5	3.21	1.17
43	543.1	3	15.43	48.78	44.24	12.12	7.17	8.98	12.41	15.02	4.7
44	558.3	5	1.17	1.22	1.44	2.38	2.18	1.19	3.32	1.49	2.07
45	560.4	5	1.88	2.27	2.05	1.64	1.31	1.11	5.94	2.6	2.47
46	562.3	3	2.21	5.8	5.5	1.95	1.36	1.28	2.29	2.56	1.56
47	573.6	4	1.24	1.46	1.61	2.08	2.18	2.54	1.27	1.1	1.35
48	575.5	4	2.02	2.15	3.28	4.79	6.79	2.43	2.57	1.6	2.49
49	576.5	3	6.37	10.31	12.09	7.21	6.12	3.91	7.71	5.08	4.81
50	592.3	2	0.98	0.88	0.78	0.66	0.61	0.63	1.25	8.21	1.18
51	599.5	4	1.98	1.37	1.72	2.71	4.83	1.97	1.69	4.03	1.55
52	616.3	1	3.54	4.09	5.73	4.27	4.91	7.5	2.39	2.11	1.73
53	618.2	3	5.79	3.21	2.64	2.15	2.26	2.88	1.78	2.68	1.41
54	628.2	4	1.25	1.22	1.49	2.18	2.81	1.15	1.12	1.09	1.23
55	650.5	4	1.25	1.62	3.05	4.56	3.54	1.48	2.26	1.99	1.52
56	652.9	2	1.71	1.39	1.16	0.96	0.83	0.88	1.65	22.18	1.43
57	688.4	3	1.34	1.7	2.18	2.03	1.6	1.1	2.37	1.33	1.51
58	689.3	5	5.25	8.87	6.27	2.77	2	1.87	14.81	7.26	4.83
59	705.2	3	31.54	66.54	66.21	28.26	17.49	15.73	33.38	26.84	11.69
60	738.1	3	5.61	3.65	7.59	7.19	4.91	3.5	6.81	4.48	3.84
61	743.5	5	0.88	0.92	0.87	0.76	0.74	0.67	0.92	0.71	2.04
62	747.0	1	2.29	2.97	2.63	3.26	2.16	6.67	1.25	2.13	1.16
63	749.1	4	4.19	4.18	7.5	11.47	11.48	6.61	2.56	4.83	1.51
64	751.0	4	1.86	2.04	4.17	5.87	4.94	2.62	1.29	1.7	1.14
65	754.5	4	1.61	1.75	2.02	2.36	2.29	1.91	1.21	1.19	1.07
66	756.6	1	3.49	4.38	5.46	9.01	6.6	14.11	3.21	4.89	1.56
67	758.7	4	6.98	6.12	14.98	29.1	33.55	12.94	10.73	11.62	5.33
68	760.7	4	2.26	2.42	6.95	13.28	12.11	4.19	3.5	3.12	1.96
69	771.0	1	2.66	2.63	2.01	2.53	2.54	4.35	1.02	2.11	1.12
70	773.0	4	4.31	2.95	3.59	6.28	8.52	4.54	1.71	3.98	4.24
71	773.4	5	3.62	2.13	1.85	2.34	3.02	2.13	1.47	2.17	4.91
72	775.0	4	2.46	1.97	3.05	4.72	4.69	2.58	1.65	2.35	1.87
73	778.5	1	2.84	2.8	2.36	3.11	3.27	7.33	1.61	2.7	1.17

74	780.7	4	5.09	4.3	4.76	7.85	8.48	9.89	4.15	7.23	1.77
75	782.7	4	6.63	3.95	7.24	16.43	25.38	8.8	6.03	9.47	3.4
76	784.6	4	2.87	2.54	4.96	10.02	10.92	4.09	2.86	3.8	2.23
77	786.7	4	1.59	1.94	3.28	5.42	4.52	1.86	1.64	1.78	2.05
78	794.6	1	5.17	7.05	6.4	8.1	5.37	17.48	2.04	5.28	1.17
79	796.6	4	10.87	10.61	18.88	28.63	28.7	17.75	6.62	13.23	2.7
80	798.6	4	4.11	4.46	10.16	15.14	12.59	6.79	2.99	4.67	1.46
81	813.6	3	1.48	1.22	1.13	1.3	1.19	1.35	1.18	4.23	1.11
82	816.5	1	2.86	3.06	2.09	2.38	2.16	6.95	1.08	2.13	1.01
83	818.5	1	6.41	5.88	4.37	6.29	6.01	11.17	1.6	5.29	1.12
84	820.6	4	10.27	6.47	8.48	15.62	20.97	11.25	3.63	10.08	1.87
85	822.6	4	4.84	3.63	6.3	10.53	10.35	5.64	2.33	4.81	1.4
86	824.6	4	1.91	1.94	3.81	5.57	4.15	2.34	1.21	2.38	1.08
87	839.6	3	0.87	0.94	0.92	0.83	0.82	0.72	1.26	2.66	1.07
88	851.3	5	3.62	2.25	2.77	2.61	2.05	1.66	11.36	4.65	5.08
89	867.4	3	22.79	16.49	32.45	30.71	20.6	13.23	28.35	18.57	13.87
90	870.6	2	2.71	1.71	2.57	2.37	1.72	1.39	3.27	28.02	2.34
91	899.9	3	4.27	2.57	4.67	5.87	4.24	2.38	5.37	4.81	3.52
92	909.6	2	2.03	1.46	1.13	1	0.87	1.42	1.26	19.12	1.19
93	917.7	3	0.93	1.03	0.95	0.83	1.35	1.42	0.95	1.06	1.12
94	919.7	3	1.03	0.97	0.95	0.83	1.49	1.42	1.1	0.9	1.17
95	923.6	3	1.04	0.96	0.9	0.82	0.91	0.94	0.92	2.45	1.08
96	926.7	5	0.89	0.97	0.94	0.82	0.74	0.78	1.52	1.57	1.11
97	934.5	4	1.69	1.29	1.73	2.26	2.33	1.34	2.11	1.92	1.85
98	953.7	3	1.42	1.17	1.27	1.43	1.24	1.53	1.25	2.58	1.05
99	955.6	3	2.09	1.15	1.28	1.68	1.85	1.36	1.98	2.08	1.15
100	975.6	3	1.65	1.4	1.23	1.39	1.79	1.95	1.5	4.07	1.26
101	977.7	3	1.47	1.16	1.21	1.66	2.04	1.48	1.31	1.97	1.16
102	979.6	4	1.38	1.07	1.23	1.82	2.66	1.25	1.36	1.77	1.21
103	1013.5	5	2.96	1.61	1.84	2.19	1.81	1.21	9.26	4.58	4.49
104	1025.7	3	0.92	0.95	0.8	0.7	0.66	0.77	0.84	2.04	1.05
105	1029.3	4	15.96	9.02	18.81	24.64	17.61	7.88	23.07	17.84	12.19
106	1061.7	5	2.66	1.58	2.77	4.11	3.25	1.51	3.89	3.56	2.93
107	1068.5	5	1.18	0.98	0.87	0.71	0.82	0.89	3.84	1.69	1.54
108	1101.5	5	2.04	1.08	0.84	0.72	0.76	0.86	1.98	1.15	1.92
109	1173.6	5	1.15	0.99	0.95	1.21	1.33	0.8	1.88	1.41	1.69
110	1175.5	5	2.23	1.22	1.37	1.76	1.65	1.06	7.13	3.75	3.79
111	1191.4	4	10.47	4.32	11.03	19.34	15.35	5.03	17.67	14.18	10.26
112	1214.7	5	0.85	0.98	0.84	0.69	0.69	0.76	4.55	1.33	1.35
113	1223.6	5	2.2	1.33	1.98	3.15	2.77	1.22	3.21	2.86	2.57
114	1230.6	5	1.26	1.07	0.91	0.76	1.01	1.14	8.51	2.98	1.81

Appendix 4: List of mean signal intensities from the MALDI MSI experiments of 14 DAP barley grains according to the selected regions of interest (ROIs). Mean signal intensities are in arbitrary units as obtained by ClinProTools v.2.2 software (Bruker Daltonics). The cluster numbers correspond to the outcomes from the Neural Gas (NG) cluster analysis. Colors represent identical cluster revealed for all three experiments; 1 – endosperm, 2 – transfer region, 3 – maternal enclosure, 4 – chlorenchyma layer, 5 – embryo. Abbreviations are: P-V, vascular tissue; NP-C, nucellar projection/cavity; ET-C, endospermal transfer cells/cavity; Emb, embryo; P, outer pericarp-ventral; Ch, chlorenchyma layer.

Index	m/z	Cluster	Mean signal intensities in selected ROIs of experiment 1							
			P-V	NP-C	ET-C	En-C	En-P	Emb	P	Ch
1	86.1	1	19.88	17.05	27.75	44.37	41.91	15.28	21.54	18.09
2	94.0	3	20.42	14.48	11.95	12.53	4.89	23.26	16.22	13.85
3	104.1	3	71.78	44.8	47.19	55.27	74.87	84.17	62.19	28.85
4	116.1	5	0.74	0.85	0.86	1.01	0.99	14.77	0.71	0.55
5	118.1	5	6.98	2.54	3.54	5.66	6.87	29	4.95	2.24
6	124.1	1	1.4	1.16	1.19	1.91	2.51	1.38	0.98	0.9
7	130.1	3	1.58	1.36	1.36	1.11	1.04	2.01	1.15	0.91
8	136.0	3	13.93	5.62	5.45	5.42	4.45	7.19	7.58	5.05
9	140.1	3	5.56	3.53	3.56	3.01	2.53	10.23	4.53	2.99
10	146.1	1	0.9	0.8	0.73	0.94	1.68	1.8	0.68	0.55
11	147.1	2	5.87	6.05	8.05	5.84	2.29	4.6	4.04	3.82
12	148.1	1	1.74	1.39	1.73	2.09	2.78	2.32	1.22	0.9
13	158.1	5	1.2	1.05	1.16	1.56	1.73	3.84	1.01	0.69
14	184.1	1	45.81	31.85	51.25	63.13	63.77	33.55	44.81	38.49
15	191.2	1	1.58	1.64	1.9	2.39	2.49	2.36	1.46	1.27
16	192.0	3	14.9	10.04	12.49	10.17	12.55	12.69	12.16	8.63
17	193.0	3	35.57	25.52	31.85	25.95	34.21	30.37	32.35	22.38
18	195.0	3	4.1	3.12	3.64	3.19	4.16	3.56	3.72	2.81
19	211.2	3	0.93	0.95	0.87	0.92	1.08	2.17	0.84	0.73
20	214.0	2	1.9	2.8	2.39	1.25	1.28	1.53	2.5	1.89
21	221.2	5	1.35	1.03	1.09	1.01	1.37	4.09	1.26	0.89
22	222.1	2	4.75	6.16	10.02	9.46	4.12	2.74	3.47	3.62
23	230.0	1	5.2	4.71	6.16	5.97	6.99	4.99	4.3	2.93
24	231.0	1	18.2	16.43	22.76	22.35	26.81	18.83	15.7	10.03
25	233.0	1	3.41	3.18	4.11	4.08	4.86	3.28	2.98	1.97
26	240.1	1	1.79	1.36	1.54	2.22	2.53	1.95	1.57	1.05
27	241.2	3	1.8	1.21	1.08	1.02	1.02	2.44	1.09	0.92
28	254.1	5	0.75	0.8	0.72	0.77	0.96	2.1	0.67	0.53
29	293.2	3	0.95	0.95	0.81	0.75	0.96	1.66	1.05	0.65
30	299.1	1	1.69	1.85	2.43	2.36	1.87	1.21	1.79	1.19
31	321.2	1	3.08	2.91	3.43	2.88	2.71	2.44	2.54	1.83
32	337.3	1	1.19	0.88	0.88	1.05	1.89	1.47	1.21	0.67
33	348.1	3	4.53	1.24	1.59	3.72	2.07	2.26	2.6	1.06
34	381.1	2	8.7	9.85	12.03	9.19	6.74	5.31	6.03	4.92
35	399.2	2	1.21	4.18	3.94	1.63	0.79	0.78	2.02	1.85
36	402.1	2	1.02	1.72	2.2	1.79	0.89	0.89	0.92	0.91
37	415.3	2	0.9	2.37	3.27	2.6	0.91	0.84	1.05	1.13

38	428.1	1	2.56	1.06	1.03	2.05	2.46	2.35	1.45	0.94
39	448.2	3	4.31	2.1	1.11	0.74	0.92	0.75	2.52	3.44
40	460.2	3	1.71	1.04	0.95	0.76	0.98	1.78	3.08	2.97
41	479.0	1	0.76	1.1	1.41	1.6	1.59	0.91	0.85	1.06
42	487.0	1	0.89	1.05	1.37	2.28	2.13	0.92	0.85	1.97
43	489.3	3	2.73	0.93	0.77	0.95	1.02	1.12	1.05	1.82
44	496.4	1	1.28	2.14	4.66	7.26	6.78	1.78	1.18	1.05
45	518.3	1	1.13	1.2	1.42	1.63	1.5	1.1	1.73	1.22
46	520.3	1	1.62	1.15	1.74	3.63	6.17	2.04	5.12	2.63
47	527.2	2	5.76	24.66	23.43	7.9	1.65	2.12	7.44	11.17
48	533.3	4	1.41	1.14	0.73	0.59	0.73	0.72	1.33	8.2
49	534.3	1	1.12	1.42	2.56	5.05	4.7	1.1	1.33	4.65
50	543.1	2	10.82	38.22	57.39	41.4	7.69	4.6	11.72	16.37
51	558.3	1	1.34	1.08	1.52	3.04	4.84	1.42	3.39	0.87
52	560.4	2	2.4	6.64	6.62	3.33	1.82	1.21	4.77	3.36
53	562.3	2	1.58	4.27	6.46	5.01	1.42	1.03	1.87	2.49
54	573.6	3	2.01	1.34	1.14	1.31	1.36	3.05	1.32	1.14
55	575.5	1	2.39	1.57	2.37	3.24	5.17	5.04	2.23	1.29
56	576.5	2	4.03	7.28	11.71	10.42	4.24	3.41	4.96	3.49
57	592.3	4	1.85	1.33	0.85	0.75	0.81	0.76	1.69	10.24
58	597.5	3	2.29	1.23	1.03	0.96	1.26	2.84	1.26	2.66
59	599.5	3	2.63	1.26	1.39	1.7	3.34	4.47	1.72	4.74
60	601.5	3	1.31	1.29	1.33	1.26	1.83	2.41	1.52	1.79
61	616.3	3	7.38	3.53	2.82	1.86	2.95	7.91	2.25	2.25
62	618.2	3	4.06	1.84	1.62	1.65	2.3	3.01	1.7	1.24
63	628.2	3	1.33	1.14	1.14	1.3	1.49	1.48	1.03	1.13
64	650.5	1	3.4	4.5	6.48	7.63	5.79	1.41	3.97	2.97
65	652.9	4	3.5	2.37	1.34	1.24	1.3	1.01	3.42	25.71
66	672.5	2	0.94	1.48	1.4	1.01	1	0.88	1.29	0.87
67	674.5	1	0.86	1.07	1.06	1.26	1.79	0.91	0.98	1.1
68	679.2	2	0.89	1.79	2.06	1.68	0.91	0.81	1	0.95
69	688.4	1	1.96	2.73	3.62	4.08	3.28	1.25	2.95	1.48
70	689.3	2	6.25	25.55	25.21	9.31	2.38	2.18	11.73	11.75
71	705.2	2	17	39.39	61.32	47.67	10.65	6.14	21.16	17.56
72	738.1	1	4.66	3.43	5.07	7.76	3.3	2.09	6.41	2.08
73	743.5	5	0.69	0.89	0.72	0.72	0.75	2.73	0.91	0.76
74	744.4	3	1.3	0.98	0.89	0.95	0.96	1.6	1.59	0.9
75	747.0	3	2.27	1.68	1.32	1.67	1.37	2.31	1.43	1.82
76	749.1	1	3.02	2.11	3.37	7.63	9.52	4.87	2.77	2.72
77	751.0	1	1.11	1.21	2.25	4.56	3.88	2.26	1.04	0.99
78	754.5	1	1.18	1.26	1.36	1.71	1.77	1.9	1.01	1.03
79	756.6	3	7.66	4.63	2.98	3.71	2.77	4.81	4.06	7.01
80	758.7	1	9.72	6.03	8.48	15.49	18.16	10.49	9.87	10.57
81	760.7	1	2.7	2.33	5.03	8.57	6.09	4.09	2.46	2.73
82	771.0	3	2.52	1.36	1	1.05	1.2	2.52	1.09	1.84

83	773.0	1	2.92	1.43	1.54	2.64	4.88	5.71	1.89	2.33
84	773.4	5	1.84	1.19	1.21	1.89	2.74	5.72	1.79	1.26
85	778.5	3	5.57	3.52	1.76	2.01	2.07	3.45	2.48	4.73
86	780.7	3	10.57	5.17	3.71	3.86	3.74	7.07	6.06	10.33
87	782.7	3	9.36	4.07	4.35	6.06	9.61	9.69	6.38	9.68
88	784.6	1	3.49	2.19	3.2	4.62	3.93	4.81	2.27	4.27
89	786.7	1	1.45	1.5	2.49	3.93	2.33	2.43	1.33	1.97
90	794.6	3	5.89	3.51	2.71	4.04	3.03	5.18	2.82	4.73
91	796.6	1	8.32	4.88	8.13	18.58	23.4	12.32	7.22	7.47
92	798.6	1	3.01	2.36	5.4	11.43	9.45	5.79	2.54	3
93	800.6	1	1.56	1.48	1.68	2.88	2.27	2.25	1.12	1.55
94	802.5	3	2.21	1.72	1.28	1.49	1.36	2.07	1.49	2.53
95	804.6	3	2.35	1.64	1.35	1.45	1.64	2.64	2.29	3.07
96	813.6	3	1.35	1.24	1.05	1.31	1.2	1.76	1.41	3.75
97	816.5	3	2.98	1.87	1.23	1.68	1.76	2.25	1.29	2.25
98	817.5	1	1.81	1.37	0.99	1.65	2.28	1.48	0.99	1.46
99	818.5	3	6.63	2.79	1.78	2.46	2.77	5.45	2.45	4.77
100	820.6	1	7.33	2.88	3.19	6.3	11.52	10.48	4.38	6.14
101	822.6	1	3.18	1.85	2.91	5.8	5.58	5.99	2.03	3.23
102	824.6	1	1.43	1.31	2.27	4.7	2.77	2.91	1.14	2
103	839.6	4	0.9	0.99	0.81	0.74	0.84	0.82	0.96	3.11
104	851.3	3	6.22	7.47	6.88	4.52	1.84	2.12	12.66	4.82
105	867.4	1	18.9	13.07	20.52	29.69	12.43	6.61	25.49	8.13
106	870.6	4	5.34	3.11	1.91	2.32	1.44	1.51	5.22	31.61
107	884.7	3	2.23	1.47	1.1	1.12	1.03	1.37	2	3.99
108	893.7	3	0.95	1.15	0.93	0.8	1.46	2.82	1.02	4.11
109	899.9	1	3.89	2.52	3.06	5.96	3.01	1.94	5.34	2.49
110	909.6	4	2.04	1.53	0.88	0.92	0.95	1.56	1.93	15.03
111	917.7	3	0.78	0.95	0.86	0.82	1.29	1.82	0.9	1.09
112	919.7	3	0.94	1.05	0.91	0.9	1.37	2.03	1.17	0.9
113	923.6	3	0.96	0.97	0.79	0.81	0.96	1.14	1.07	1.96
114	934.5	1	1.71	1.34	1.29	2.36	1.84	1.35	2.15	1.27
115	953.7	3	1.11	1.04	0.99	1.17	1.11	1.31	1.07	1.65
116	955.6	1	1.34	1.03	1.07	1.64	1.97	1.19	1.33	1.31
117	957.6	3	0.97	0.98	0.87	1.11	1.23	1.07	1.03	1.04
118	975.6	3	1.39	1.2	0.94	1.19	1.3	2.72	1.29	2.78
119	979.6	1	1.02	1.07	1.15	1.46	3.18	1.29	1.08	1.81
120	981.6	3	0.9	0.99	0.93	1.11	1.6	1.14	0.95	1.8
121	1006.7	1	0.89	0.99	0.94	1.43	1.32	0.94	0.95	1.03
122	1013.5	3	5.04	4.72	3.79	3.55	1.68	1.57	10.41	3.68
123	1025.7	3	0.92	1.03	0.75	0.68	0.72	0.77	0.97	2.51
124	1029.3	1	14.65	8.19	10.92	23.24	11.4	4.28	20.63	6.13
125	1061.7	1	2.99	1.87	2	4.58	2.42	1.32	4.2	1.54
126	1068.5	3	4.04	0.98	0.74	0.72	0.77	0.98	4.06	0.98
127	1101.5	3	2.55	1.14	0.74	0.85	1.01	1.82	2.63	1.52

128	1173.6	3	1.46	1.07	0.89	1.49	1.24	0.89	2.02	0.92
129	1175.5	3	4.16	3.26	2.36	3.02	1.46	1.36	8.53	2.96
130	1191.4	1	11.9	5.4	6.35	20.21	9.71	3.39	17	4.88
131	1214.7	3	2.46	1.11	0.73	0.73	0.74	0.85	4.21	1.16
132	1223.6	1	2.35	1.43	1.3	3.25	1.76	1.08	3.13	1.16
133	1230.6	3	6.67	1.09	0.75	0.77	0.87	1.19	7.29	1.44

Index	m/z	Cluster	Mean signal intensities in selected ROIs of experiment 2							
			P-V	NP-C	ET-C	En-C	En-P	Emb	P	Ch
1	86.1	1	10.27	7.26	14.44	17.38	15.51	5.82	8.95	8.28
2	94.0	3	7.8	9.22	3.73	2.68	2.13	8.87	9.59	8.98
3	104.1	3	63.77	77.32	43.13	24.75	44.16	90.54	44.93	40.03
4	116.1	5	0.61	0.65	0.68	1.21	0.86	14.48	0.55	0.59
5	118.1	5	6.55	6.32	5.76	7.44	7.49	52.62	9.11	4.91
6	124.1	1	1.12	1.2	1	2.33	2.42	1.11	1	1.1
7	130.1	3	1.31	1.26	0.9	0.78	0.79	1.87	0.98	0.72
8	136.0	3	5.04	3.88	3.43	3.68	2.92	3.93	6.49	3.36
9	140.1	3	2.97	3.41	3.1	2.03	1.68	7.13	4.81	3.28
10	146.1	3	0.9	0.83	0.78	0.88	1.26	1.77	0.76	0.73
11	147.1	2	7.74	8.6	5.13	1.93	1.47	5.09	2.34	3.74
12	148.1	1	2.05	2.13	1.93	2.25	2.79	2.89	0.89	1.26
13	158.1	5	1.69	2.13	1.55	3.31	1.79	7.86	1.5	1.34
14	184.1	1	29.3	22.5	42.9	45.22	38.07	14.91	32.97	24.12
15	191.2	5	1.15	0.89	1.28	1.83	1.75	6.42	1.15	0.94
16	192.0	2	28.23	37.69	23.68	11.97	13.53	16.15	23.31	17.93
17	193.0	2	66.62	89.04	59.36	32.57	34.65	42.42	55.58	43.96
18	195.0	2	8.26	11.32	7.05	4.06	4.51	5.06	7.22	5.49
19	211.2	3	0.68	0.72	0.73	0.89	0.89	1.84	0.82	0.64
20	214.0	2	1.99	2.95	3.13	1.1	1.08	1.16	2.57	2.4
21	221.2	5	1.44	1.38	1.48	1.17	1.38	12.5	2.1	1.17
22	222.1	2	9.95	14.48	10.3	5.26	2.78	2.63	2.75	5.17
23	230.0	2	12.37	21.93	9.05	5.02	6.61	5.87	6.57	7.85
24	231.0	2	45.04	75.21	34.75	18.44	24.15	21.84	25.19	28.95
25	233.0	2	8.15	14.5	6.2	3.55	4.63	4.1	4.68	5.32
26	240.1	1	1.28	1.17	1.55	3.15	1.96	1.5	1.5	0.97
27	241.2	3	1.39	1.5	0.95	1.18	0.92	1.96	1.08	1.05
28	254.1	5	0.69	0.76	0.64	0.92	0.87	2.8	0.7	0.61
29	293.2	3	1.11	1.09	1.05	1.3	0.99	2.42	1.46	0.86
30	299.1	2	2.07	2.62	2.69	2.73	1.62	1.25	2.13	1.5
31	321.2	2	5.58	7.22	7.25	2.72	2.3	1.53	5.63	2.03
32	337.3	1	0.99	0.89	1.31	1.78	2.5	1.63	1.82	0.73
33	348.1	3	4.34	1.86	2.38	5.24	2	2.98	4.49	1.56
34	381.1	2	23.15	34.26	17.43	8.9	7.95	4.63	7.71	14.7
35	399.2	3	1.77	1.15	1.05	1.26	1.18	1.59	1.73	1.48
36	402.1	2	1.24	2.17	2.28	1.54	0.87	1.09	1	1

37	415.3	2	1.17	3.07	3.16	1.51	0.85	1.06	1.07	1.16
38	428.1	1	2.46	1.47	1.54	2.98	2.55	2.49	2.05	1.69
39	448.2	3	4.43	3.32	0.84	0.85	0.92	0.95	5.24	3.37
40	460.2	3	1.95	1.45	0.87	0.88	1.12	1.72	6.3	1.7
41	479.0	2	1.92	3.33	2.55	1.39	1.48	1.12	1.18	1.28
42	487.0	1	1.03	0.95	1.07	2.42	2.11	1.13	0.99	1.2
43	489.3	3	2.02	1.1	0.69	1.23	1.18	1.05	1.12	1.59
44	496.4	1	1.41	1.97	5	10.96	8.24	2.03	1.58	1.2
45	518.3	3	1.29	0.95	1.2	1.72	1.39	1.2	2.42	1.41
46	520.3	1	1.85	1.33	2.4	7.18	8.52	2.45	11.56	2.28
47	527.2	2	4.89	11.22	21.6	3.05	1.37	1.52	6.28	7.01
48	533.3	4	1.84	0.68	0.63	0.75	0.88	0.8	0.85	3.99
49	534.3	1	1.57	1.26	2.14	6.15	5.38	1.4	1.64	2.6
50	543.1	2	23.52	67.05	65.71	23.35	5.84	5.21	14.46	20.75
51	558.3	1	1.4	1.32	1.58	4.67	6.15	1.93	7.23	1.33
52	560.4	2	1.22	1.84	3.35	2.1	1.95	1.23	3.55	1.74
53	562.3	2	1.73	4.28	4.93	2.61	1.35	1.31	1.64	2.01
54	573.6	3	2.12	1.63	1.51	1.48	1.39	2.26	1.58	1.64
55	575.5	1	2.62	2.21	5.06	4.94	6.94	4.32	3.27	1.66
56	576.5	2	2.91	7.2	9.15	7.08	4.4	2.98	4.51	2.74
57	592.3	4	3.83	0.75	0.73	0.92	1.11	0.87	1.19	8.45
58	597.5	3	2.8	1.57	1.19	1.12	1.5	2.36	1.36	2.66
59	599.5	3	5.17	1.92	2.52	2.66	5.5	4.64	2.48	5.74
60	601.5	1	1.78	1.07	1.48	1.61	2.89	2.48	1.37	1.94
61	616.3	3	8.75	3.79	3.22	2.69	4.36	7.73	2.91	5.07
62	618.2	3	4.85	2.38	1.95	2.19	2.7	3.11	2.01	2.52
63	628.2	1	1.93	1.35	1.82	2.58	2.21	1.51	1.32	1.42
64	650.5	2	1.84	4.08	8.5	6.42	3.35	1.22	2.95	2.22
65	652.9	4	9.25	1.37	1.61	1.37	2.16	1.19	1.84	21.9
66	672.5	2	0.78	1	1.76	1.11	0.9	0.86	1.15	0.82
67	674.5	1	0.98	1.59	2.52	2.99	2.12	0.98	1.04	1.22
68	679.2	2	0.84	1.74	1.62	1.15	0.84	0.94	0.99	0.86
69	688.4	2	1.6	3.13	4.81	3.48	2.5	1.24	3.73	1.55
70	689.3	2	3.09	8.84	17.73	3.41	1.67	1.35	8.85	5.32
71	705.2	2	16.38	53.04	56.68	24.19	7.56	4.88	22.62	15.85
72	738.1	1	1.19	1.95	3.14	4.27	2.35	1.65	6.38	1.37
73	743.5	5	0.77	0.76	0.75	0.91	0.9	8.78	0.84	0.85
74	744.4	5	0.91	0.95	1.01	1.04	0.99	4.72	2.28	1.07
75	747.0	3	5.2	3	1.56	1.77	1.57	2.06	1.56	4.21
76	749.1	1	6.95	4.4	8.39	13.01	15.78	4.7	4.06	5.66
77	751.0	1	2.02	1.71	4.2	6.06	5.66	2.16	1.31	1.67
78	754.5	1	1.91	1.57	2.42	3.55	2.44	1.75	1.28	1.51
79	756.6	3	15.13	6.87	5.71	5.26	3.17	3.58	5.57	12.99
80	758.7	1	18.56	9.57	27.17	34.63	31.03	8.62	16.79	16.09
81	760.7	1	4.27	2.68	12.83	14.42	9.58	3.24	3.92	3.62

82	771.0	3	5.52	2.45	1.24	1.4	1.58	2.48	1.22	4.43
83	773.0	1	6.34	2.9	3.26	5.71	10.54	9.45	2.78	5.04
84	773.4	5	2.65	1.88	1.48	2.22	3.73	10.53	2.05	2.09
85	778.5	3	8.5	3.75	2.92	2.63	3.2	2.74	2.83	8.09
86	780.7	3	17.79	6.39	8.47	5.62	5.28	4.93	7.72	16.63
87	782.7	1	17.07	5.94	12.47	16.14	21.62	8.63	12.11	15.14
88	784.6	1	5.74	2.4	7.5	9.22	8.23	3.85	4.11	5.49
89	786.7	1	2.03	1.47	6.08	6.94	4.26	2.05	1.98	2.03
90	794.6	3	16.91	8.96	4.52	4.49	3.77	4.38	3.76	13.4
91	796.6	1	22.42	13.53	24.15	33.65	37.99	12.07	12.59	18.11
92	798.6	1	6.55	4.45	12.42	16.33	15	5.04	3.94	5.36
93	800.6	1	1.95	1.47	2.89	3.61	3.23	1.72	1.27	2.16
94	802.5	3	2.28	1.33	1.59	1.72	1.7	1.47	1.4	3.17
95	804.6	3	2.36	1.22	2.3	1.94	2.25	1.86	2.6	3.39
96	813.6	3	2.7	1.28	1.12	1.4	1.52	2.02	1.77	4.46
97	816.5	3	6.7	3.31	1.83	1.98	2.63	2.26	1.56	5.63
98	817.5	1	3.85	2.1	1.53	2.86	4.15	1.55	1.14	3.25
99	818.5	3	17.3	7.07	3.02	3.55	4.54	5.31	3.08	13.47
100	820.6	1	19.27	8.02	8.88	15.02	25.53	11.79	7.79	15.26
101	822.6	1	7.18	3.35	6.43	9.48	11.58	5.88	3.41	6.26
102	824.6	1	2.43	1.69	4.97	6.58	5.39	2.63	1.46	2.78
103	839.6	3	1.88	0.68	0.76	0.94	1.13	0.92	0.88	3.18
104	851.3	3	1.14	1.74	3.73	2.31	1.54	1.31	11.56	1.86
105	867.4	1	3.93	9.39	16.1	19.76	9.75	4.96	32.62	5.59
106	870.6	4	14.29	1.18	1.61	1.83	3.24	1.72	4.28	31.14
107	884.7	3	3.09	1.08	1.17	1.12	1.39	1.41	1.75	4.6
108	893.7	3	1.51	1.24	1.36	0.92	3.43	3.74	0.92	3.96
109	899.9	1	1.31	1.52	2.27	3.73	2.54	1.5	5.3	1.86
110	909.6	4	11.48	1.27	0.79	1	2.11	1.69	1.71	23.76
111	917.7	1	0.92	1.15	0.95	0.9	3.21	2.31	0.86	1.17
112	919.7	1	0.77	1.16	0.93	0.96	3.13	2.55	1.07	0.88
113	923.6	3	2.03	0.88	0.77	0.88	1.66	1.32	0.91	3.3
114	934.5	1	1.01	0.93	1.05	1.97	2.02	1.2	2.13	1.14
115	953.7	3	1.55	1.09	1.31	1.46	1.6	1.41	1.34	1.86
116	955.6	1	1.82	1.24	1.8	2.5	4.4	1.38	1.91	1.73
117	957.6	1	1.01	0.87	1.13	1.45	2.17	1.16	1.16	1.13
118	975.6	3	2.27	1.7	0.95	1.25	1.87	3.22	1.83	3.53
119	979.6	1	1.38	0.98	1.77	2.3	7.46	1.47	1.33	1.95
120	981.6	1	1.15	0.83	1.18	1.48	3.37	1.31	1.06	1.86
121	1006.7	1	1.2	0.94	1.78	1.94	1.86	1.11	1.19	1.18
122	1013.5	3	1.05	1.22	2.08	1.99	1.44	1.13	9.71	1.68
123	1025.7	3	1.72	0.7	0.62	0.76	0.98	0.88	0.93	2.85
124	1029.3	1	2.82	4.97	8.4	16.33	10.01	3.31	27.28	4.32
125	1061.7	1	0.94	1.1	1.46	3.33	2.16	1.18	4.58	1.23
126	1068.5	3	0.83	0.76	0.6	0.83	1.02	0.91	4.25	1.2

127	1101.5	3	1.02	0.84	0.63	0.91	1.05	1.52	1.87	1.14
128	1173.6	3	0.64	0.77	0.67	1.18	1.34	0.94	2.62	0.79
129	1175.5	3	0.85	0.94	1.32	1.83	1.4	1.07	8.9	1.37
130	1191.4	1	1.92	2.75	5.18	15.26	10	2.89	24.82	3.41
131	1214.7	3	0.71	0.84	0.6	0.8	0.88	0.88	1.58	0.97
132	1223.6	1	0.76	0.85	0.99	2.39	1.86	1.03	3.65	0.92
133	1230.6	3	0.85	0.8	0.61	0.88	1.27	0.98	3.91	1.48

Index	*m/z*	Cluster	Mean signal intensities in selected ROIs of experiment 3							
			P-V	NP-C	ET-C	En-C	En-P	Emb	P	Ch
1	86.1	1	2.63	1.92	2.87	5.71	5.5	2.39	2.18	1.52
2	94.0	5	3.29	2.33	2.86	1.63	1.64	16.9	4.29	1.59
3	104.1	3	98.06	58.83	40.74	32.43	55.08	68.38	57.96	19.81
4	116.1	5	0.87	0.85	0.69	0.93	0.96	6.96	0.82	0.69
5	118.1	5	12.14	7.2	7.31	8.09	8.07	46.85	8.55	2.43
6	124.1	1	1.3	0.9	1	2.27	2.05	1.6	0.94	0.66
7	130.1	3	1.38	1.07	1.1	1.03	0.91	1.56	0.99	0.7
8	136.0	3	2.9	1.76	2.52	2.54	2.24	2.23	3.02	1.55
9	140.1	5	4.1	2.64	2.36	1.43	1.58	9.44	3.89	1.79
10	146.1	3	1.5	0.84	1.08	1.18	1.27	1.67	0.96	0.68
11	147.1	2	9.04	5.57	5.01	1.88	1.38	2.5	4.37	1.59
12	148.1	1	3.04	1.67	1.96	2.5	2.39	1.82	1.67	0.75
13	158.1	5	3.55	2.24	1.61	1.65	1.95	9.27	2.58	0.89
14	184.1	1	8.96	8.13	16.07	21.44	17.11	6.88	6.74	5.93
15	191.2	5	1.01	0.92	0.95	1.46	1.4	8.42	0.9	0.82
16	192.0	2	25.13	24.16	27.48	13.2	15.75	17.23	21.77	9.24
17	193.0	2	63.34	61.36	68.6	37.26	41.89	42.42	55.09	24.78
18	195.0	2	8.1	7.84	8.95	4.54	5.3	5.34	6.99	3.17
19	211.2	5	0.75	0.79	0.71	0.9	0.92	5.57	0.81	0.6
20	214.0	3	2.84	2.51	2.47	0.98	1.11	1.31	3.16	2.1
21	221.2	5	3.75	1.68	1.39	1.5	2.06	14.28	1.93	0.82
22	222.1	2	7.28	5.94	5.25	2.42	1.51	2.37	3.95	2.23
23	230.0	3	13.09	10.32	8.6	4.73	6.76	6.41	11.55	4.4
24	231.0	3	48.75	39.36	33.32	18.17	25.35	24.13	43.1	16.03
25	233.0	3	9.03	7.16	6.12	3.36	4.59	4.56	8.03	3.13
26	240.1	1	1.06	0.94	1.03	1.81	1.61	1.2	0.92	0.64
27	241.2	5	1.51	1.05	0.85	1	1	4.53	1.31	0.75
28	254.1	5	1.01	0.84	0.62	0.81	0.86	2.77	0.92	0.6
29	293.2	5	1.19	0.96	0.84	0.92	0.96	5.74	1.03	0.67
30	299.1	1	1.52	1.37	1.44	1.5	1.35	1.17	1.2	0.87
31	321.2	2	2.93	5.79	6.25	2.65	2.21	1.98	2.5	2.73
32	337.3	1	0.92	0.87	0.97	1.7	2.05	1.09	0.96	0.6
33	348.1	3	4.61	2.17	4.52	4.37	2.79	3.76	5.28	1.38
34	381.1	3	21.41	14.72	11.92	8.21	7.73	6.32	17.5	9.3
35	399.2	3	5.01	1.66	1.72	1.84	1.61	3.12	5.32	2.26

36	402.1	2	1.35	2.07	2.16	1.18	1.07	1.08	1.22	1.04
37	415.3	2	1.15	2.07	1.87	1.12	0.88	0.87	0.96	1.2
38	428.1	1	2.86	1.23	1.67	4.15	3.37	2.23	2.07	1.43
39	448.2	3	2.68	1.84	0.98	0.93	0.93	1.08	2.95	1.88
40	460.2	3	1.44	1.25	0.91	0.95	1.02	1.06	1.68	1.14
41	479.0	2	3.29	4.77	3.66	1.63	2.03	1.52	3.41	1.95
42	487.0	1	1	1.05	0.91	1.66	1.65	1.28	1.21	0.98
43	489.3	3	2.38	1.03	0.96	1.66	1.4	1.42	2.71	1.58
44	496.4	1	0.96	1.73	2.19	6.2	4.86	1.48	1.1	0.85
45	518.3	1	0.79	0.96	0.82	1.33	1.14	1.01	1.48	0.82
46	520.3	1	0.94	1.27	1.24	4.5	4.86	1.59	3.97	1.09
47	527.2	2	5.84	11.33	12.07	2.35	1.49	1.74	4.9	11.14
48	533.3	3	0.82	0.81	0.67	0.82	0.86	0.81	0.92	1.65
49	534.3	1	0.87	1.24	1.19	3.92	3.54	1.17	1.24	1.27
50	543.1	2	21.27	50.02	50.85	15.34	5.02	5.38	10.47	24.53
51	558.3	1	1.13	1.32	1.09	3.32	4.18	1.57	5.84	1.06
52	560.4	3	1.13	1.9	1.79	1.69	1.64	1.18	2.65	2.74
53	562.3	2	1.57	3.33	3.19	1.84	1.26	1.21	1.48	2.27
54	573.6	1	1.23	1.25	1.51	1.69	1.42	1.75	1.1	1.07
55	575.5	1	2.21	2.94	5.42	5.18	5.67	2.79	1.97	1.46
56	576.5	2	2.58	5.08	5.93	4.01	3.49	2.17	2.58	4.02
57	592.3	4	1.09	0.93	0.81	0.85	0.91	0.91	1.1	3.43
58	597.5	2	1.23	1.61	1.73	1.22	1.24	1.15	1.38	1.33
59	599.5	1	3.32	1.58	2.08	2.84	4.03	2.11	1.7	3.26
60	601.5	1	1.7	1.13	1.31	1.58	2.26	1.3	1.53	1.84
61	616.3	3	5.37	2.3	2.87	3.19	3.15	2.66	3.01	2.48
62	618.2	3	5.91	1.93	2.03	2.62	2.53	2.01	5.64	2.85
63	628.2	1	1.74	1.63	2.44	2.48	2.36	1.39	1.45	1.37
64	650.5	2	1.77	2.37	2.29	1.31	1.36	1.13	1.73	1.9
65	652.9	4	2.33	2.58	2.42	1.24	1.5	1.17	1.95	12.75
66	672.5	2	1.64	2.5	2.05	1.04	1.19	0.97	1.73	1.28
67	674.5	2	1.38	1.88	1.54	1.02	1.2	1.06	1.51	1.35
68	679.2	3	1.02	1.35	1.17	0.93	0.93	1.1	1.17	1.06
69	688.4	3	1.1	1.44	1.41	1.27	1.2	1.13	2.14	1.25
70	689.3	2	4.27	11.63	12.16	2.1	1.45	1.48	4.75	15.83
71	705.2	2	19.55	48.44	49.78	18.31	7.15	6.4	15.41	35.41
72	738.1	3	1.82	1.75	2.22	3.57	2.26	2.21	3.26	3.84
73	743.5	3	0.93	0.94	0.77	0.88	0.93	0.91	1.74	0.92
74	744.4	3	1.06	1.02	0.82	0.91	0.93	0.94	2.22	1.23
75	747.0	3	3.21	2.32	2.02	2.74	2.02	2.45	1.92	2.81
76	749.1	1	6.08	4.78	8.63	15.07	15.72	5.43	4.59	4.84
77	751.0	1	2.14	2.33	5.03	7.55	6.57	2.36	2	1.94
78	754.5	1	1.7	1.9	2.93	3.02	2.89	1.82	1.44	1.57
79	756.6	3	6.1	5.47	7.63	7.29	4.52	5.97	3.18	6.98
80	758.7	1	11.7	12.92	29.79	37.78	32.66	13.05	8.35	12.44

81	760.7	1	2.68	4.61	15.33	17.11	11.45	3.76	2.44	3.65
82	771.0	3	3.86	2.29	1.97	2.18	2.05	2.42	2.16	3.34
83	773.0	1	6.34	3.25	3.9	7.37	9.99	3.96	4.32	5.26
84	773.4	1	2.78	1.8	1.55	2.66	3.37	1.83	3.03	2
85	778.5	3	4.91	2.88	3.35	3.5	3.4	2.95	2.74	5.72
86	780.7	3	10.38	6.16	8.35	7.36	6.31	6.68	5.91	13.21
87	782.7	1	12.38	7.89	14.52	20.03	21.46	9.04	8.02	14.08
88	784.6	1	4.07	4.81	11.41	13.27	9.59	3.71	3.28	8.07
89	786.7	1	2.2	3.89	8.6	8.1	4.82	2.39	2.12	3.79
90	794.6	3	9.09	6.2	5.94	7.78	5.43	6.77	4.65	8.52
91	796.6	1	18.37	14.72	26.31	40.23	40.63	16.1	13.43	15.69
92	798.6	1	5.7	6.09	15.14	21.71	18.26	5.89	4.82	6.46
93	800.6	1	1.87	1.77	3.44	4.84	4.12	1.67	1.68	2.39
94	802.5	3	2.13	1.35	1.41	1.74	1.78	1.24	1.63	3.61
95	804.6	3	2.85	1.65	1.93	1.91	2.2	1.41	2.59	5.04
96	813.6	4	2.02	1.45	1.3	1.51	1.4	1.29	1.85	6.55
97	816.5	3	4.36	2.25	2	2.64	2.94	2.41	2.42	3.92
98	817.5	1	2.61	1.71	1.81	3.99	4.96	1.65	1.63	2.4
99	818.5	3	11.92	5.1	4.04	6.27	6.15	6.03	5.28	10.32
100	820.6	1	18.65	8.66	11.34	20.47	27.46	10.97	11.76	15.68
101	822.6	1	6.78	4.52	9.28	14.83	13.35	4.7	4.99	9.88
102	824.6	1	2.33	2.76	6.59	8.73	5.93	2.08	2.07	4.52
103	839.6	3	1.04	1.07	0.96	1.06	1.11	1.02	1.18	2.4
104	851.3	4	2.17	2.29	3.01	2.28	1.76	1.84	4.59	9.38
105	867.4	3	8.7	9.1	14.99	20.4	11.23	9.97	17.4	24.05
106	870.6	4	3.16	1.52	1.77	2.06	2.03	1.68	2.76	23.35
107	884.7	3	1.96	2.13	1.87	1.31	1.31	1.19	1.76	3.01
108	893.7	4	1.63	1.41	1.26	1.22	2.84	2.09	1.22	5.54
109	899.9	3	2.06	1.87	2.21	3.15	2.38	1.68	3.29	3.89
110	909.6	4	3.53	1.38	1.17	1.17	1.54	1.22	2.35	22.84
111	917.7	1	1.21	1.27	0.95	1.03	2.39	1.47	1.27	1.37
112	919.7	1	1.09	1.3	0.94	1.06	2.29	1.37	1.26	1.18
113	923.6	3	1.28	1.1	0.87	0.97	1.41	0.97	1.29	2.72
114	934.5	1	1.31	1.18	1.17	1.87	1.93	1.45	1.66	1.83
115	953.7	3	1.53	1.26	1.51	1.76	1.51	1.28	1.48	3.6
116	955.6	1	1.98	1.4	1.68	2.95	3.66	1.48	2.28	2.28
117	957.6	1	1.28	1.1	1.12	1.61	1.89	1.22	1.46	1.52
118	975.6	4	2.32	1.57	1.21	1.65	1.72	1.74	1.65	7.43
119	979.6	1	1.46	1.36	1.78	3.9	6.86	1.46	1.47	2.25
120	981.6	1	1.21	1.18	1.32	2.26	3.18	1.26	1.31	2.18
121	1006.7	1	1.63	2.44	3.56	3.3	2.92	1.4	1.62	2.07
122	1013.5	4	1.98	1.58	1.93	1.84	1.51	1.37	4.09	8.37
123	1025.7	3	1.12	1.03	0.82	0.9	0.94	0.97	1.16	2.6
124	1029.3	3	7.75	5.09	8.83	16.8	9.77	5.87	15.86	21.59
125	1061.7	3	1.54	1.31	1.52	2.96	1.93	1.49	2.73	3.21

126	1068.5	3	1.15	0.94	0.81	0.95	0.98	1.06	2.88	2.62
127	1101.5	3	1.11	0.98	0.82	0.99	0.92	0.99	1.19	1.6
128	1173.6	3	1	0.9	0.8	1.18	1.13	1.06	1.47	1.84
129	1175.5	4	1.85	1.1	1.3	1.66	1.3	1.47	3.7	7.27
130	1191.4	3	5.85	2.33	5.2	15.49	8.75	5.3	12.47	18.19
131	1214.7	3	1.02	0.98	0.87	0.97	0.88	0.98	1.9	2.36
132	1223.6	3	1.39	1.04	1.16	2.19	1.51	1.22	2.26	2.88
133	1230.6	3	1.47	1.11	1.09	1.08	1.07	1.2	4.73	4.67

Appendix 5: Quantity of sugars in stem tissues from barley. Stem samples were cut directly below the spikes at defined time points in relation to the stages of grain development (DAP, days after pollination). Measurements were performed by LC and electrochemical detection (in collaboration with Prof Win Van den Ende, KU Leuwen, Belgium).

Seed age	Sugar content of stem tissues [mg/g FW]							
	Glucose	**Fructose**	**Sucrose**	**1-Kestose**	**6-Kestose**	**Neokestose**	**Nystose**	**Bifurcose**
7 DAP	1.18	0.49	1.12	0.05	0.14	0.00	0.02	0.72
10 DAP	0.30	0.40	1.62	0.18	0.10	0.00	0.00	0.34
10 DAP	0.44	0.32	0.56	0.07	0.19	0.00	0.01	0.46
14 DAP	0.20	0.18	0.42	0.04	0.07	0.00	0.00	0.09
14 DAP	0.68	0.26	0.79	0.04	0.07	0.00	0.00	0.20
20 DAP	0.44	0.24	1.49	0.05	0.18	0.00	0.01	0.22
20 DAP	0.14	0.10	1.09	0.09	0.10	0.00	0.00	0.08